

CR-18415
537464



INTERSONICS
INCORPORATED

FINAL REPORT

Contract NAS8-37592

Submitted To:

GEORGE C. MARSHALL SPACE FLIGHT CENTER

**NATIONAL AERONAUTICS & SPACE
ADMINISTRATION**

Prepared By:

**INTERSONICS INCORPORATED
NORTHBROOK, ILLINOIS**

March 28, 1991

(NASA-CR-18415) DEVELOPMENT OF HIGH
TEMPERATURE CONTAINERS PROCESSING
EQUIPMENT AND THE DESIGN AND EVALUATION OF
ASSOCIATED SYSTEMS REQUIRED FOR MICROGRAVITY
MATERIALS PROCESSING AND PROPERTY

63/35 Unclass
0014414



INTERSONICS
I N C O R P O R A T E D

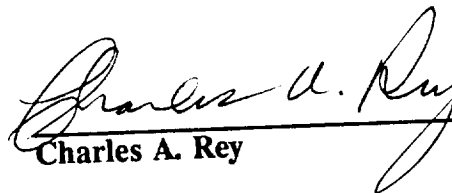
CONTRACT NAS8-37592

FINAL REPORT

Prepared For: George C. Marshall Space Flight Center
Marshall Space Flight Center
Alabama, 35812

Prepared By: Intersonics, Incorporated
3453 Commercial Avenue
Northbrook, Illinois 60062

Submitted By:



Charles A. Rey

March 28, 1991

TABLE OF CONTENTS

INTRODUCTION	1
EXECUTIVE SUMMARY	1
1. Brassboard Acoustic Levitation Facility (ALF)	1
2. Special Studies	2
2.1 ALF Special Studies	2
2.2 NCTM Brassboard	2
2.3 Division of Amplitude Polarimetric Pyrometer (DAPP)	3
2.4 Contamination Control	3
2.5 Beam Heating	3
3. High Temperature Acoustic Levitator (HAL)	4
3.1 HAL Results Summary and Capabilities Assessment	5
4. Recommendations	5

APPENDIX A: AGEMA NCTM SYSTEM BRASSBOARD FINAL REPORT

APPENDIX B: DIVISION OF AMPLITUDE POLARIMETRIC PYROMETER (DAPP) FINAL REPORT

APPENDIX C: STUDY AND EVALUATION OF THE FEASIBILITY OF PROVIDING IMPROVED
CONTAMINATION CONTROL FOR AN ELECTROMAGNETIC LEVITATION SYSTEM

APPENDIX D: SURVEY AND EVALUATION OF BEAM HEATING SYSTEMS FOR APPLICATIONS IN
CONTAINERLESS EXPERIMENTATION

APPENDIX E: CONTAINERLESS PROCESSING AT HIGH TEMPERATURES USING ACOUSTIC
LEVITATION

INTRODUCTION

This is the Final Report on NASA Contract NAS8-37592. The contract effort was directed towards the development of high temperature containerless processing equipment and the design and evaluation of associated systems required for microgravity materials processing and property measurements. Some of the work carried out under the present contract continued work which was initiated under contract NAS8-33742.

Effort was directed towards the following task areas:

- o Design and development of a High Temperature Acoustic Levitator (HAL) for containerless processing and property measurements at high temperatures.
- o KC-135 testing of the HAL module to establish this technology for use as a positioning device for microgravity uses.
- o Construction and evaluation of a brassboard hot wall Acoustic Levitation Furnace (ALF).
- o Construction and evaluation of a noncontact temperature measurement (NCTM) system based on an AGEMA thermal imaging camera.
- o Construction of a prototype Division of Amplitude Polarimetric Pyrometer (DAPP) for NCTM of levitated specimens.
- o Evaluation of and recommendations for techniques to control contamination in containerless materials processing chambers.
- o Evaluation of techniques for heating specimens to high temperatures for containerless materials experimentation.

The work in each of these areas is described in the Executive Summary, and the individual project reports are included as appendices to this report.

The project reports include recommendations for future work. These recommendations are based on technical feasibility and on the needs identified by the microgravity science community during the Workshop on Containerless Experimentation in Microgravity held at JPL in January, 1990.

EXECUTIVE SUMMARY

1. Brassboard Acoustic Levitation Facility (ALF)

The brassboard ALF is a hot wall furnace design intended for service up to 1750°C. Its purpose is to provide a test facility for an eventual high temperature Acoustic Levitation Facility for containerless materials processing in micro-gravity. Primary development for this facility was carried out under the previous contract (NAS8-33742). This technology is an extension of the

Single Axis Acoustic Levitator (SAAL) technology and subsequent research performed under that contract. Further information on that work can be found in the final report for that contract which was submitted August 24, 1989.

This facility was intended for KC-135 testing under this contract. Due to a re-direction of effort toward the NCTM development project, the KC-135 flight module was not completed and the tests were not performed. Limited ground-based testing was carried out prior to task redirection.

2. Special Studies

Much of the work performed in this contract was to study and evaluate subsystems for a containerless processing facility. The purpose was to cover the necessary furnace development and acoustic integration tasks associated with the ALF R&D program. This work progressed from May through September of 1989 before task redirection. This redirection was to accommodate the need for a Thermal Imaging NCTM device. Also included in the additional tasking was further development work on the Division of Amplitude Polarimetric Pyrometer (DAPP). Subsequent task additions included a study of contamination control techniques in electromagnetic levitation facilities and a study of beam heating techniques. The following is a summary of these tasks.

2.1 ALF Special Studies:

These studies were intended to characterize the ALF high temperature hot wall furnace configuration for a variety of different aspects. Furnace liners, heating elements, and other chamber materials were to be further evaluated with respect to contamination, thermal cycling, mechanical stability, etc. Further acoustic testing was planned including SPL and force measurements at high temperatures, acoustic field mapping, temperature mapping, sample deformation from acoustic pressure, sample gas quench cooling feasibility, and sample rotation capability. In addition to these, a number of acoustic transducer studies were also planned. Among these were studies to measure transducer output at high temperatures and verify resonance tracking feasibility of six transducers at high temperature.

Plans were developed to accomplish these tasks which required considerable preparation activities. Development of a hot probe microphone for use at temperatures up to 1600°C was initiated along with an automated xyz translation device for acoustic field and temperature mapping. Other preparations included force meter and furnace design modifications, signal conditioning electronics and a data acquisition system. Much of this work was completed and some testing had been carried out when task redirection occurred in October, 1989.

2.2 NCTM Brassboard

This project ensued following a task directive issued October 5, 1989. Its purpose was to establish the feasibility of integrating an AGEMA Infrared Thermal Imaging camera into the DPM flight module and to subsequently carry out the task. Feasibility was confirmed and the

development project was carried out. The design approach employed for this instrument was to digitize the analog video signal produced by an AGEMA 870 scanner and prepare the digital data for downlink via the shuttle telemetry system. Custom electronics and optics were designed for this system. The system performed nominally as designed but testing determined that the AGEMA scanner is not suitable for precision temperature measurement applications. Details of this can be found in the NCTM Brassboard Final report which is attached as Appendix A.

2.3 Division of Amplitude Polarimetric Pyrometer (DAPP)

The objective of this task was to demonstrate a polarimetric method for precisely measuring spectral emissivity and other optical properties of specular and partly specular surfaces. Included in this effort was the design, fabrication, testing, calibration and delivery of a prototype instrument to NASA. This project was successfully completed and very good results were obtained. The instrument was calibrated and tested at 633nm and the accuracy of stokes vector measurements at this wavelength was determined to be 0.5 - 1%. Spectral emissivity measurements with this device provide .5% absolute accuracy. This is probably the first absolute thermodynamic temperature and optical property measuring device available. A detailed report on DAPP is included in Appendix B.

2.4 Contamination Control

The purpose of this study was to evaluate techniques to minimize and control contamination in an electromagnetic levitator. Control of gaseous and particulate impurities were considered. Approaches examined include operation in vacuum, inert gas, chemically active gases, chemically purified gases, gettering, filtering, etc. This study and other work being pursued at Intersonics indicate that in many cases the use of a gaseous atmosphere has significant advantages over operation in a vacuum. However, the best techniques for reducing and controlling contamination are dependent on the type of material being processed. This and other specific experimentation requirements must be known before the best methods can be specified. Contamination control is covered in greater detail in the report attached in Appendix C.

2.5 Beam Heating

This study looked at the factors affecting beam heating of samples and various techniques for non-isothermal heating. Approaches considered included; focused lamps, electron beam, lasers (gas and solid state), solar and electromagnetic induction heating. Each of these has advantages and disadvantages, and particular applications for which they are well suited. Energy conversion efficiencies vary widely and system optimization is essential to reduce power consumption in space based applications. Other factors considered include; safety, size, and power requirements.

The most promising prospect for future microgravity experiments requiring beam heating is solid state laser diode technology. This rapidly

advancing technology may provide a versatile, efficient (both in size and power conversion) and safe method of beam heating specimens to high temperatures. They are small, can provide up to 50% conversion efficiency, and are relatively easy to drive (no high voltage required).

However, as is pointed out in the report included in Appendix D, electrical to optical power conversion is only part of the total efficiency. Energy can only be delivered to a sample if it absorbs light at the wavelength where the source is emitting the light. For example, a CO₂ laser emitting at 10.6 μm is very efficient for heating glasses and ceramics but not for metals. These factors must be taken into account when specifying a suitable beam heating source for a particular application. There is no single technique that can provide high efficiency heating for all materials. Recommendations include; the development of laser diode systems and the consideration of a high power CO₂ laser for micro-gravity applications.

3. High Temperature Acoustic Levitator (HAL)

The HAL facility is a three axis acoustic levitation system similar to ALF but designed to operate with beam heating instead of the isothermal hot wall design of ALF. This system was developed under NASA contract NAS8-33742 and was being prepared for its first KC-135 flight at the commencement of this contract. Further description of HAL can be found in the Final Report for NAS8-33742 and in Appendix E.

Intersonics personnel performed the first KC-135 flight tests of HAL in May of 1989. The equipment performed well and demonstration of the technique was accomplished including melting of an aluminum sample. Minimal equipment related problems were encountered during the first week of flights and a large number of samples were processed. After a brief period of data analysis, minor equipment repairs and modifications, the equipment was prepared for a second week of testing. Flight testing in June of 1989 confirmed information from the previous flights but provided only modest improvements in results.

Following testing, work began on upgrading the HAL capabilities. Specifically, the Sample Injection and Retrieval System (SIRS) was redesigned, an optical pyrometer was built and a closed loop specimen stabilization system was installed. The latter provides the ability to continuously monitor the specimen position and correct for motion via phase adjustments to the appropriate sound sources. This is made possible by the use of the opposed sound source configuration used in the HAL system.

These system modifications were effected between June and December, 1989. In January, 1990 the third set of KC-135 flights took place. This flight established the ability to damp and reduce sample motions with the application of closed loop feedback. The SIRS modifications proved to be very effective. Aircraft problems substantially reduced the total flight time and another week of flights were scheduled for March.

The March flights were postponed due to aircraft problems but testing resumed after 2 weeks. During these tests positioning was maintained on samples up to ~ 1300°C and several aluminum samples were melted. A large amount of data was obtained and their subsequent analysis demonstrated the effectiveness of the closed loop feedback system.

3.1 HAL Results Summary and Capabilities Assessment

A considerable amount of testing and analysis has been performed to assess the current and potential capabilities of the HAL system. The KC-135 tests provided partial proof of the feedback damping concept. In some cases specimen motion control was outstanding and in others it was ineffective. Some of this was attributable to intermittent electronic noise but other causes were also identified. Conditions affecting damping effectiveness include system gain, sound level, specimen velocity (oscillation frequency) and lighting conditions.

Data analysis and post-flight testing indicated some minor deficiencies in the feedback system. It was determined that the basic position feedback was ineffective in correcting for slow specimen motion (i.e. < 1Hz). Since the velocity feedback amplitude decreases with frequency, the low frequency perturbations were unaffected. In addition, the feedback system was also susceptible to problems induced by the large dynamic range of lighting conditions (i.e. low to high emissivity, arc lamps on/off). Suitable techniques for eliminating these problems were identified and the modifications have been effected.

Laboratory testing indicates that there may be no limit to the temperature differential (between the sample and the ambient) that can be tolerated with the HAL system. This has been demonstrated up to 2700K in tests performed on Al₂O₃ samples. Based on these results and the post flight analysis, it is apparent that an adequate demonstration of the full capabilities of the HAL was not obtained in these KC-135 flights. We are very confident that future testing of HAL would be quite successful in establishing those capabilities.

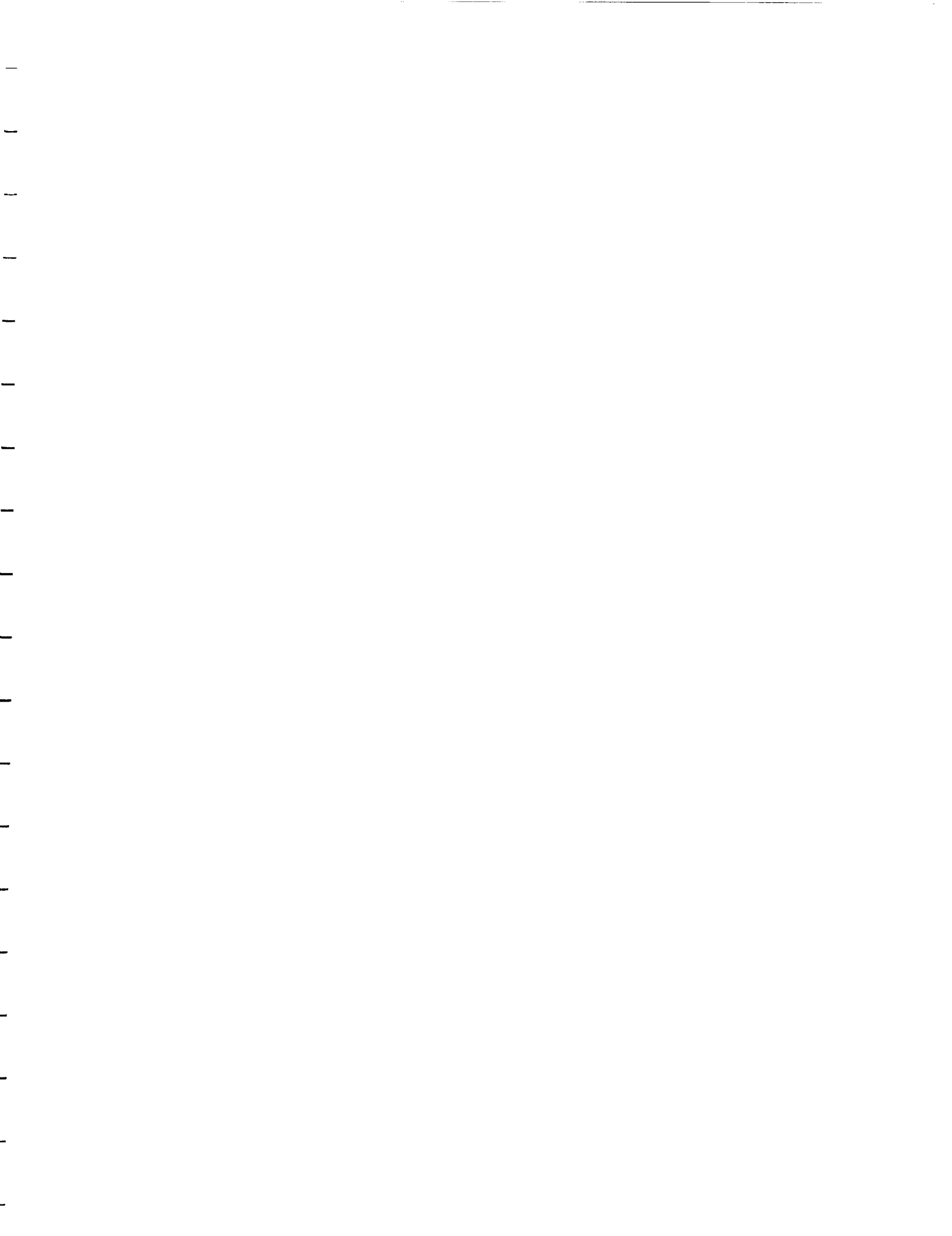
4. Recommendations

Information presented in this report indicates the status of all work performed under this contract. Significant progress was made in many areas and it is strongly recommended that work in some of these areas be continued.

KC-135 and laboratory testing of HAL indicate that this is a very viable technique for high temperature containerless processing. It appears as though there may be no upper temperature limits on the ability of HAL to position samples. This system is applicable to both conducting and nonconducting materials. We, therefore, strongly recommend continued development and testing of this technique.

The DAPP technology is producing unprecedented results in noncontact temperature measurement. Sample temperature is some of the most important data in the field of containerless materials processing and the DAPP technology can make a significant contribution to precision measurement. Continued development work in this area is also recommended.

Beam heating of containerlessly positioned samples is also an area requiring attention. Safety requirements and limited power availability on the Space Shuttle and Station make this a very important development area. Work in this area should begin as soon as possible to ensure capabilities for the next generation of flight hardware.





INTERSONICS
I N C O R P O R A T E D

CONTRACT NAS8-37592

AGEMA NCTM SYSTEM BRASSBOARD

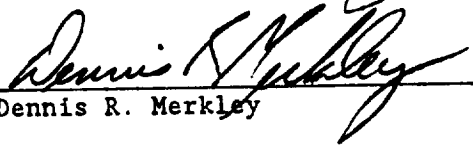
FINAL REPORT

Report of Work Completed Period Ending: December 31, 1990

Prepared For: NASA, George C. Marshall Space Flight Center
Marshall Space Flight Center
Alabama 35812

Submitted By:


Charles A. Rey


Dennis R. Merkley

3.2.3	System Calibration with the Dual Zone Chamber	23
3.2.4	Sweet Spot Detection	28
3.2.5	Measurement Sensitivity to Target Location	28
3.2.6	Optical Parameters	33
3.2.6.1	Focal Range	33
3.2.6.2	Depth of Focus	33
3.2.6.3	Field of View	33
3.2.7	Hot Sapphire Window Emission	33
3.2.8	Electrical Characteristics	34
3.2.8.1	Video Conditioning Filter Response	34
3.2.8.2	System Power Measurements	34
4.	<u>PERFORMANCE EVALUATION</u>	37
4.1	NCTM System Performance	37
4.1.1	Electronics	37
4.1.2	Optics	37
4.1.3	Temperature Measurement	38
4.1.3.1	Baseline Temperature Measurement Ranges	38
4.1.3.2	Measurement Sensitivity To Target Location	38
4.1.3.3	Sweet Spot Detection	38
4.1.3.4	Temperature Resolution/Error Effects	41
4.1.3.4.1	Scan Line Error	41
4.1.3.4.2	Periodic Scan Errors	41
4.1.3.4.3	Asynchronous Digitization Error	42
4.1.3.5	Optics Train Effects/DZC Characteristics	42
4.1.3.6	Temperature Measurement Summary	43
5.	<u>RECOMMENDED SYSTEM MODIFICATIONS</u>	47
5.1	Electronics	47
5.2	Optics	47
5.3	Ground Support Equipment	48
6.	<u>RECOMMENDED SYSTEM MODIFICATIONS (FUTURE FLIGHT SYSTEM)</u>	49
6.1	Data Handling	49
6.2	Automated Filter Selection	49
6.3	Optics	49
6.4	Ground Support Equipment	50
7.	<u>SUMMARY AND CONCLUSIONS</u>	52
7.1	AGEMA NCTM Brassboard Performance	52
7.2	Dual Zone Chamber Radiance Measurements	53

TABLE OF CONTENTS

<u>1. SYNOPSIS</u>	1
<u>2. SYSTEM DESCRIPTION</u>	2
2.1 Agema Thermovision	2
2.2 NCTM System Description	2
2.2.1 Objective Optics	3
2.2.2 Mechanical Assembly (MA) Board Functions & Description	3
2.2.2.1 Power Supplies	8
2.2.2.2 Power Switching	8
2.2.2.3 Scanning Motor Current Limit	8
2.2.2.4 TE Cooler Control	8
2.2.2.5 Video and Sync Relay Buffers	11
2.2.2.6 Bus Interface/Registers	11
2.2.3 Controller Assembly (CA) PWA Functions & Description	12
2.2.3.1 Video Conditioning Circuitry	12
2.2.3.2 Video & Sync Digitization	12
2.2.3.3 Controller Assembly Bus Interface	12
2.2.3.4 Interleave Control	15
2.2.3.5 Timing Control & P/S Conversion	17
2.2.4 Ground Support Equipment (GSE) Functions & Description	17
2.2.4.1 S/P Conversion & Word Sync	20
2.2.4.2 Registers/Register Control	20
2.2.4.3 Video Reconstruction	20
2.2.4.4 Pixel Addressing	20
2.2.4.5 Target Pixel Processing	21
2.2.5 Dual Zone Chamber (DZC) Mock-Up Description	21
<u>3. SYSTEM TESTING AND CALIBRATION</u>	22
3.1 Tests and Facilities	22
3.1.1 Test and Calibration List	22
3.2 Test Descriptions and Results	22
3.2.1 Baseline Blackbody Calibration	22
3.2.2 Temperature Resolution	23
3.2.2.1 Electrical Noise	23
3.2.2.2 Dark System Noise	23
3.2.2.3 Temperature Measurement Uncertainty	23

- APPENDIX A: AGEMA 870 Thermovision Specifications
- APPENDIX B: Mechanical Drawings of Objective Optics
- APPENDIX C: Test and Calibration Facilities
- APPENDIX D: Specifications

LIST OF FIGURES

- Figure 1: NCTM Functional Block Diagram
- Figure 2: AGEMA/DZC Test Facility
- Figure 3: Cassegrainian Objective Lens
- Figure 4: Afocal Imaging of On-Axis and Extreme Off-Axis Target Points
- Figure 5: PWA Functions
- Figure 7: Controller Assembly PWA Block Diagram
- Figure 8: Output Bit Assignment
- Figure 9: Interleave Timing Diagram
- Figure 10: Word Cycle Timing Diagram
- Figure 11: GSE Functional Diagram
- Figure 12: Polynomial Approximation of $(V)T$
- Figure 13: Polynomial Approximation of $(V)T$
- Figure 14: Temperature Measurement Statistics
- Figure 15: Temperature Measurement Statistics
- Figure 16: Polynomial Approximation of $V(T)$
- Figure 17: Polynomial Approximation of $V(T)$
- Figure 18: Horizontal Scan Through Sweet Spot
- Figure 19: Measurement Sensitivity to Target Location
- Figure 20: Video Conditioning Circuit Response
- Figure 21: System Power Measurements
- Figure 22: Temperature Measurement Range
- Figure 23: Temperature Measurement Range
- Figure 24: Emissivity of Sapphire Window
- Figure 25: Periodic Optical Error Effects
- Figure 26: POCC Hardware Block Diagram

Abstract

The AGEMA NCTM System Brassboard was completed under NASA contract NAS8-37592. The goal was to provide a system for noncontact temperature measurement of levitated specimens in the DPM Dual Zone Chamber experiment. The system was to include an AGEMA 870 Thermal Imaging camera and necessary support systems developed and integrated into the DPM prior to the USML-1 mission. The project proceeded on schedule prior to the cancellation of the DZC experiment in May, 1990, which negated the requirement for flight qualified hardware. With this exception, the system design, development, testing, and calibration was completed as planned.

The completed hardware provides a digitized version of the analog video output of the AGEMA 870 camera. This digital data is intended for downlink via the space shuttle telemetry system. For ground-based testing, additional hardware was developed to decode and convert the digital data back to analog format, thereby allowing the use of the AGEMA support electronics, computer, TV monitor, and other supporting hardware. This system provides the capability of directly acquiring digital data for precise temperature measurement of any single, selectable pixel.

It is possible with this NCTM device to achieve a temperature resolution of 0.35°C under ideal conditions. It has been determined, however, that optical radiance measurement in the Dual Zone Chamber is far from ideal. This could substantially reduce the temperature measurement capability of this or any optical NCTM device.

1. SYNOPSIS

This report represents the completion of the NCTM Brassboard Development task performed under NASA contract NAS8-37592. The goal of this effort was to provide a temperature measurement system for the DPM Dual Zone Chamber in time to allow integration into the DPM for the USML-1 mission. This report provides closure to both the "Brassboard Development" and the "AGEMA Calibration and Evaluation" Statements of Work. The hardware which was designed, developed, tested, calibrated, and evaluated under these tasks will be described.

Effort began in October, 1989 with an analysis of the AGEMA 870 Thermal Imaging System, which was selected by JPL for this application. It was followed by a study to determine the feasibility of integrating this system into the DPM within the constraints of time, budget and physical system design compatibilities. Several primary design drivers surfaced in these studies:

- 1) No facilities would be available for in-flight data manipulation or storage. Therefore, all data required downlinking.
- 2) The Swedish designed AGEMA scanner head produces a video frame rate of 25 fps, unlike the NTSC standard 30 fps. This made video downlink impractical or impossible on the space shuttle telemetry system.
- 3) The AGEMA system was designed for large area scanning. No lenses were available to provide the required field of view (15mm X 15mm).

A conceptual plan was developed in this study which indicated a high success probability for completing this task within the constraints. It included the use of a Cassegrainian type lens designed by JPL and a technique for digitizing the video signal for downlink. System design began in January, 1990 and continued through the Requirements Definition Review (RDR) on March 30, 1990. Due to the accelerated development schedule, detailed design activities immediately followed the RDR.

This work continued on schedule until May 21, 1990, when notification of the Dual Zone Chamber deletion from USML-1 was received. Activities in this area were reduced to a minimum at that point pending further re-direction of effort.

At a review meeting at JPL on June 15, 1990 Intersonics' staff presented a project status report. In addition, recommendations for an enhanced capability system were presented. In July, JPL decided to continue with the original design scheme, but to relax the requirement for flight qualifiable hardware. The project was completed under this scenario.

This report will describe the hardware developed by ISI, including hardware developed for flight, ground support, and for testing purposes. It will discuss the tests and calibrations performed and assess the performance capabilities of the system.

2. SYSTEM DESCRIPTION

2.1 Agema Thermovision

The AGEMA Thermovision is a Swedish made Thermal Imaging system designed to monitor thermal radiation over a scanned area and calculate temperatures accordingly. In its simplest form the system operates with the model 870 Scanner Head, the model 800V Control Unit and a video monitor. The Scanner Head produces a differential video output at 25 fields/sec and separate horizontal and vertical sync signals. The 800V Control Unit scan converts this signal to provide compatibility with a standard video monitor for image display. It also displays intensity information in the form of intensity units (IU) which, in conjunction with AGEMA supplied calibration curves, can be used to derive temperature information.

Temperature calculation, as well as many other functions, can be accomplished by interfacing a computer to the 800V. In this configuration, the video information is digitized and sent to the computer along with other information supplied by the scanner head and 800V Control Unit. This is the most useful and versatile configuration. Specifications for the AGEMA system are included in Appendix A to indicate the capabilities of the "off the shelf" system.

2.2 NCTM System Description

Intersonics designed the NCTM Brassboard to provide compatibility with the JPL Drop Physics Module. To accomplish this, several design drivers and criteria were considered. They include:

- o Support electronics must be electrically and mechanically compatible with the DPM.
- o No on-board data processing (i.e. temperature calculation) is feasible.
- o No on-board data storage is available.
- o AGEMA's 25 frame/sec video is not compatible with shuttle video telemetry.
- o No lenses are available to provide the required 15mm X 15mm field of view.
- o Appropriate optics must fit within the mechanical constraints of the DPM.
- o Absolute measurement accuracy and resolution must approach AGEMA specifications.

The resulting design described in Figure 1 accommodates these items by utilizing the AGEMA scanner head with custom designed optics and electronics. It employs a Cassegrainian optics design, initiated by Antonio Puerta at JPL. This lens provides the required field of view and working distance but some reduction in light collection efficiency is concomitant.

Data handling is accomplished by digitizing the video signal at high speed and high resolution and preparing the data for downlink via the shuttle telemetry system. It can then be stored and processed by ground based facilities. Two DPM compatible printed wire assemblies (PWA) provide the entire flight support system. One board is designed for installation into the DPM Mechanical Assembly (MA) and the other interfaces with the Controller Assembly (CA). Both boards provide limited interface capability with the DPM controller.

For test and demonstration purposes, the system has been assembled into a stand-alone unit. For the same purposes, we developed an additional processing device to approximate the ground support equipment. This device accepts the serial digital data stream directly from the CA PWA, bypassing the downlink process in the absence of the shuttle telemetry system. It then processes the digital data to provide calibrated temperature measurement and to reconstruct the analog video signal. A detailed description of the completed hardware follows.

2.2.1 Objective Optics

The two-reflector, $f/7.9$ Cassegrainian objective lens was designed by Antonio Puerta (JPL) to image a field of practical dimensions at the required target distance. This system was chosen over a relay lens design because of its achromaticity, compact size, and minimal impact upon the DZC video optics. The reflectors (two sets) were fabricated by Tucson Optical Research Corporation. The mounts for these, the housing, and its interface to the AGEMA scanner head were designed and fabricated at Interionics. Figure 2 shows the overall optical layout of the NCTM portion of the DZC. Mechanical drawings of the objective lens housing are included in Figure 3 and Appendix B.

Figure 4 depicts the afocal imaging of on-axis and extreme off-axis target points by the objective and AGEMA macro optics. Incident light that is not blocked by the secondary reflector mounting is focused by the primary reflector to create a virtual object for the secondary. The secondary re-focuses the rays onto a curved focal plane. The AGEMA macro lens then collimates the rays, and delivers them through the exit pupil into the scanner head optics. All parts outside the head are fixed except for the secondary, which is mounted on a threaded shaft for focusing. Once a focus is achieved, a locking nut secures the secondary in place.

2.2.2 Mechanical Assembly (MA) Board Functions & Description

This board supplies power to the scanner, controls the thermo-electric (TE) cooler element attached to the detector, and buffers the video and sync signals for relay to the Controller Assembly (CA) PWA. It also provides

NCTM FUNCTIONAL BLOCK DIAGRAM

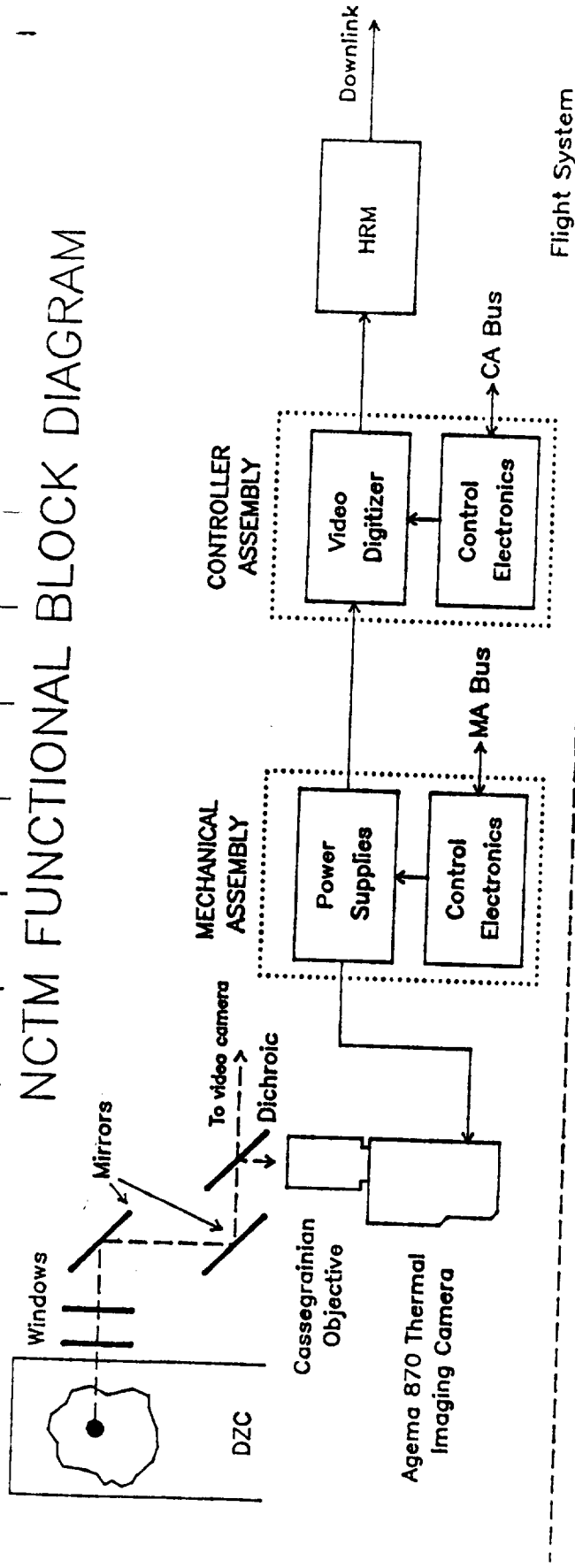


Figure 1

AGEMA/DZC TEST FACILITY

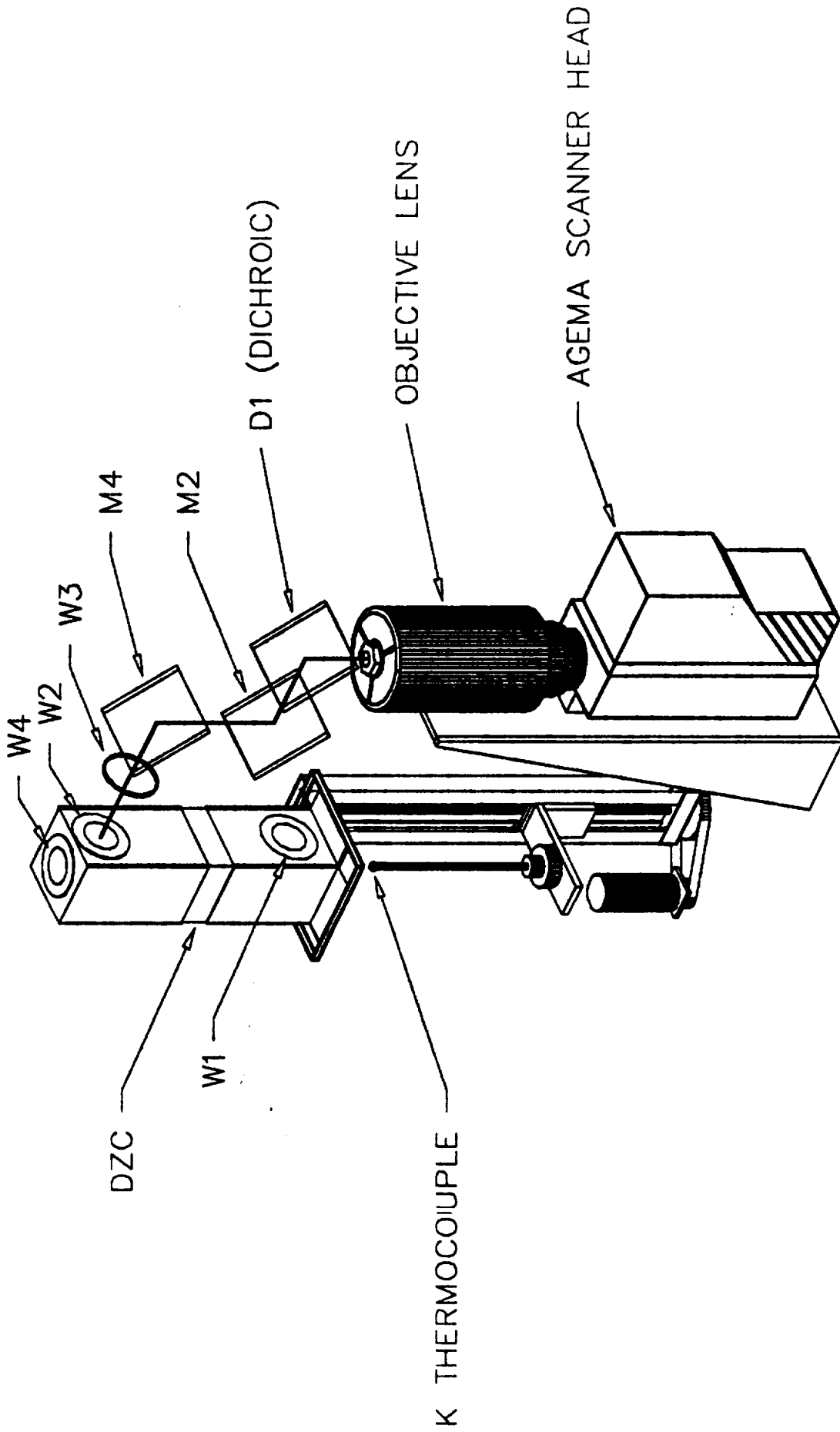


Figure 2

CASSEGRAINIAN OBJECTIVE LENS

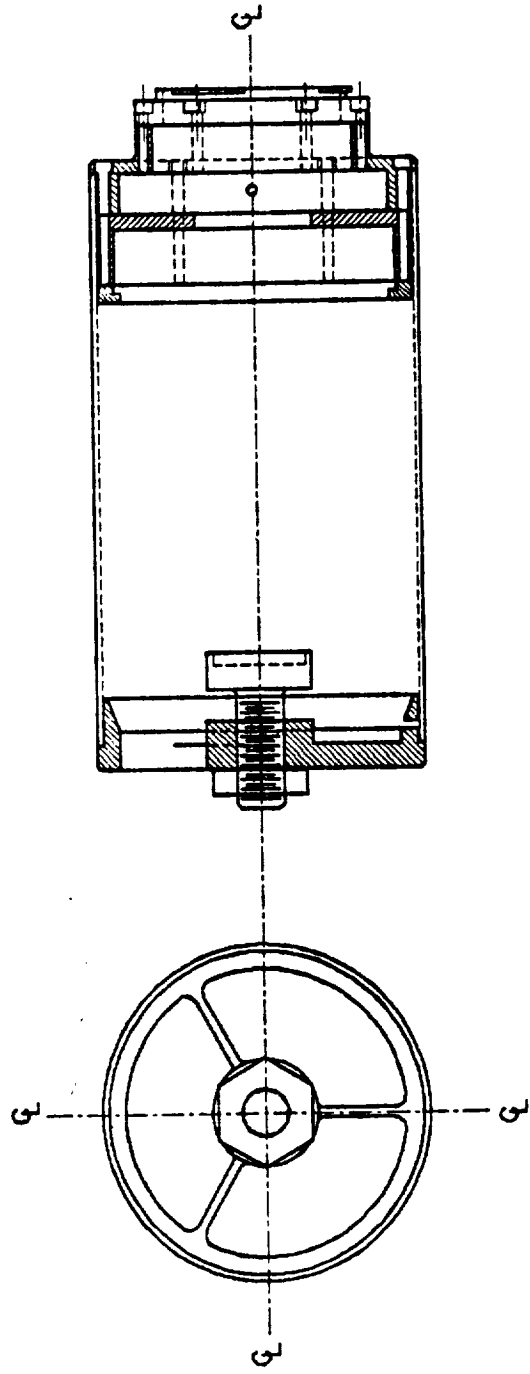


Figure 3

AFOCAL IMAGING OF ON-AXIS AND EXTREME OFF-AXIS TARGET POINTS

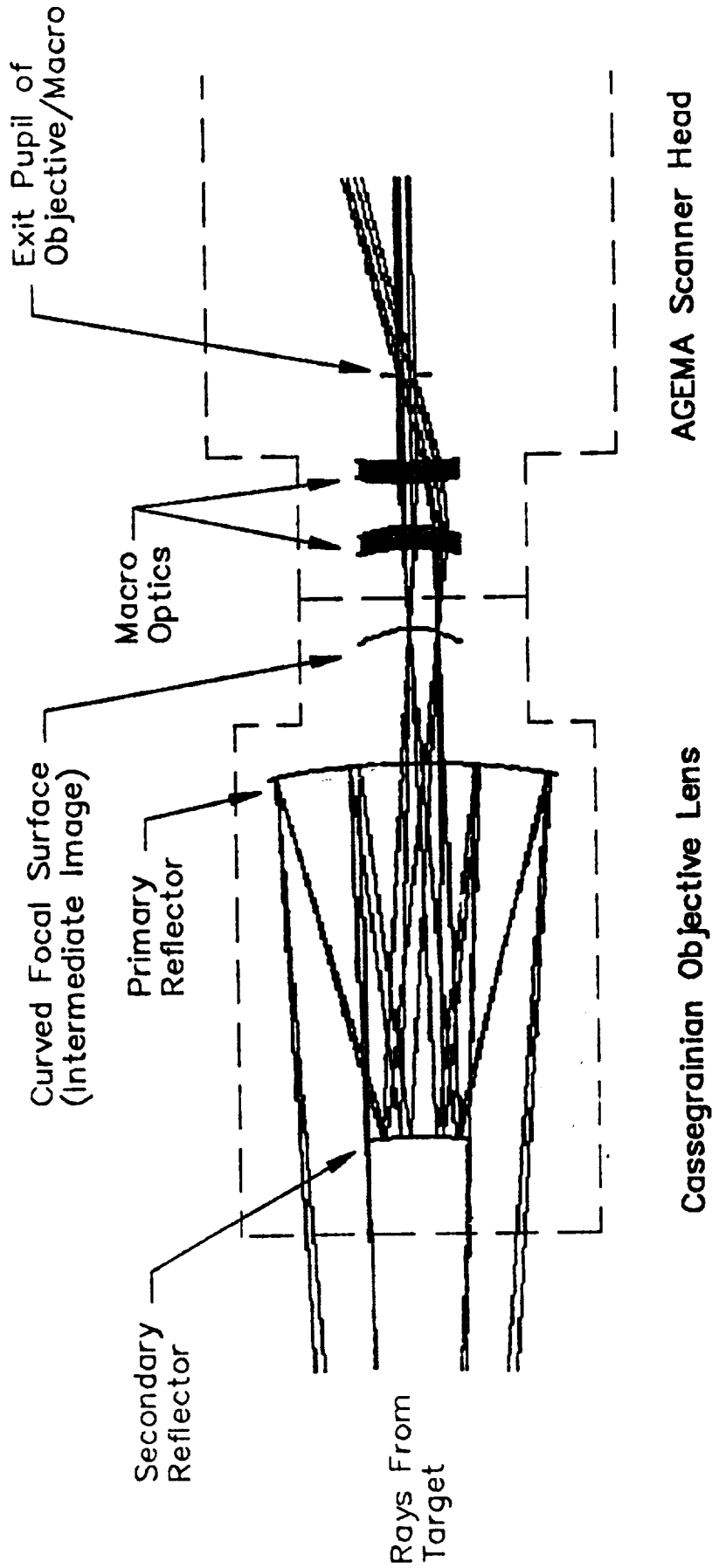


Figure 4

interface with and status information to the local governing controller. The MA PWA functions are shown in Figure 5. Figure 6 is a Functional Block Diagram of the MA PWA.

2.2.2.1 Power Supplies

The Agema scanner requires six power supply voltages which are supplied by the MA PWA. The MA PWA requires power from the DPM MA bus at $\pm 12V$ and $+5V$ to provide this power. The scanner requires two $+8V$ supplies, two $-8V$ supplies, (analog and digital circuits use separate supplies) one $+12V$ scanning motor supply, and a $+5V$ supply. The two $\pm 8V$ supplies are provided via four voltage regulators on the MA PWA. The input power for the regulators comes from the DPM $\pm 12V$ supplies available in the MA. The scanning motor and $+5V$ supplies are FET switch controlled extensions of the MA supplies.

2.2.2.2 Power Switching

The power for the scanner and circuitry devoted to scanner functions is controlled by opto-isolated FET switches in the $+12V$, $-12V$, and $+5V$ paths. The regulators which supply the $\pm 8V$ supplies to the scanner are powered by the switched $\pm 12V$. The scanner is turned on and off via commands written to the on board status/control register (see Sec. 2.2.2.6). The status of the FET switches is available on the bus when this register is read. When the command for power on is issued, three opto-isolators are turned on which in turn drive the FETs into their low impedance state. This allows current to flow to the scanner with negligible resistance. Conversely, power off command puts the FETs into their high impedance state, turning the scanner and associated circuitry off.

2.2.2.3 Scanning Motor Current Limit

The scanning motor normally draws about 2 amps at $+12V$ during start up. A circuit in the return leg of the motor supply circuit limits the current available to the scanning motor to about 1 amp during start up. After the motor's start up period the motor current drops to its steady state level of 0.63 amps and the motor speed control regulates the motor voltage.

2.2.2.4 TE Cooler Control

The TE cooler attached to the detector in the Agema scanner uses power from the $+5V$ source. Adjustment of the current into the TE cooler (and therefore its temperature) is achieved by comparing a temperature related signal from the detector (TE CTRL) to the time integral of the current through the cooler. This continuous adjustment maintains proper detector temperature. This circuit is based on the circuit used in the Agema 800V controller.

PWA FUNCTIONS

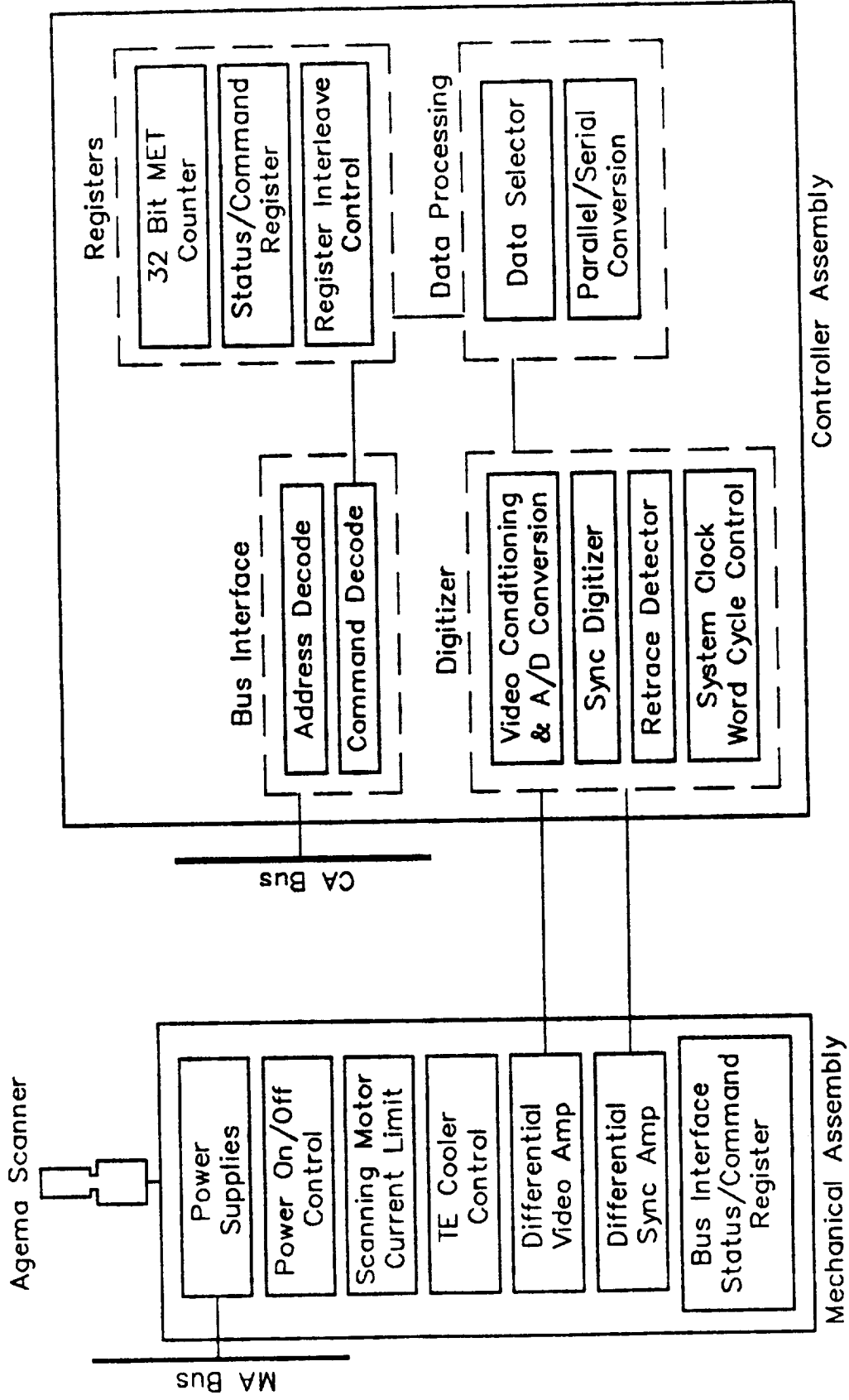


Figure 5

MECHANICAL ASSEMBLY PWA BLOCK DIAGRAM

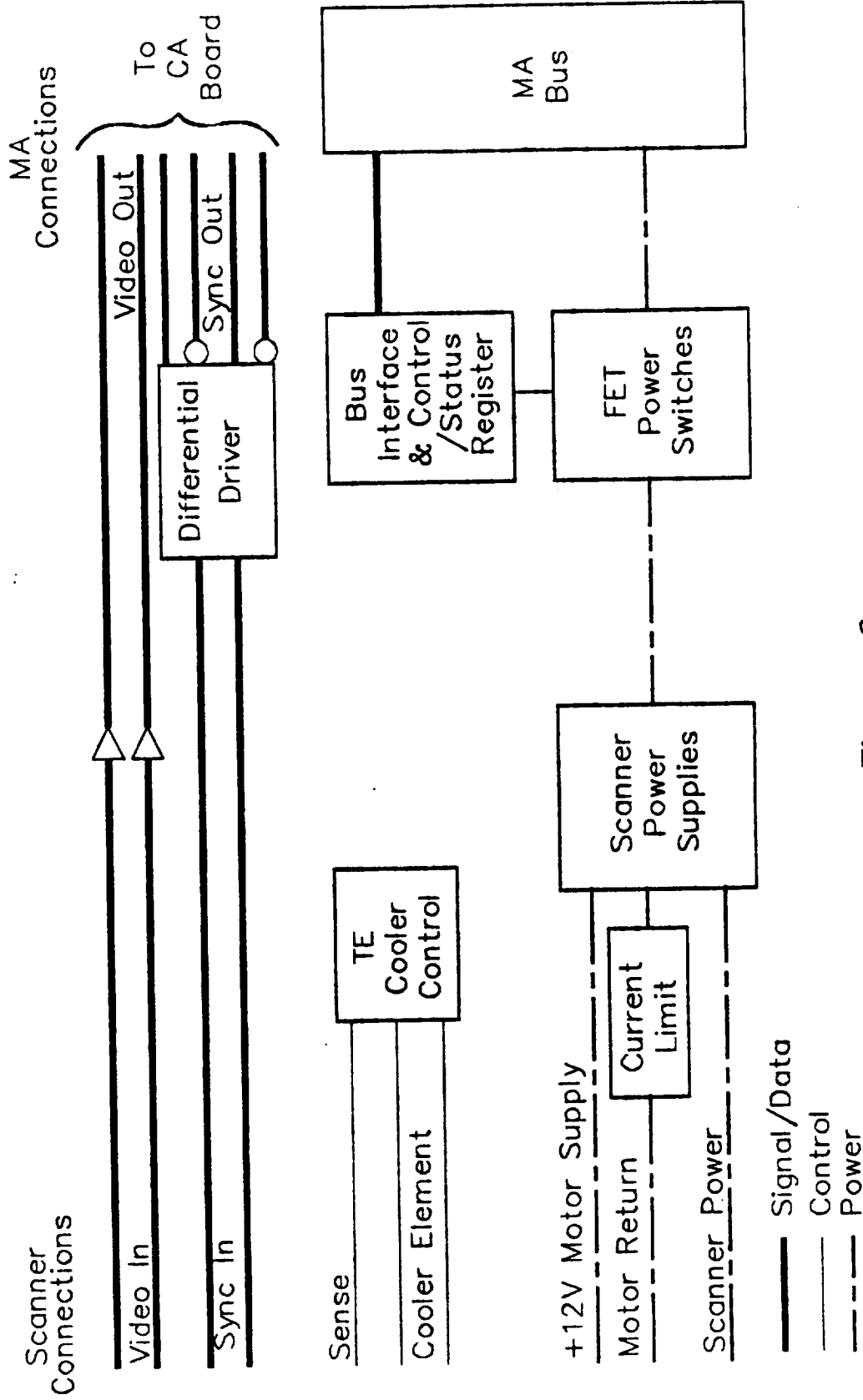


Figure 6

2.2.2.5 Video and Sync Relay Buffers

The differential video from the scanner is routed to the CA PWA via two inverting unity gain amps. The sync signals H-TRIG and V-TRIG are converted to differential for relay to the CA PWA. This is to improve noise immunity and to maintain ground isolation between the Mechanical and Controller Assemblies.

2.2.2.6 Bus Interface/Registers

The interface circuitry on the MA PWA follows the specification for the MA system bus. Although the capability of supporting four commands exists, only two are currently defined: power on and power off. The two least significant bits (bit 0 and bit 1) of the data bus are devoted to command functions. The remaining 6 bits are used for data. Commands are issued by placing the desired bit pattern on bits 0 and 1 of the system bus and writing to the status register (register 00 as addressed by the bus signals RSO* AND RS1*) on the MA board. The command bit patterns are listed below.

bit 1	bit 0	Command
0	0	Power off
0	1	Power on

The remaining 6 bits of the status register are devoted to supplying status information to the system upon request. The bits and their meanings are shown below.

bit	Meaning
2	V-TRIG status.
3	H-TRIG status.
4	Switched +12V supply status.
5	Switched +5V supply status.
6	Switched -12V supply status.
7	-- Undefined --

In each case above, a 1 (logic high) represents the nominal condition on the MA PWA. Since the bus transceiver is an inverting device, a 0 (logic low) corresponds to nominal as read by the MA system. This information is put on the bus when the MA board register is read. In addition, the two command bits are placed into bits 0 and 1 for a read-back of the last command issued.

The determination of the MA board status discussed above is made with two types of circuits. The status of the video sync signals is determined by timer circuits which are re-triggered by every pulse of the signal in question. If the signal is interrupted, the circuit will time-out

indicating an error condition. The indicators for the switched power supplies compare the output voltage of the power FETs to un-switched reference voltages to produce a TTL level indicating the current state of the switched power.

2.2.3 Controller Assembly (CA) PWA Functions & Description

The functions of the CA PWA, shown in Figure 5, revolve around formation of a sequence of 16 bit digital words that represent the video output of the scanner. In addition to this basic process, the board performs the interleaving of system time and other data into the digital output and supports interface with the CA bus. Figure 7 is a Functional Block Diagram of the CA PWA.

2.2.3.1 Video Conditioning Circuitry

This circuit transforms the differential video received by the CA PWA into a format appropriate for A/D conversion. It consists of a differential amp, a gain stage, and a 4 pole anti-aliasing filter. The output of these stages is a single ended version of the Agema video output amplified by a factor of 1.42 V/V to take full advantage of the resolution of the A/D converter.

2.2.3.2 Video & Sync Digitization

The conditioned video is converted to 12 bit digital by a Datel ADS-112 A/D converter at a rate of 228 kHz. The sync signals, H-trig and V-trig (already TTL compatible), are simply latched by the same clock that initiates A/D conversion of the video signal. The digitized sync signals are then placed in bits C and D of the output word respectively. Bit E is a flag bit that indicates whether the word is video or interleaved data and Bit F is unassigned. The interleaved data is discussed in Sec. 2.2.3.4.

The table in Figure 8 indicates the bit assignments in the 16 bit output words. The left column indicates the format for video information and the right is for interleaved data. The digital video is placed into the 12 least significant bits of the output word (bits 0 - B).

Digitization of the video and sync is asynchronous with respect to the Agema signals.

2.2.3.3 Controller Assembly Bus Interface

The interface circuitry to the address and data busses is compatible with the Multibus I standard used in the Controller Assembly. Only the lower 8 bits of the data bus are supported on the CA PWA. The address space reserved for NCTM is 200_H - 21F_H. Since this represents many more

CONTROLLER ASSEMBLY PWA BLOCK DIAGRAM

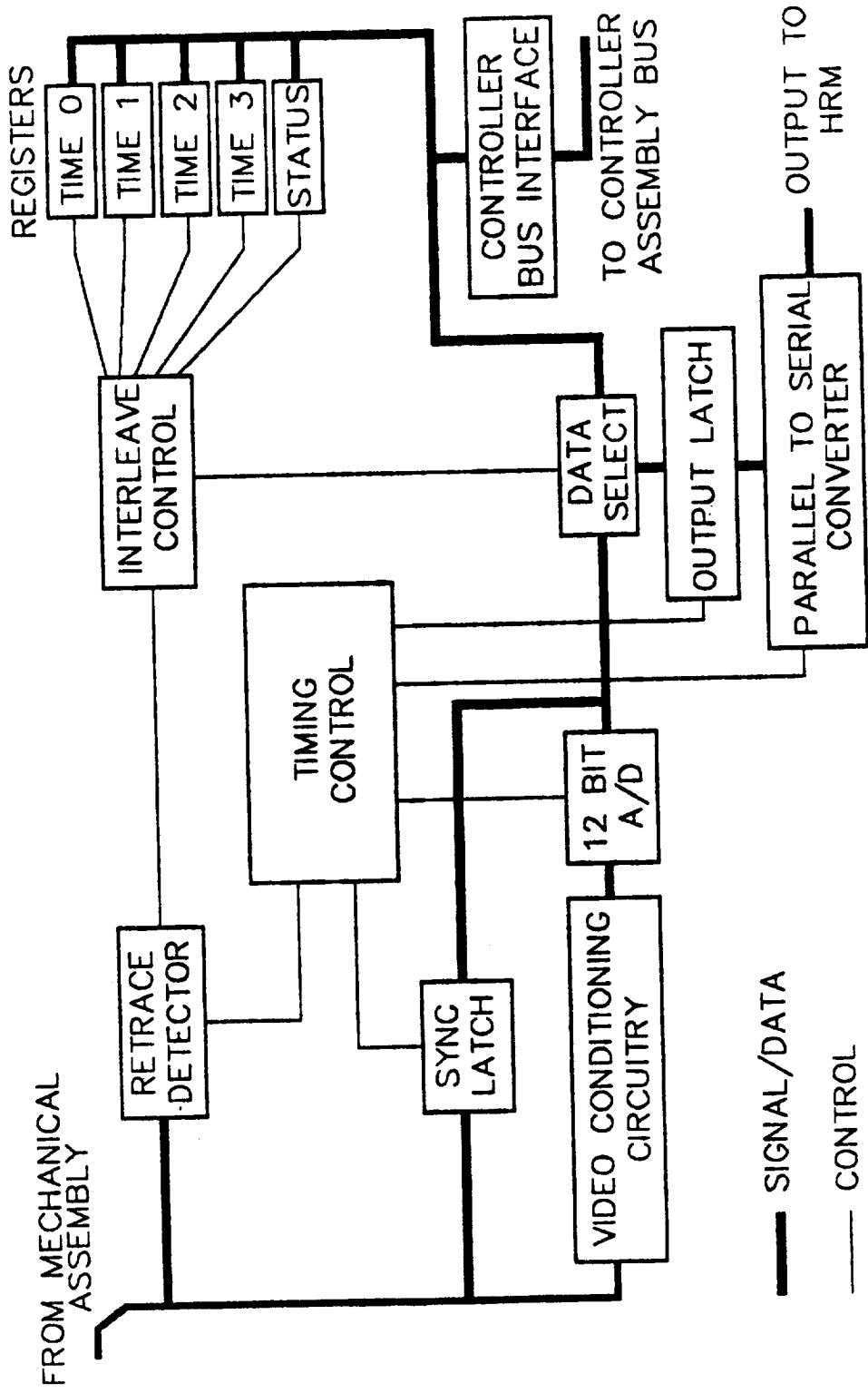


Figure 7

OUTPUT WORD BIT ASSIGNMENT

bit	Video Word	Data Word
0	Video LSB	Data LSB
1	Video	Data
2	Video	Data
3	Video	Data
4	Video	Data
5	Video	Data
6	Video	Data
7	Video	Data MSB
8	Video	ID code LSB
9	Video	ID code
A	Video	ID code MSB
B	Video MSB	-- Unused --
C	H-TRIG	H-TRIG
D	V-TRIG	V-TRIG
E	Flag (0 = Video)	Flag (1 = Data)
F	-- Unused --	-- Unused --

Figure 8

commands than are needed, the current design recognizes addresses 200_H - 20F_H and supports commands at addresses 200_H - 205_H as described below:

I/O Address	Access	Function
200 _H	(R&W)	System time register, bits 0-7.
201 _H	(R&W)	System time register, bits 8-15.
202 _H	(R&W)	System time register, bits 16-23.
203 _H	(R&W)	System time register, bits 24-31.
204 _H	(W)	Increment system time register command.
205 _H	(R&W)	Control/status register.
206 _H - 21F _H	Reserved	Currently unused

External access to the CA PWA is inhibited when on-board bus access is under way.

2.2.3.4 Interleave Control

To affect interleave of the system time and status information into the data stream, an output data selector is employed to choose either the digitized video information or the on board data storage. Figure 9 is a timing diagram which shows this event sequence. Circuitry is included on the CA PWA which detects when the scanner is in a vertical retrace period and announces this by driving RTC high on the next rising edge of WCLK. This switches the output data selector to route data rather than the video to the output latch. The signal LATCH* then loads the selected word into the output latch. The remaining time and status registers are placed one at a time into the output stream until all have been included. The interleave controller then resets the output data selector to route video to the output latch.

The system time and status registers are placed one at a time into bits 0-7 of the output word, as shown in Figure 8. Bits 8 - F are then available for other tasks. It is convenient to dedicate bits C and D to the signals H-TRIG and V-TRIG respectively regardless of whether data or video is being output. This maintains proper video sync with minimal complication. It is also useful to insert the 3 signals DSELO - DSEL2 into bits 8 - A respectively to identify each byte of data. These ID codes are shown below.

Code	Byte
000	Time LSB
001	Time 2SB
010	Time 3SB
011	Time MSB
100	Status register

Interleave activity inhibits external access to the data bus on the CA PWA.

2.2.3.5 Timing Control & P/S Conversion

This circuitry controls all the internal activity of the CA PWA. It is conceptually comprised of a crystal oscillator master clock, a synchronous 6 bit counter, and a binary decoder. The master clock drives the counter at 8.192 MHz. The counter outputs drive the binary decoder which produces control pulses that trigger the actions that make up a word cycle. The word cycle timing diagram is shown in Figure 10.

The word cycle begins with the high going pulse WCLK. This pulse triggers the A/D converter and the sync latch to produce a video word. The next pulse that occurs is LATCH* which loads the current output word (subject to the interleave controller) into the output latch.

The next action is to load the output latch into the shift register in preparation for serial output. The pulse S/L triggers this step.

The final control action is a pulse that enables the serial output stage. This automatic re-enabling of the serial output is intended as part of a word sync protocol between the CA PWA and the HRM. The other part of the protocol is provided by the HRM and consists of a pulse input to the CA PWA that disables the serial output. This disabling pulse must occur after the HRM latches the 16th bit of an output word and before the re-enabling pulse produced by the CA PWA controller. This pulse needn't occur after every output word but the more frequently it occurs, the less likely a word sync error is to persist.

Concurrent with the generation of each video word is the serial output of the previously produced word. The least significant output bit of the counter is used to generate BITCLK, a gated 4.096 MHz square wave which is the clock for this process. The BITCLK waveform consists of groups of 16 pulses separated by 600 ns. The CA PWA puts each bit of the output word (MSB first) on the serial data output line in time for the next rising edge of BITCLK to latch it into the HRM.

2.2.4 Ground Support Equipment (GSE) Functions & Description

The GSE prototype for the Agema NCTM system decodes the encoding that is performed by the CA PWA and reconstructs the analog differential video and sync signals for relay to the 800V. It also provides a "Pixel Grabber" feature which enables a single pixel to be selected from the incoming data stream and routed to a computer for processing and temperature read out. Calibrated temperature measurement is provided by this device from the digital data before it is converted back to analog format. A Functional Block Diagram of the Data Decoder and Pixel Grabber is shown in Figure 11.

INTERLEAVE TIMING DIAGRAM

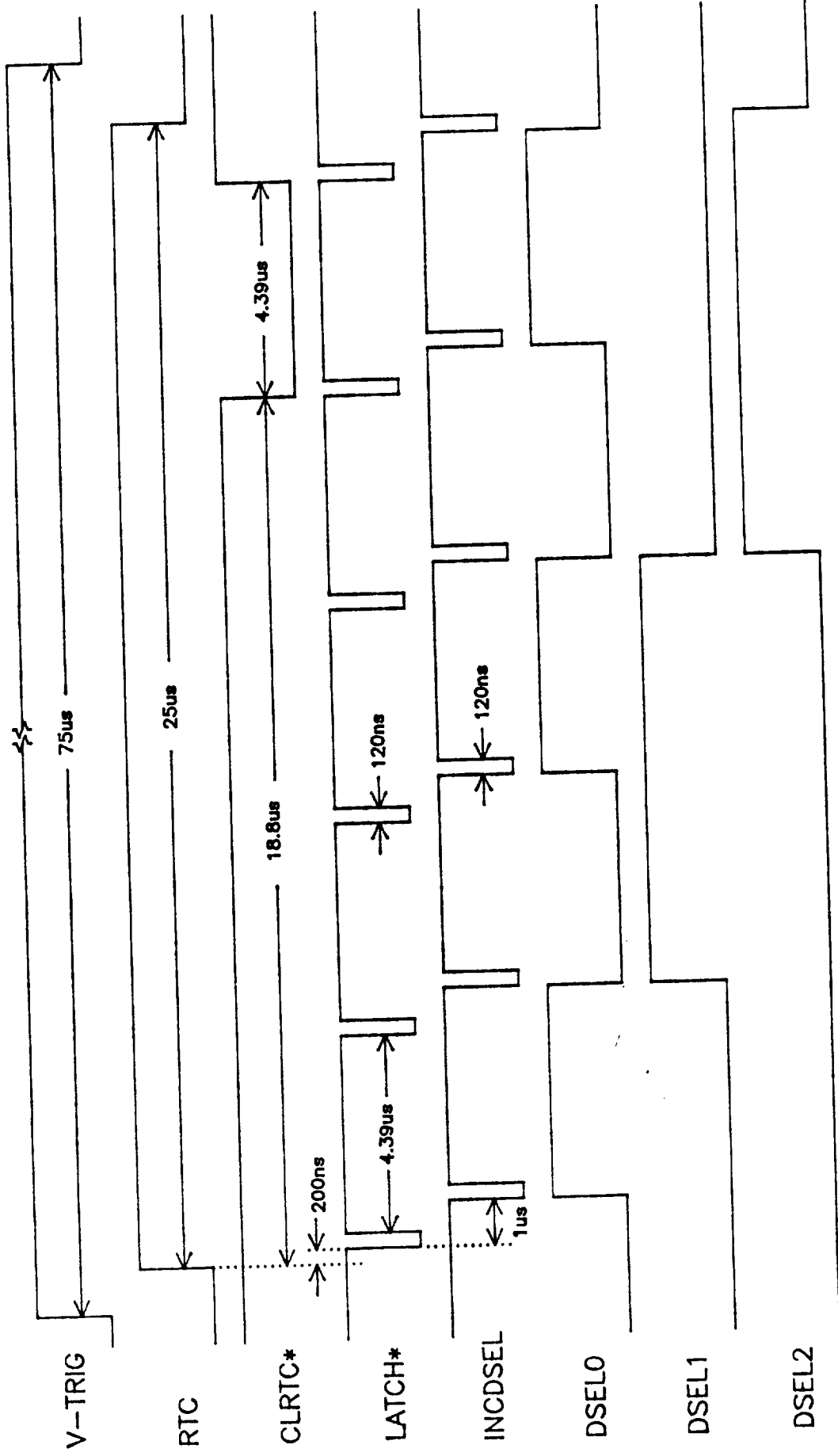


Figure 9

WORD CYCLE TIMING DIAGRAM

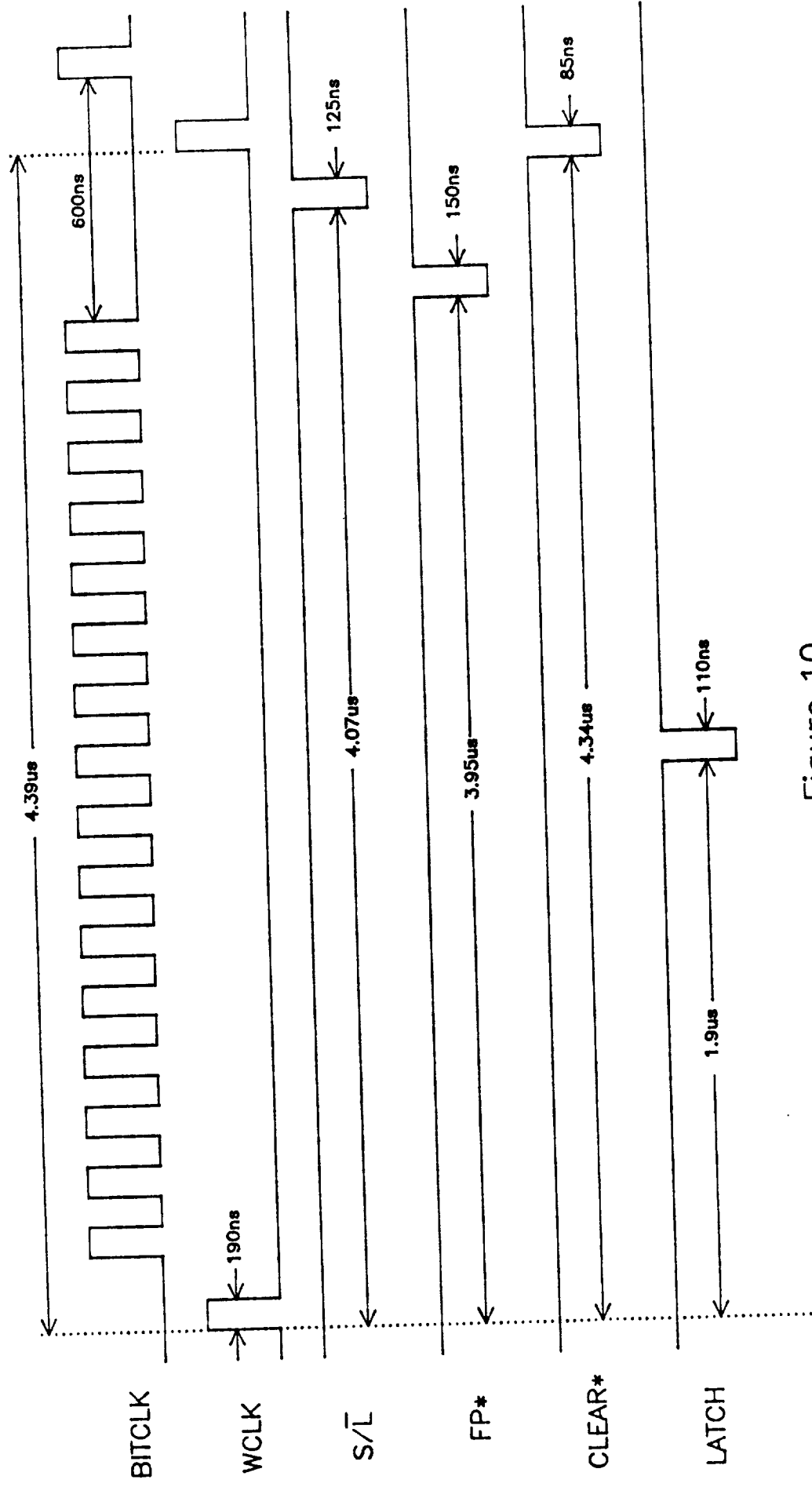


Figure 10

GSE FUNCTIONAL DIAGRAM

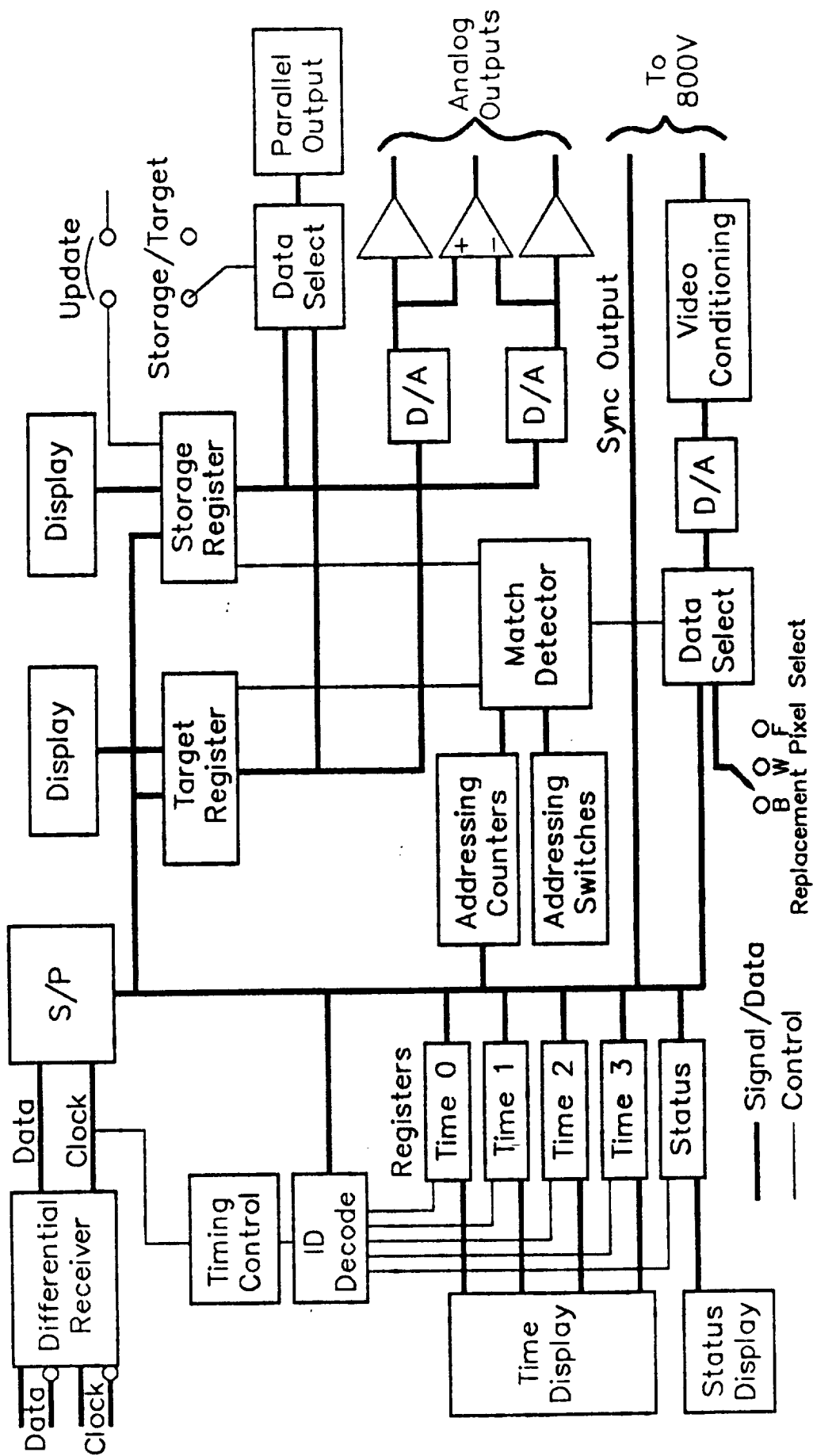


Figure 11

2.2.4.1 S/P Conversion & Word Sync

This circuitry receives the serial data and clock signals from the CA PWA and converts them back to 16 bit words. It also produces a pulse after every 16th bit in compliance with the word sync protocol discussed in Sec. 2.2.3.5.

2.2.4.2 Registers/Register Control

When bit E of the received word (the data/video flag bit) is high, indicating that a received word is data rather than video, the word is parsed as follows: bits 8-A are decoded to identify the incoming data and address the register in which the low byte of the word (the actual data) belongs. This enables the register and a subsequent signal loads the data into the register. The contents of the time and status registers are displayed in hexadecimal in seven-segment displays on the face of the GSE prototype.

2.2.4.3 Video Reconstruction

The video words of the digital input are separated into the 12 bit video code and the two sync bits, the latter of which are already in an acceptable format for the 800V controller. The video information is routed to a D/A converter to reproduce the single-ended video signal. It is then passed through an anti-imaging filter and gain stage to undo the amplification of the video conditioning circuitry on the CA PWA. Finally the video signal is converted to differential and the reconstructed video and sync signals are routed to the 800V controller for display.

2.2.4.4 Pixel Addressing (Pixel Grabber)

By counting scan lines and pixels relative to a reference, recognition and readout of any pixel in the image is achieved. In order to affect the addressing of individual pixels in the video signal, field, scan line, and pixel counters are employed. The field counter is implemented as a 2-bit counter to specify the four distinct fields (0 through 3) and can be disabled so the specified pixel in all fields is recognized. The scan line counter is incremented by the H-TRIG signal to provide an address for each scan line. This counter is cleared with the V-TRIG signal resetting it at the beginning of each field. Similarly, the pixel counter is incremented by the WCLK signal and reset by the H-TRIG signal to maintain pixel addresses.

When a specified address matches the field, scan line, and pixel specified, the signal HIT is driven high to indicate that the target pixel is now available and the data is stored in the target register.

To provide a visual reference for the location of the target pixel, the Pixel Grabber replaces it in the output to the 800V with one of three switch selectable images. Steady white and black replacement pixels are available, as is a black/white flashing pixel.

2.2.4.5 Target Pixel Processing

When HIT goes high, indicating the target pixel is now present at the output of the S/P converter, the digitally encoded video level is latched into the 12 bit target register. This register is updated every time HIT goes high providing continuous readout of the video level at the point of interest. A duplicate register exists which is updated only when HIT is high and an external button is pressed. This storage register provides a way to freeze the readout for greater ease in manual measurement.

The contents of both the target and storage registers are converted to analog and are output from the Pixel Grabber. To aid in comparisons over time or between pixels, the difference of these two analog signals is also available. In addition to these analog outputs, a parallel output is provided on a standard 37 pin D type connector. A switch is provided to select either the target or storage register as the source for this output.

2.2.5 Dual Zone Chamber (DZC) Mock-Up Description

A DZC mock-up test facility was built by Intersonics, Inc. for testing purposes. The configuration of key elements of the mock-up is shown in Figure 2. The heart of this system is a 2.75" X 2.75" X 10" Inconel chamber provided by JPL/Loral. Sapphire viewing windows are located in the cold zone (W1), hot zone (W2), and chamber top (W4). The upper (hot) zone of the chamber is heated with four 500W resistive elements, which are held against the outside of the chamber by fibrous ceramic insulating boards. A temperature of 900°C can be attained in the hot zone. Precise closed-loop temperature control is achieved using a calibrated "K" type thermocouple and a solid-state temperature controller, which regulates the current to the heating elements. The thermocouple is mounted on a motor-controlled translator such that it may be embedded into spherical test samples and placed anywhere within the hot zone field of view. This thermocouple was calibrated in our blackbody reference source (See Appendix C).

An aluminum support structure for the chamber also supports the intermediate elements in the DZC optical train, which consists of a second sapphire window (W3), two front-surface aluminum mirrors (M4 & M2), and a dichroic beam-splitter (D1). Finally, the structure supports the mounting hardware for the AGEMA scanner and objective lens. The clear apertures and locations of all optical elements are as per JPL drawings #10134325, the limiting aperture being the Cassegrainian objective. The support structure may also accommodate beam heating through the top window.

3. SYSTEM TESTING AND CALIBRATION

3.1 Tests and Facilities

Testing and calibration was performed to verify the performance of this equipment. Since the requirement for flight ready hardware was relaxed, the testing associated with flight qualification was waived. The tests performed focussed primarily on the ability of the system to measure temperature accurately and determine the feasibility of using this technique for its intended purpose. A list of some of the key facilities utilized is included in Appendix C.

This section will discuss the test and calibration procedures employed and results obtained. The information and data presented in this section will be discussed further in Section 4.

3.1.1 Test and Calibration List

The following is a list of tests and calibrations performed on this device.

1. Baseline Blackbody calibration.
2. Temperature resolution.
3. System calibration with the Dual Zone Chamber.
4. Sweet spot detection.
5. Measurement sensitivity to target location.
6. Optical parameters.
7. Hot sapphire window emissions
8. Electrical characteristics.

3.2 Test Descriptions and Results

3.2.1 Baseline Blackbody Calibration

The NCTM head assembly was mounted on a tripod and focused onto the orifice of the M300 blackbody furnace. Using the Pixel Grabber and thermal image monitor, two image locations were chosen to measure the 12 bit digital video signal (voltage). These points are located at the pixel/line addresses of 49/62 (center of field), and 49/36 (top center of field). The signals at these locations are the extremes of the apparent radiance range produced by the head assembly optics over an iso-radiance target (see Section 3.2.5). Each "measurement" is actually the arithmetic mean of 5 measured values. Data points for filter position 0 (no filter) were recorded between 425K and 775K in 25K increments. Measurements for filter position 1 (3.7 to 4.0 micron) were recorded between 800K and 1375K in 25K increments. The digital numbers corresponding to these data points were then converted to voltages based on a full scale of 10 VDC at FFF_H .

From these voltage vs. temperature data, polynomial expressions were fit for both filter settings. The calibration curves for the center pixel, along

with their corresponding 2nd order polynomial expressions are shown in Figures 12 and 13. These figures also show the actual data points recorded and the error included in the polynomial fit to this data.

In addition to this calibration the R, B and F constants were approximated for entry into the AGEMA TIC 8000 computer. This enables temperature data to be calculated and displayed on the video monitor. This is a convenient, real-time approximation of temperature and is not for precision measurements.

3.2.2 Temperature Resolution

Several tests were performed to determine the temperature resolution of this system.

3.2.2.1 Electrical Noise

A 1.5 VDC battery source was input to the Mechanical Assembly board in place of the video signal. A large number of digital data points (>450) were recorded and the distribution of data was plotted. Analysis of this data indicates an approximate electrical noise equivalent of 2.2 mV RMS.

3.2.2.2 Dark System Noise

This test was performed with all systems powered and operational but with a lens cap covering the optics to prevent light from entering the scanner head. This is essentially a room temperature measurement performed with no filter in place. The resultant data distribution analysis indicates the system dark noise is 2.6 mV RMS

3.2.2.3 Temperature Measurement Uncertainty

In these tests the scanner head viewed the Mikron Blackbody source and the DZC. The blackbody temperature was held constant at 800K and 1350K and a large number of data points (>450) were obtained for each setting. These tests were repeated at 800K and 1117K with a .25" diameter oxidized Monel sample located in the DZC. The data was taken at the sweet spot of this sample under equilibrium conditions.

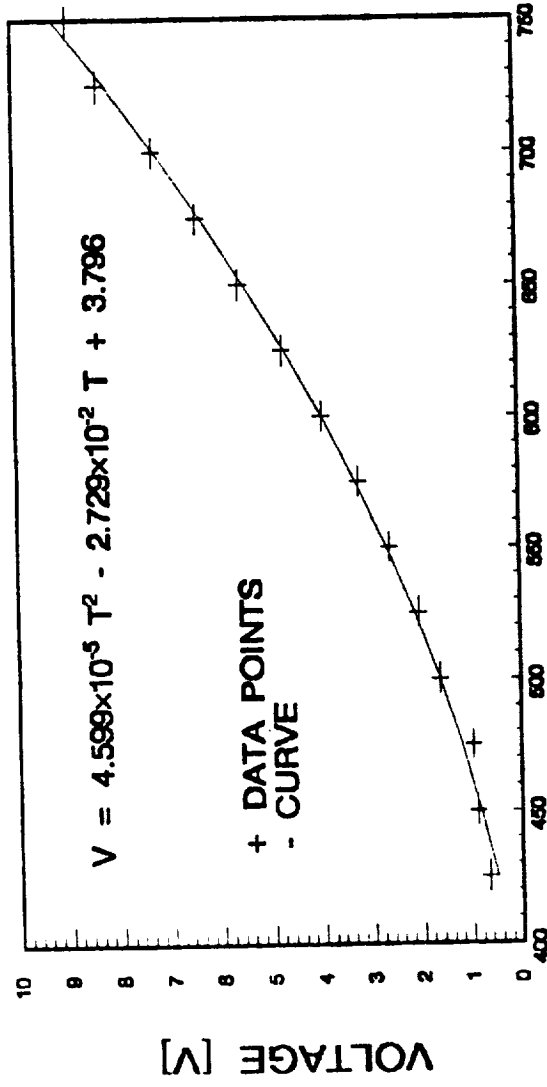
Data distribution plots for these are shown in Figures 14 and 15. Beam heating was not used in these tests. Therefore the maximum temperature in the DZC was limited to <1150K.

3.2.3 System Calibration with the Dual Zone Chamber

The NCTM head assembly was mounted in a position such that all of the NCTM optical components in the DZC mock-up assembly were included in the optical path. A .25" diameter Monel specimen with a 1mm diameter blackbody hole was installed on the calibrated "K" thermocouple and was placed in the specimen position in the DZC mock-up. In this way the thermocouple was still utilized for temperature measurement and the blackbody hole was near the center pixel where the calibration took place. Eleven digital readings were

POLYNOMIAL APPROXIMATION OF V(T)

Black Body Target No Filter



TEMPERATURE [K]

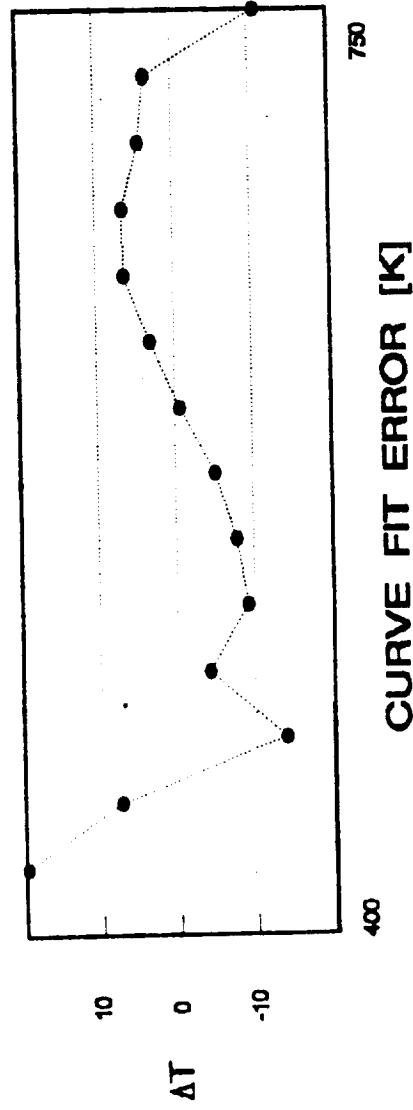
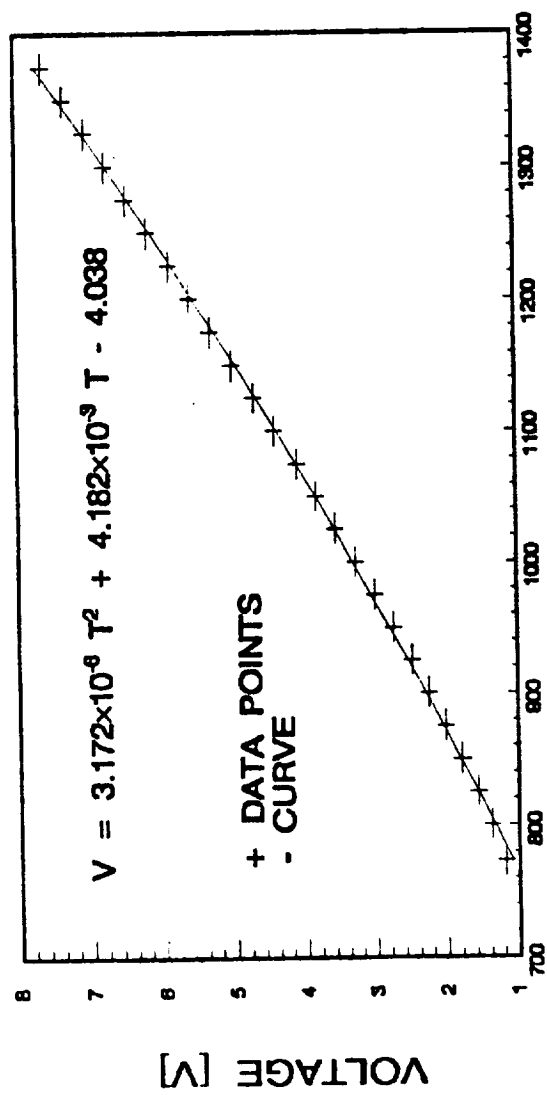


Figure 12

POLYNOMIAL APPROXIMATION OF V(T)

Black Body Target 3.7-4 μm Filter



Recorded Data

Temperature	Voltage
773	1.189
800	1.387
825	1.572
850	1.794
875	2.012
900	2.246
925	2.485
950	2.742
975	3.003
1000	3.281
1025	3.569
1050	3.845
1075	4.102
1100	4.424
1125	4.712
1150	5.015
1175	5.310
1200	5.603
1225	5.884
1250	6.196
1275	6.489
1300	6.772
1325	7.046
1350	7.339
1375	7.634

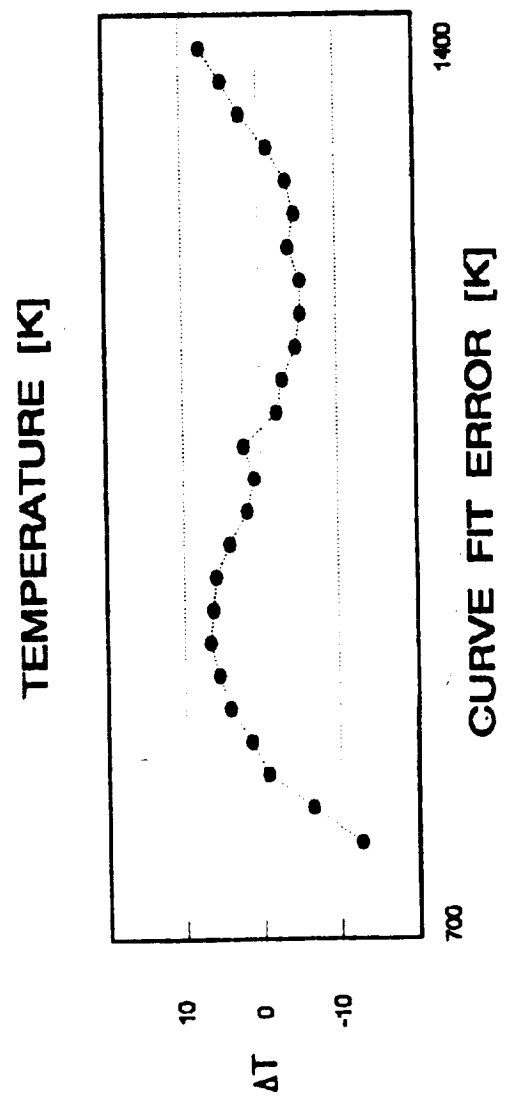
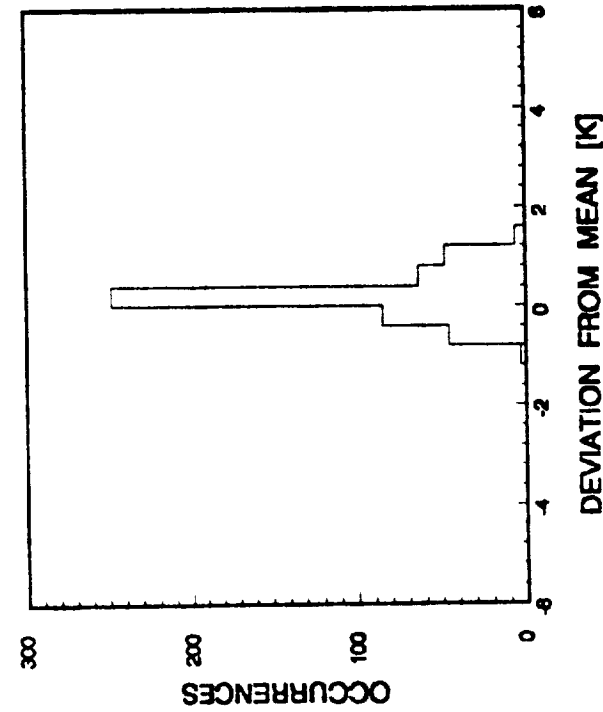


Figure 13

TEMPERATURE MEASUREMENT STATISTICS

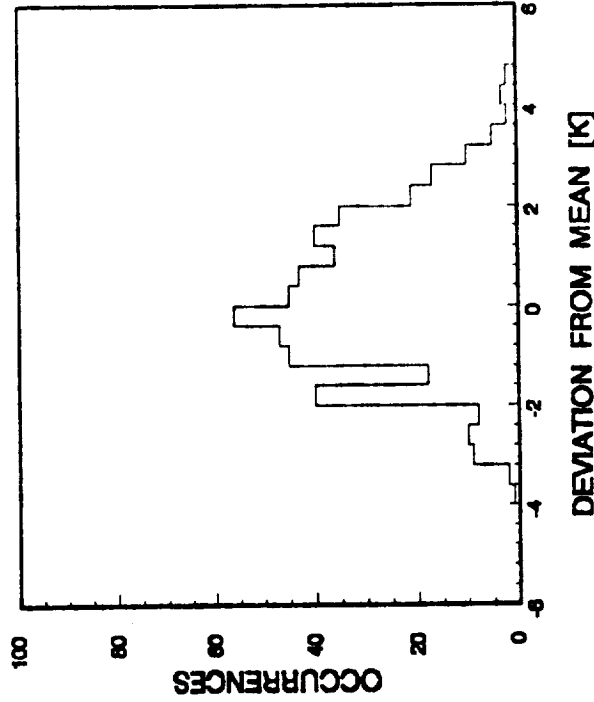
Readings of Mikron M300 Black Body



500 Data Points

Target Temperature: 800K

Standard Deviation: .41



495 Data Points

Target Temperature: 1350K

Standard Deviation: 1.5

Figure 14

TEMPERATURE MEASUREMENT STATISTICS

Measurements of Sweet Spot Temperature in the DZC

Sample: .25" Monel

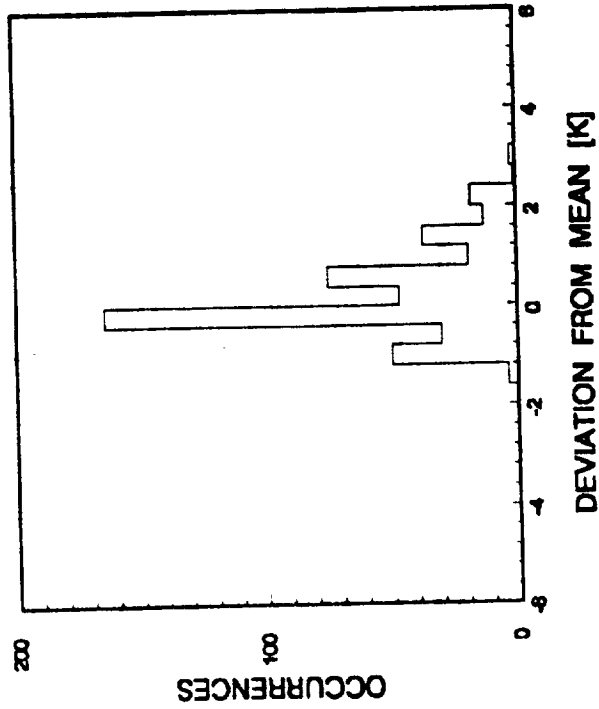


Figure 15(a)

461 Data Points

Sample Temperature: 800K

Standard Deviation: .83

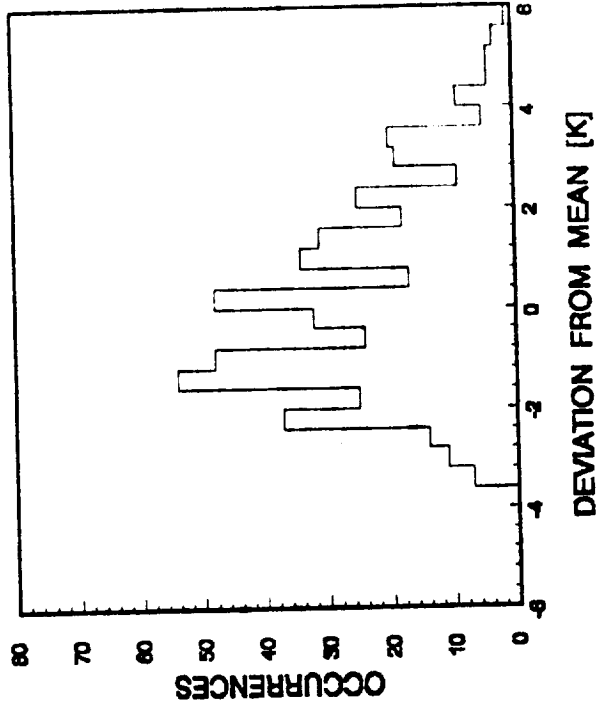


Figure 15(b)

500 Data Points

Sample Temperature: 1117K

Standard Deviation: 2.0

Figure 15

taken under equilibrium conditions between 471K and 767K for filter position 0, and 16 readings between 741K and 1150K for filter position 1. The calibration data curves, 2nd order polynomial functions, and recorded data for the two filter settings are shown in Figures 16 and 17.

3.2.4 Sweet Spot Detection

The sweet spot, as it is referred to in this report, is that spot on a specular sphere where no light emanating from the chamber walls will be reflected into the camera lens. It is the only spot which, in principle, is emitting light uncontaminated by reflections from other hot sources.

In these tests, a spherical target was placed onto the calibrated thermocouple bead, and was inserted into the specimen position in the hot zone of the DZC. Once equilibrium was reached, the thermal image was stored, and the horizontal scan line passing through the center of the sphere was located by the Pixel Grabber. The voltage level across this line was measured by the storage oscilloscope and was stored for analysis. This measurement was performed at 800K and 1100K for .125" and .250" diameter oxidized Monel spheres. The emissivity of these samples is estimated to be between .5 and .7. For a .25" diameter specimen in this configuration the sweet spot is calculated to be ~ .87mm diameter.

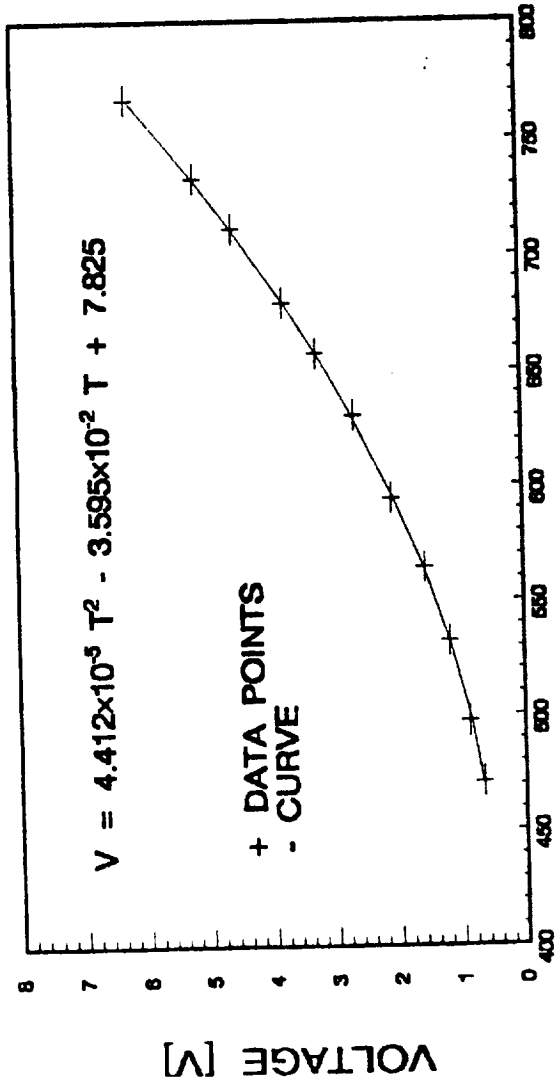
Figure 18 shows the thermal image of the .25" diameter Monel sphere and a horizontal scan line passing through the sweet spot. As the scan line passes through the narcissus region, the detected radiation is reduced. This is due to the fact that light radiated from this area includes less wall reflections and is therefore more dependent on the specimen emissivity. In the center of this region is the actual sweet spot. From the aforementioned calculation, the sweet spot diameter for this sample is .87mm. Since this constitutes more than three pixels with this system, sweet spot detection should be well within its capabilities. While Figure 18 demonstrates the ability to locate the sweet spot, the actual size and purity of it cannot be clearly defined due to the fact that this is not a specular surface.

3.2.5 Measurement Sensitivity to Target Location

Figure 19 is the thermal image of the DZC hot zone at 800K, upon which are superimposed a vertical and a horizontal line. A false gradient can be seen (primarily along the vertical axis) in the image of what is an iso-radiant target. Using the Pixel Grabber, the average A/D signal levels were recorded at 12 locations across the horizontal line, and at 15 locations along the vertical line. The plots in the figure indicate the approximate temperature deviations that can be expected from the center pixel, where all of the calibrations were performed.

POLYNOMIAL APPROXIMATION OF V(T)

Black Body Specimen in DZC
All Optics No Filter



Recorded Data

Temperature	Voltage
471	0.661
497	0.880
532	1.186
564	1.561
594	2.079
630	2.658
657	3.256
679	3.775
711	4.552
733	5.154
767	6.229

TEMPERATURE [K]

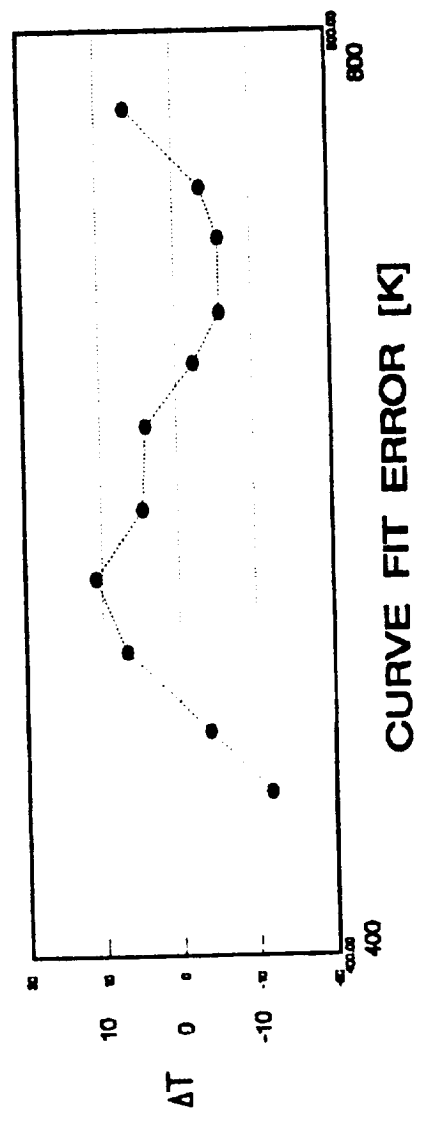


Figure 16

POLYNOMIAL APPROXIMATION OF V(T)

Black Body Specimen in DZC
All Optics 3.7 - 4 μm Filter

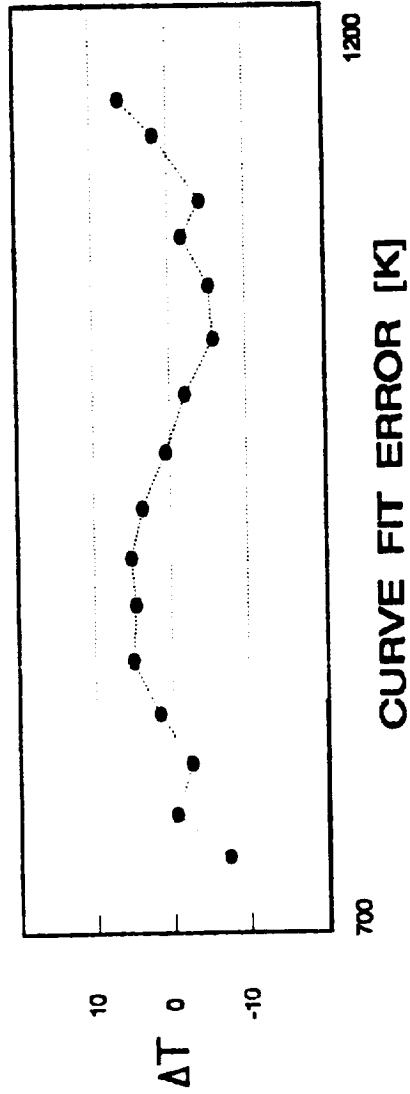
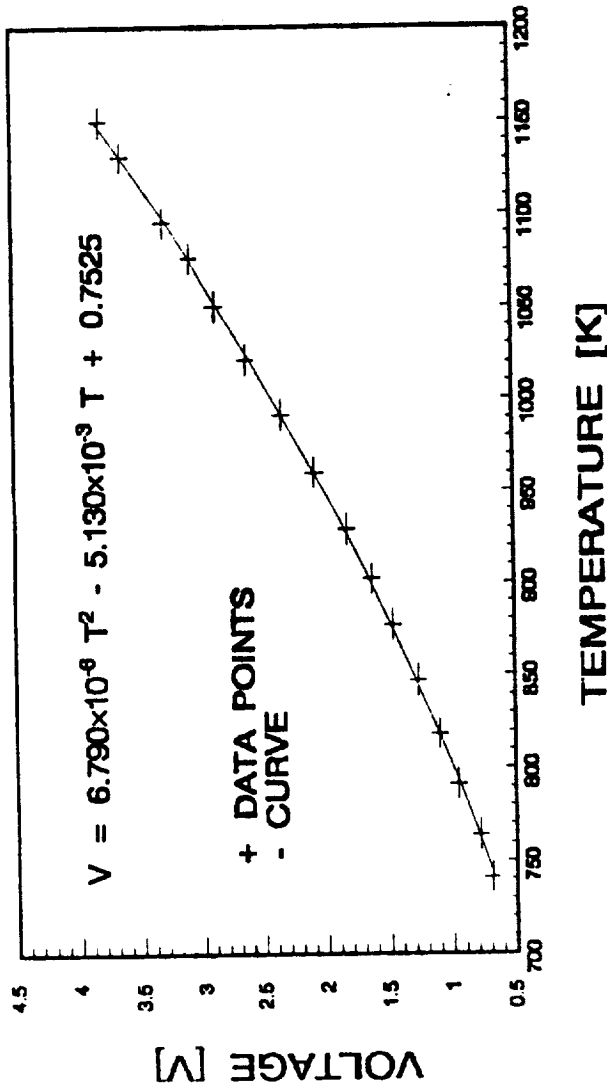
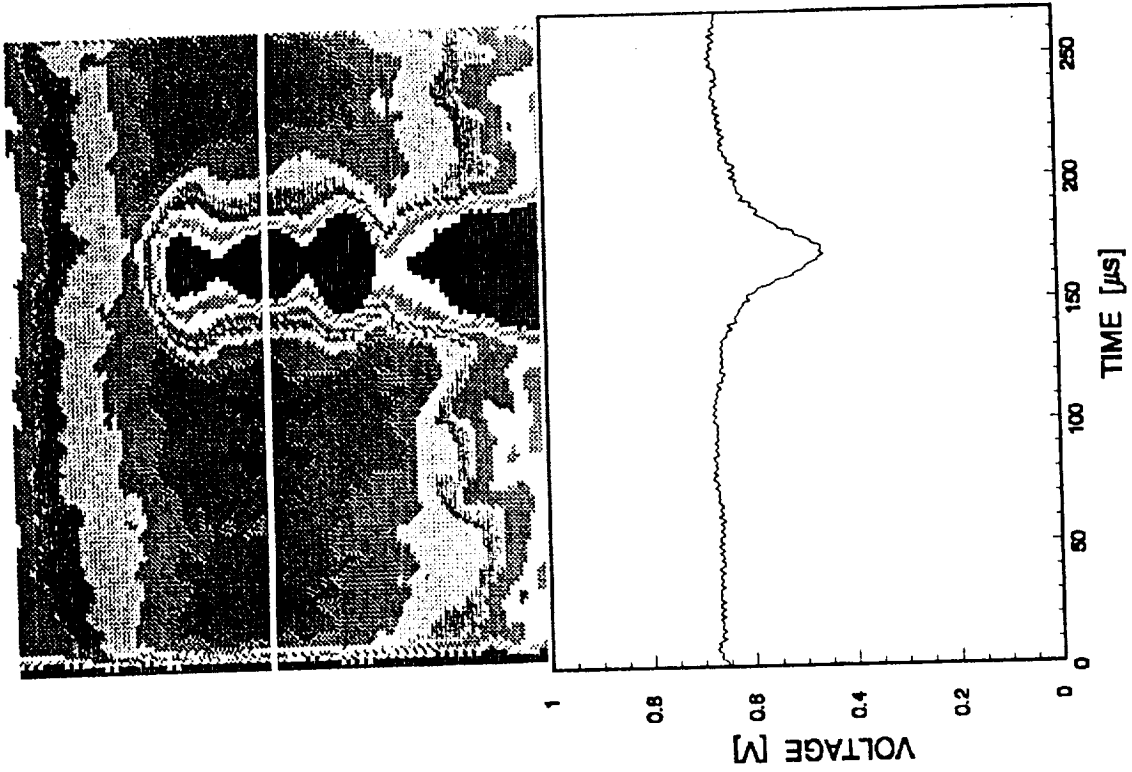


Figure 17

HORIZONTAL SCAN THROUGH SWEET SPOT

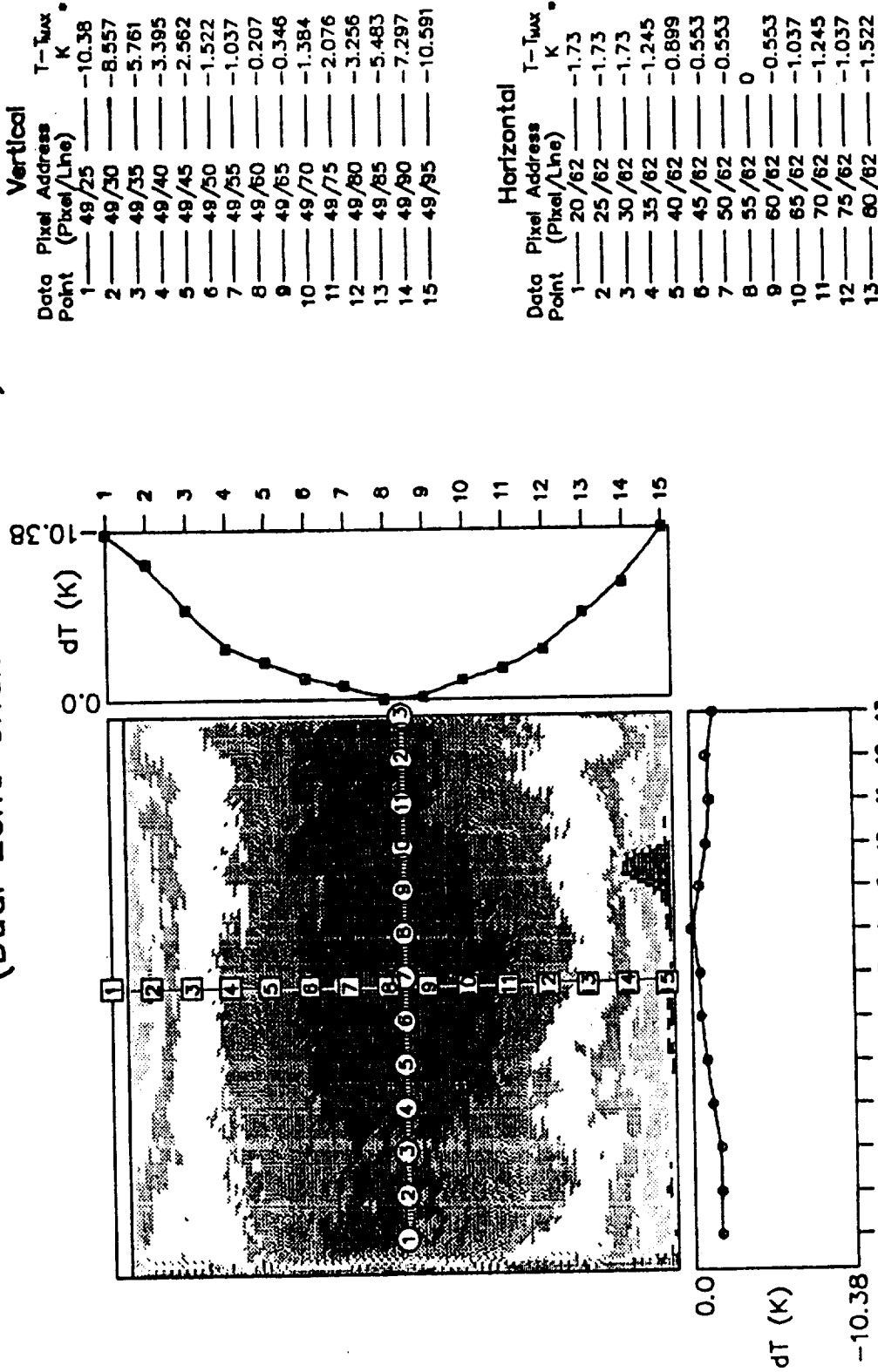


Sample: 0.25" Dia Monel

$$0.5 \leq \epsilon \leq 0.7$$

Figure 18

MEASUREMENT SENSITIVITY TO TARGET LOCATION (Dual Zone Chamber at 800K)



* Calculated from a polynomial

Figure 19

3.2.6 Optical Parameters

3.2.6.1 Focal Range

Using a fine heated wire as a target, the secondary reflector was moved to its furthest position toward the target, and the target was moved until it came into sharpest focus. The distance between the target and objective fore was measured. This was repeated for the secondary at its opposite extreme position.

Total focusing range: 254mm to 424mm
Nominal range: 390mm.

3.2.6.2 Depth of Focus

The scanner head was focused on the edge of a razor blade oriented vertically in front of the Mikron blackbody furnace orifice. A scan line that crossed the edge of the blade was displayed on the RAPID Systems storage scope. The 25%-75% rise time of the video signal was measured to be 5 μ s, which is just over 1 pixel. This measurement was repeated for displacements from the scanner position toward and away from the target image and the rise times were recorded.

The resulting data, which forms an inverted bell shaped curve, was fitted with a polynomial. This function was evaluated to find the displacement from the focal distance that resulted in a $\sqrt{2}$ factor increase in the rise time. The distance between these two positions is taken to be the depth of focus and is given below:

Depth of Focus: 9mm.

3.2.6.3 Field of View

The NCTM head assembly was placed at the nominal distance from the heated blackbody orifice, and the jaws of a vernier caliper were closed until their edges came into the thermal image field, both horizontally and vertically. Electronically, the field is 65 pixels (horizontal) by 70 lines (vertical). From these measurements, the spatial resolution was calculated.

FOV: 15.4mm (horizontal) X 16.0 (vertical)
Spatial Resolution: 237 micron X 229 micron

3.2.7 Hot Sapphire Window Emission

To determine the amount of radiation emitted from the hot window (W2), a copper block at room temperature was inserted into the chamber and simultaneous measurements were made of the scanner output. The furnace was stabilized at 1100K and the block was inserted such that virtually all light in the chamber was shielded from the window. The remaining light was that

radiated directly by the window and that radiated from the window into the furnace and reflected by the copper. The signal detected was ~15% of the signal produced by the freely radiating Dual Zone Chamber, which is known from separate experiments to be approximately a blackbody.

3.2.8 Electrical Characteristics

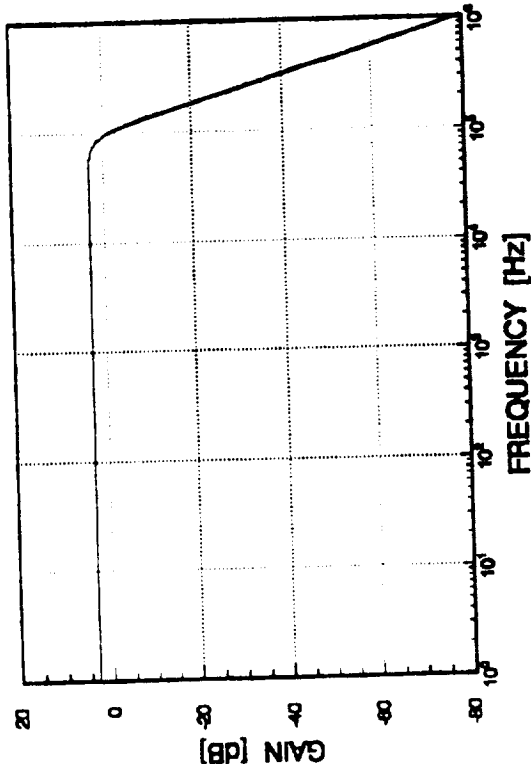
3.2.8.1 Video Conditioning Filter Response

The frequency response of the video conditioning circuitry was determined with the use of Tatum Labs "Electronic Circuit Analysis" simulation software. The simulation uses models for the op amps that reflect the characteristics of the OP-37's used in the actual circuit. The response of the actual circuit was checked against the simulation at several points and agreement was excellent. The amplitude response of the simulation is shown in Figure 20 along with a typical scan line before and after processing. The indication is that this filter has very little adverse effect on the integrity of the video signal.

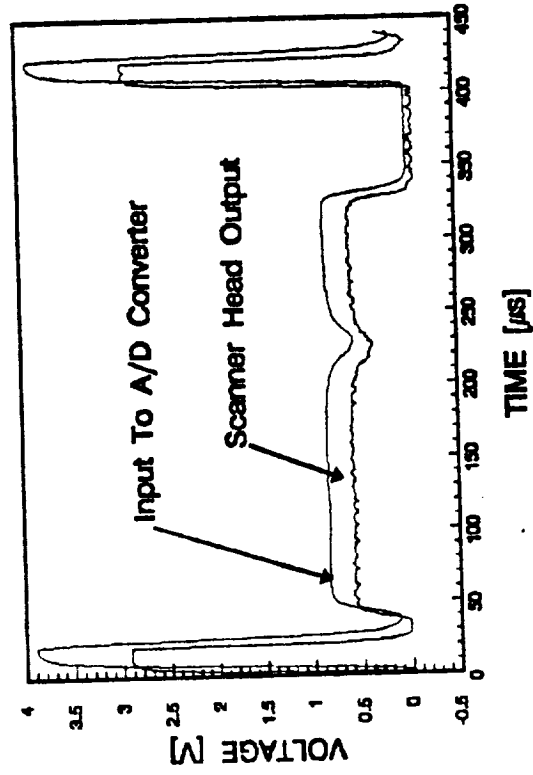
3.2.8.2 System Power Measurements

The power and currents required by the CA and MA boards are given in Figure 21.

VIDEO CONDITIONING CIRCUIT RESPONSE



Filter Type:
4th Order Butterworth
-3dB Point \approx 91kHz



Sample: .25" Monel
T \approx 815K

Figure 20

SYSTEM POWER MEASUREMENTS

CONTROLLER ASSEMBLY PWA

V	I	P
+12.2 V	35.6 mA	430 mW
+5.0 V	200 mA	1.0 W
-12.2 V	46.4 mA	570 mW

MECHANICAL ASSEMBLY PWA

V	I	P	COMMENTS
+12.2 V	1/15 mA	14 mW	Scanner Off
+12.2 V	1.07 A	13 W	During Motor Start-Up (0-5s)
+12.2 V	.54 A	6.6 W	Before Vertical Scanning Motor Starts (5-15s)
+12.2 V	.63 A	7.7 W	Steady State
+5 V	62.1 mA	310 mW	Scanner Off
+5 V	.89 A	4.45 W	Scanner On
-12.2	11.3 mA	140 mW	Scanner Off
-12.2	.12 A	1.5 W	Scanner On

Figure 21

4. PERFORMANCE EVALUATION

This evaluation is the result of the tests and calibrations performed and calculations based on data obtained. The capabilities of the completed hardware as a NCTM device will be discussed and presented. A summary of the system specifications is included in Appendix D.

It is important to note that curve-fitting software was utilized to obtain analytical expressions of the calibration data. While the use of polynomial functions was required to complete this analysis, some error is introduced as a by-product of their use. Some of the calculated data presented in this section and the previous one are based on these polynomials and therefore may not represent the ultimate capabilities of this system. The best possible results would be achieved if empirically generated look-up tables were employed.

4.1 NCTM System Performance

4.1.1 Electronics

The system electronics performs nominally as designed. It is DPM compatible, provides adequate digitization rate and resolution, and has sufficiently low noise to provide minimal measurement uncertainty. Improvement in electrical S/N ratio, currently measured at 73dB, would further improve the ultimate temperature measurement capabilities of the system. This, however, is not the limiting aspect of this systems' ability to measure temperature.

4.1.2 Optics

The Cassegrainian Objective provides a field of view of 15.4mm (H) X 16.0mm (V) at the specified target distance of 390mm. Although the image clarity is equal or better than that of standard AGEMA objectives, its radiance collection characteristics produce a false vertical gradient in the image of a uniform target (see Figure 19, Section 3.2.5). The cause of this appears to be a poor match between the exit pupil of the objective/macro optics and the entrance pupil (or pupils) of the scanner head. The problem is severe enough to render the system useless when using the two smallest scanner head apertures, which are not believed to be apertures in the purest sense.

This does not present a problem when using the standard AGEMA objectives, presumably because of their low f-numbers (nearly one compared to f7.9 for the center-obscured Cassegrainian system). The true cause of this phenomenon and the best method of correction can only be ascertained by gaining a more thorough understanding of the scanner head optics, which may involve proprietary information from the manufacturer.

This deficiency will reduce the effective performance of temperature measurement in the DZC. However, this performance degradation can be minimized since the entire specified temperature range can be measured by

switching in attenuating filters rather than apertures, and since the signal dependence upon field location can be corrected by calibration.

4.1.3 Temperature Measurement

4.1.3.1 Baseline Temperature Measurement Ranges

Using the polynomials obtained from the blackbody and DZC calibrations, the measurement ranges vs. target emissivity for filter positions 0 and 1 were calculated. The results are shown graphically in Figures 22 and 23. When correcting for emissivity, it must be noted that the spectral bandpass of the system is restricted to between 3.7 and 4.0 microns when using filter position 1, while position 0 utilizes the entire 2 to 5 micron bandpass of the AGEMA optics and detector.

4.1.3.2 Measurement Sensitivity To Target Location

As was previously discussed some false non-uniformity is present over the scanned image of an isothermal target. It is possible however, to generate a weighting factor array which will correct for this. This could be accomplished by measuring the signal at every pixel in the field, and dividing its value by the signal value of the "hottest" pixel. The resulting weighting factor can then be divided into the signal value for any thermal image of interest, to obtain the "true" signal to be used for temperature calculation for the pixel. Without this correction, additional temperature measurement errors on the order of those shown in Figure 19 can be expected.

4.1.3.3 Sweet Spot Detection

The results presented in Section 3.2.4 are evidence for the ability of the NCTM system to locate the sweet spot of any spherical sample. It can be seen on small fairly high emissivity targets (see Figure 18). However, since liquid materials cannot be suspended in this device in the laboratory, these tests were not carried out on completely specular surfaces. Attempts at investigating this with gold plated spheres resulted in evaporation of the plating and were therefore unsuccessful. The data obtained with non-specular samples and the spatial resolution of the device indicate that adequate sweet spot detection can be accomplished.

It should also be noted here that all three sweet spots, which result from windows W2, W4, and the bottom of the chamber, are visible in this image. This could be very valuable in determining true temperature gradients across the specimen. The center and bottom sweet spots would be unaffected by the use of beam heating from the top since very little light from the heater would reach these spots. This is particularly important if xenon arc heating is employed. While the Xenon Arc Spectrum does not cover the 3.7 to 4 um range, the anode of the lamp glows extremely hot (up to 2800K) and its radiation will be imaged onto the specimen. Potentially, this radiation could produce a significant error source.

TEMPERATURE MEASUREMENT RANGE

Mikron M300 Black Body Target

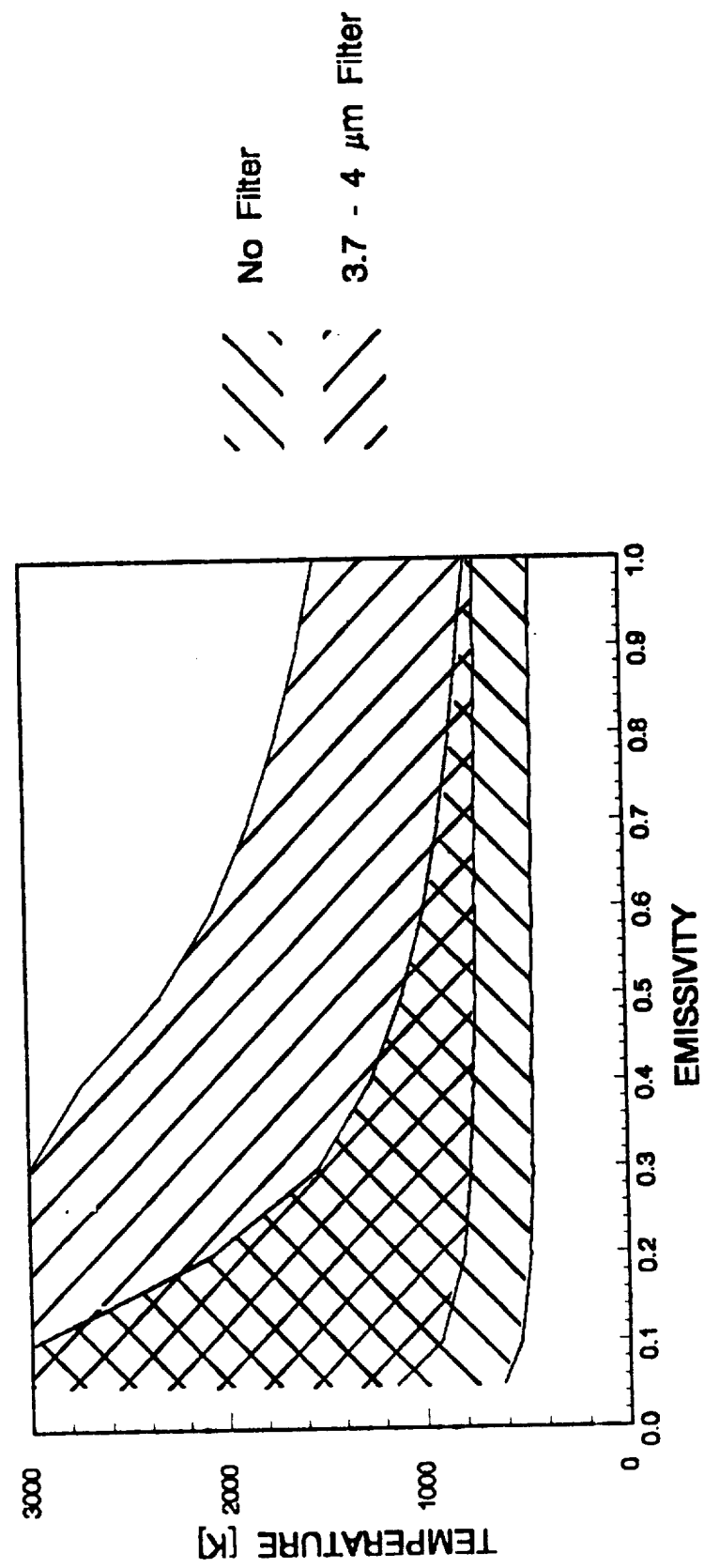


Figure 22

TEMPERATURE MEASUREMENT RANGE

DZC Target With Optics

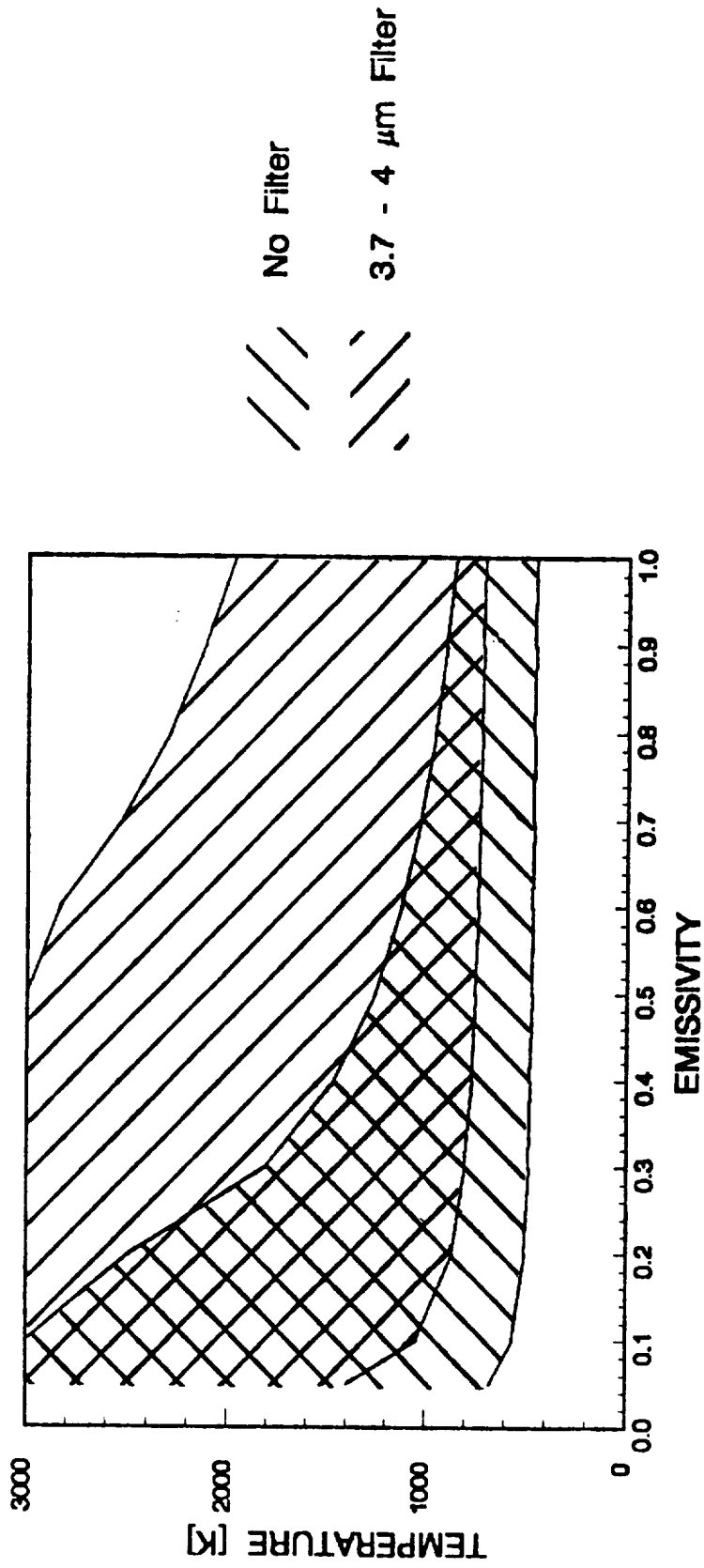


Figure 23

Another potentially large error source in sweet spot measurements may result from the radiance contributed by the hot window mounted to the furnace. This effect is discussed in Sec. 4.1.3.5.

4.1.3.4 Temperature Resolution/Error Effects

The histograms displayed in Sec. 3.2.2.3, Figures 14 & 15 indicate the uncertainty in temperature measurement for several different conditions. In all of these cases the temperature distribution data was calculated from the actual measured data.

The unusual aspect of this data is that the temperature resolution gets worse as the temperature increases. This is due to the fact that the electrical noise, as measured in Sec. 3.2.2.1, is not the only contributing factor to the measurement distribution. Several other factors have been found to contribute to this.

Optical irregularities internal to the AGEMA Scanner head produce errors which are in addition to those from the electrical noise in the system. It is apparent from the tests performed at ISI, that the 10-sided rotating horizontal scanning mirror is not regular. The exact nature of this irregularity is not known but the result is that the scan lines produced by different mirror facets vary with a period traceable to the 10 mirror sides. It is apparent that the asynchronous nature of the video digitization process adds to the overall error as well. These aspects must be considered independently.

4.1.3.4.1 Scan Line Error

For any given scan line through an iso-radiant field, some amount of optical induced irregularity will appear as a " Δv " from a constant horizontal line. This error has two sources, the first being the non-uniformity in the objective optics light collection which was discussed in Sec. 4.1.2. The second source is an apparent non-uniformity in the mirror surfaces within the AGEMA scanner. It is likely that all of the mirrors are contributing to this error. This means that a perfectly constant scan line is not achievable regardless of how isothermal the target is. The resulting " Δv " increases as the detector signal (v) increases. While $\Delta v/v$ remains fairly constant over the operating range, the increase in Δv at the higher temperature ranges shows up as an increase in the apparent temperature deviation across an iso-radiant field.

4.1.3.4.2 Periodic Scan Errors

In addition to the errors induced within a scan line it is also apparent that substantial differences exist between individual scan lines. Therefore, adjacent pixels in consecutive scan lines may appear much brighter or darker than they actually are due to the optical irregularities between two adjacent mirror facets. As will be explained, this error is periodic and therefore predictable.

Due to the nature of the vertical and horizontal scanning mechanism in the scanner head, the same mirror facet does not always produce the same scan line in the field image. Analysis has determined that a given mirror facet scans the same line in space only once in 40 fields, or 10 frames. (1 frame = 4 fields).

Each mirror facet produces a characteristic scan line which appears every 10th line and moves upward (as viewed on the video monitor) at the rate of 10 lines in ~ 1.6 sec. As a result, the exact same scan line occurs in the same location on the monitor only once every ~ 1.6 sec. Therefore, if the Pixel Grabber is used, the data collected will include all of the fluctuations produced by the individual mirror facets unless only one in forty data points is accepted.

If this is done, the resolution can approach the limit imposed by the electrical noise spec of 2.2mV RMS. If no other error sources were present, this would result in a temperature resolution capability of ~.25°C.

4.1.3.4.3 Asynchronous Digitization Error

The asynchronous nature of the digitization process is also responsible for some additional systematic error. When a single pixel is monitored, the actual location of that pixel on the scan line is only known to within 4 μ s or 237 micron. This is due to the fact that the horizontal sync pulses, which are the reference for the "Pixel Grabber", may be skewed in time by up to that amount. This is not a problem for a constant line since the measured voltage would not be affected by what point it is measured at. However, since truly constant lines are not the case here, the possibility of measuring different points on a slope with consecutive pixel measurements is quite high. At the highest temperatures where the " ΔV " across a scan line can get rather large, additional errors of $\pm 1^\circ\text{C}$ may occur as a result of this if averaging is not employed.

4.1.3.5 Optics Train Effects/DZC Characteristics

There are several important aspects of the DZC and the optics path which must be considered and understood. They include:

- o Transmission of optics
- o Radiant Emission from the hot window (W2)
- o Purity of the sweet spot

Transmission losses through most of the optics path are straightforward and can be assumed constant. This is easily accounted for in the system calibration, simply by including all of the components in the path when the calibration is performed. This, however, is not true for the hot window (W2) mounted to the furnace.

This window, which is at approximately the same temperature as the furnace walls, will radiate according to its temperature and emissivity. This is potentially a large source of error since the absorption coefficient of sapphire is significant at the temperatures and measurement wavelengths in question (700 to 1100K, 3.7 to 4 micron). The emissivity of a 3mm thick sapphire window and its dependence on temperature and wavelength are shown in Figure 24. This shows a strong dependence of emissivity on temperature and wavelength making it very important to know the window temperature if any corrections are to be possible. The errors induced by this effect will become larger as the specimen emissivity decreases and if the specimen temperature is significantly different from the window temperature.

Results from the copper block test described in Sec. 3.2.7, are consistent with the data shown in Figure 24. The approximate emissivity of the window at 1100K is .05 at 3.85 micron. Assuming a blackbody approximation for the DZC, this would constitute ~5% of the total signal. This could nearly double when the reflection from the cold copper block is included. The additional 5% is likely accounted for by several considerations. Firstly, the actual properties of this window are certainly not given precisely by the theoretical data on Leuco Sapphire. This window may also have been contaminated from the prior use of this facility in extensive laboratory testing. Other considerations potentially having an impact on this test are light leakage around the copper, the actual emissivity of the copper, and the actual emissivity of the chamber. Regardless of the approximations in the test, the effect is quite significant.

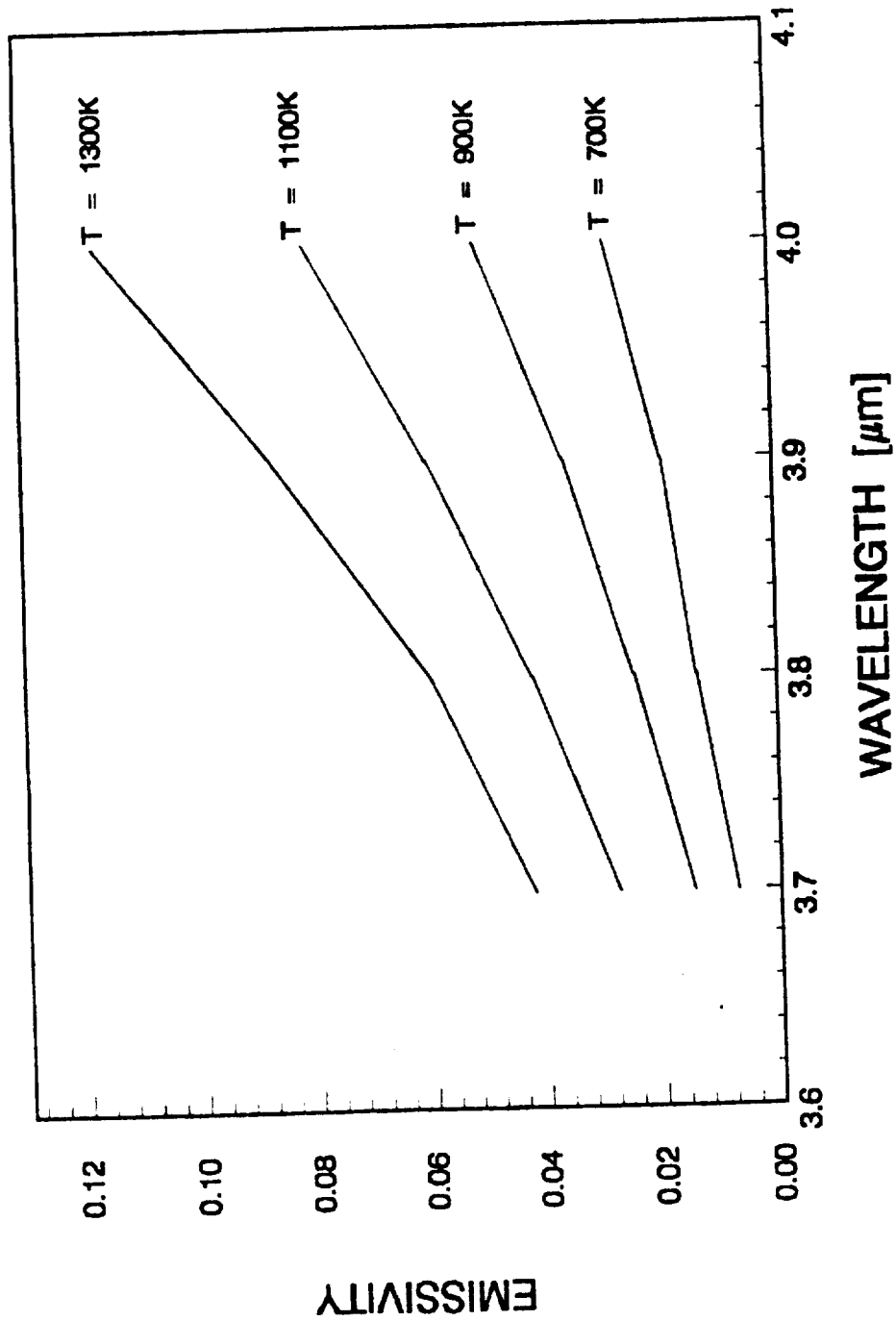
Further, it can be noted from this discussion that radiation from W2 will affect the purity of the sweet spot. This spot cannot be assumed to be completely free of reflected or scattered light originating from the hot window itself. For highly reflective specimens, e.g. gold, the radiance contributed by the window will be greater than that contributed by the sample. In any case, window radiance must be considered as a sweet spot contaminant.

4.1.3.6 Temperature Measurement Summary

Error sources have been identified which can limit the temperature resolution that can be realized with this device. However, the systematic and periodic nature of them can allow much of this error to be removed by careful selection of data obtained, by averaging and by calibration.

The effects produced by the hot window, however, are quite complex and further work is required to fully characterize and adequately correct for them. The calibrations performed that included this window were performed with a blackbody target inside the DZC and with the furnace under equilibrium conditions. Under these circumstances all of the effects are accounted for in the calibration. Any departure from these conditions would require considerable measurement corrections.

EMISSIVITY OF SAPPHIRE WINDOW (W2)*



* Data selected from "Optical Properties of Leucosapphire at High Temperatures" YU. K. Litgart et. al. Teplofizika Vysokikh Temperatur, Vol.20, No.5, pp672-680

Figure 24

Figure 25 shows the periodic nature of some of the errors and the resultant temperature resolution achievable by data selection and averaging. A blackbody target was measured and the data was selected to remove the periodic error effects previously discussed. The periodicity of the acquired data can be seen in Figure 25b and the data distribution is shown in Figure 25a. This data distribution reflects data selected to correct for the periodic error, i.e. every 40th field. The temperature resolution indicated by this data which also includes the polynomial error, is $\sim .35^{\circ}\text{C}$. This is in direct comparison to the data displayed in Figure 14, which is not corrected for the periodic errors. The data shown in Figure 15, which includes the hot window, is also uncorrected for the periodic errors. Improvement could be expected if this correction were applied to this data but it must again be pointed out that this is a narrowly defined set of conditions (i.e., blackbody target, equilibrium conditions).

PERIODIC OPTICAL ERROR EFFECTS

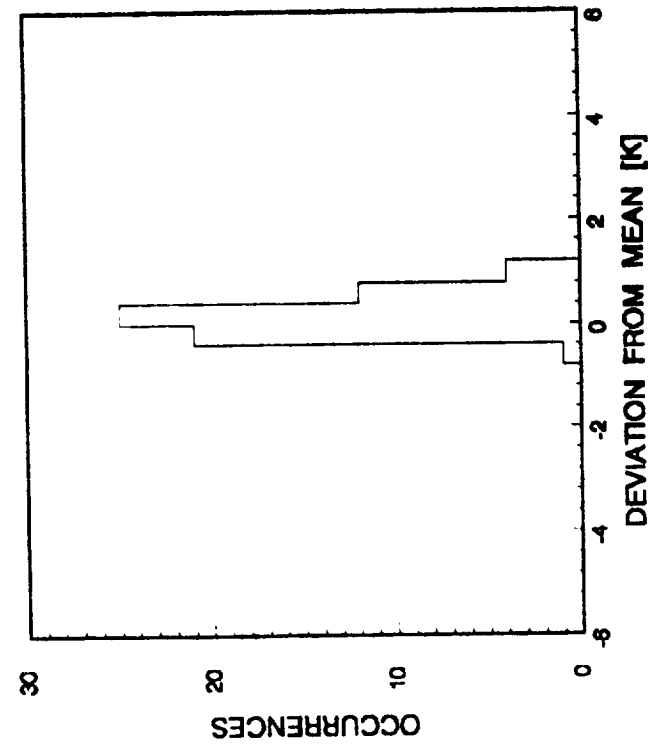


Figure 25(a)

Distribution Of Data Corrected For
Periodic Variation in Optical Path

Target Temperature: 1350K
Standard Deviation: .35

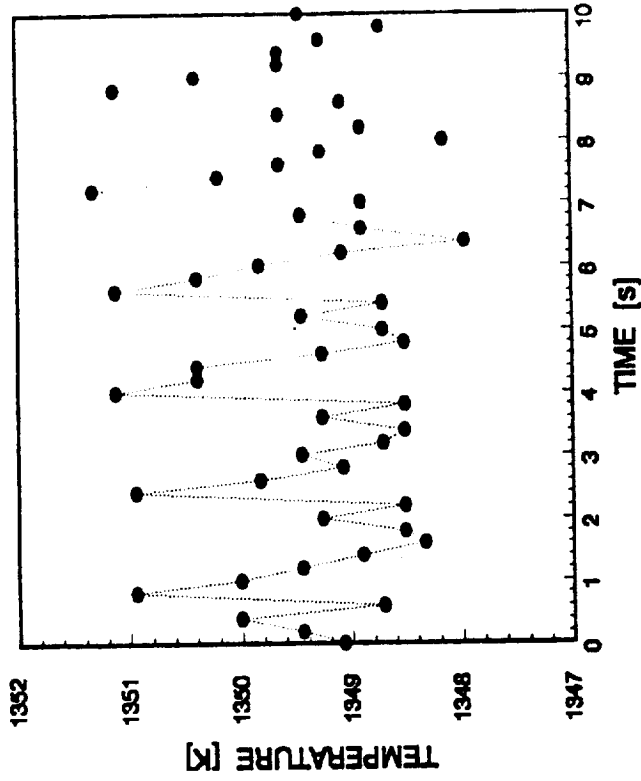


Figure 25(b)

Temperature Readings Taken From
The Same Pixel Every 5th Field.
8 Data Points Represent 40 Fields.

Figure 25

5. RECOMMENDED SYSTEM MODIFICATIONS (Existing Hardware)

This section will discuss minor modifications to the completed hardware that are necessary or desirable either for up-grade to flight quality status or for improved performance.

5.1 Electronics

The circuit boards in this equipment are first generation and would require some modification before they could be considered flight ready. While they are mechanically and electronically compatible with the DPM, they are not flight qualifiable and would require some minor circuit changes. Additionally, manufacture by an approved board house would be required along with the use of high reliability electronic components. The minimum required circuit board modifications include:

- o A few minor trace routing errors must be rectified.
- o Heavier ground traces are required for some signals to reduce voltage drop.
- o MA board video repeater improvement is required. The current output stage of this simple circuit is an OP37 op amp. In the lab with a short cable between the CA board and the MA board, this isn't a problem. However, to handle the requirement for a longer connection cable between assemblies, high current line drivers should be added.
- o Transmit disable is required. The serial output to the HRM is not switchable on command. Gaging to allow this should be incorporated to prevent meaningless signals from reaching the HRM input.
- o HRM interface capability is required. The current output of the CA board does not contain the header information nor is it in the precise format required by the HRM. Since the board already performs the interleaving of other data into the output, the extension of this process to include header info. and control the output format should not involve any major design changes.
- o The digitization process should be converted from asynchronous to synchronous. Digitization is currently done asynchronously and therefore produces a slight instability in the horizontal position of the pixels as seen on the video monitor. In addition, as was previously discussed, the asynchronous nature of the digitizer also effects the temperature resolution of the system and complicates data correction.

5.2 Optics

- o The secondary reflector of the Cassegrainian objective is currently held in its mount with silicon adhesive (RTV). It is recommended that the flight hardware version use a permanent epoxy.

- o Baffling: Ray tracing has shown that radiation from angles between 5.7 and 15.1 degrees with respect to the primary mirror intermediate image can enter the scanner head without ever encountering the objective optics. In the event that any thermal source along these directions is of sufficient radiant strength to influence the signal, a conical baffle should be placed about the hole in the primary reflector.
- o Mechanical Support: Currently, the objective housing is supported only by the CRES steel bayonet connector, which is held to the head by the macro mounting flange. To meet G-loading and vibration requirements, it will be necessary to provide additional support for the objective housing when interfacing to the DPM optical bench.

5.3 Ground Support Equipment

The Pixel Grabber substitutes a selectable digital code for the target pixel in the output to the 800V as discussed in Sec. 2.2.4.4. This replacement takes place prior to the filtering of the output video. Consequently, what would be a distinct, accurately located spot on the display suffers from delay and dispersion in the filter causing it to appear more than one pixel wide and slightly to the right of the actual pixel that is replaced. A better implementation would be to perform the substitution after the filter with an analog switch to reduce these effects.

6. RECOMMENDED SYSTEM MODIFICATIONS (FUTURE FLIGHT SYSTEM)

Due to the accelerated nature of this task, some design compromises were necessary. To fully take advantage of this technique for temperature measurement some design and technical approach modifications should be made. The following is a list of recommendations for enhancing the performance and versatility of this system.

6.1 Data Handling

The current data rate of ~4Mbs creates data downlinking problems for the shuttle telemetry system. The use of the HRM for high speed data downlinking precludes simultaneous video transmission. This affects every data station in the POCC which poses an obvious conflict between the users.

This problem can be solved by employing any one (or a combination) of several data compression techniques in the flight hardware which will reduce the data rate to < 2Mbs. Data rates in this range can be accommodated by the Low Data Rate transmission so that the simultaneous video downlink of other users is not precluded.

An additional modification, which could be considered complimentary to the above, or as an alternative, is to provide full data transfer compatibility to the local governing computer system, i.e. the DPM Controller. If desired, real-time temperature calculation could be done on board and/or selective data could be processed or stored while the rest is discarded or downlinked. This would greatly reduce the amount of data storage that would be required in-flight thereby making local data storage feasible. In addition, the full interface compatibility between the controller and the NCTM electronics would increase the overall system flexibility by allowing full control by the DPM software. Automated system trouble-shooting would also become possible.

6.2 Automated Filter Selection

To accommodate the temperature and emissivity ranges required with this device selectable filter(s) should be utilized. This function should be automated and software controllable.

6.3 Optics

Some of the problems associated with the existing optics system were discussed in Sect. 4.1.2. These problems might be easily corrected by changing the objective design from a Cassegrainian telescope to a refractive element relay lens system in the NCTM path, which could significantly reduce the f-number (possibly at the expense of image clarity, and certainly at the expense of achromaticity). Such a system would also require an analysis and possible re-design of any other optical system (e.g. video) using common elements in the NCTM train. Further investigation of the internal AGEMA optics is also necessary.

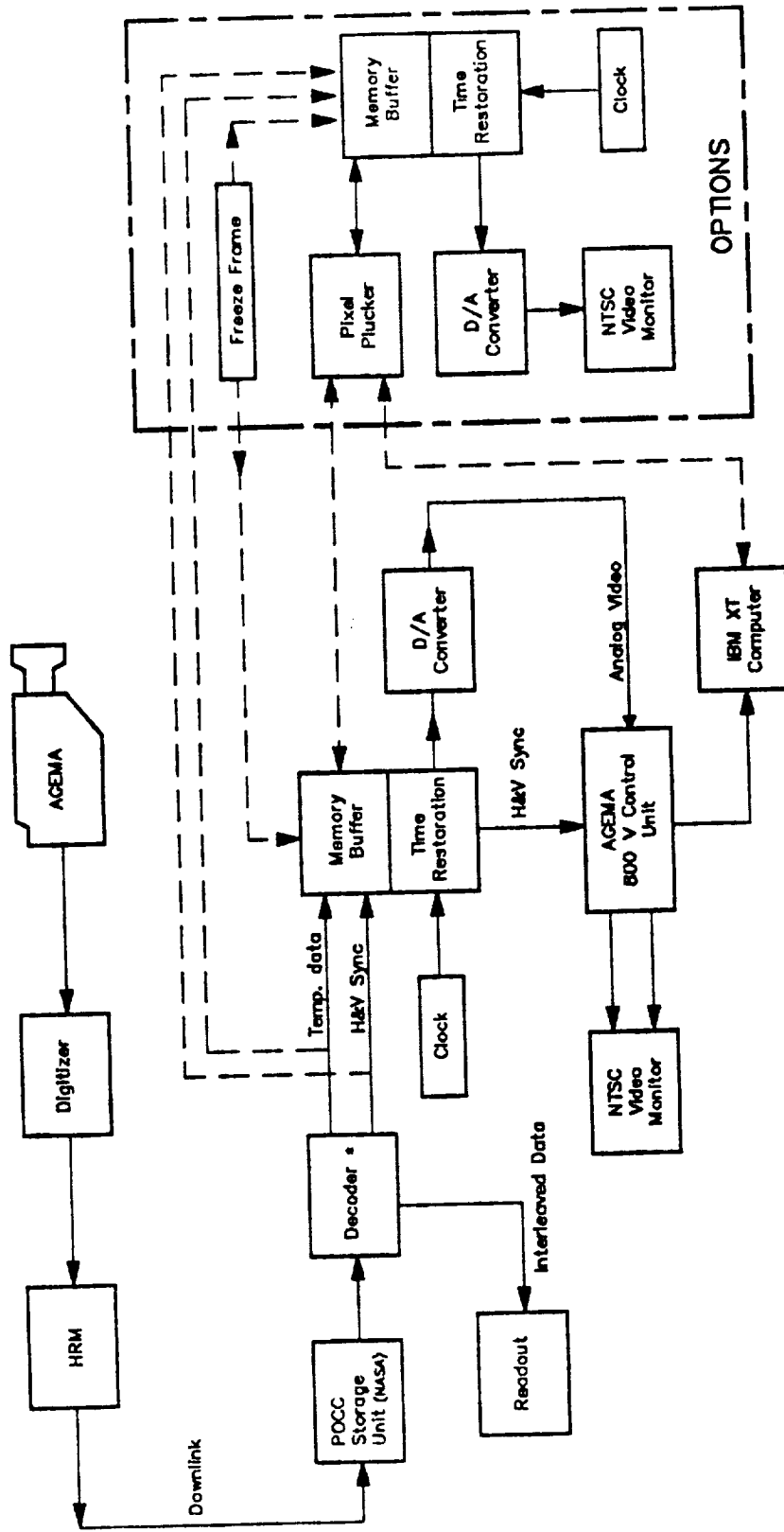
6.4 Ground Support Equipment

The current GSE was developed to provide the minimum functions required to test the flight system. Substantial upgrades to this are required to provide a true Ground Support System suitable for POCC operations. Figure 26 is a block diagram of the POCC GSE, that was proposed by Intersonics, Inc. It begins with a Data Decoder, the complexity of which is determined by the in-flight data handling procedure and the downlink format. The Memory Buffer and Time Restoration block is necessary to collect the data, which is being transmitted asynchronously and with some amount of randomness, and to re-create the video data stream as it exited the A/D converter in the flight system. It also provides other functions such as allowing direct access by a computer to the digital data, a Pixel Grabber feature and a video freeze frame option.

The digital data stream can then be D/A converted to recreate the original video signal. This can be fed into the AGEMA 800V Control Unit thereby allowing access to virtually all the features available with the AGEMA Thermovision system. It is also possible, by changing the clock rate to the Memory Buffer/Time Restoration block, to obtain a different video scan rate than the 25 frame/sec AGEMA standard. Therefore, direct conversion to the NTSC 30 frame/sec can be accomplished without the use of the AGEMA 800V Control Unit if desired.

In addition to providing calibrated radiance measurements, this system would be capable of determining the "sweet spot" location on the specimen. From this, accurate specimen temperature can be determined.

POCC HARDWARE BLOCK DIAGRAM



• Complexity of this increases when data is compressed in flight.

Figure 26

7. SUMMARY AND CONCLUSIONS

An AGEMA Thermal Imaging System was evaluated to determine its feasibility for use as a temperature measurement device for the DPM Dual Zone Chamber, USML-1 Spacelab mission. Feasibility was established and a development project was carried out by Interasonics, Inc. to provide this capability. This development included the design and manufacture of custom objective optics for the AGEMA 870 scanner head, which was the sole component of the AGEMA system that was retained for this application. All support electronics were custom designed for integration compatibility with the DPM.

The NCTM System Brassboard was built, tested, and calibrated at Interasonics. It was integrated into a stand-alone system for testing purposes and is a fully operational system as such. Two electronic PWA's make up the support system and video digitizer for the AGEMA Thermal Imaging Scanner. A ground support simulating device provides access to the digital data to allow temperature measurement to take place prior to the conversion back to analog video. This device also allows the use of AGEMA support facilities by providing a regenerated analog video signal virtually unaltered by the digitization process.

Testing of this equipment was directed toward performance evaluation since the requirement for flight qualifiable hardware was removed. This is reflected by the tests performed and the data presented in this report. Significant attention was paid to determine the temperature resolution achievable with this system and the error sources affecting it. This specification is indicative of the ultimate accuracy that can be achieved through careful calibration and is therefore highly important. Additional tests, either directly or indirectly relating to temperature resolution were performed. These included; general electrical tests, spatial resolution, sweet spot determination, and voltage vs. temperature calibrations.

To appropriately summarize the results presented in this report it is necessary to independently assess the inherent capabilities of the NCTM system and the combined NCTM/DZC performance.

7.1 AGEMA NCTM Brassboard Performance

Electronically, the device performs nominally as designed. The digitization process is fairly transparent with the exception of the slight ($\leq 4\mu s$) uncertainty in the sync pulses caused by the asynchronous nature of the process. The system was designed and built to be mechanically and electrically compatible with the DPM. Although full system integration with the DPM has not taken place, minimal difficulty is anticipated. Necessary or recommended upgrades and redesigns (some of which have been presented here) would take place prior to the development of flight hardware.

The Cassegrainian optics performs adequately but appears to provide a slightly irregular image over its field of view. Specifically, the light collection efficiency appears highest near the center of the image with decreasing efficiency in the vertical directions. It is also apparent that the switchable apertures in the AGEMA scanner cannot be used in conjunction with

this lens. Range changes can (and must) be accomplished by filtering. To understand and possibly correct for this would require additional analysis of the scanner optics and consultation with AGEMA Infrared Systems.

Optical effects internal to the AGEMA scanner produce an additional source of errors. While these errors can substantially reduce the temperature resolution of the device, they are periodic in nature and can therefore be corrected by synchronizing the data collection with this period. If this is not corrected the resolution decreases as the target radiance increases, degrading from .4°C at 800K to 1.5°C at 1350K. If this correction is made the resolution remains fairly constant over this range at .35°C. While the asynchronous digitization technique accounts for some of this uncertainty, primarily it is the electrical noise that is the ultimate limit in resolution capability. It is important to note that the resolution specification of .35°C is not based on single pixel measurements. High temperature, single pixel measurements would be subject to an error of $\pm 4^\circ\text{C}$. However, measurements taken with a blackbody target and corrected for periodic errors indicate that the system is quite capable of making radiance measurements with a fairly high degree of accuracy if averaging is employed.

7.2 Dual Zone Chamber Radiance Measurements

This measurement accuracy will degrade considerably when the measurement target is located in the Dual Zone Chamber. Approximately 30% signal loss is encountered through the optics path between the specimen and the objective optics. This alone is not highly detrimental since its effect is included in the calibration technique and can be assumed to be fairly constant. However, this is not true for errors due to radiation from the sapphire window mounted to the furnace wall, which may be large.

The potential effects of a hot sapphire window, as in the DZC, are numerous and complex. Testing has verified that the errors induced by this window can be substantial. A complete analysis of this error source was not carried out under this task but some of the effects of a hot window have been identified. Two primary errors result from direct window radiation into the detector and onto the specimen sweet spot. The greatest impact will be on low emissivity targets and under conditions where the specimen and window are at different temperatures. This area requires further investigation.

Another important factor is the ability to adequately resolve the sweet spot. Testing has determined that this device has sufficient spatial resolution to do so and can indeed detect the sweet spot. Liquid specimens cannot be levitated in the DZC in the laboratory so testing was limited to non-specular solid spheres. Therefore, this testing verified the ability to resolve the sweet spot, but not to determine its precise size. Also, as was previously discussed, this is further complicated by window emission.

It is not feasible with the current data and information available to make definitive estimates on the absolute measurement capability of the integral system under all possible conditions. It is possible to achieve reasonable radiance measurements on specimens in the DZC but the conditions must be narrowly defined and calibrated. As an example, measurement of a blackbody

target under equilibrium conditions in the DZC can result in similar accuracy to that of the blackbody calibration target. However, any deviation from this calibration point will require input from a complex matrix of system parameters. These include:

- o Specimen emissivity
- o Temperature of the hot window and the resultant radiated energy
- o The relationship between the specimen temperature and the window temperature
- o The relationship between the specimen emissivity and the window emissivity
- o Specimen surface (specular or partially specular)
- o Wavelength acceptance (spectral sensitivity functions)

To conclude, it can be stated that a system has been built which could fly aboard the DPM and is capable of measuring thermal radiance with a fairly high degree of accuracy. However, the ability to make precise measurements is greatly inhibited by the configuration of the Dual Zone Chamber. Calibration is possible which takes all of the error sources into account but this must be done for a narrowly defined set of conditions. If this device is to be used successfully, these conditions must be defined so calibrations can be performed accordingly. These conditions would then need to be strictly adhered to in flight. A redesign of the DZC window configuration, specifically W2, should be considered.

AGEMA 870 Thermovision Specifications *

Specification	
Scanner	870 shortwave
Infrared detector	SPRITE, thermoelectrically cooled MCT.
Spectral response	SWB version with broadband coating 2-5 microns.
Temperature range	-20° to 500°C (extended to 1500°C with filter)
Field frequency	25Hz
Line frequency	2500Hz
Lines per frame	280 (interlace 4:1)
Resolution elements/line	90 (50% SRF)
Apertures	Three, externally selectable
Infrared filters	Two, externally selectable
Sensitivity NETD	0.1°C at 30°C object temperature
System operating temperature - storage -	-15°C to +50°C -40°C to +55°C
Dimensions (without lens)	92 x 150 x 205 mm (W x H x L)
Weight (without lens)	2.5kg
Length of detachable cable	1.5 m
Lenses	7°, 12°, 20°, 40° field of view
Display Unit	
Thermal image size	50 x 50 mm framed by temperature measurement scale and range digit display
Thermal range	9 calibrated ranges from 2 to 1000 (IU)
Thermal level	5-turn graduated control
Picture modes	Normal, inverted, black, gray scale, gray step
Isotherm function	Width (2 to 30%) and two levels continuously adjustable within selected thermal range
Power	Power supply/battery charger unit for 100 to 240V, 50/60Hz, 35VA or separate battery for 8 to 15V DC, 20W
Dimensions	W x H x D: 235 x 129 x 322 mm
Weight	4.5 kg

* Reprinted from AGEMA Operating Manual

Appendix A

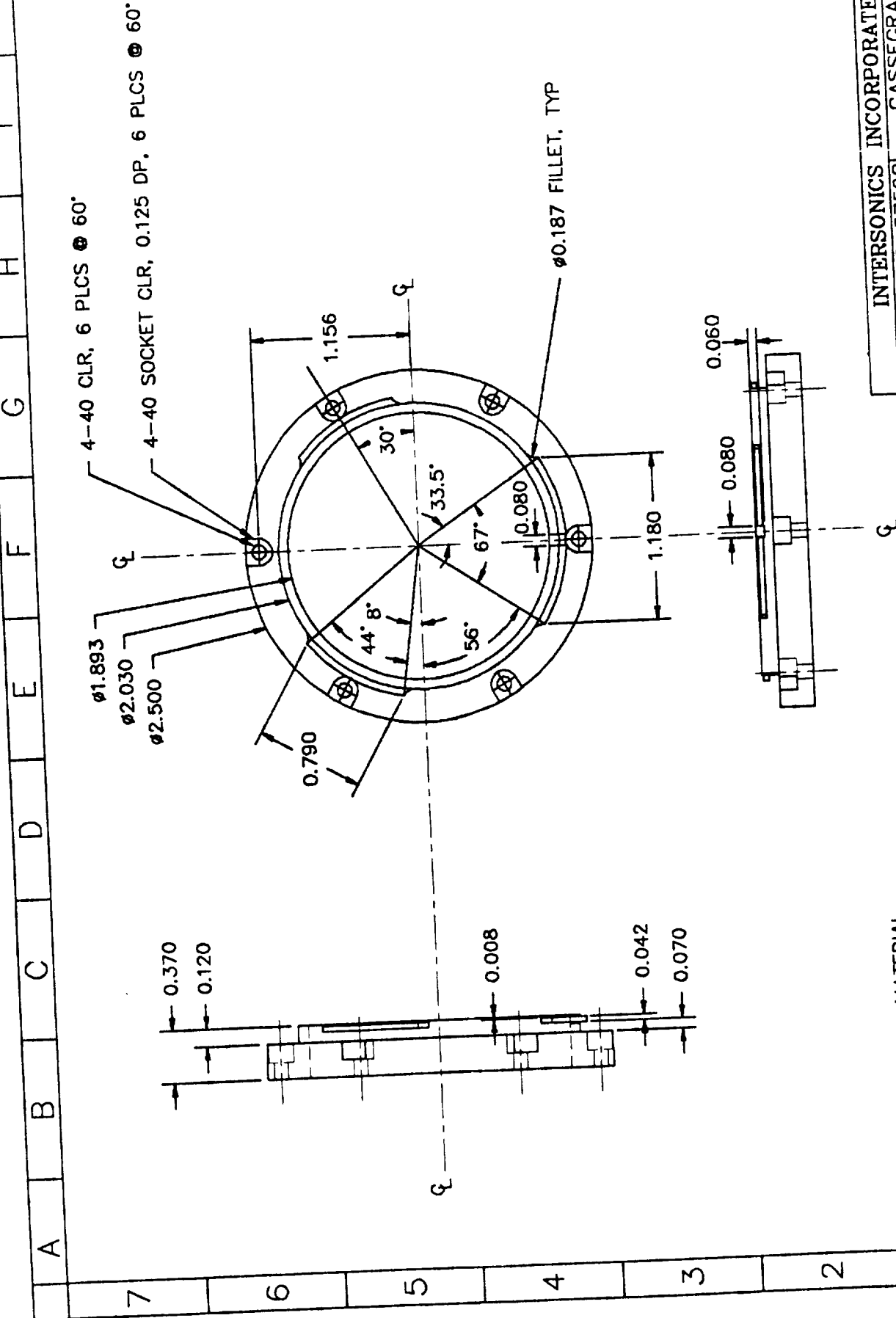


INTERSONICS
INCORPORATED

NCTM BRASSBOARD

Appendix B

MECHANICAL
DRAWINGS OF
OBJECTIVE OPTICS

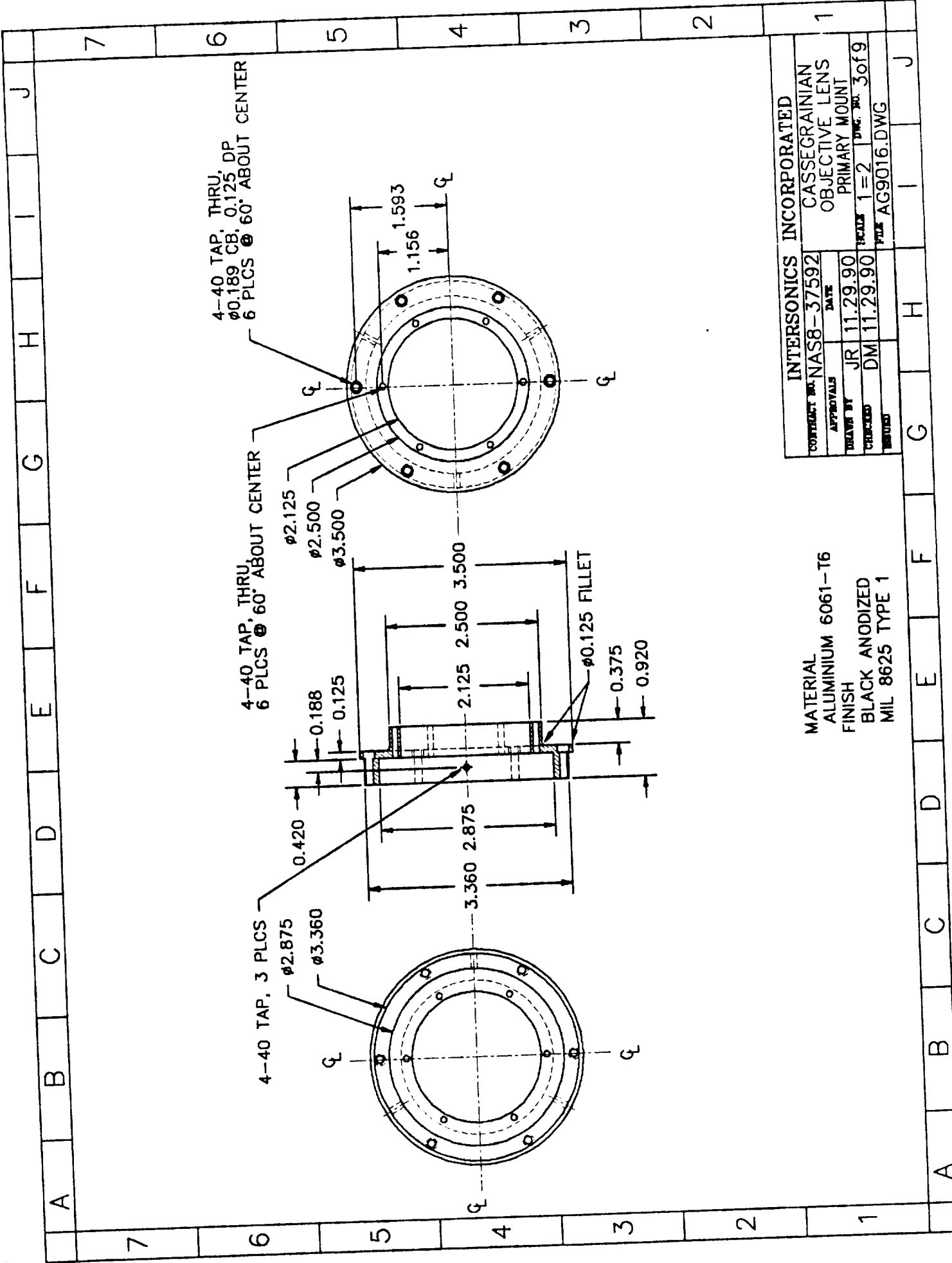


MATERIAL
STAINLESS STEEL P-90
FINISH
MACHINE

INTERSONICS INCORPORATED	
CONTRACT NO. NAS8-37592	CASSEGRAINIAN
APPROVALS	OBJECTIVE LENS
DESIGNED BY JR 11.29.90	BAYONET MOUNT
CHECKED BY DM 11.29.90	SCALE 1=1
REVISED	DWG. NO. 2019
	SIZE AG9016.DWG

7 6 5 4 3 2 1

A B C D E F G H I J



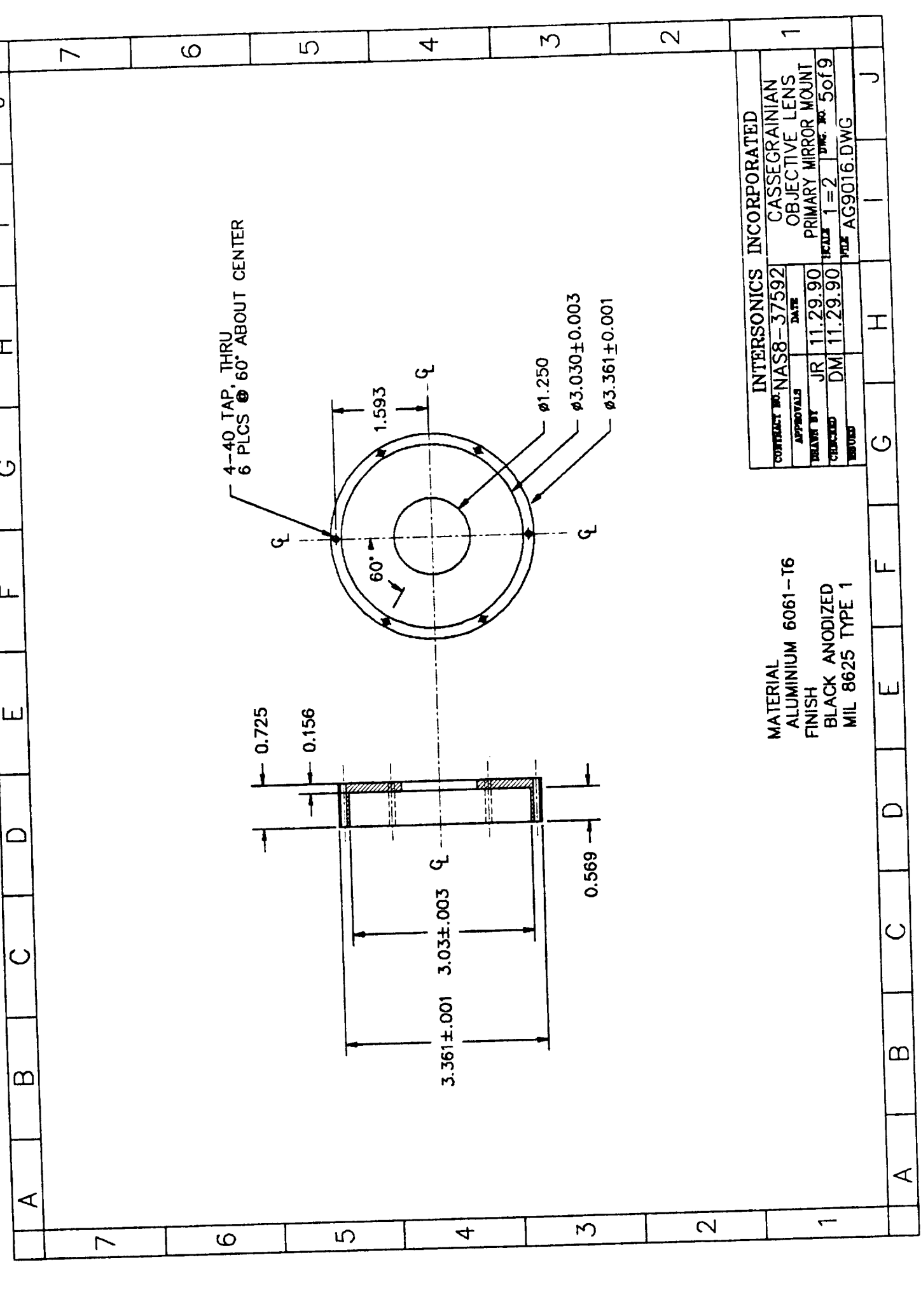
MATERIAL
ALUMINIUM 6061-T6
FINISH
BLACK ANODIZED
MIL 8625 TYPE 1

INTERSONICS INCORPORATED	
CONTRACT NO. NAS8-37592	CASSEGRAINIAN OBJECTIVE LENS PRIMARY MOUNT
APPROVALS	DATE
DESIGNED BY JR	11.29.90
CHECKED BY DM	11.29.90
SCALE 1=2 DWG. NO. 3 of 9	
TITLE AG9016.DWG	

7 6 5 4 3 2 1

A B C D E F G H I J

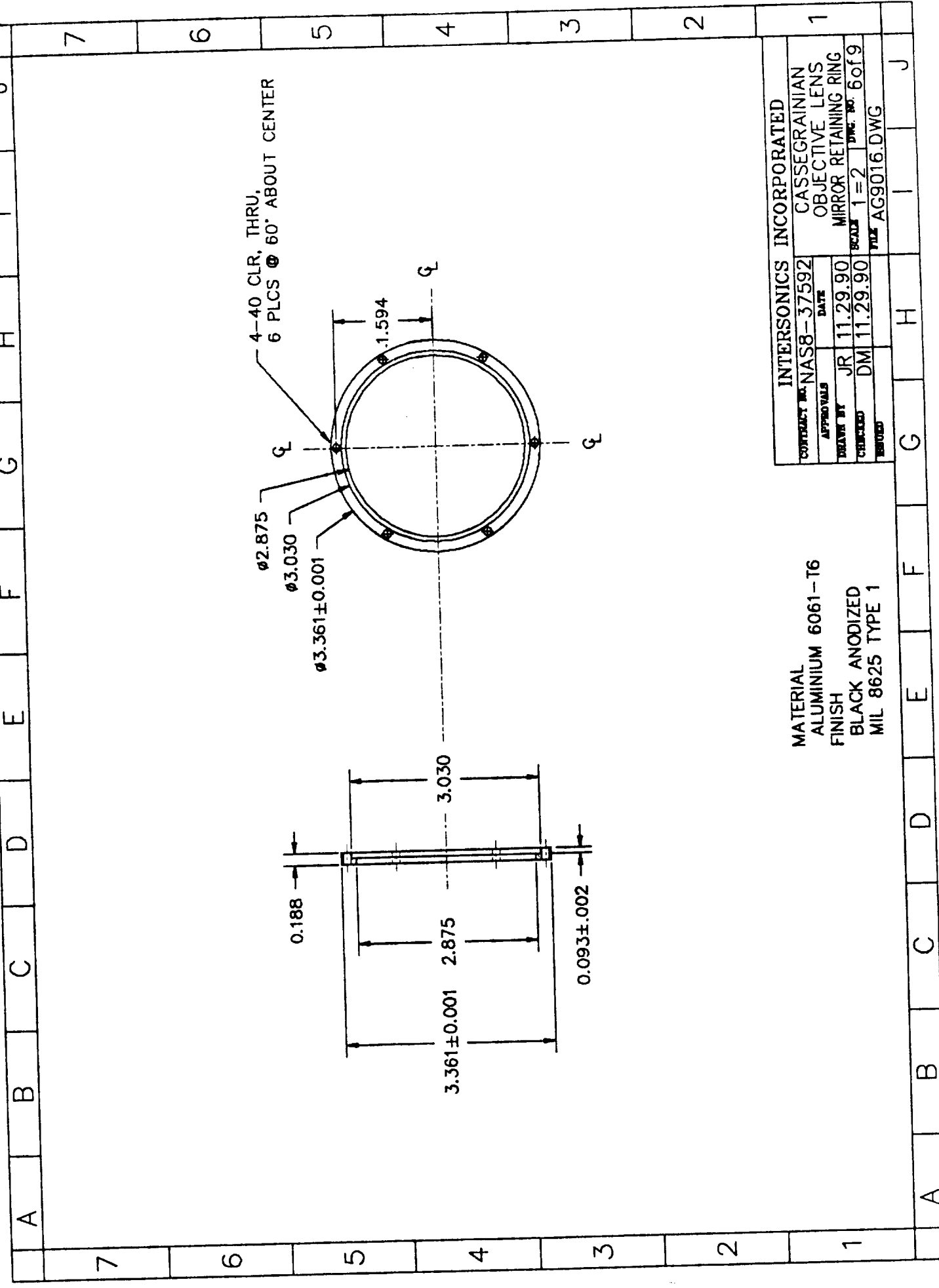
7 6 5 4 3 2 1



MATERIAL
ALUMINIUM 6061-T6
FINISH
BLACK ANODIZED
MIL 8625 TYPE 1

INTERSONICS INCORPORATED	
CONTRACT NO. NAS8-37592	DATE
APPROVALS	
DESIGNED BY JR 11.29.90	DATE
CHECKED DM 11.29.90	SCALE 1=2 DWG. NO. 5 of 9
REVISED	FILE AG9016.DWG

A B C D E F G H I J



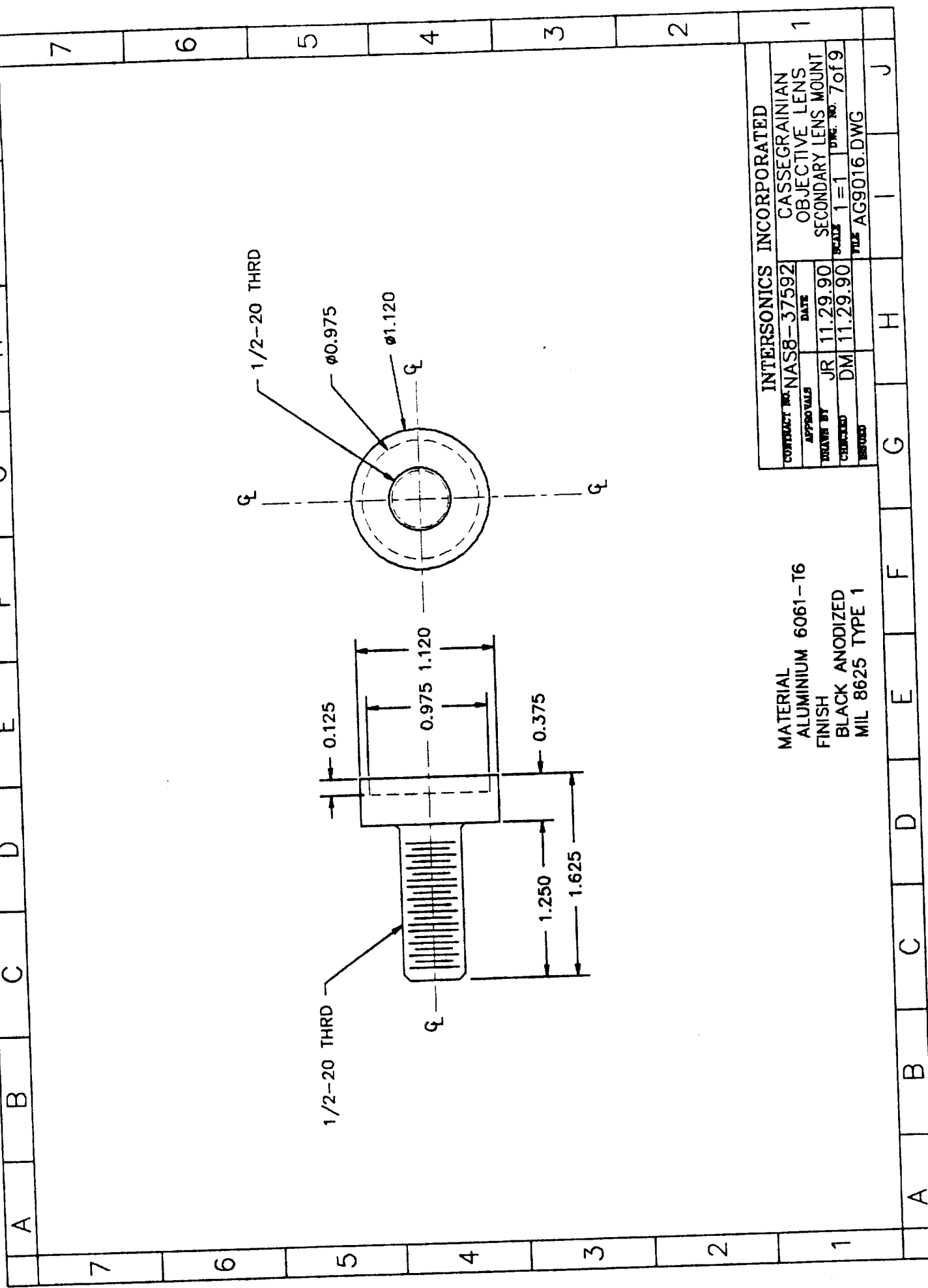
4-40 CLR. THRU,
6 PLCS @ 60° ABOUT CENTER

MATERIAL
ALUMINIUM 6061-T6
FINISH
BLACK ANODIZED
MIL 8625 TYPE 1

INTERSONICS INCORPORATED	
CONTRACT NO. NAS8-37592	CASSEGRAINIEN OBJECTIVE LENS MIRROR RETAINING RING
APPROVALS	DATE
DRAWN BY JR	11.29.90
CHECKED BY DM	11.29.90
ISSUED	SCALE 1=2 DWG. NO. 6 of 9
	FILE AG9016.DWG

A B C D E F G H I J

7 6 5 4 3 2 1

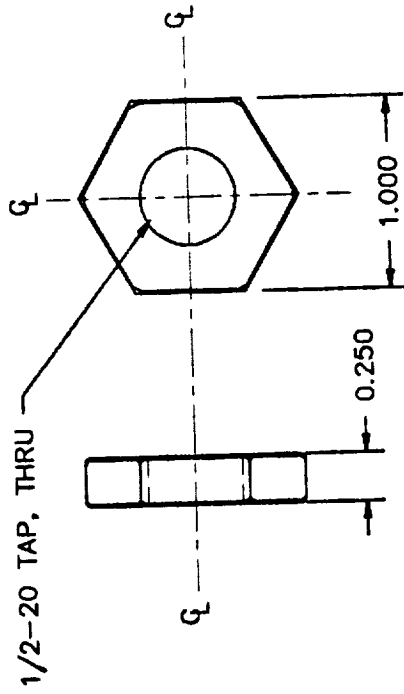


MATERIAL
ALUMINIUM 6061-T6
FINISH
BLACK ANODIZED
MIL 8625 TYPE 1

INTERSONICS INCORPORATED	
CONTRACT NO. NAS8-37592	CASSEGRAINIEN OBJECTIVE LENS SECONDARY LENS MOUNT
APPROVALS	DATE
JR	11.29.90
DM	11.29.90
CHECKED	SCALE 1=1 DWG. NO. 7 of 9
ISSUED	TITLE AG9016.DWG

A B C D E F G H I J
7 6 5 4 3 2 1

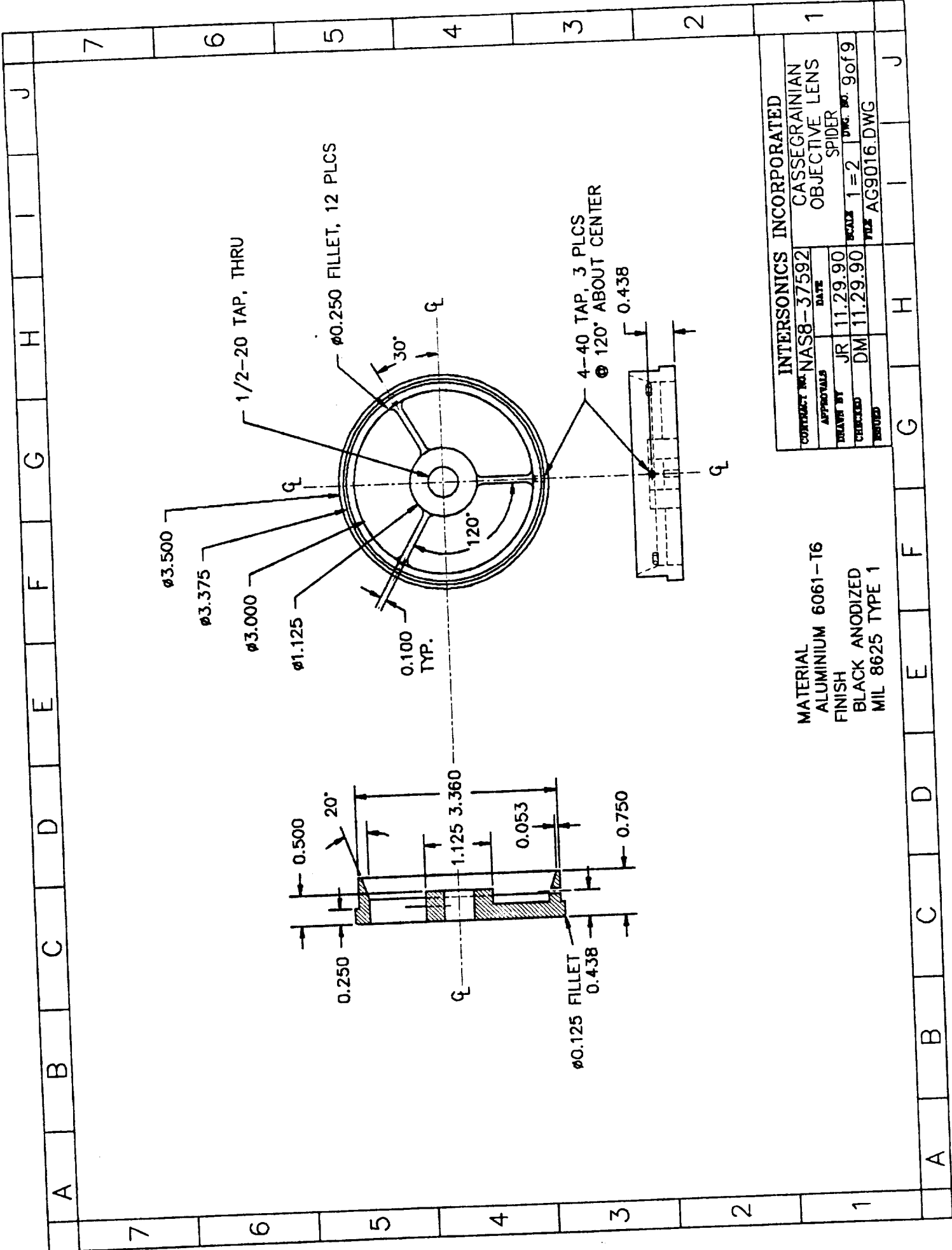
	A	B	C	D	E	F	G	H	I	J
7										
6										
5										
4										
3										
2										
1										
	A	B	C	D	E	F	G	H	I	J



MATERIAL
ALUMINIUM 6061-T6
FINISH
BLACK ANODIZED
MIL 8625 TYPE 1

INTERSONICS INCORPORATED

CONTRACT NO. NAS8-37592	CASSEGRAINIAN	
APPROVALS	DATE	OBJECTIVE LENS
BY JR	11.29.90	LOCKING NUT
CHECKED DM	11.29.90	SCALE 1=1
REVISED		DWG. NO. 8 of 9
		FILE AG9016.DWG



MATERIAL
ALUMINIUM 6061-T6
FINISH
BLACK ANODIZED
MIL 8625 TYPE 1

INTERSONICS INCORPORATED

CONTRACT NO. NAS8-37592		DATE	
APPROVALS	JR	11.29.90	
DELIVER BY	DM	11.29.90	
CHECKED			SCALE 1=2 DWG. NO. 9 of 9
DESIGNED			FILE AG9016.DWG

CASSEGRAINIAN
OBJECTIVE LENS
SPIDER

A B C D E F G H I J

7 6 5 4 3 2 1

A B C D E F G H I J

TEST AND CALIBRATION FACILITIES

- 1) Complete AGEMA system including:
 - 2- AGEMA Model 870 scanner heads, #'s 4150, 4154
 - 1- AGEMA 800 V control unit
 - 1- TIC 8000 computer
 - 1- Polaroid video freeze frame recorder
 - 1- Panasonic Model NV 180 video cassette recorder
 - 1- Sony Model PVM-1390 trinitron video monitor
 - 1- Canon Model PJ-1080A printer
 - 1- AGEMA Infrared lens 20° sw
 - 1- AGEMA Infrared lens 7° sw

- 2) Pyrometer Instrument Co, Inc. Micro-optical pyrometer, NIST traceable
- 3) Mikron M300 blackbody source, calibrated against the above pyrometer
- 4) Mikron M900 1.1-1.65 micron digital infrared pyrometer, calibrated against Mikron M300 blackbody source
- 5) K type Thermocouple and Omega 115KC Digital Thermometer calibrated against Mikron M300
- 6) Rapid systems R350 spectrum analyzer/storage oscilloscope
- 7) Tektronix 2465 300 MHz oscilloscope
- 8) Dual Zone Chamber Mock-up assembly
- 9) Miscellaneous laboratory and test equipment

APPENDIX C

NCTM BRASSBOARD

SPECIFICATIONS

PRINTED WIRE ASSEMBLIES

Mechanical Assembly (MA)

Size 6.25 x 12 (DPM MA Compatible)
Power Requirements + 12 VDC @ 1.07 A (Transient)
(includes power to scanner) + 12 VDC @ 630 ma (Steady State)
..... - 12 VDC @ 120 ma
..... + 5 VDC @ 890 ma
Inputs Differential Video @ 25 fps
..... Horizontal and Vertical Sync
..... TE Cooler Temperature
..... MA Bus Interface
..... Differential Video
Outputs Differential Horizontal & Vertical Sync
..... TE Cooler Regulator Current
..... MA Bus Interface

Controller Assembly (CA)

Size 9.35 x 8.65 (DPM CA Compatible)
Power Requirements + 12 VDC @ 35.6 ma
..... - 12 VDC @ 46.4 ma
..... + 5 VDC @ 200 ma
Inputs Differential Video
..... Horizontal & Vertical Sync
..... CA Bus Interface (Multibus I)
..... Datel ADS112MC 12 bit A/D Converter
Video Digitizer 228 kHz (asynchronous)
Conversion Rate 100 H x 100 V 65 x 70 Visible
Pixel Resolution 4 pole, 91 kHz Low Pass
Anti-aliasing Filter

APPENDIX D



SPECIFICATIONS - continued

Controller Assembly (CA) continued

Outputs Digitized video and interleaved data
transmitted serially @ 4.166 MHz (max)
CA Bus Interface
73 dB

System Electrical S/N Ratio

THERMAL IMAGING DEVICE AGEMA 870
(See Appendix A)

OBJECTIVE OPTICS

Size 7" L x 3.5" Dia.
(See Appendix B)
Cassegranian

Type
7.9

f# Canon FD Bayonet

Mounting 254 mm to 424 mm (390 nominal)

Focal Range 15.3 mm(H) x 16.0 mm (V)

Field of View 237 μ (H) x 229 μ (V)

Spatial Resolution (65 pixels x 70 lines)

TEMPERATURE MEASUREMENT CHARACTERISTICS (Blackbody Target)

Resolution 0.35 $^{\circ}$ C*

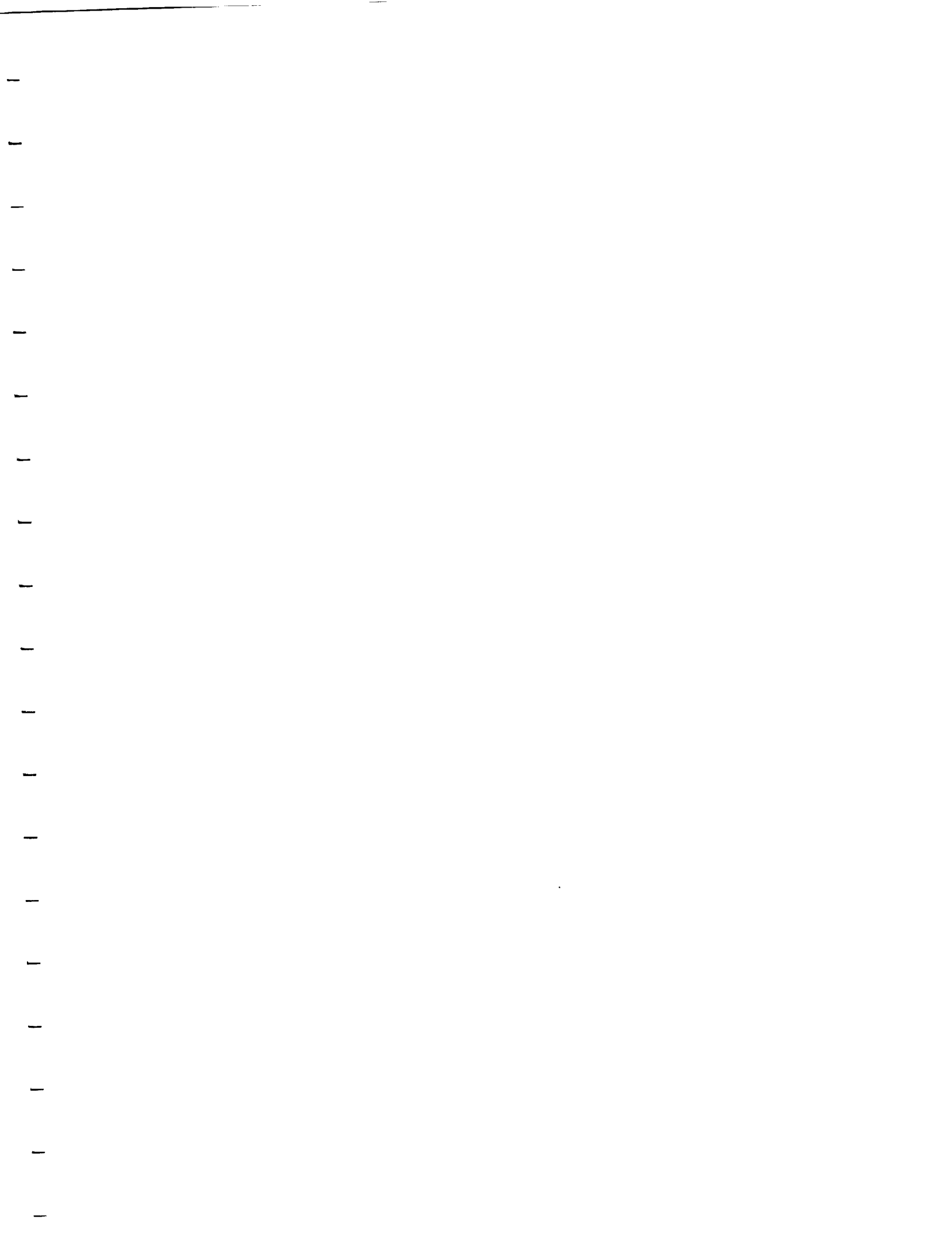
Range 425K to 750K (No filter, Aperture O)
750K to 1600K (3.7-4 Micron Filter,
Aperture O)

* Measured at 800K and 1350K, corrected for periodic error in scanner



INTERSONICS
INCORPORATED

NCTM BRASSBOARD





INTERSONICS
I N C O R P O R A T E D

FINAL REPORT

DIVISION OF AMPLITUDE POLARIMETRIC PYROMETER (DAPP)

Period of Performance January 1 through Dec. 31, 1990

Prepared For: George C. Marshall Space Flight Center
Marshall Space Flight Center
Alabama 35812

Prepared By: InterSonics, Incorporated
3453 Commercial Avenue
Northbrook, IL 60062

Submitted By: Shankar Krishnan
Charles A. Rey
D. Scott Hampton
Paul C. Nordine

Work done under NASA CONTRACT NAS8-37592

PREFACE

Research to develop the Division of Amplitude Polarimetric Pyrometer, DAPP, is described in this report. The purpose of this instrument is to make optical property and temperature measurements in containerless experiments in space. The present NASA-sponsored work was carried out to build, calibrate, and test a breadboard device which will be delivered to NASA.

The report goes beyond the scope of the DAPP work statement because it includes some research on polarimetric techniques carried out with support from Intersonics' internal funds and from an SBIR grant from the National Science Foundation.

Technical questions should be addressed to Dr. Shankar Krishnan, who is the principal author of this report and the principal investigator of Intersonics' R&D on DAPP and other applications of laser polarimetry.

Approved:
Intersonics, Incorporated

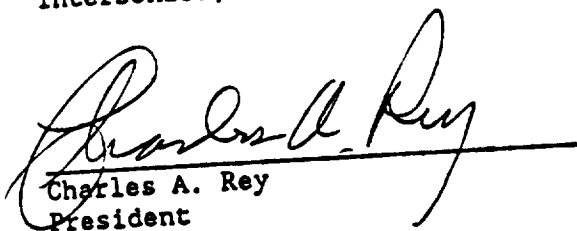

Charles A. Rey
President

TABLE OF CONTENTS

1.	PROJECT SUMMARY	1
2.	RESEARCH OBJECTIVES	2
3.	TECHNICAL APPROACH	2
3.1.	BACKGROUND	3
3.2.	OVERVIEW OF THE TECHNIQUE	6
3.3.	OVERALL PROTOTYPE INSTRUMENT DESIGN AND DESCRIPTION	6
	3.3.1 Optical System	8
	3.3.2 Electronics	9
	3.3.3 Computer/Software Interface	12
	3.3.4 Polarimetric Data Analysis	
4.	CALIBRATION, TESTING, AND MEASUREMENT USING DAPP	14
4.1.	CALIBRATION PROCEDURE	14
	4.1.1 4-Point Calibration Method	15
	4.1.2 Equator-Poles Calibration Method	17
4.2.	TESTING AT ROOM TEMPERATURE	29
4.3.	ACCURACY	36
4.4.	PRECISION AND REPEATABILITY	39
5.	TECHNICAL FEASIBILITY CONCLUSIONS	39
6.	ACKNOWLEDGEMENTS	43
7.	REFERENCES	44

LIST OF FIGURES

Figure 1	Schematic of DAPP Optical Layout	7
Figure 2	DAPP Detector/Demodulator Circuit	10
Figure 3	Quadrant Detector/Beam Alignment Block Diagram	11
Figure 4	Comparison of Measured and Predicted Values of S1	18
Figure 5	Comparison of Measured and Predicted Values of S2	19
Figure 6	Comparison of Measured and Predicted Values of S3	20
Figure 7	Deviation of Measured S1 From Predictions	21
Figure 8	Deviation of Measured S2 From Predictions	22
Figure 9	Deviation of Measured S3 From Predictions	23
Figure 10	Normalized Detector i1 Response Versus Polarizer Azimuth	25
Figure 11	Normalized Detector i2 Response Versus Polarizer Azimuth	26
Figure 12	Normalized Detector i3 Response Versus Polarizer Azimuth	27
Figure 13	Normalized Detector i4 Response Versus Polarizer Azimuth	28
Figure 20	Histogram Showing Deviation of S1 From Prediction	29
Figure 21	Histogram Showing Deviation of S2 From Prediction	40
Figure 22	Histogram Showing Deviation of S3 From Prediction	41
		42

LIST OF TABLES

TABLE 1	38
TABLE 2	38

1. PROJECT SUMMARY

The primary objective of this program was to develop an instrument to measure, instantaneously, the true surface temperature of freely radiating bodies based on measuring both the spectral emissivity and the apparent temperature (pyrometry) using polarization techniques. The design, fabrication and preliminary testing of the breadboard Division of Amplitude Polarimetric Pyrometer (DAPP) demonstrates the feasibility of this approach. The spectral emissivity is determined by performing time-resolved measurements of all four Stokes vectors of laser light reflected from the target surface. This determines the spectral emissivity and optical constants of the target surfaces in real-time. The instrument has been calibrated and tested at 0.6328 μm . The absolute accuracy of Stokes vector measurement is 0.5 - 1% at 0.6238 μm . The absolute accuracy of spectral emissivity measurements is 0.5%. The DAPP is probably the first absolute thermodynamic temperature and optical property measuring device to be made available.

2. RESEARCH OBJECTIVES

- a. Demonstrate the feasibility of a polarimetric method to measure precisely the spectral emissivity and optical properties of specular and partly specular surfaces. The emissivity measured by the instrument would be used to make corrections to radiometric measurements (made by a conventional pyrometer) to determine the true surface temperatures of freely radiating bodies.
- b. Design, fabricate, calibrate, and test such an instrument for materials processing and optical property measurement in containerless experiments.
- c. Deliver a prototype instrument to NASA for evaluation.

3. TECHNICAL APPROACH

The research completed thus far has addressed the major objectives outlined above. The demonstration of feasibility of the polarimetric technique together with a prototype instrument development has been accomplished and the results will be presented in this report. The ultimate objective of our project is to develop an instrument capable of measuring both the optical properties and the spectral emissivities of freely radiating target surfaces together with a measure of the apparent temperature to obtain the true thermodynamic temperature. We will present, briefly, the scientific basis for the instrument design and the implementation of the design in terms of optics and electronics. The results from calibration, verification and testing procedures are detailed. The feasibility of such an instrument design for measuring emissivity and optical properties is demonstrated.

3.1. BACKGROUND

The measurement of temperature by noncontact radiation thermometry necessitates knowledge of spectral emissivities. However, the temperature and wavelength dependence of spectral emissivities is strongly influenced by the nature of the surface. Factors which affect the spectral emissivity include the degree of surface roughness, the chemical nature of the surface and, finally, its intrinsic optical properties.

The measurement of thermodynamic temperature of radiating surfaces by noncontact radiation thermometry must incorporate spectral emissivity data. Any method that does not incorporate an emissivity measurement together with radiance brightness measurement is prone to large errors. This is particularly true when the surface emissivity is not known or changes with time or temperature.

Traditionally, spectral emissivities are measured by comparing the radiation from a radiating body to that of a blackbody when the two are in thermal equilibrium. A common approach in measuring emissivities of

solids is to drill a hole in the sample and compare its emittance to that of the surrounding material, making the assumption that the hole approximates blackbody conditions. However, this technique does not lend itself to emissivity measurements on liquids which is required in high-precision thermodynamic measurements.

There have been two major approaches to temperature measurement that have attempted to circumvent the emissivity problem. The first, and perhaps the most misunderstood one, is multi-wavelength pyrometry (multi-color). Coates [1], Nordine [2], Nordine and Schiffman [3] and McElroy and Fulkerson [4] among others have examined the problem of multi-color pyrometry and conclude that emittance corrections cannot be eliminated by increasing the number of spectral intensity measurements. The second approach uses reflection measurements of laser light to obtain the reflectance of diffuse scattering surfaces thereby inferring the effective emissivity. This approach is severely restricted to diffusely reflecting surfaces.

The new approach developed during this project has been based on earlier studies using ellipsometry and polarimetry of the optical properties of various materials. A detailed account of the emissivity measuring technique and the results have been published and include optical property measurements on solid and liquid Si, Al, Cu, Ag, Au, Ni, Pd, Pt, Zr, Ti, Hf, Nb, Mo, Ir, Ta, and V. [5-12]

3.2. OVERVIEW OF THE TECHNIQUE

The technique involves the measurement of a change in polarization on reflection of light reflected from a sample surface. By measuring the amplitude and phase change of light polarized, both parallel and perpendicular to the plane of incidence, a precise measurement of; 1) spectral reflectivities, 2) spectral emissivities and 3) the optical constants of the surface such as dielectric constants and refractive indices are obtained. A simultaneous measurement of the self emission of the sample then provides the absolute thermodynamic temperatures. According to Wien's approximation to Planck's law, the flux distributions from a blackbody per unit solid angle can be written as a function of wavelength and brightness temperature:

$$J_{\lambda} = c_1 \cdot \exp \left[\frac{-c_2}{\lambda \cdot T_B} \right] \quad (1a)$$

where C_1 and C_2 are the first and second Planck radiation constant, respectively and J_{λ} is the intensity of radiation from the surface. Eq. 1a has been shown to be accurate to 1% for $T < 2897.8 \text{ umK}$. For a real body with emissivity, ϵ_{λ} , Eq. 1a can be written as:

$$J_{\lambda} = c_1 \cdot \exp\left[\frac{-c_2}{\lambda \cdot T_{Th}}\right] \cdot E_{\lambda, T} \quad (1b)$$

A useful form of Wien's approximation is obtained by taking the ratio of the real-body radiated flux distribution to that of a blackbody. Equating the radiances of the two bodies, we have:

$$\frac{1}{T_{Th}} - \frac{1}{T_B} = \frac{\lambda \cdot \ln[E_{\lambda}]}{c_2} \quad (1c)$$

where T_B is the measured brightness temperature, T_{Th} the thermodynamic (blackbody) temperature, and ϵ_{λ} is the normal spectral emissivity of the real body at the wavelength, λ .

We shall briefly present the fundamental expressions that relate the optical constants of surfaces. Under the assumption that the sample in question is a specular reflector (most liquid metals and alloys and many solids are specular reflectors) we can derive the following relationship relating the reflected intensities with the optical constants of the surfaces in question. Kirchoff's law can be stated as follows:

$$E_{\lambda} + R_{\lambda} = 1 \quad (2)$$

where ϵ_{λ} is the emissivity and R_{λ} is the reflectivity for a specular surface. The subscript denotes the wavelength dependence of these quantities.

From Maxwell's relations, the complex refractive index is defined as:

$$\bar{n} = n - i \cdot k \quad (3a)$$

where n_0 is the refractive index and k is the extinction co-efficient. Likewise, the complex dielectric constant $\bar{\epsilon}$ is defined as:

$$\bar{\epsilon} = \epsilon_1 - i \cdot \epsilon_2 \quad (3b)$$

where ϵ_1 and ϵ_2 are the real and imaginary parts of the dielectric constant respectively. ϵ_1 and ϵ_2 are related to the refractive indices through the following relations:

$$\epsilon_1 = n^2 - k^2 \quad (3c)$$

$$\epsilon_2 = 2 \cdot n \cdot k \quad (3d)$$

If ϵ_1 and ϵ_2 are experimentally determined, then all of the optical constants of the material in question can be obtained. The normal incidence reflectance is then obtained from:

$$R_\lambda = \frac{[n - n_0]^2 + k^2}{[n + n_0]^2 + k^2} \quad (3e)$$

where n_0 is the refractive index of the ambient transparent medium. Using Eq. 2, the emissivity can then be obtained. Simultaneous determination of radiance brightness at the same angle of measurement provides the thermodynamic temperature from Eq. 1c.

Traditionally, ellipsometric and polarimetric techniques have been employed for the measurement of the optical properties in the visible and near infrared. In this approach, the changes in amplitudes and phase of the two orthogonally polarized components of light reflected from the target are measured. However, most ellipsometric designs use moving parts and are not suitable for time-resolved measurements or for monitoring transient events. The present design of DAPP incorporates no moving parts. It is also a "complete polarimeter", i.e., one that measures all four Stokes parameters with no sign ambiguities.

The experimental approach is to illuminate the sample or target surface with light of known polarization, and measure the state of polarization of the reflected light (specular). The instrument measures the Stokes parameters of the reflected light. The magnitude and sign of the Stokes parameters together with the incident polarization are sufficient to provide the ellipsometric parameters Ψ , and Δ , which then give the optical properties of the material in question. An analysis of the Stokes parameter measurement and the equations which govern this are given in Sec. 3.3.4.

3.3 OVERALL PROTOTYPE INSTRUMENT DESIGN AND DESCRIPTION

Intersonics, Incorporated has developed a breadboard Division of Amplitude Polarimetric Pyrometer (DAPP) instrument. Detailed design and testing of this instrument has been performed to demonstrate the proof of concept and feasibility. This device is composed of three distinct modules; 1) the optical system, 2) the electronics, and 3) the computer/controller and interface. A schematic of the optical system is shown in Fig. 1. The optical system includes the laser, source polarization and collimating optics. The remaining part of the optical system includes the light collection and analyzing optics. The electronics consists of analog signal processing modules that condition the signals from the detectors. Additionally, we have incorporated position sensitive detectors to enable accurate alignment of the instrument. A computer performs data acquisition and data reduction in addition to providing the spectral emissivities and optical properties.

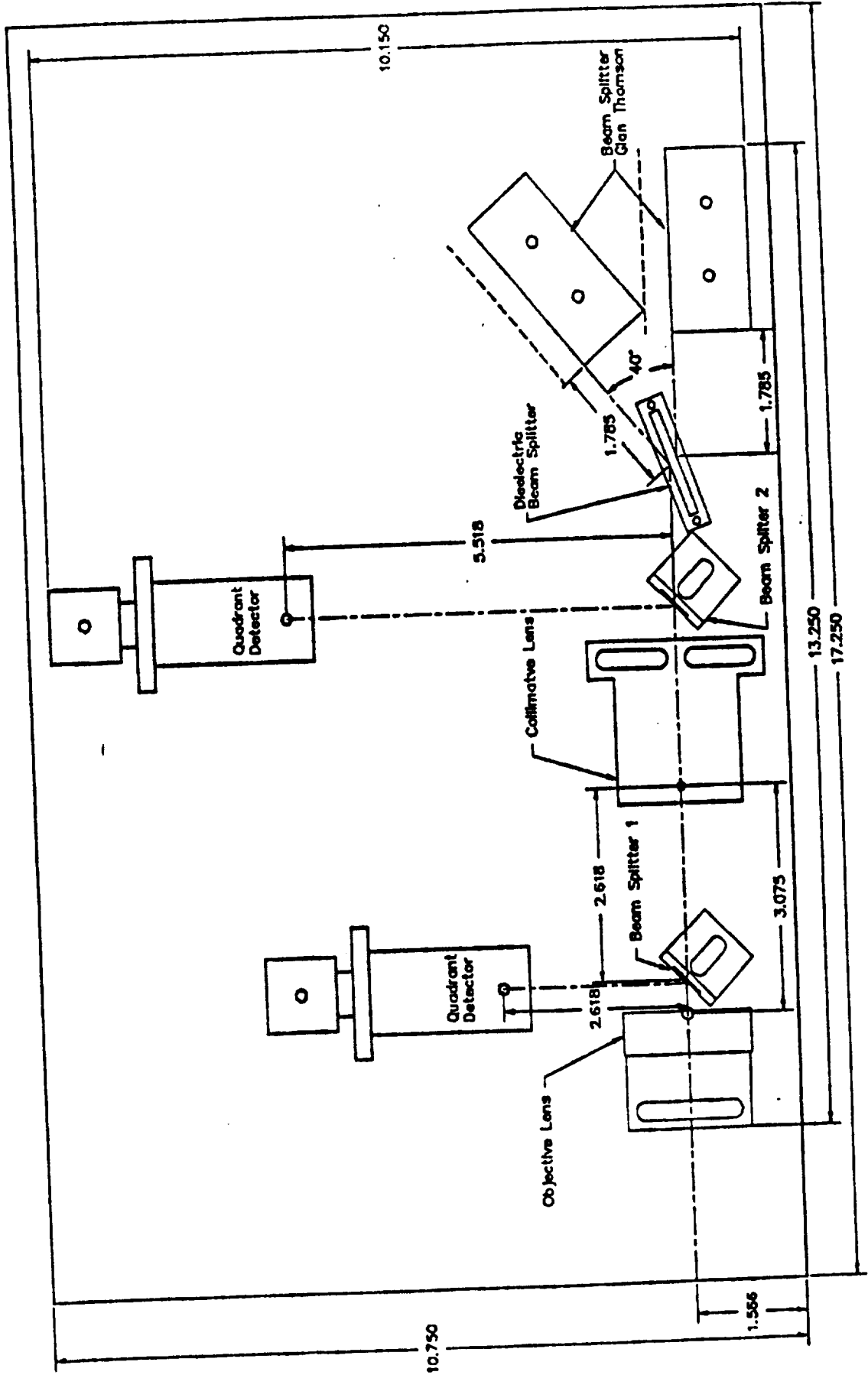
In addition to the optical properties, we must measure the radiant intensity from the sample in order to be able to compute the true surface temperature from Planck's law. This is usually accomplished by measuring the sample self emission over a narrow wavelength band (10 nm) using a radiometer (pyrometer). One of the DAPP designs incorporated the radiometer in the DAPP instrument itself, as a separate detector, with a wavelength band centered around the laser wavelength. Other designs incorporated a separate radiometer (standard pyrometers) at normal incidence also centered at the laser wavelength. Since the normal incidence emissivity is measured by the DAPP, direct correction to the apparent temperature using Planck's law could then be made. If the radiometer viewed the target at the same angle as the DAPP, an angular emissivity was calculated from the optical constants measured by the DAPP using standard expressions. We now present a detailed analysis of the functional components of the instrument that was designed and tested at Intersonics, Incorporated.

3.3.1 Optical System

The optical system consists of a laser, source polarizers, collimating optics, lenses, a coated beamsplitter, and analyzing prisms. The light reflected by the sample is analyzed for its polarization by a special detector arrangement which results in the determination of the Stokes vectors of reflected light. The incident laser source is modulated with the aid of an optical chopper to discriminate it from background radiation. Light that is both reflected and emitted from the sample reaches the polarimeter. The reflected light is used to determine the optical properties.

The polarimeter primarily consists of a beamsplitting, phase shifting coated dielectric. The beam incident is both reflected and transmitted by the dielectric material. The two beams are then analyzed by a total of four detectors, D1-D4, which produce intensities denoted as $i_1 - i_4$. A schematic of the polarimetric assembly is shown in Fig. 1.

Figure 1. Schematic of DAPP Optical Layout



The two beams which are reflected and transmitted by the beamsplitter are incident on two identical Glan Thompson beam splitting polarizers. A total of four beams are produced and the intensity of these four are measured by four individual detectors. Each of the detectors is placed in a metallic housing and a lens is placed in front of each detector to focus the incoming light onto each detector. The analyzer consists of a beam-splitting Glan Thompson prism which produces two beams, the o-beam and e-beam. The e-beam is undeviated and the o-beam is totally internally reflected at 45 degrees to the e-beam.

Two metal coated beamsplitters are also inserted into the optical path. A fraction of the beams are focussed onto two silicon quadrant detectors. The path lengths that the two beams travel are different and the two position signals that are generated from these two detectors are used to align the instrument. Using this approach, it is possible to correct for x-y and tilt-rotation errors while analyzing a reflected beam from the sample and during calibration.

The instrument has two operating modes; Calibration (straight-through) and Measurement mode. This will be discussed further in the section on instrument operation.

3.3.2 Electronics

Several electronics modules were developed to support the needs of the DAPP instrument. These include the signal processing electronics, the alignment electronics and the data acquisition interface.

The signal processing electronics module consists of a.c.-coupled demodulator circuitry that discriminates the modulated laser signal from the background radiation resulting from sample self-emission or background radiation. The output from the analog processing circuitry is supplied to the computer interface. The modulation-demodulation provides high signal-to-noise, and is not affected by extraneous or scattered light.

During our initial investigations, it was determined that the instrument alignment was critical. Displacements of 1 mm produced errors in the Stokes vector measurements. To maintain and detect alignment, additional electro-optical techniques were incorporated. These included two silicon quadrant detectors that received a fraction of the beam using a pair of partially reflecting metal coated beamsplitters. The signal processing from these quadrant detectors included automatic gain control, logarithmic digital L.E.D. display, and a TTL output for the computer interface. When the instrument is aligned the quadrant detectors provide a 5V signal to the computer. When the alignment is not correct, the output from the detectors goes low. A schematic of the detector electronics

designs is shown in Fig. 2. A functional block diagram of the position detection is shown in Fig. 3.

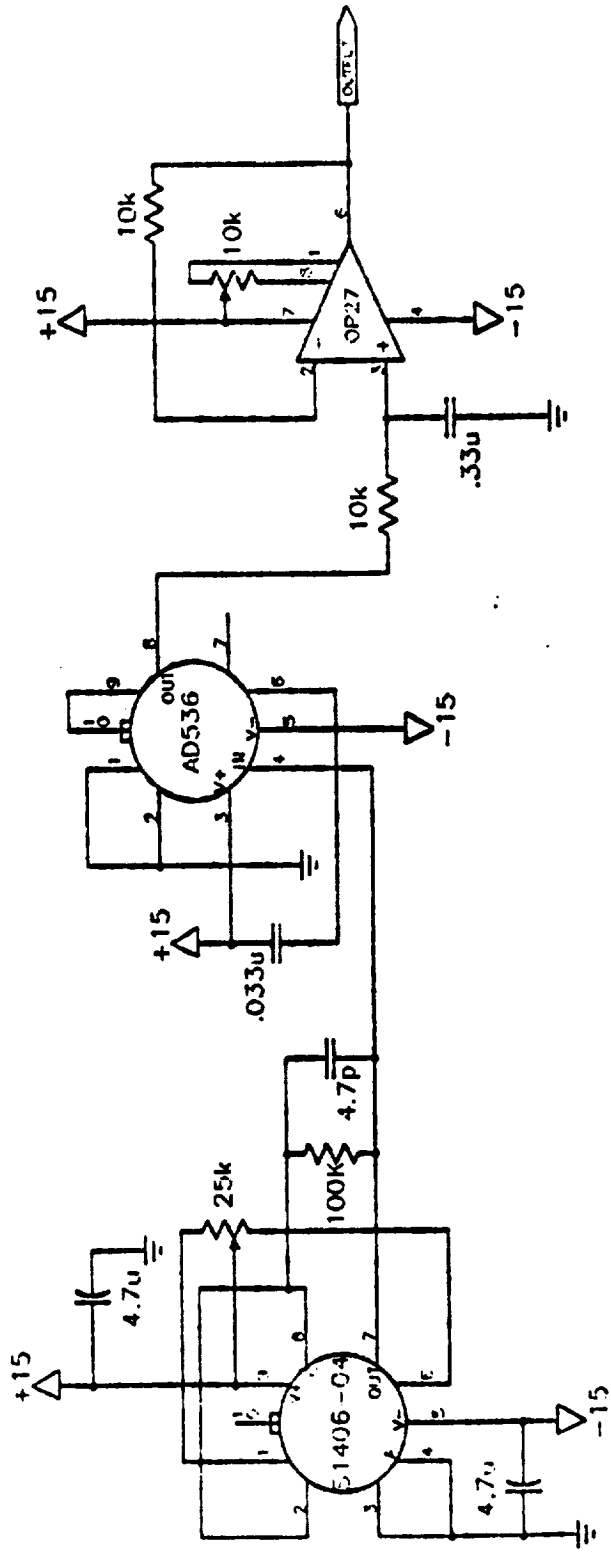
3.3.3 Computer/Software Interface

The computer and software interface includes a laboratory personal computer (Compaq 286), a 16 bit data acquisition board (Strawberry Tree Inc.) and proprietary software to carry out the numerical reductions in the computer. The data acquired by the PC includes four voltages corresponding to the four detector outputs together with an additional signal corresponding to the radiance detector (pyrometer). The outputs of the four detectors together with the calibrated instrument matrix give unambiguously the four Stokes vectors of light reflected by the target sample. If the source polarization is known, then the optical properties of the sample, including the complex dielectric constant, the indices of refraction and the spectral emissivity and reflectivity can be immediately computed. The following section is devoted to outlining the polarimetric system of measurement including the method by which the Stokes vectors of reflected light can be used to measure the material optical properties.

Additional inputs to the computer system include the TTL signals from the alignment detectors. Data are acquired by the computer only when both position detectors provide positive going TTL signals. The data are acquired by the computer, a continuous printout of the measured optical properties and temperature is provided and on-screen display of the same results is provided.

In the following subsection, we provide an analysis of polarized light detection, a definition of the various parameters of interest and the methods by which a measurement of polarized light states is sufficient to determine the optical properties of a sample surface.

DAPP DETECTOR/DEMODULATOR CIRCUIT



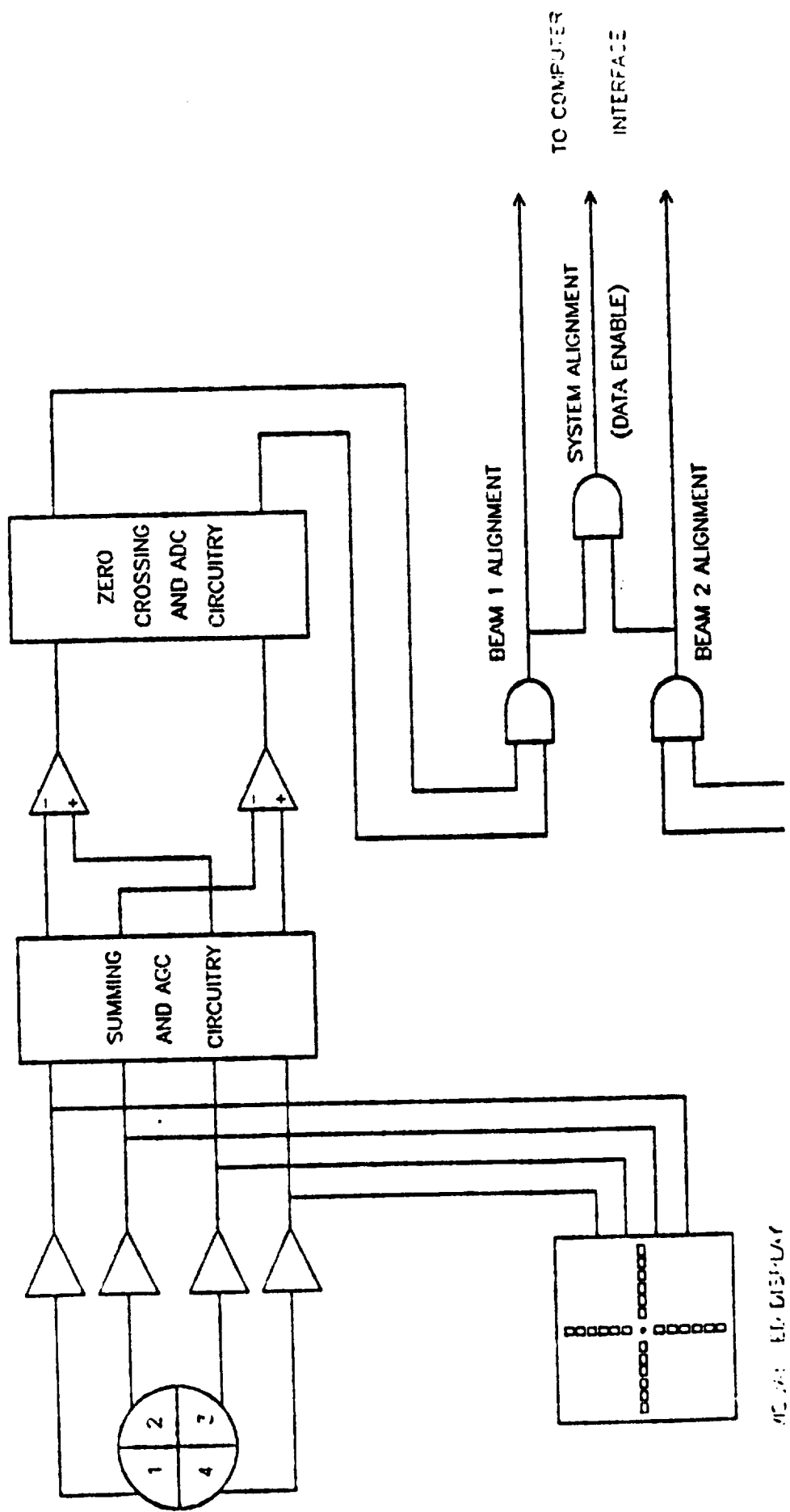
1 POLE FILTER

RMS-TO-DC CONVERTER

FM TO DC CONVERTER/AMP

Figure 2

QUADRANT DETECTOR / BEAM ALIGNMENT BLOCK DIAGRAM



FROM SECOND DETECTOR CIRCUIT

VIDEO DISPLAY

Figure 3

3.3.4 Polarimetric Data Analysis

The most general representation of a polarized state is the Stokes vectors or the Stokes parameters. They are related to the azimuth α and ellipticity χ of the polarized component, the degree of polarization p , and the overall intensity I by the following: [13,14]

Stokes Vectors $[S_0, S_1, S_2, S_3]^T$:

$$S_0 = I \quad (4a)$$

$$S_1 = S_0 \cdot p \cdot \cos(2\chi) \cdot \cos(2\alpha) \quad (4b)$$

$$S_2 = S_0 \cdot p \cdot \cos(2\chi) \cdot \sin(2\alpha) \quad (4c)$$

$$S_3 = S_0 \cdot p \cdot \sin(2\chi) \quad (4d)$$

Polarimetric and Ellipsometric Parameters:

$$I = S_0 \quad (5a)$$

$$p = \frac{\sqrt{S_1^2 + S_2^2 + S_3^2}}{S_0} \quad (5b)$$

$$\alpha = 0.5 \cdot \arctan \left[\frac{S_2}{S_1} \right] \quad (5c)$$

$$\chi = 0.5 \cdot \arctan \left[\frac{S_3}{\sqrt{S_1^2 + S_2^2}} \right] \quad (5d)$$

The ellipsometric sample parameters of interest are Ψ and Δ . In order to determine Ψ and Δ of a target surface, it is necessary to fix the source polarization to some known value. In our studies, we have used laser sources, polarized linearly at +45 degrees to the plane of incidence. Under these conditions, the ellipsometric parameters, Ψ and Δ are given by: [15]

$$\Psi = 0.5 \cdot \arctan \left[\frac{\sqrt{S_3^2 + S_2^2}}{-S_1} \right] \quad (6a)$$

$$\Delta = \arctan \left[\frac{-S_3}{S_2} \right] \quad (6b)$$

These values are then used to compute the complex dielectric constant, the indices of refraction and the spectral emissivity from standard expressions. [5]

The measurement of the Stokes vectors by the instrument can be understood in terms of Muller-Stokes calculus. Let us consider light that enters the DAPP (reflected, emitted, or straight through as in calibration) with Stokes vectors $S = [S_0, S_1, S_2, S_3]^t$, where t stands for the transpose. The response of the DAPP system to light is given by four voltages (intensities), $I_m = [I_1, I_2, I_3, I_4]^t$. The intensity column matrix I_m , is given by the product of the Muller matrix M of the DAPP system times the input Stokes vector S .

$$I = M \cdot S \quad (7a)$$

where I_m is a column vector of intensities, S is a column vector of the unknown (or incoming) Stokes parameters, and M is a 4x4 matrix that is a characteristic of the instrument. If the instrument matrix M is known, then the input or unknown Stokes vector can be calculated from the inverse relationship:

$$S = M^{-1} \cdot I \quad (7b)$$

The instrument matrix can be computed numerically by multiplying the products of the Muller matrices of all the elements in the system. However, such a cumbersome process can be circumvented by illuminating the instrument with known Stokes states and determining the response. In general, a set of four linearly independent states such as three linearly polarized states and one circularly polarized state can be used. However, from the point of view of accuracy, substantially more complicated calibration procedures have to be used. A discussion of the calibration procedure is outlined in the section on calibration.

4. CALIBRATION, TESTING, AND MEASUREMENT USING DAPP

The subsections 4.1 - 4.5 will describe the calibration procedure and results of tests with the DAPP. These sections deal with the measurement of the Stokes parameters, the spectral emissivity and optical constants.

4.1 CALIBRATION PROCEDURE

As stated in Sec. 3.3.4, the aim of the calibration procedure is the determination and verification of the Muller matrix of the DAPP instrument. Two different calibration procedures were outlined by Azzam [16-18], both of which were implemented in the work on DAPP. Each of the calibration procedures involves introducing states of known polarization into the DAPP, and determining the response. These states must however, be linearly independent, i.e., all of the states cannot lie on the same latitude on the Poincare sphere. A practical way to generate four states is to use a combination of a linear polarizer followed by a quarter wave retarder (or compensator). Under these conditions, the incident Stokes parameters are given by: [16]

$$S_0 = 1 \quad (8a)$$

$$S_2 = \frac{1}{2} \cos(2 \cdot P) + \frac{1}{2} \cos(4 \cdot C - 2 \cdot P) \quad (8b)$$

$$S_3 = \frac{1}{2} \sin(2 \cdot P) + \frac{1}{2} \sin(4 \cdot C - 2 \cdot P) \quad (8c)$$

$$S_4 = \sin(2 \cdot C - 2 \cdot P) \quad (8d)$$

where P represents the azimuth of the polarizer and C represents the retarder fast axis orientation.

The DAPP was placed in a Calibration (straight-through) mode by allowing the laser light to enter directly into the entrance pupil of the device.

The light first passed through a Glan Thomson linear polarizer, followed by a Mica quarter wave plate. The zero reference of the polarizer was established outside the frame of reference of the DAPP. The zero of the retarder was established by crossing two polarizers and inserting the retarder in between and preserving the extinction. The fast axis was then identified based on the polarizer zero.

Since we anticipated carrying out hundreds of calibration and verification tests involving the rotation of the polarizers and retarders, we automated the rotation of the polarizers and retarders. This was accomplished with the use of two rotary stepper motor stages (Oriel model #13049) together with a stepper motor controller (Oriel model #20010). These were driven from the computer program via the asynchronous communication port at 2400 baud. Rotation of the components was required during the calibration phases and during the verification phases of the testing of the instrument.

Azzam has discussed both the calibration procedures employed in several publications [16-18]. The first procedure is referred to as the 4-point calibration and the second is called the equator-poles calibration method.

The basic approach of both calibration techniques is essentially as follows: if the polarimeter is illuminated with four linearly independent states, one obtains a 4x4 matrix (S_m) of Stokes vectors corresponding to which we have a 4x4 matrix of voltages (I_m). The columns of the Stokes matrix S_m are the Stokes vectors of each state, and the response voltages are also arranged by columns. The response of the polarimeter to input Stokes states is given by the equality:

$$I_m = M \cdot S_m \quad (9a)$$

where I_m is the 4x4 response matrix, S_m is the input Stokes matrix, and M is the instrument Muller matrix which we want to evaluate. Eq. 9a can be rewritten as:

$$M = I_m \cdot S_m^{-1} \quad (9b)$$

4.1.1 4-Point Calibration Method

This calibration procedure, as the name implies, uses exactly four linearly independent input states to calibrate the polarimeter. The mathematical basis for this procedure is exactly represented by Eq. 9b. A set of four carefully chosen states on the Poincare sphere [16] provide the constituents of S_m , and M is readily evaluated.

Let the four states be represented by four points on the Poincare sphere. The best choice of states is the four points on the vertices of a tetrahedron inscribing the largest volume. This optimum selection results in choosing the vertices of an equilateral triangle inscribed in a circle of latitude distance of 1/3 below the plane of the equator of the unit radius of the Poincare sphere. These three states have an ellipticity of -9.736 degrees with an axial ratio of 0.1716 and are 60 degrees apart in azimuth. The last calibration state is the vertex of the tetrahedron representing the right circular state. These criteria result in the following azimuth pairs for (P,C) = (0,45), (10,0), (-50, -60), and (70,60).

During the development of this instrument, we performed several hundred calibration and verification experiments. The verification procedure was based on using the same optical train of the polarizer and retarder and determining the accuracy and precision of the DAPP to correctly predict the Stokes parameters, i.e., one could test if the instrument could accurately measure known Stokes states (states other than those used for calibration). In practice, this could be accomplished in several ways. By rotating the quarter wave retarder, and fixing the polarizer at zero, a continuum of linear, circular and elliptical states could be obtained. Presented below is an example of our calibration procedure. For laser light at 0.6328 μm , we present some results below.

For the states listed above, S_m is:

$$S_M = \begin{bmatrix} 1 & 0 & 0 & 0 \\ 0 & 0.940 & -0.470 & -0.470 \\ 0 & 0 & -0.814 & 0.814 \\ 1 & -0.342 & -0.342 & -0.324 \end{bmatrix} \quad (9c)$$

In one of our tests using the four point approach, we obtained the intensity matrix I_m as:

$$I_m = \begin{bmatrix} 0.4145 & 0.0213 & 0.4377 & 0.3499 \\ 0.2411 & 0.1054 & 0.4582 & 0.6000 \\ 0.1750 & 0.3271 & 0.2574 & 0.0355 \\ 0.2161 & 0.3112 & 0.2150 & 0.2260 \end{bmatrix} \quad (9d)$$

The instrument Muller Matrix was:

$$M_{4P} = \begin{bmatrix} 0.3053 & -0.2624 & -0.0570 & 0.10911 \\ 0.3505 & -0.3005 & 0.0871 & -0.1094 \\ 0.1975 & 0.1281 & -0.1362 & -0.0270 \\ 0.1939 & 0.1329 & 0.1256 & 0.0222 \end{bmatrix} \quad (9e)$$

To establish that the instrument can now measure the Stokes parameters correctly, we carried out a verification procedure in which we provided a continuum of known Stokes states. These states included linear, circular and elliptical states, similar to those encountered in the case of a sample reflection. In the verification procedure, we fixed the Glan Thomson polarizer at zero and rotated the retarder through 360 degrees. The plots in Figs. 4 - 6 show the predicted behavior indicated by solid lines for the normalized Stokes parameters S_1 , S_2 , and S_3 , while the measurements (in 10 degree intervals) by DAPP are shown by the squares(\diamond).

If the polarizing optics were perfect, then one could plot the error between the measurements and predictions in all three Stokes parameters (Figs. 7 - 9). Here, we have connected all the discrete points to produce a continuous line. As seen in these plots, the absolute error in any Stokes parameter does not exceed 0.04. The average error summed over all possible states is 0.015.

In spite of the greatest care in the calibration and verification procedure, we could not reduce the "error" as defined by the difference between the predicted and measured points in the verification procedure. Initially we attributed this to systematic instrument error but finally determined that it was due to imperfection in the polarizing components of the calibration equipment and not of the instrument. This will be discussed further in this report.

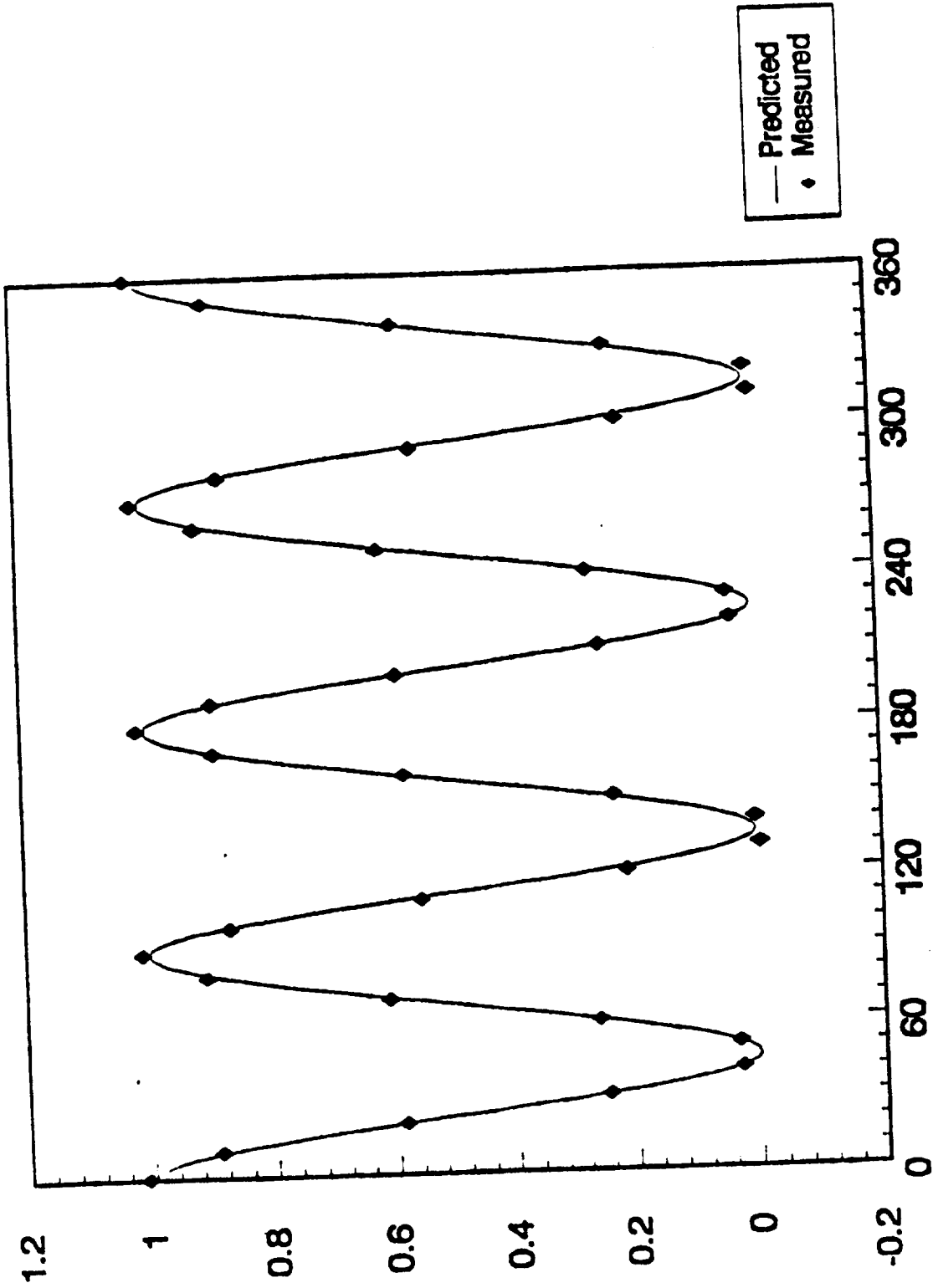
Azzam has discussed imperfections in polarizing elements and suggested the use of the Equator-Poles calibration technique as a means of calibrating a polarimeter. [18,19] We discuss this approach and results from its implementation in our laboratory in the next section.

4.1.2 Equator-Poles Calibration Method

The procedure that we will outline in this section has been reported by Azzam. [18] The basic goal of this calibration procedure is to accurately determine the instrument Muller matrix using an imperfect polarization state generator (PSG). The PSG consists of a linear polarizer and a quarter wave retarder (QWR).

The major imperfections of a PSG are in the retarder. These imperfections have been described well in the literature. [20]

Comparison of measured and predicted values of S1

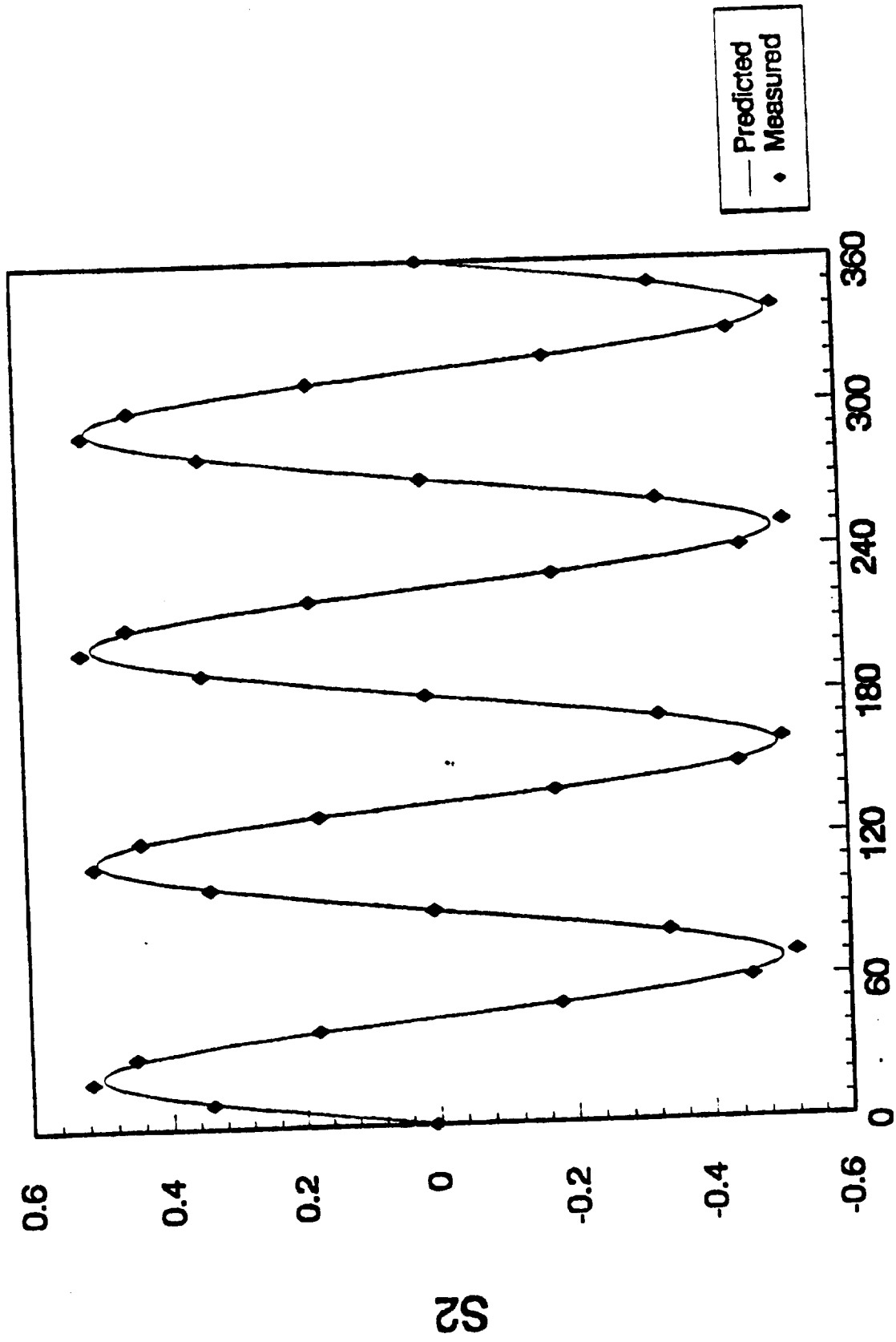


Retarder Fast Axis, C

FIG 4

S1

Comparison of measured and predicted values of S2



Retarder Fast Axis, C

FIG 5

Comparison of measured and predicted values of S3

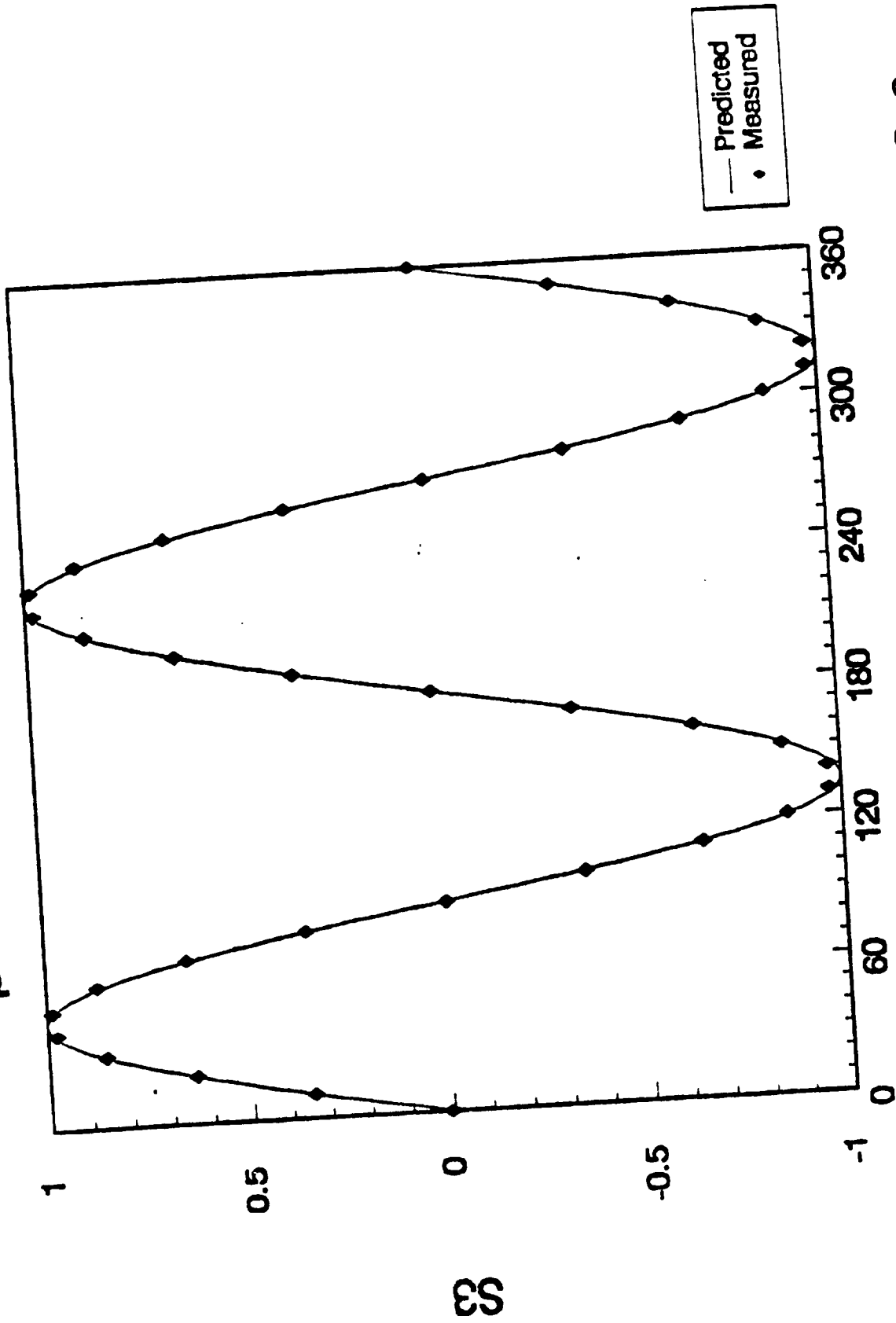
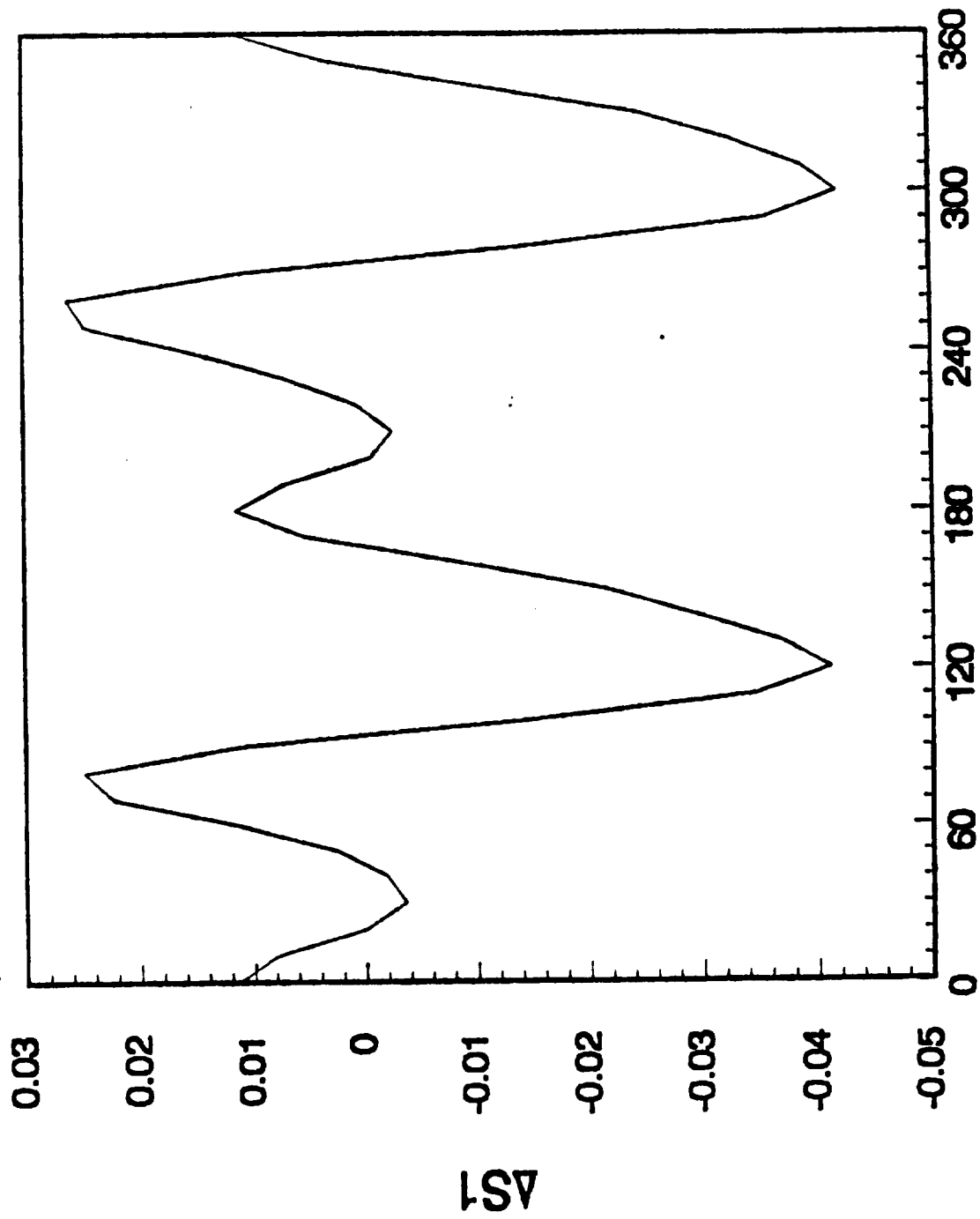


FIG 6

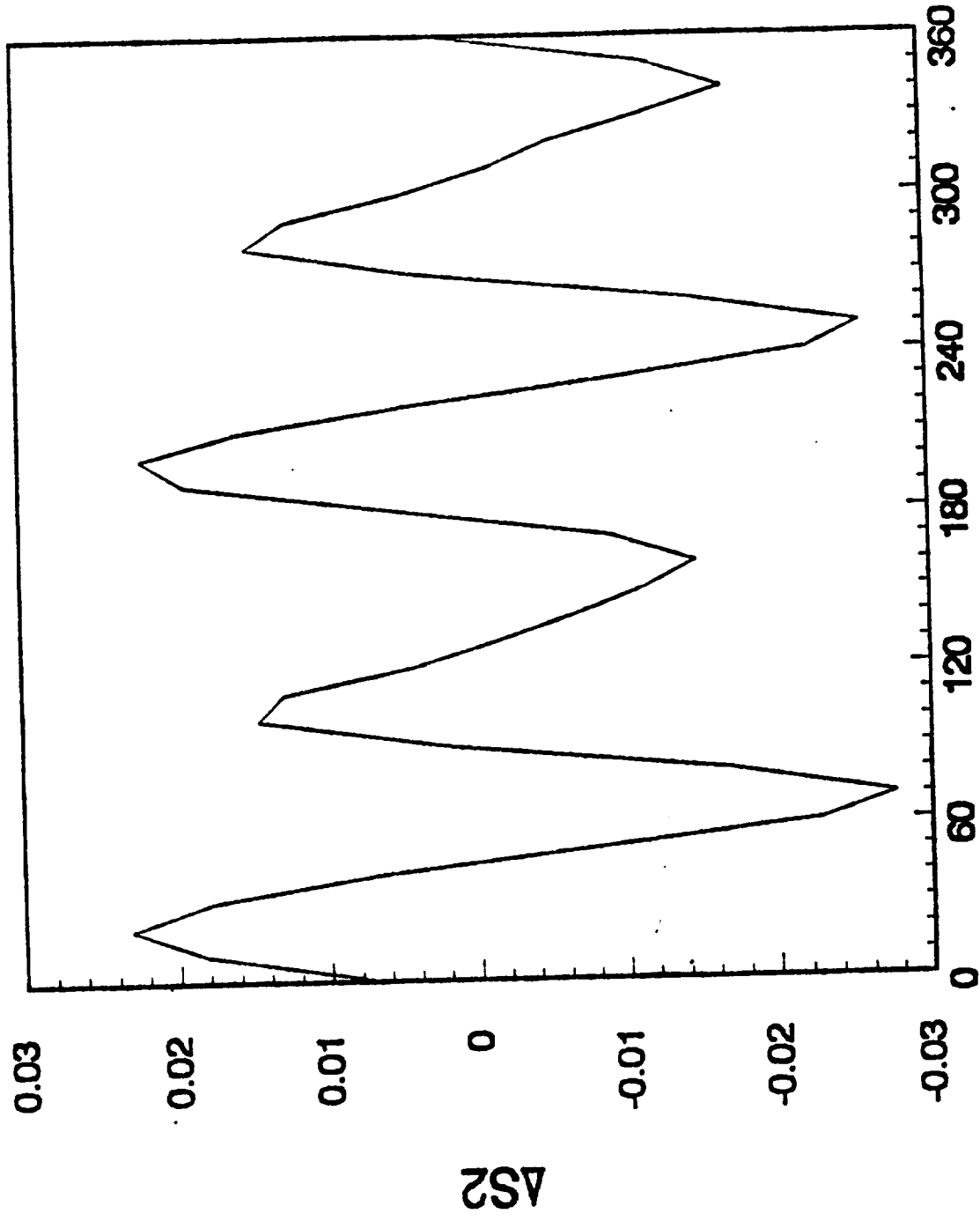
Retarder Fast Axis, C

Deviation of measured S1 from predictions



Retarder Fast Axis, C FIG 7

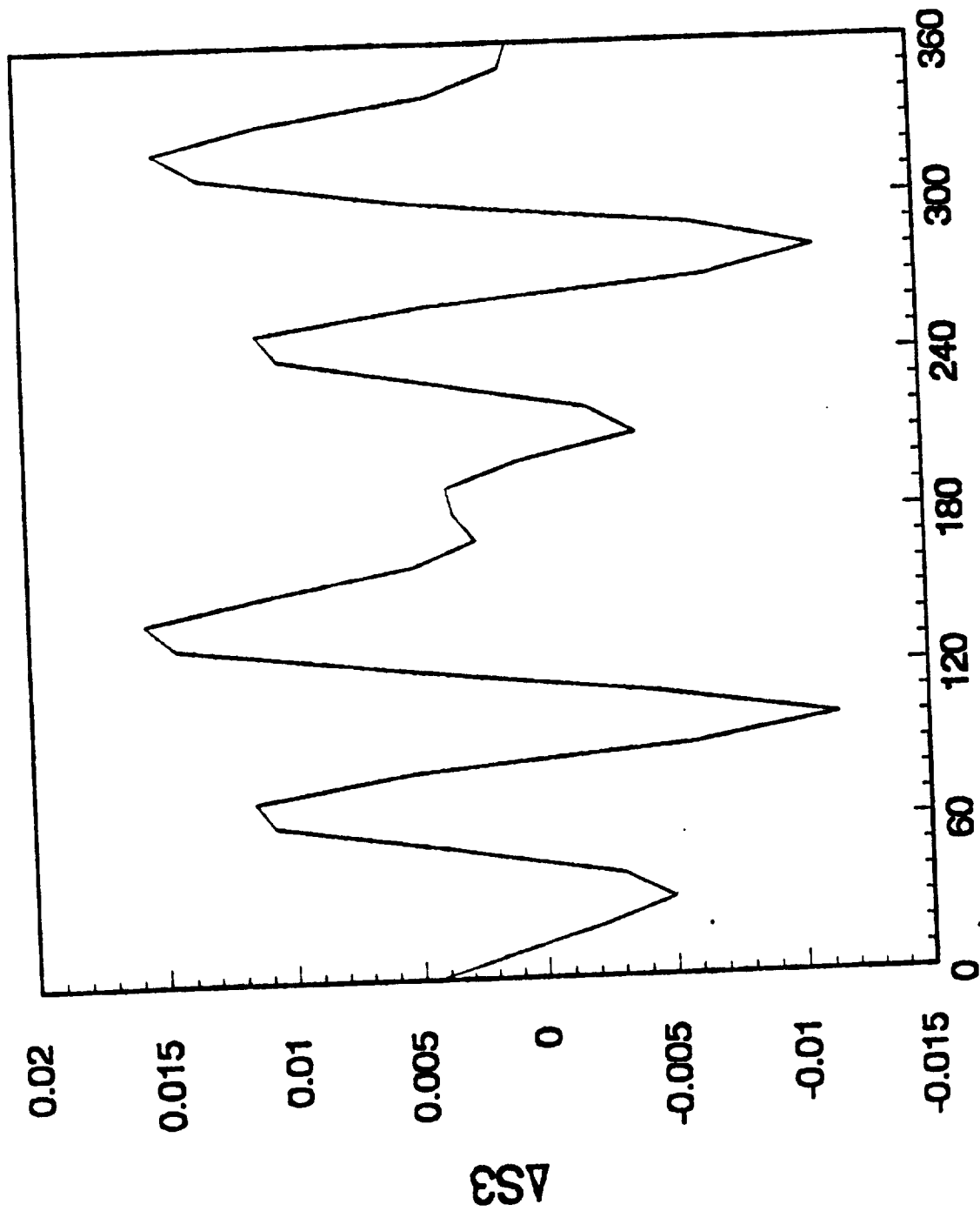
Deviation of measured S2 from predictions



Retarder Fast Axis, C

FIG 8

Deviation of measured S3 from predictions



AS3

Retarder Fast Axis, C

FIG 9

Hence, the determination of M should minimize the use of the QWR as much as possible. If the column vectors of M are written as $[M_0 \ M_1 \ M_2 \ M_3]^t$, a linear polarizer can be used to determine the first three elements of M.

$$M = \begin{pmatrix} M_0 & M_1 & M_2 & M_3 \end{pmatrix} \quad (10a)$$

The Stokes vectors of incident linearly polarized light of azimuth P are given by:

$$S(P) = \begin{pmatrix} 1 & \cos(2 \cdot P) & \sin(2 \cdot P) & 0 \end{pmatrix}^t \quad (10b)$$

The use of Eq. 10a and Eq. 10b gives the response equation:

$$I(P) = M_0 + M_1 \cdot \cos(2 \cdot P) + M_2 \cdot \sin(2 \cdot P) \quad (10c)$$

If the output of DAPP is measured as a function of P (0-180), and the response is fitted to the Fourier series (Eq. 10c), the three Fourier components immediately give the three elements of M. Figures 10-13 give the response of the DAPP to linear polarization. The normalized voltage outputs as a function of polarizer azimuth are plotted in these figures. The continuous curves represent the least squares fit to the data while the solid points are the measured points (in 10 degree intervals).

The measurement of the last element of M requires the generation of the circular polarized state with the use of the retarder. The fourth element is determined by taking the average of the difference in response of the left and right circular states.

$$S(CP) = \begin{pmatrix} 1 & 0 & 0 & \pm 1 \end{pmatrix}^t \quad (11)$$

where + and - apply to right and left circular states respectively. The equation that determines M_3 is:

$$M_3 = \frac{1}{2} [I_{RCP} - I_{LCP}] \quad (12)$$

However, it is practically impossible to generate left and right circular states exactly. Therefore, following Azzam's recommendations, we assume that each left or right state is an elliptical near circular state (ENCS). Rotation of an ENCS around 360 azimuth in 10 degree intervals then yields a more accurate average for the two circular states. The use of Equation 12 then produces the last column of the Muller matrix of the instrument.

Normalized detector i1 response
versus polarizer
Azimuth

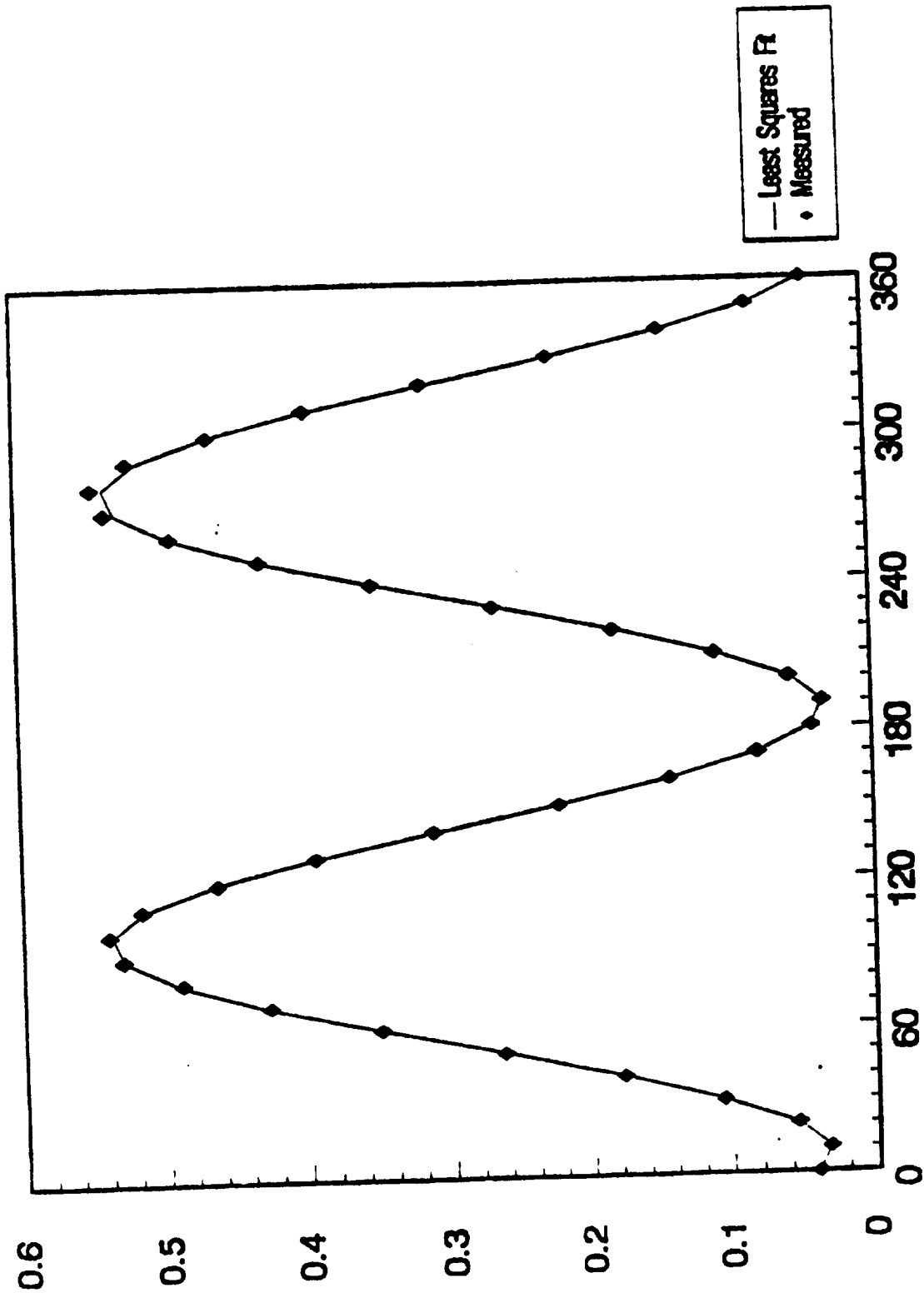
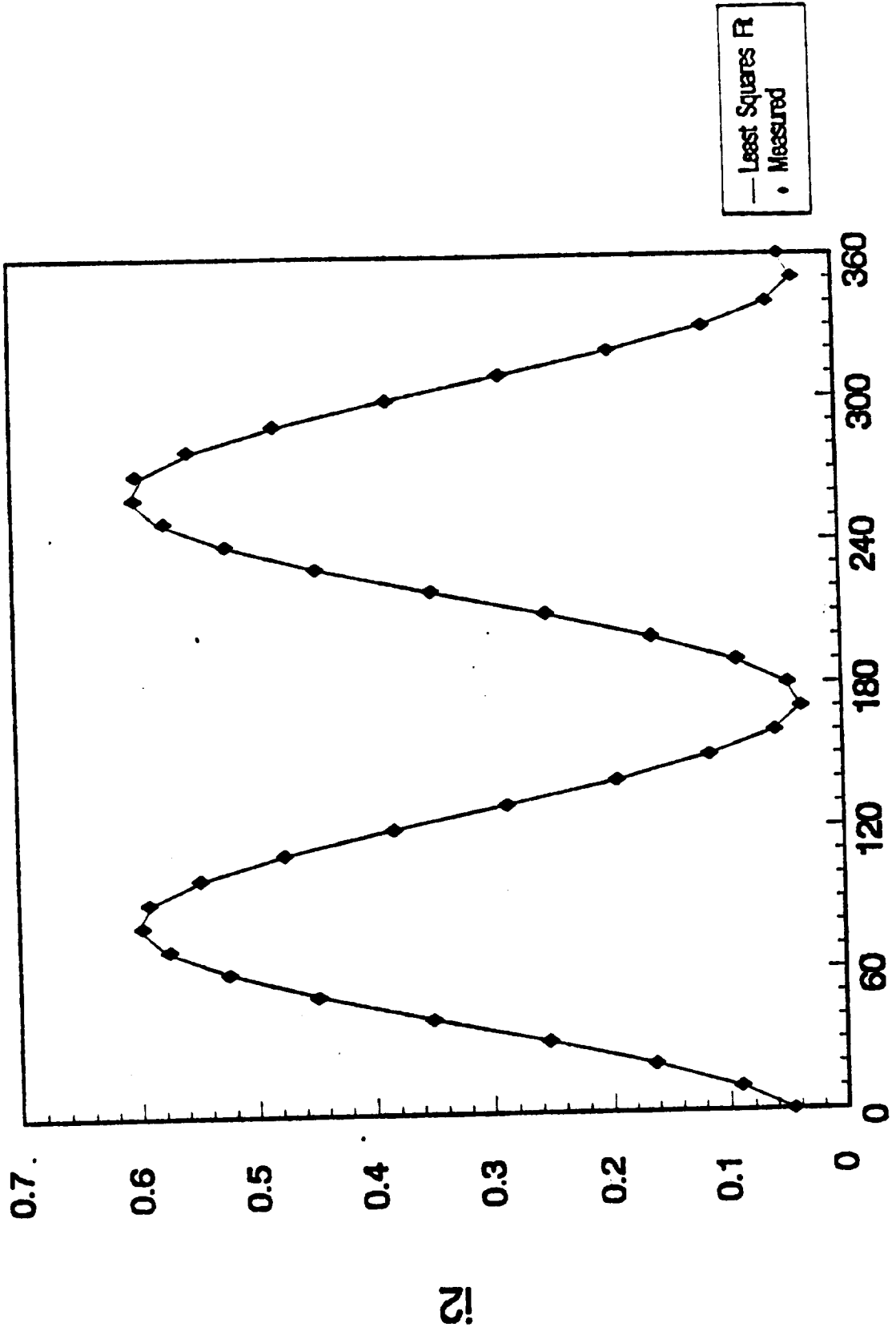


FIG 10
Polarizer Azimuth, P

Normalized detector i2 response
versus polarizer Azimuth



Polarizer Azimuth, P

FIG 11

Normalized detector i3 response
versus polarizer
Azimuth

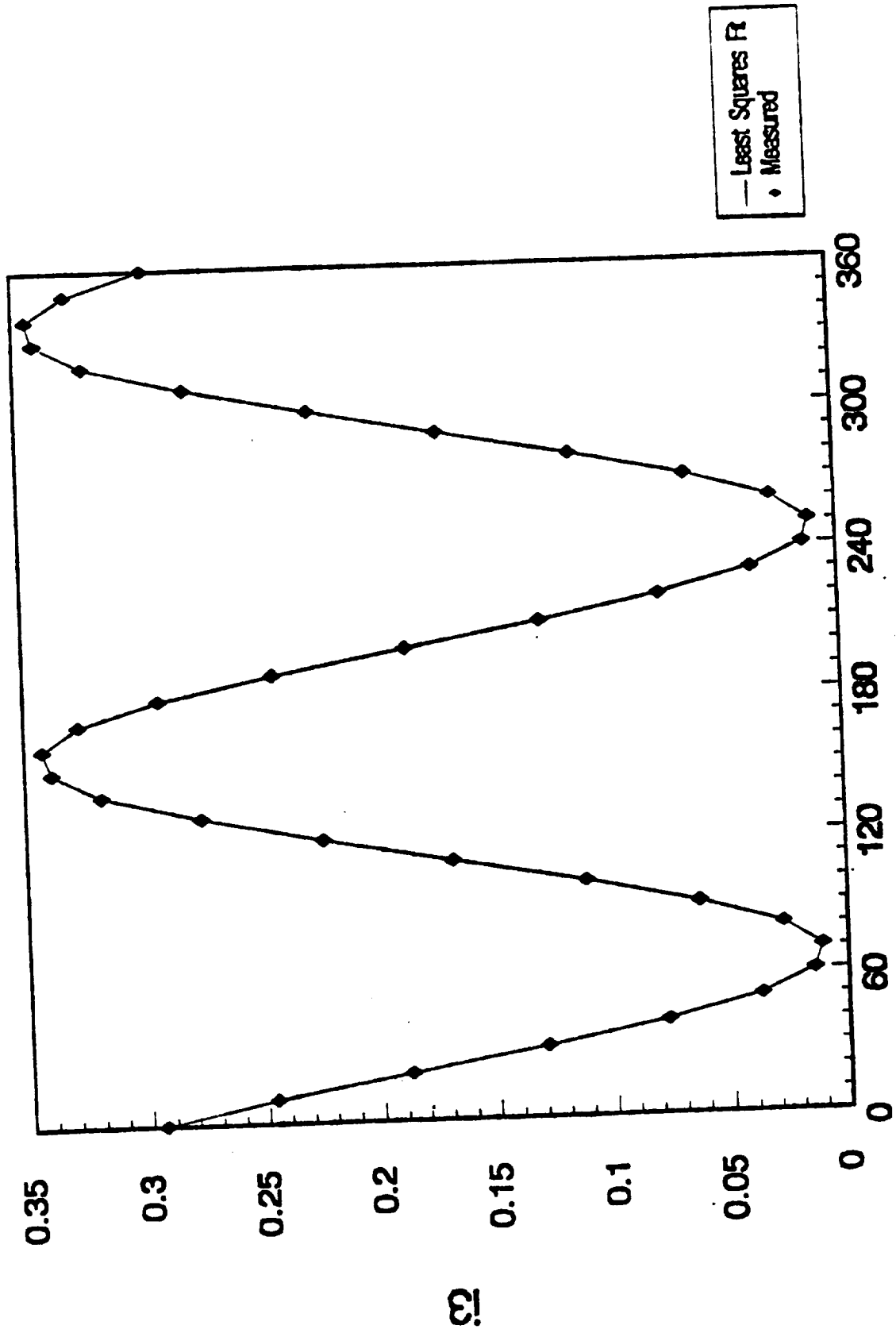


FIG 12

Polarizer Azimuth, P

Normalized detector i4 response
versus polarizer Azimuth

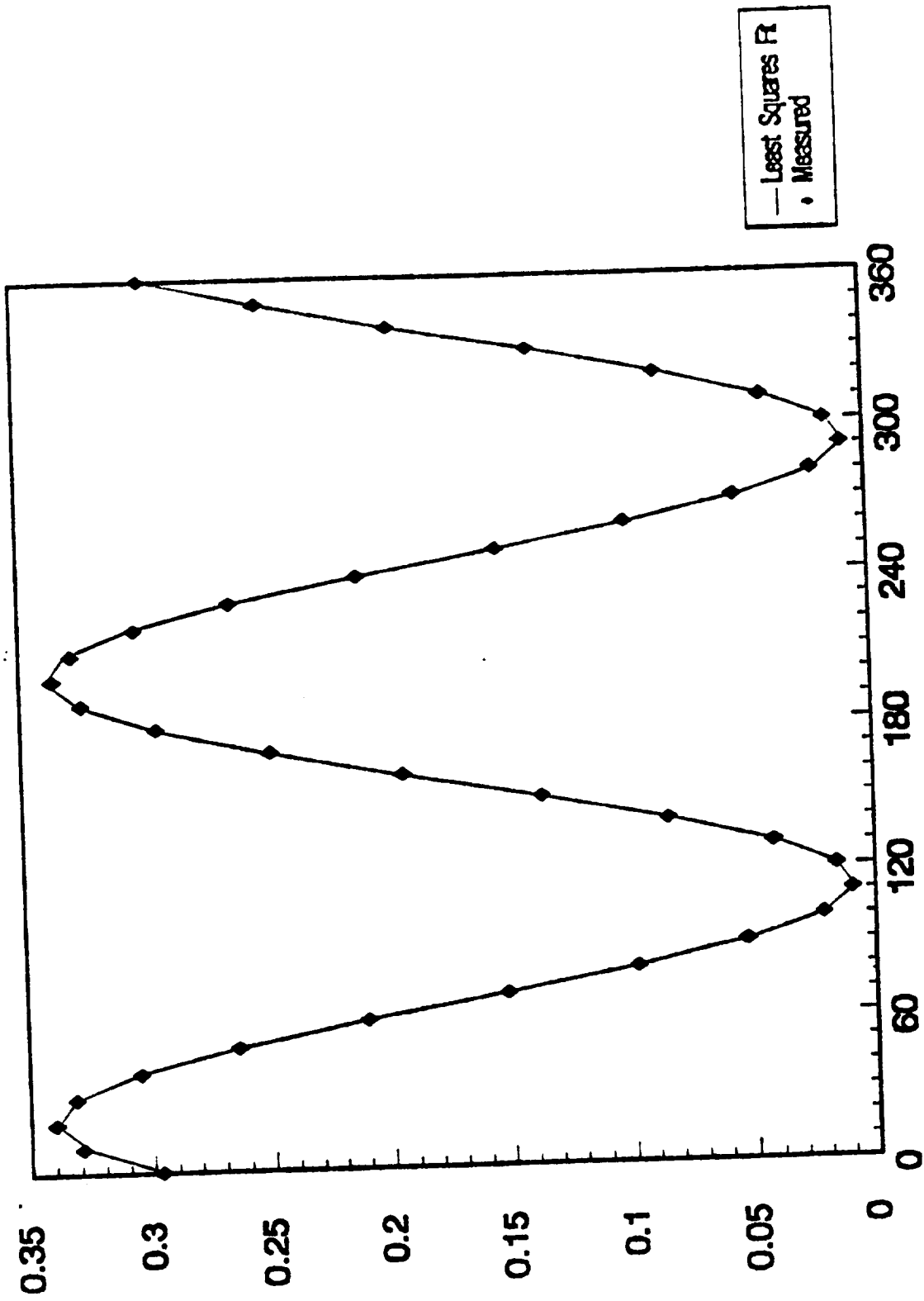


FIG 13
Polarizer Azimuth, P

We now compare the instrument matrix obtained using this approach with that in the previous section. The matrix M, was:

$$M_{E-P} = \begin{bmatrix} 0.2858 & -0.2438 & -0.0670 & 0.1011 \\ 0.3183 & -0.2714 & 0.0813 & -0.1029 \\ 0.1772 & 0.1154 & -0.1211 & -0.0232 \\ 0.1738 & 0.1216 & 0.1216 & 0.0207 \end{bmatrix} \quad (13)$$

This matrix is similar to the matrix obtained by the 4-point technique but differs in some of its elements. The verification procedure outlined in the previous section was utilized to measure known Stokes states. The predicted and measured normalized Stokes parameters S_1 , S_2 and S_3 , as a function of the retarder fast axis are shown in Figs. 14 - 16. The deviation from the predicted Stokes parameters are shown in Figs. 17 - 19. The systematic errors that existed using the previous calibration approach are somewhat reduced. Azzam [18] has stated that any residual differences between prediction and measurement are imperfections in the components and not errors in the system. We have achieved excellent calibration and have done so with an imperfect PSG. Our experiments prove, as does Azzam [18], that the equator-poles calibration procedure does produce superior results. Our estimates in the error analysis section is based on the use of the equator poles technique, and not the 4-point technique.

It may be added that the use of this calibration procedure enables one to produce a nearly perfect polarization state detector (PSD) using an imperfect polarization state generator (PSG).

4.2 TESTING AT ROOM TEMPERATURE

To demonstrate that the instrument does measure the spectral emissivity accurately (and consequently the true surface temperature), we carried out several measurements on bare, polished silicon wafers. The testing of DAPP on materials of known properties has been carried out at room temperature. Test results on clean polished silicon, whose properties are extremely well documented in the literature, are reported here. At 0.6328 μm , the reported values for silicon are $n = 3.840$ and $k = 0.028$. [21]

In these experiments, we first cleaned the surfaces thoroughly with acetone to remove any surface contaminants. Aspnes [22] and Vedam [23] have discussed contamination by oxide films and its effect on the complex dielectric function of silicon. In order to remove films from the surface, we used a solution of 5% hydrofluoric acid in water. Measurement of the Stokes parameters and the complex index of refraction were carried out immediately following the removal of the surface oxide. The angle of incidence used was 70 degrees, and an average of 500 measurements were taken by the computer.

Comparison of measured and predicted values of S1

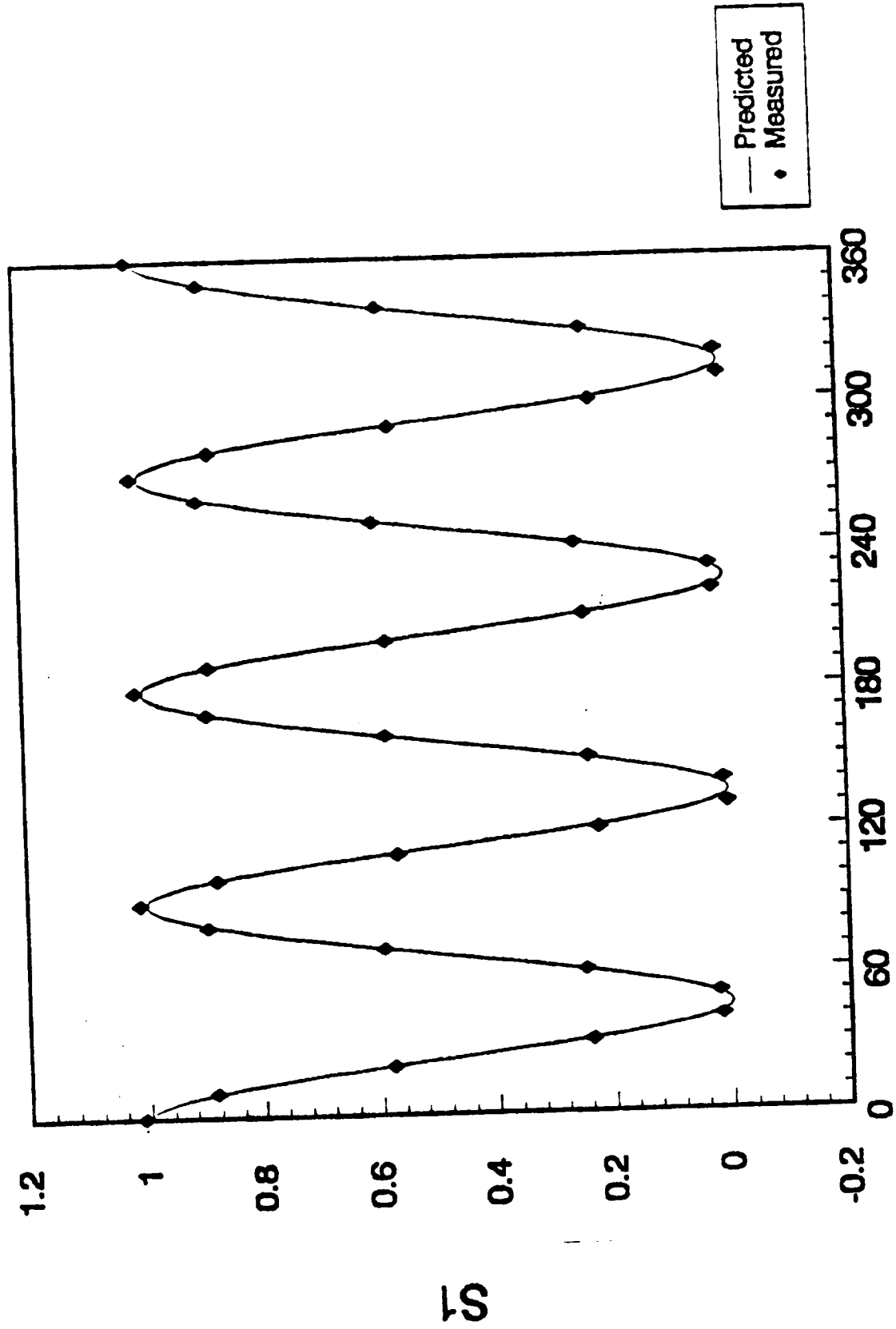
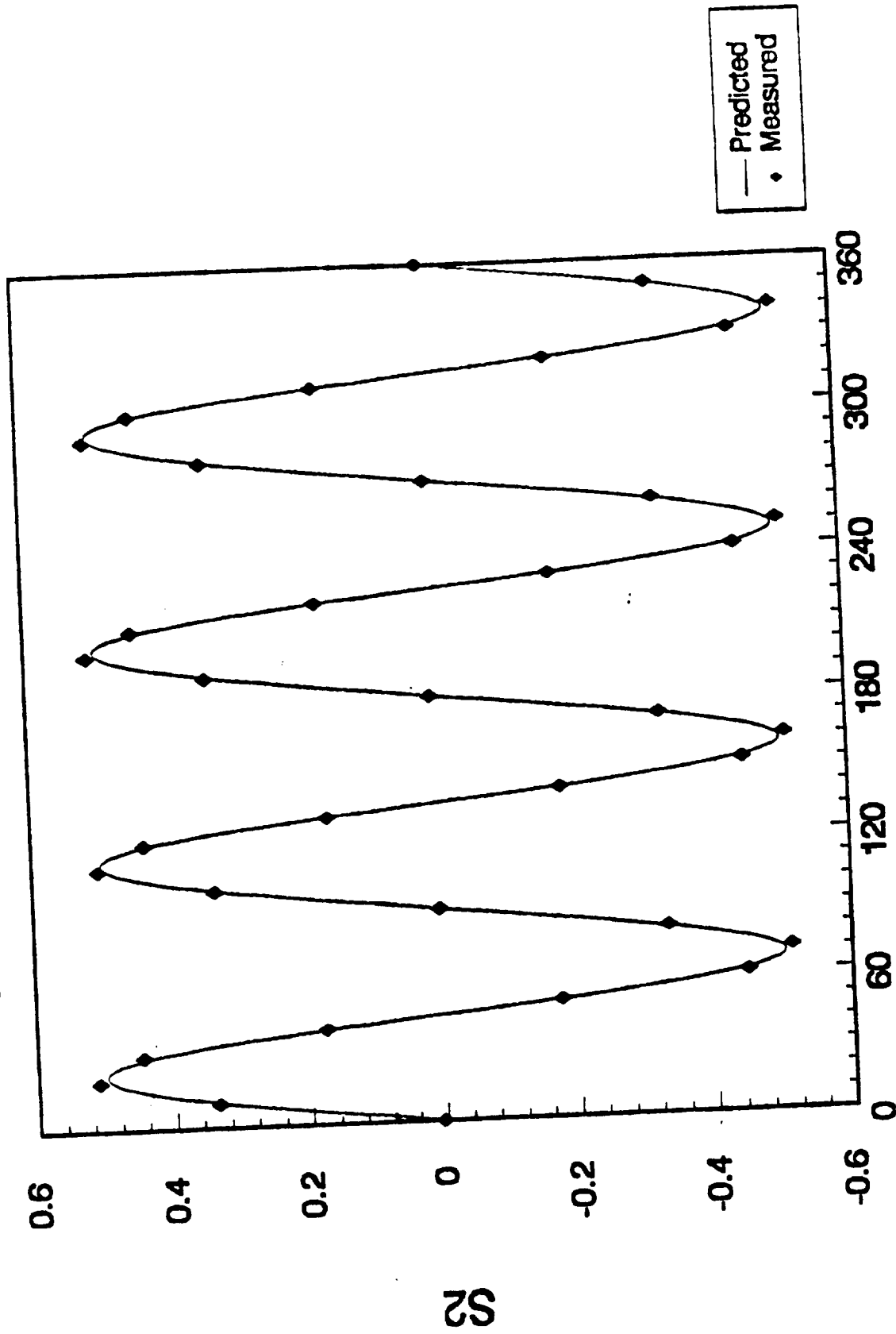


FIG 14
Retarder Fast Axis, C

Comparison of measured and predicted values of S2



Retarder Fast Axis, C

FIG 15

Comparison of measured and predicted values of S3

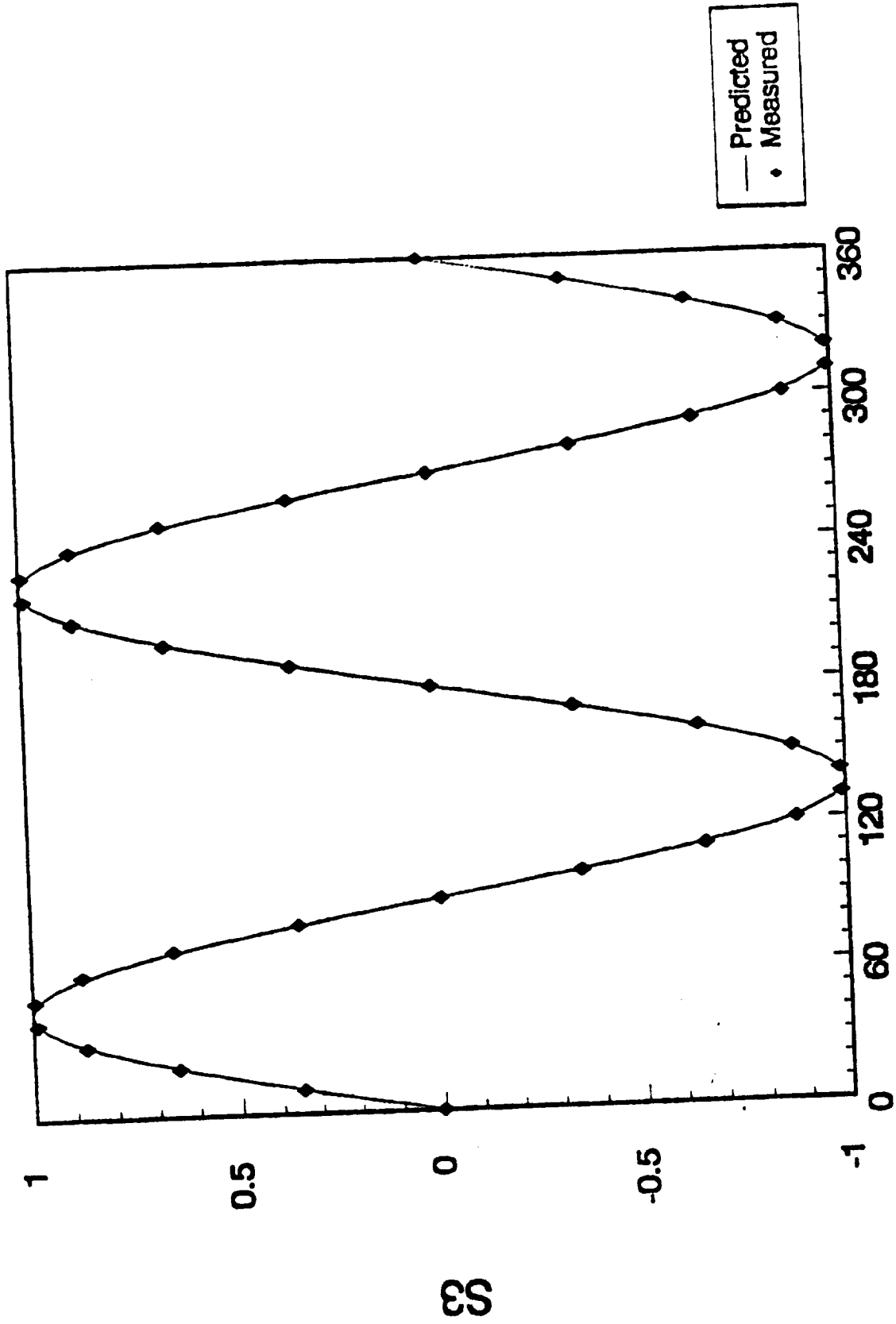
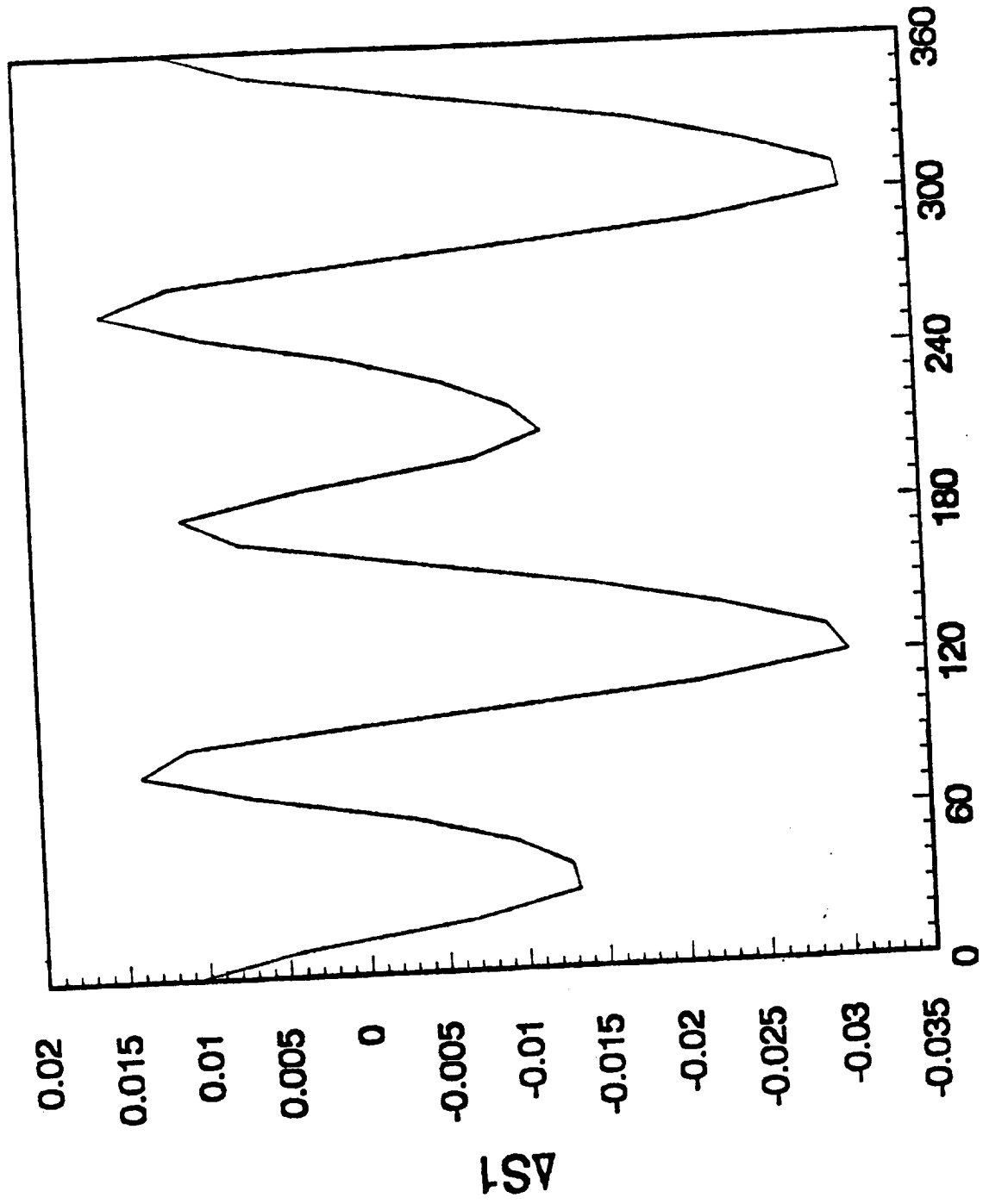


FIG 16

Retarder Fast Axis, C

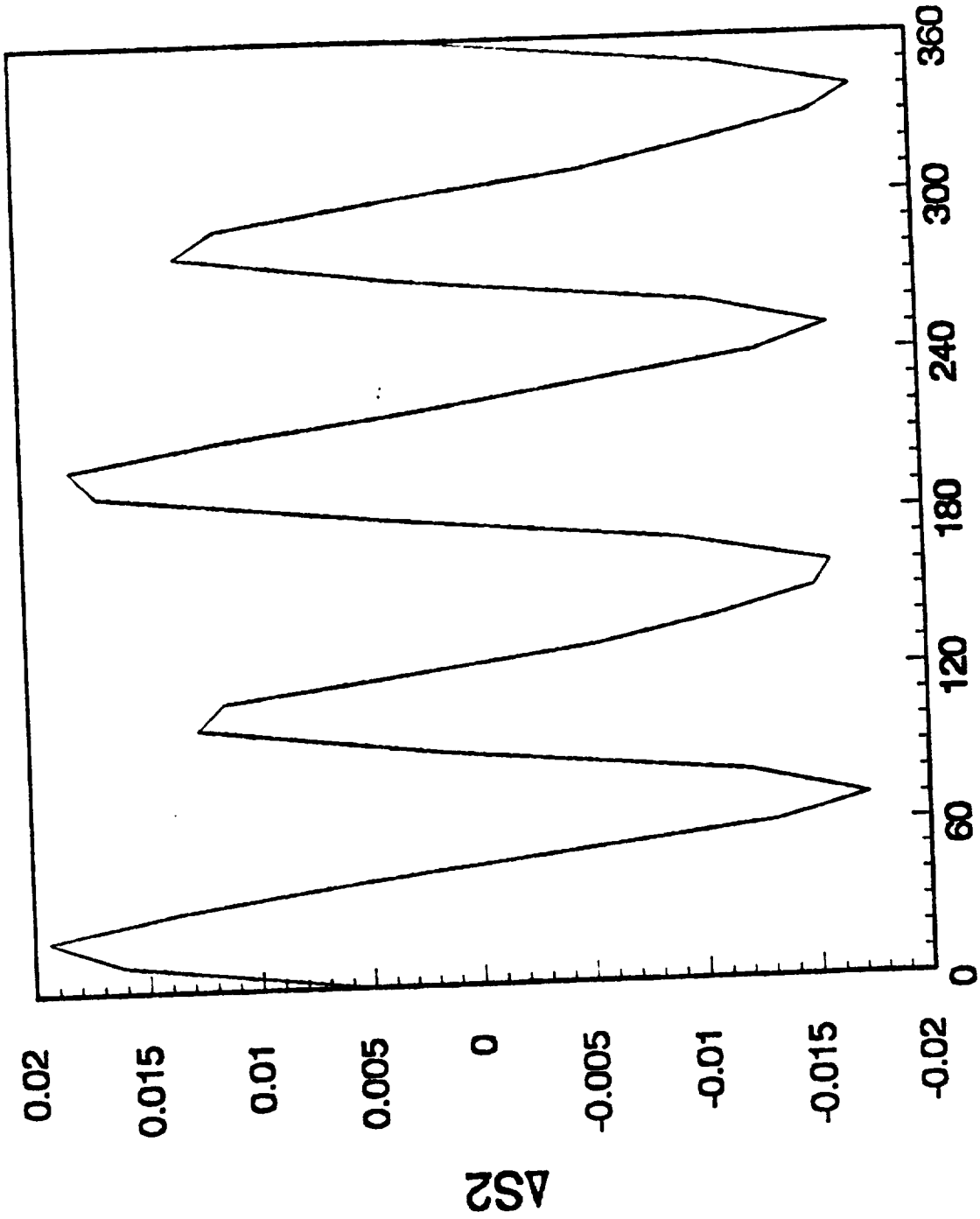
Deviation of measured S1 from predictions



Retarder Fast Axis, C

FIG 17

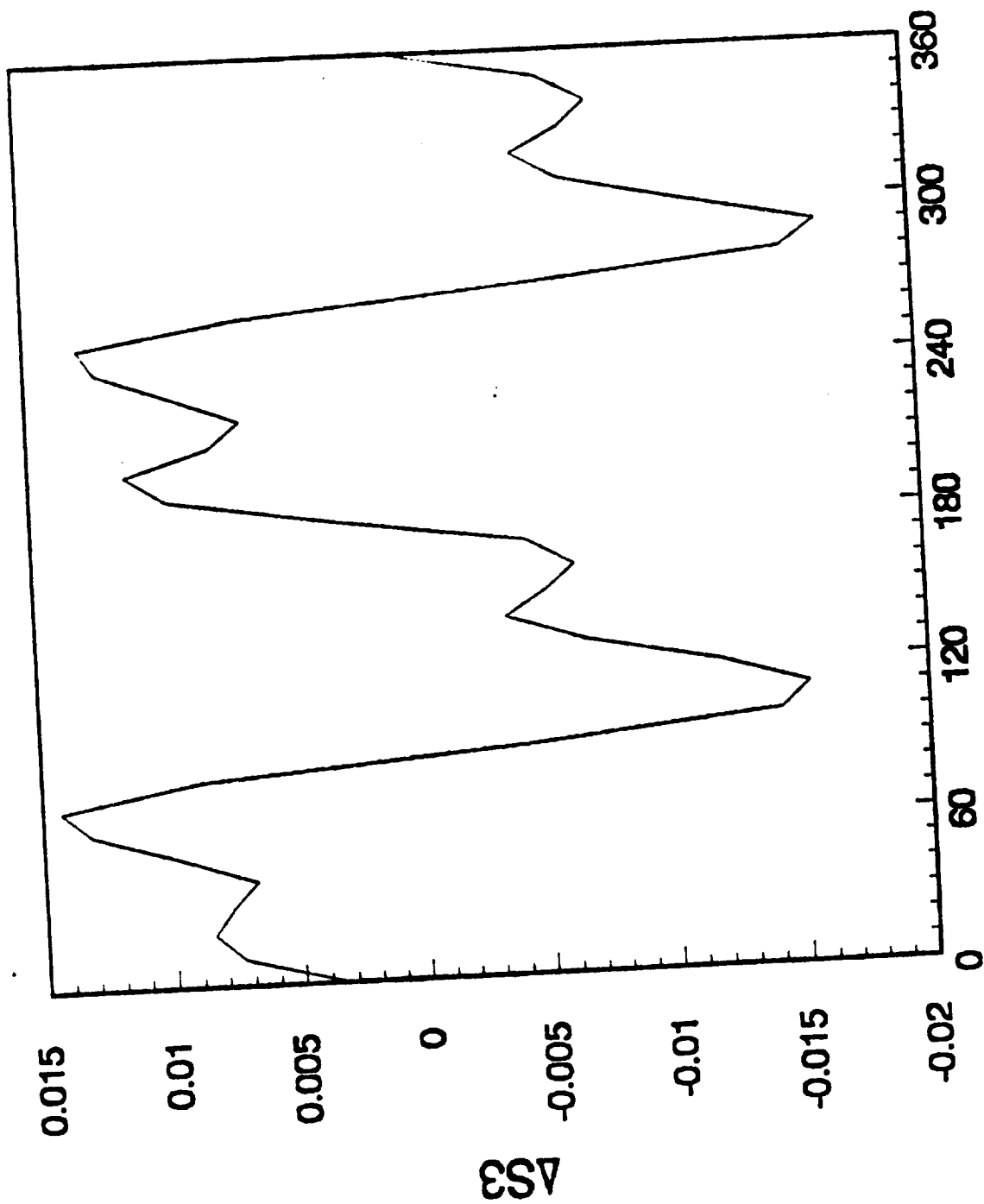
Deviation of measured S2 from predictions



Retarder Fast Axis, C

FIG 18

Deviation of measured S3 from predictions



Retarder Fast Axis, C

FIG 19

Measurements on Silicon:

Wavelength = 0.6328 μm
Angle of incidence = 70 degrees

n measured = 3.826 \pm	0.002	n literature = 3.840
k measured = 0.047 \pm	0.002	k literature = 0.028
e measured = 0.657 \pm	0.001	e literature = 0.656
R measured = 0.343 \pm	0.001	R literature = 0.344

The slight discrepancies in the measured and reported values of the indices of refraction may be due to imperfections on the sample surface, the presence of contaminants and most importantly, the method of sample preparation. Vedam [23] has discussed the scatter in measurements of the optical properties of silicon prepared under different conditions.

The sample was allowed to sit for 1 hour, and measurements were repeated. The new values of n and k were used to compute the thickness of an oxide film which easily forms on silicon. A thickness of 45 Angstroms was calculated which is in agreement with the observation that oxide films on silicon saturate at about 50 Angstroms on exposure to air. Cleaning the surface again produced the results reported above to within 0.002 for both n and k.

4.3 ACCURACY

We will now discuss the accuracy of the measurement, which is influenced primarily by the systematic errors. The accuracy can be estimated in several ways. The most rigorous way is to generate an error Muller matrix and determine its effect on the measured Stokes parameters. Alternatively, one can assume that the polarization state generator (PSG) is perfect and determine the deviations from the predicted states as a measure of the absolute accuracy. This procedure will produce a more conservative estimate of the absolute systematic error.

Based on the difference between measured and predicted curves, the following give the absolute accuracy of the DAPP for measuring the polarization state and hence the optical properties and spectral emissivities. Table 1 summarizes the results of the DAPP as a polarization state detector at 0.623 μm . In this table, we list quantities that are pertinent to the measurement of the state of polarization of

light reflected from a sample surface. The polarization state errors are based on deviations from predictions while the ellipsometric parameters are based on measurements on silicon and are presented in Table 2.

The absolute accuracy in the optical constants, n and k , is 0.02 based on our experiments with silicon. However, for silicon, k is very small, and affected easily by surface preparation method or contamination. In retrospect, silicon is not really a perfect standard. The true measure of the accuracy of this instrument will be to establish the accuracy of temperature measurement when this instrument is used in conjunction with a standard radiometer to measure the true surface temperature and compare this result with that obtained from a thermocouple located on the sample. This will demonstrate that the surface emissivity is measured correctly, which is the ultimate objective of this project. However, most metals and alloys have large values of n and k ($n > 2$, $k > 2$). In this case, the accuracy in the measurement of optical constants is better than 1%.

TABLE 1

Polarization State Accuracy at 633 nm

Quantity	ERROR (Absolute units)
S_1	0.009
S_2	0.010
S_3	0.008
Amplitude, Ψ	0.05°
Phase, Δ	0.05°
Azimuth, α	0.05°
Ellipticity, χ	0.05°
Axial Ratio	0.05°
Degree of Polarization, P	0.005
Degree of Linear Pol.	0.008
Degree of Circular Pol.	0.004

TABLE 2

Accuracy in Optical Properties at 633 nm
(Based on measurements on silicon)

Quantity	Absolute error (%)
Refractive Indices	
n	0.5-1 (n > 2.0)
k	0.5-1 (k > 2.0)
Spectral emissivity	
e	0.5

4.4 PRECISION AND REPEATABILITY

The precision of any measurement is limited by the noise in the measurement. The repeatability of the DAPP to measure the same state of polarization was tested by making measurements every 5 minutes for a 24 hour period. Statistical analysis of the results produced the histograms shown in Figs. 20-22. In each figure, the deviations of the measured Stokes parameters with that predicted from the PSG is plotted. If each histogram is approximated by a Gaussian, standard deviations of 0.17%, 0.12% and 0.10% were obtained for S_1 , S_2 and S_3 respectively. This precision is quite satisfactory and can be improved further with low noise electronics.

5. TECHNICAL FEASIBILITY CONCLUSIONS

We present below, scientific and technical conclusions that derive from our experience in the design, fabrication and preliminary testing of a prototype DAPP device to demonstrate the feasibility of this technique for emissivity measurements of solid and liquid surfaces.

- 1) The DAPP can measure all four Stokes parameters of arbitrarily polarized light instantaneously, and permit fast, time-resolved polarimetry, ellipsometry and spectral emissivity measurements, ultimately leading up to fast temperature measurement.
- 2) The accuracy of Stokes parameter measurement is 0.5 - 1% at the laser wavelength of 0.6328 μm . The errors are attributed to imperfections present in the retarding elements, and not the instrument design.
- 3) The accuracy can be improved with use of a better polarization state generator. Alignment at longer wavelengths would be more critical than at shorter wavelengths where the angular acceptance of the polarizing elements are greater.
- 4) The spectral emissivity can be measured to within 0.5% or better, and the indices of refraction are accurate to within 1%. These are worst case estimates and the values are based on measurements on silicon at room temperature.
- 5) The high accuracy in spectral emissivity measurements will enable the true surface temperature to be determined to within 0.5% when the instrument is used concurrently with a radiometric measurement such as a standard commercial pyrometer.
- 6) Safe, non-visual and accurate alignment of the instrument was achieved with the use of two quadrant detectors. This provided a very high degree of reproducibility in alignment and positioning of the instrument for laboratory use.

**Histogram showing deviation
of S1 from prediction**

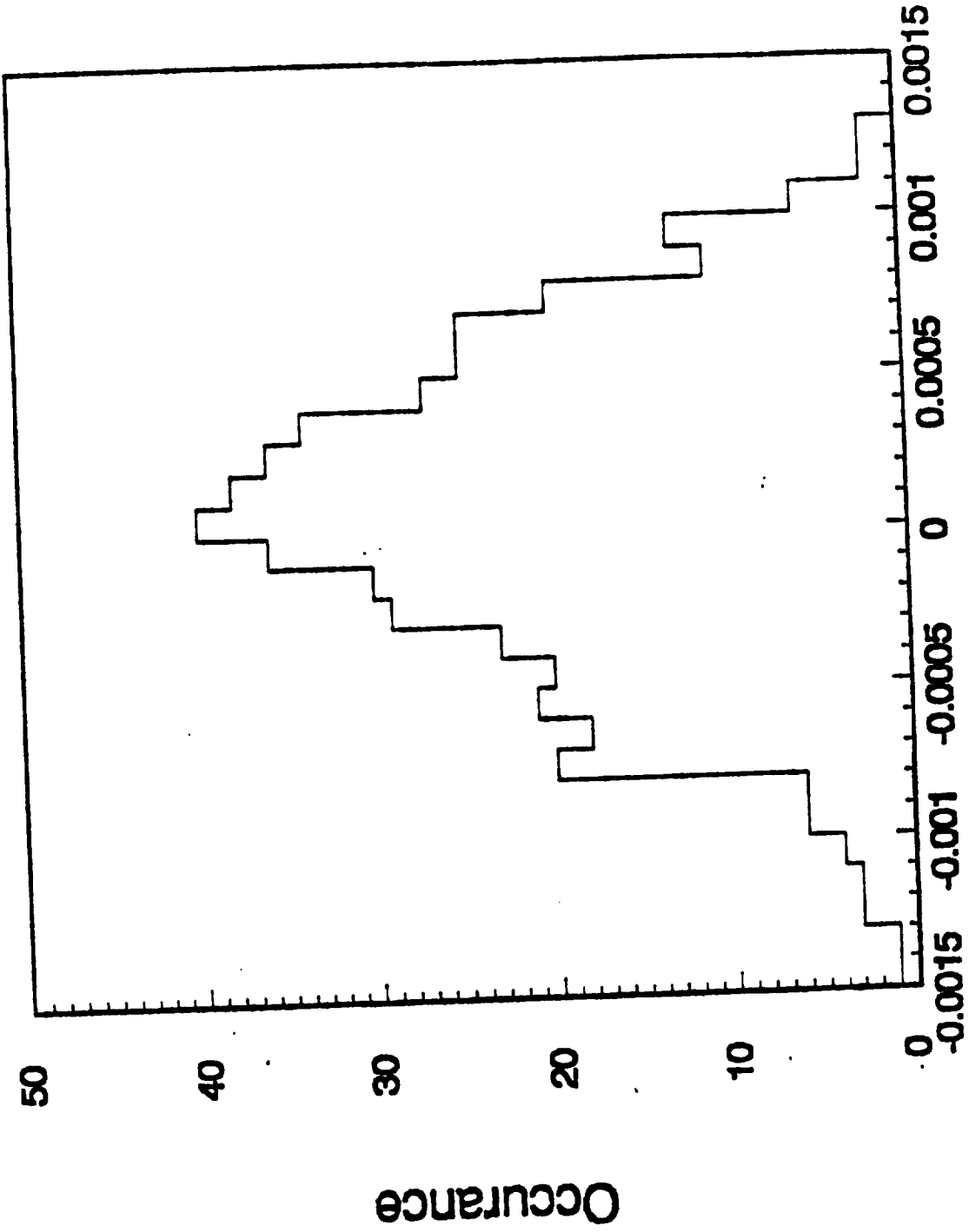


FIG 20

Error in S1

Histogram showing deviation of S2 from prediction

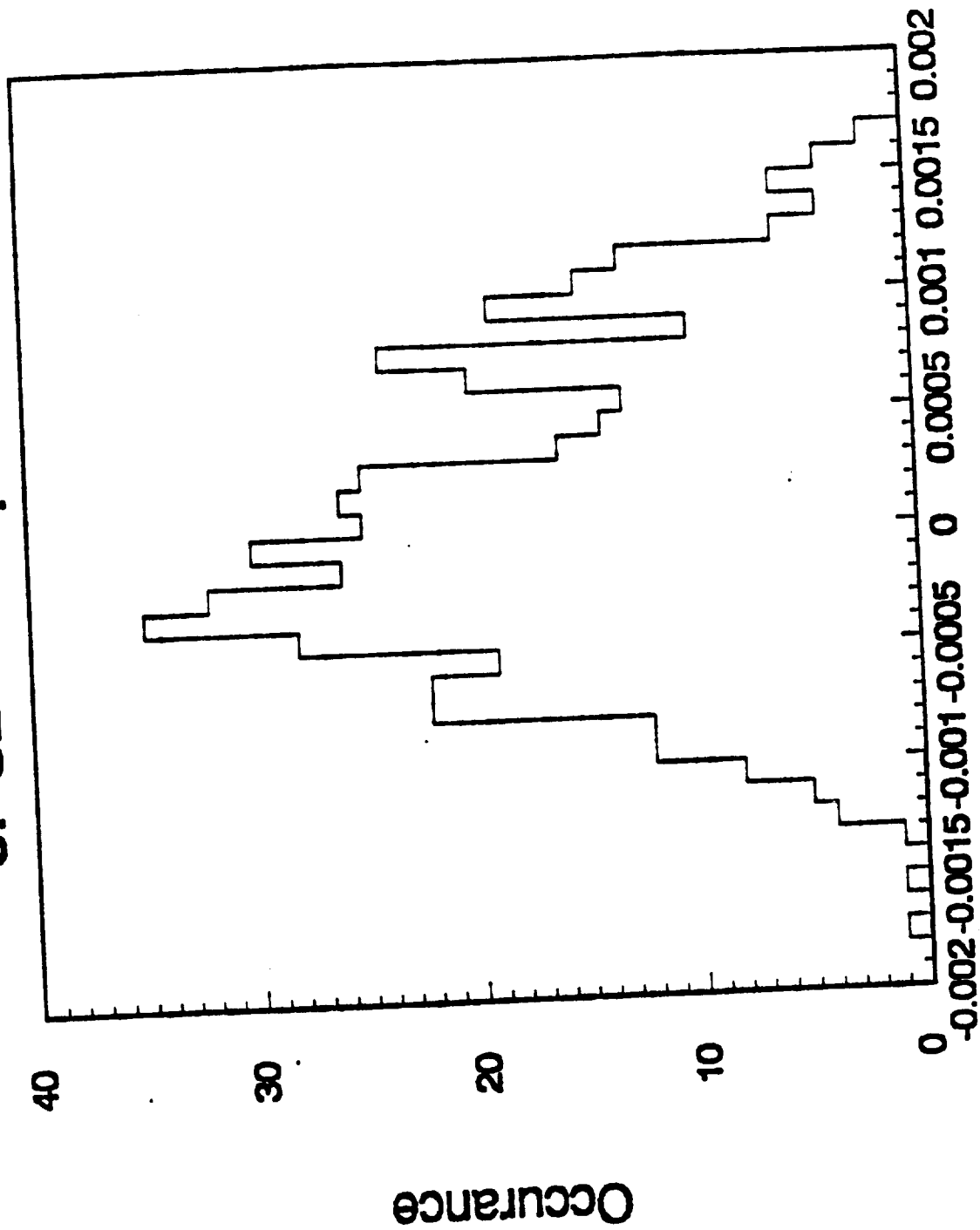


FIG 21

Error in S2

**Histogram showing deviation
of S3 from prediction**

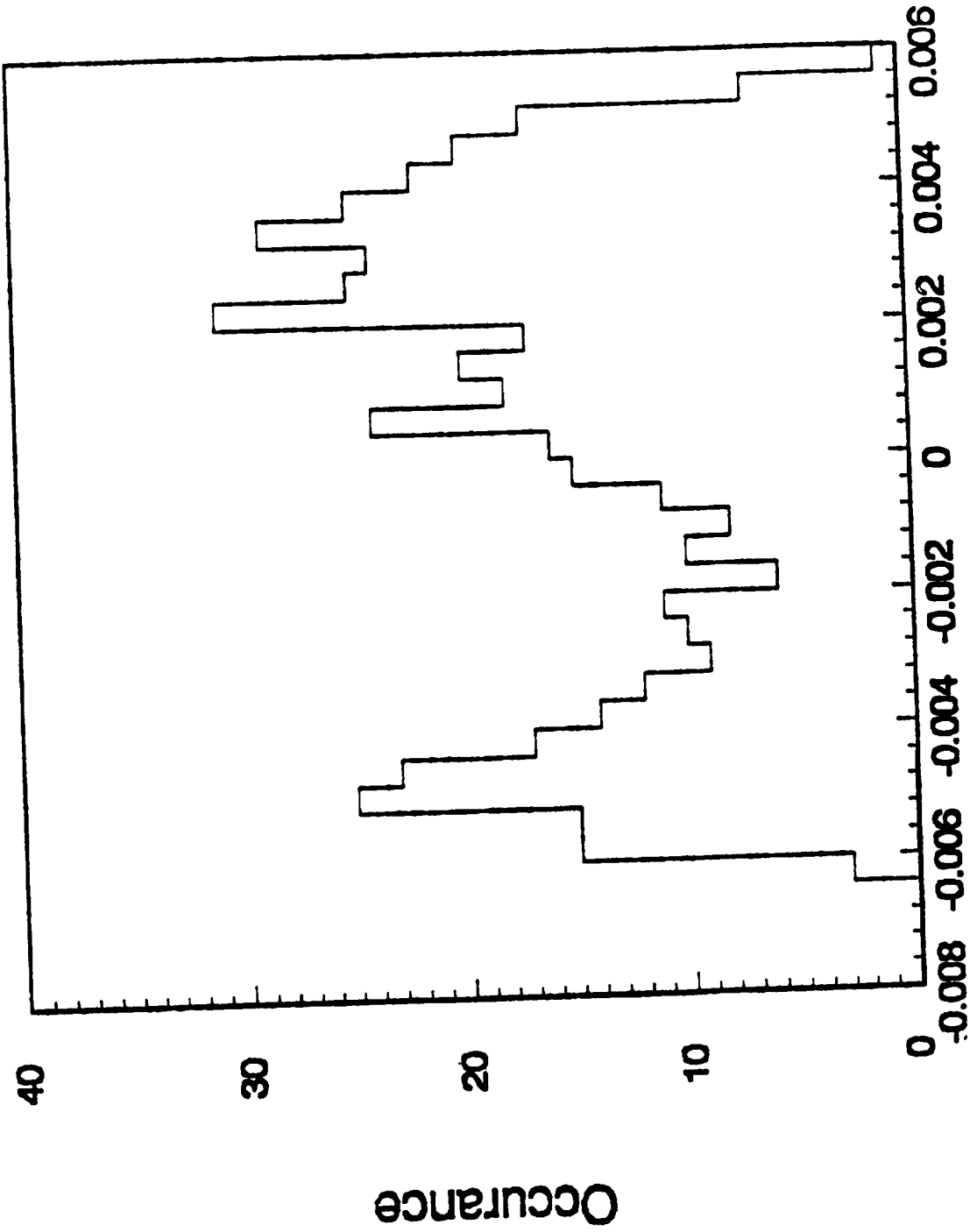


FIG 22

Error in S3

7) The DAPP has been calibrated by two independent methods, both of which produced nearly identical results. The 4-point method uses the bare minimum of optimized polarization states on the Poincare sphere. It is slightly less accurate compared to the equator-pole method.

8) Short and long-term drift tests suggest that the resolution of the instrument is better than 0.2% in any Stokes parameter. This is partly attributed to incorporation of light-modulation techniques into the design of DAPP.

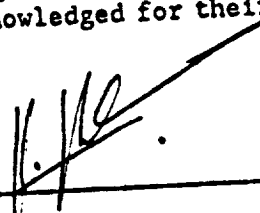
9) The response time of the instrument, in determining the Stokes parameters is limited only by the electronics and the time required for matrix inversion and numerical reduction. Initial tests suggest that the intensity measurements could be made in a time as small as 0.1 us.

10) The simplicity of the design and electronics, and the ease of data reduction make it an ideal instrument for use in laboratories and in process control applications for the measurement of temperature.

6. ACKNOWLEDGEMENTS

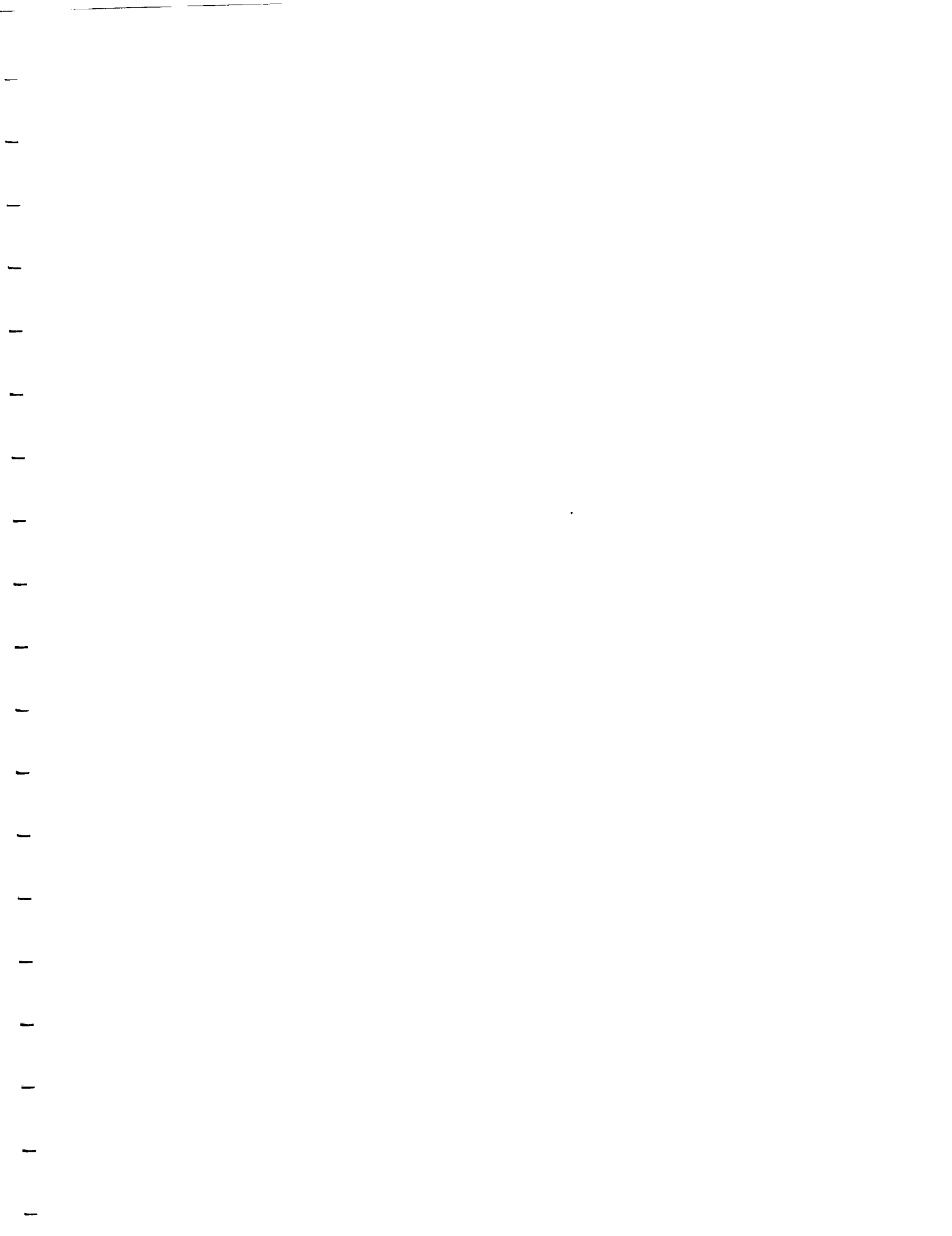
I would like to acknowledge Dr. Paul Nordine's help throughout this project and in preparing this report. Dr. Charles A. Rey, the Project Director was always a source of inspiration and guidance. Scott Hampton provided substantial help in the design and implementation of the optical and electronic systems. Dennis Merkley, Mark Zatarski and Eric Granderson were instrumental in the electronics design. Dr. Richard Weber is deeply acknowledged for his help with the test chambers and with other experiments. Lastly, our desktop publishing and proposal preparation staff are acknowledged for their help in making this report possible.

Submitted By: _____


Shankar Krishnan, Principal Investigator

7. REFERENCES

1. P.B. Coates, "Metrologia", 17,103 (1981)
2. P.C. Nordine, High Temp. Sci., 21, 97 (1986).
3. P.C. Nordine and R. A. Schiffman: Presented at NASA Non-Contact Temperature Measurement Workshop, Washington, D.C., April 30, 1987.
4. D.L. McElroy, and W. Fulkerson, Temperature Measurement and Control, John Wiley & Sons, Inc., New York, Techniques of Metals Res., vol.1, 1968, Ed. R.F. Bunshah, p.489.
5. S. Krishnan, G.P. Hansen, R.H. Hauge, and J.L. Margrave, High. Temp. Sci., 29, 17 (1990).
6. S. Krishnan, Ph. D Thesis, Rice University, Dec. 1988.
7. S. Krishnan, G.P. Hansen, R.H. Hauge, and J.L. Margrave, Met. Trans., 19A, 1939 (1988).
8. G.P. Hansen, S. Krishnan, R.H. Hauge, and J.L. Margrave, Met. Trans., 19A, 1889 (1988).
9. G.P. Hansen, S. Krishnan, R.H. Hauge, and J.L. Margrave, Applied Optics, 28, 1885 (1988).
10. S. Krishnan, R.H. Hauge and J.L. Margrave, "Spectral Emissivities and Optical Constants of Electromagnetically Levitated Liquid Metals as Functions of Temperature and Wavelength", NASA JPL-89-16, June 1989.
11. S. Krishnan, G.P. Hansen, R.H. Hauge, and J.L. Margrave, "Emissivities and Optical Constants of Electromagnetically Levitated Liquid Metals as Functions of Temperature and Wavelength", in Press, High Temp. Sci., and in Press, Sixth IUPAC Proceedings, Washington D.C. Apr. 3-9, 1989.
12. J.K. Richard Weber, R.A. Schiffman, Shankar Krishnan, and P.C. Nordine, VIIth European Symposium on Materials and Fluid Sciences in Microgravity, Oxford, England, Sep., 1989.
13. P.S. Hauge, SPIE Proc., Vol. 88, p. 3 (1976).
14. P.S. Hauge, SPIE Proc., Vol. 112, p. 2 (1977).
15. P.S. Hauge, Surf. Sci., 96, 108 (1980).
16. R.M.A. Azzam, E. Masetti, I.M. Elminyawi, and F.G. Grosz, Rev. Sci. Instr., 59, 84 (1988).
17. R.M.A. Azzam, I.M. Elminyawi, and A.M. El-Saba, J. Opt. Soc. Am. A, 5, 681 (1988).





INTERSONICS
I N C O R P O R A T E D

Study and Evaluation of the Feasibility of Providing Improved
Contamination Control for an Electromagnetic Levitation System

Report on NASA Contract #NAS8-37592

By
J.K. Richard Weber
Dennis R. Merkley
Charles A. Rey

To
George C. Marshall Space Flight Center
Marshall Space Flight Center
Huntsville, AL 35812

March 1, 1991

InterSonics, Incorporated
3453 Commercial Avenue
Northbrook, IL 60062-1818

Preface

This work was carried out under NASA Contract NAS8-37592 through NASA Marshall Space Flight Center, Huntsville, AL. It was conducted by a team of engineers and research scientists who have experience with the design and construction of flight hardware and ground-based scientific research in the areas of containerless processing and materials science.

The report contains recommendations for environmental cleaning and monitoring in electromagnetic levitation systems. Areas requiring further studies or equipment development are identified and a design layout for a gas handling system is suggested.

Questions regarding the content of this report should be addressed to Richard Weber (708) 272-1772.

Table of Contents

1. Executive Summary	3
2. Introduction	3
3. The Scope of The Problem	4
3.1 Gaseous Impurities	5
3.1.1 Approaches to Gas Purification	7
3.1.1.1 Operation in High Vacuum	7
3.1.1.2 Getter Techniques	7
3.1.1.3 Chemisorption	7
3.1.1.4 Catalytic Adsorption	8
3.1.1.5 Cryogenic Purification	8
3.1.1.6 Molecular Sieves	8
3.1.1.7 Palladium Filters	9
3.2 Summary	9
3.3 Particulate Impurities	9
3.3.1 Filtration Systems	10
3.3.2 Window Coating	10
3.4 Power and Cooling Requirements	10
3.5 Safety Requirements	11
4. Discussion	11
4.1 Operation in Ultra High Purity Atmospheres	11
4.2 Operation in High Vacuum	12
4.3 Operation in a Reducing Gas	12
4.4 Particulate Contaminants	13
4.5 Summary	14
5. Recommendations	14

5.1 Case 1	15
5.2 Case 2	17
5.3 Case 3	17
5.4 Case 4	17
6 Recommendations for Further Work	17
6.1 Scientific Issues	17
6.2 Instrumentation Issues	18
7. References	19
Figure 1	6
Figure 2	16
Appendix I	20
Appendix II	21
Appendix III	23
Appendix IV	25
Appendix V	27

1. Executive Summary

The requirements for environmental purity for containerless processing of metals have been evaluated. Recommendations for the design parameters for practical systems to meet a variety of processing requirements are presented.

The formation of oxide and nitride impurities has been identified as a major source of contamination in the processing of several metals and alloys of potential interest. These may be removed by evaporation or decomposition at high temperatures if residual gas impurity levels are small. The presence of particles in the processing environment may interfere with experiments which require undercooling of liquid metals and alloys.

A number of approaches to the prevention of contamination are described and discussed. These include operation in vacuum, inert gas, chemically active gases and chemically purified gases.

Electromagnetic levitation is frequently carried out in high vacuum processing chambers. The use of high vacuum limits the types of experimentation and processing which can be carried out. Experiments have demonstrated that processing in a gas atmosphere has several advantages over the use of high vacuum, particularly when specimen cleanliness is of importance.

When the highest purity is required, the use of recirculated inert gas, purified by passing it through getter and particle filtering systems is recommended. Recirculation provides the potential for achieving the highest purity by reacting gaseous impurities with vapor emanating from the material being processed. Condensed phases can subsequently be removed by filtration. The gas stream can be used to entrain and remove material from the region around the specimen and allows control of temperature.

The best technique for reducing contamination depends on the material being processed and can be specified only when the experimental requirements are known. In many cases, operation in a reasonably pure gas has technical and scientific advantages over working at very low pressure where chamber outgassing is a problem. There is still work required to adapt or specify equipment and the following areas have been identified as needing further research; gas handling systems, gas analysis systems, particle removal systems, techniques to prevent coating of windows and gas quality specification for specific metal or alloy systems.

2. INTRODUCTION

The purpose of this study is to evaluate techniques which may control and minimize the level of contamination in an electromagnetic levitator. The techniques considered fall into two categories: control of gaseous impurities and control of

particulate impurities. A section on gas quality analysis is included in Appendix I.

Containerless processing is carried out for at least two principal reasons. The first is to eliminate contamination of materials by dissolution and reaction with crucibles at high temperatures. The second reason is that, in the case of liquids, elimination of contact with a solid prevents heterogeneous nucleation of solid phases. This enables liquids to be undercooled and allows non-equilibrium states to be accessed. Containerless processing can also be used to clean materials of impurities by evaporation or gasification at high temperatures.^(1,2)

Electromagnetic levitation and heating is one method for containerless processing of solid and liquid conductors. The technique can be used in vacuum or in gaseous atmospheres. Other containerless processing techniques may require the presence of a gas atmosphere to operate.

3. The Scope of The Problem

The ambient environment can be characterized in terms of materials it contains and the way in which these interact with the material being processed. The environment can be considered to have gaseous and solid aspects as follows:

Gaseous:

- o Inert
- o Oxidizing
- o Reducing
- o Reactive
- o Vacuum

Solid Aspects:

- o Containment vessel boundaries
- o Particles of the material being processed
- o Particles of impurities
- o Subcritical nuclei

For many applications, especially those involving space flight, a number of engineering constraints also apply. These constraints typically are:

- o Power Requirements
- o Weight Limitations
- o Size Limitations
- o Cooling Requirements
- o Safety Requirements
- o Maintainability

3.1 Gaseous Impurities

Processing in gas atmospheres may be desirable because it can decrease evaporation rates of volatile materials and it affords a convenient method of temperature control. In general the gas is passive and is not intended to react with the material being processed. Impurities which can react with the specimen may result in formation of impurity phases such as oxides or nitrides.

Reactive impurities may include any or all of the following:

Oxygen, Nitrogen, Water, Carbon Dioxide, Carbon Monoxide, Hydrocarbons and Hydrogen. Carbon oxides, water, hydrogen and oxygen can exist together as redox mixtures in equilibrium concentrations determined by the ambient pressure and temperature.

Figure 1⁽³⁾ is a phase stability diagram for formation of oxides from metals and oxygen or oxygen-bearing gases. This diagram suggests several methods which might be used to prevent formation of oxides:

- o Addition of a gas such as hydrogen, has a greater affinity for oxygen than the material being processed,
- o Remove oxygen by reaction with a "getter" or material with greater oxygen affinity than the specimen.
- o Operate in a vacuum with a pressure less than the decomposition pressure of the oxides of the materials being studied.

Next to oxygen, a similar situation exists for the elimination of nitrides and in some cases carbides. In general, when the oxide impurity formation is prevented, the next most stable impurity phase will form, this is frequently a nitride.

TEMPERATURE-PRESSURE DIAGRAMS

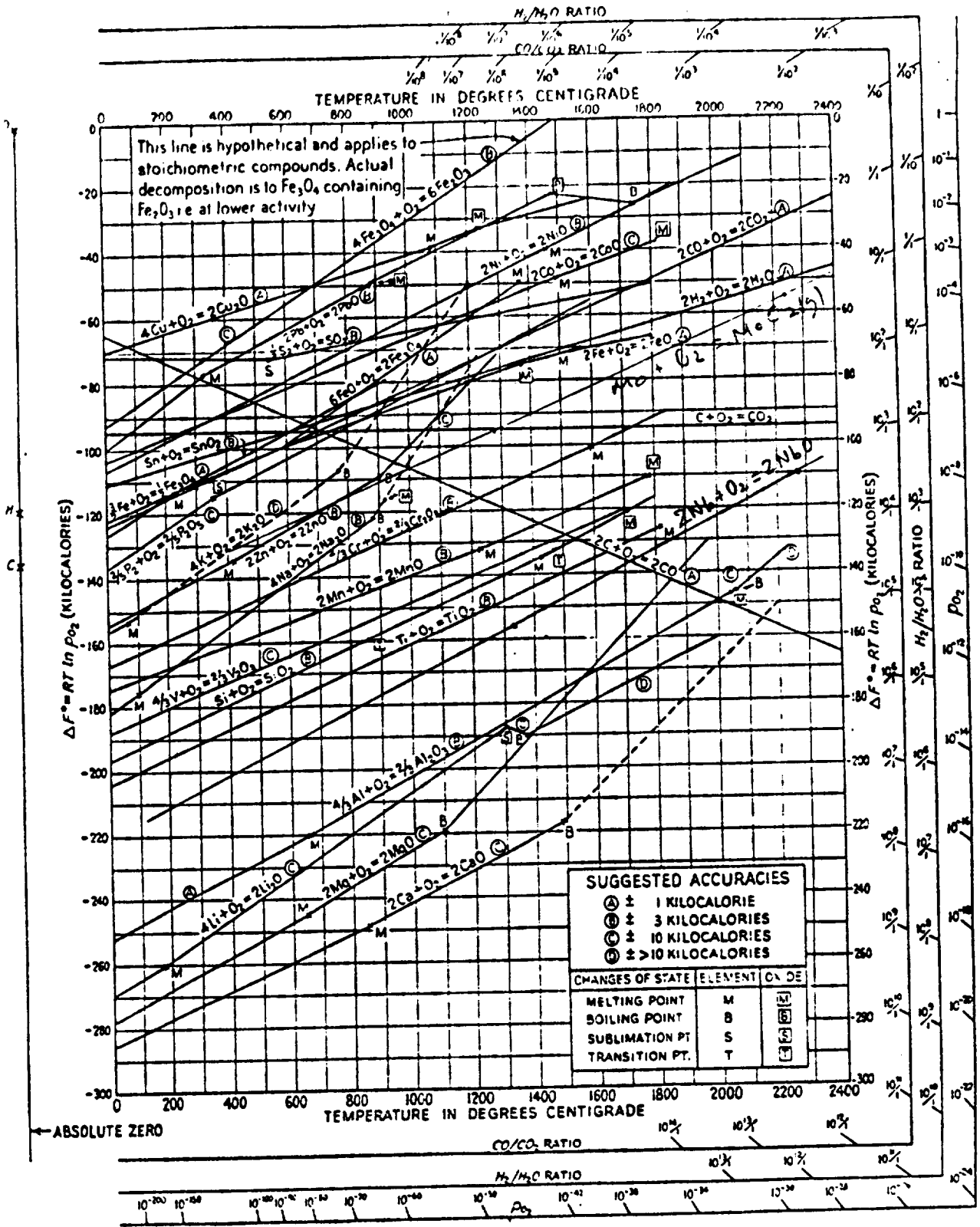


FIGURE 1 DECOMPOSITION PRESSURE VS TEMPERATURE FOR VARIOUS METAL OXIDES

ORIGINAL PAGE IS
OF POOR QUALITY

3.1.1 Approaches to Gas Purification

High purity inert gases typically contain 1 part in 10^6 (1 ppm) of impurities. A well designed gas handling system which has been purged and cleaned can maintain this purity from a storage cylinder to the processing chamber.

However, the gas can be further purified by a number of techniques. Several techniques have been developed for applications in the semiconductor processing industry and the technologies are mature and well understood.

The following section describes approaches which can be used to decrease the effects of impurities on an experiment.

3.1.1.1 Operation in High Vacuum

When this is possible, operation in a high or ultra high vacuum (pressure = ca. 10^{-9} Torr) decreases the amount of gas which can come into contact with a specimen. As discussed in section 3.2, this pressure is still sufficient to allow formation of a number of metal oxides and nitrides. Since, in the absence of a processing atmosphere, impurity transport cannot be controlled or monitored, the use of vacuum is limited in controlling impurities outgassing from the chamber walls or small particles within the system.

3.1.1.2 Getter Techniques

Getters react irreversibly with impurities to form a stable, bound product. Getters are made from alloys based on reactive metals such as titanium and zirconium. These alloys are available in the form of pellets or compacts which purify a gas stream which passes through them. They can remove a wide variety of reactive gases and lend themselves well to purification of gas for use in metals processing applications.

Many getters require heating in order to operate efficiently. The reliability of getter-based systems has been demonstrated in the semiconductor industry. Information on a system manufactured by SAES is provided in Appendix II.

Getter systems have the advantage that they are solid-state and robust. The power requirements are modest, typically under 100 W and well insulated canisters can further reduce this power. A disadvantage of getter systems is that they require flow through a porous medium and this may result in the need for a pumping system. Spall or dust from the getter substrate also needs to be removed, adding a particulate filtering requirement to the system.

3.1.1.3 Chemisorption

This technology is similar to gettering. The principal difference

is that impurities react with organometallic agents impregnated into a substrate material rather than with metals. Chemisorption can be used to remove a wide range of impurities, including those found in high quality inert gases. Systems are available which can operate at various temperatures from ambient to several hundred degrees. Information on a system manufactured by Semi-Gas is provided in Appendix III.

The principal advantage of chemisorption systems over getter systems is that they can be designed to operate at ambient temperature and therefore do not consume as much power. Their application however, is limited since they do not remove nitrogen.

3.1.1.4 Catalytic Adsorption

This technique is useful for removing redox gases. Oxidizing and reducing gases are reacted together to produce water or carbon dioxide which are easily removed by molecular sieves. Catalytic adsorption can remove hydrocarbon impurities by oxidizing them, provided there is sufficient oxygen in the atmosphere. The products formed by oxidation must be removed by a second stage of purification. A number of systems can be used for this.

Catalytic purification is limited by two factors. First, the residual oxygen pressure is determined by the redox reaction. This may result in an unacceptably high residual oxygen pressure. Second, gases which do not participate in the redox reaction are not removed and a supplementary system is required to remove these products formed.

3.1.1.5 Cryogenic Purification

Gas to be purified is passed over a series of cooled surfaces, usually tubes. Impure species whose partial pressures in the ambient gas exceed their vapor pressures at the cryogenic temperature will condense on the cooled surface. Obviously, this can be used to remove only those impurities which are much less volatile than the gas to be purified.

Cryogenic purification is a reliable technique. It requires that the cryogenic cell is maintained at its operating temperature at all times. Heating of the cell results in release of the condensed gases and immediate contamination of the gas stream. The cryogenic technique consumes relatively large amounts of power because a refrigerator is used for cooling the cryogenic cell.

3.1.1.6 Molecular Sieves

These selectively remove molecules which are larger than a critical size from a gas stream which passes through them. Molecular sieves are well suited to removal of large molecules, such as carbon dioxide, water vapor and hydrocarbons. They are ideally suited to

removing oil vapor released by an oil-sealed pump. They are not well suited to separating smaller sized molecules such as nitrogen, oxygen and argon.

3.1.1.7 Palladium Filters

These rely on the fact that palladium is permeable to hydrogen. Hydrogen can be separated from other gases by filtering through a palladium membrane under pressure.

3.2 Summary

Table 1 summarizes the features of the purification systems described.

TABLE 1

TECHNIQUE	PURIFICATION EFFICIENCY	POWER REQUIRED TO OPERATE	COMMENTS
HIGH VACUUM	FAIR - GOOD	HIGH (PUMPS)	RAPID TRANSPORT OF CONTAMINANTS
GETTERS	BETTER THAN 1PPB	30-100 W TYPICAL	COMPACT, LOW-POWER REQ., RELIABLE
CHEMISORPTION	1PPB	ONLY IF HEATING REQUIRED	COMPACT, RELIABLE DOES NOT REMOVE N ₂
CATALYTIC	FAIR FOR REDOX ONLY	MODERATE (HEATING)	ONLY STRIP REDOX GASES, NEED ADDITIONAL SYSTEM
CRYOGENIC	1PPB	LARGE REFRIGERATION	FAIL IF COOLING NOT MAINTAINED
MOLECULAR SIEVES	PPM	YES (PUMPS)	DO NOT STRIP ALL CONTAMINANTS
PALLADIUM	GOOD FOR HYDROGEN	YES (PUMPS)	ONLY SUITABLE FOR H ₂

3.3 Particulate Impurities

Particulate impurities can arise from a variety of sources which include contamination from gas handling equipment, pumps, the processing chamber, and condensed material from heated specimens. The latter may result from ablation of surface coatings or from condensation of vapors. The number of particles in an atmosphere can be defined in a number of ways, the specifications pertaining

to particulate matter suspended in a gaseous media are ASTM F 25, and MIL-STD-1246B.

3.3.1 Filtration Systems

Particles can be removed by filtering the gas stream. The technology for this is advanced and filter membranes may be made of ceramics or polymers. Filters can provide up to 99.9999999% removal of particles in the size range down to 10 nm.

If large particle loads need to be removed, filters can be arranged in series to remove smaller and smaller particles until the required purity is reached. The pressure drop across a filter membrane depends on its active surface area and the flow rate. Pumping is required to generate flow and this will require energy to operate the pump and flow control system.

The placement of the filter is an important consideration because outgassing of a filter may provide a source of gaseous impurities into the gas stream. Conversely, the gas purification system may provide a source of particulate contamination. A multi-stage filtering system could be designed to control both of these situations simultaneously.

Information on commercially available gas filtration systems are given in Appendix IV.

3.3.2 Window Coating

The coating of optical windows by condensed vapor emanating from hot specimens results in errors in radiation pyrometry. This coating interferes with visual or photographic observations and with all measurements by optical techniques. One approach in eliminating these problems is to protect critical windows with a gas purge. Alternatively, a laminar gas flow can be used to entrain particles and remove them from the processing chamber. If operation in high vacuum is required, transport of vapor to windows will be a significant effect. Techniques to prevent this require further development.

3.4 Power and Cooling Requirements

These will of course depend on the scale of the process and the system which is selected. In general, gas purification systems capable of handling flow rates, of a few liters per minute have modest power requirements. For example, getter systems require on the order of 30-100 W to operate them. This energy is converted to heat and this is dissipated into the gas stream and into the surroundings.

Vacuum pumps may be the largest power consuming component. The power required by recirculating pumps will vary with the amount of

gas being pumped. Other power consuming components will be electrically operated valves and flow control systems.

3.5 Safety Requirements

The systems evaluated do not require the use of toxic materials. Some getter systems contain small quantities of reactive metals and these can be activated by heating them to several hundred degrees. Pumps, valves, storage tanks and other gas handling equipment would be selected to meet the appropriate specifications pertaining to their operation and testing.

Reducing and oxidizing gases may form explosive mixtures when they are combined. Carbon monoxide which is toxic may be present in some redox mixtures.

4. Discussion

The ultimate purity of a system will be determined by its construction. In systems which have a sufficient concentration of gaseous impurities to stabilize impurity phases, the degree of specimen contamination will depend on the kinetics of impurity formation.

The interaction of the gas handling, cleaning and particle removal systems will play a key role in determining how well the gas quality can be maintained. Outgassing and dusting of components in the gas handling and purification train will contribute to the total impurity level in a system. Careful placement and specification of each component can reduce the contamination levels to a minimum.

4.1 Operation in Ultra High Purity Atmospheres

These atmospheres are obtainable from good quality, correctly handled and purified gases. The reactive impurity concentration will be of the order of 1 part in 10^6 (1ppb).

As shown in Figure 1, the decomposition pressure of many metallic oxides is less than 10^{-9} atm. This means that the oxide is stable if the oxygen content of the gas is equal to or greater than this value. However, as suggested by Brewer and Rosenblatt⁽¹⁾ and demonstrated in work at Intersonics^(2,5), many metals, including some of the more reactive ones such as titanium and aluminum, can be cleaned of oxide by evaporation of suboxides. The reaction used to remove oxide is of the type $MO_x(s) + M(s) = M_2O_x(g)$

The criterion for cleaning by this method is that the vapor pressure of the volatile suboxide is sufficient to remove it at a useful rate. A pressure of 10^{-6} atmospheres corresponds to evaporation of about one monolayer per second.

Processing in gas atmospheres has several advantages over the use of vacuum processing. The gas atmosphere forms a boundary layer at the specimen surface. This may control the evaporation rate from the specimen and can be particularly important in the processing of alloys which preferentially lose one component by evaporation.

A further effect which may occur is that metal vapor is contained (rather than deposited on the processing chamber walls and windows) in the gas and produces an inert atmosphere around a specimen by gettering of the gas adjacent to it. This offers a means of purifying gas of all reactive species for a given material. If the gas is then cleaned of condensate, it can be recirculated.

Gas flow may control and stabilize the temperature of a specimen. Mixtures of helium and argon can provide a range of temperatures which may not be accessible by control of electromagnetic power alone. In microgravity, where the positioning forces are small, gas may also provide a means to damp specimen motion.

4.2 Operation in High Vacuum

Some of the advantages of gas-based processing are lost when processing is carried out in a vacuum. For example, gas quenching is no longer possible and temperature control capabilities are diminished.

Operation in high vacuum has the disadvantages that, by increasing the mean free path of the gas molecules, it has the effect of making the specimen seem closer to the chamber walls. This results in an increased flux of material from the specimen to the windows. Also, rapid transport of outgassed species from the chamber walls to the specimen and increased rates of specimen evaporation and composition change due to incongruent evaporation.

4.3 Operation in a Reducing Gas

Figure 1 shows that a number of metal oxides will be reduced in an atmosphere of hydrogen or carbon monoxide. This approach would therefore prevent oxide formation of these materials.

Processing in reducing atmospheres has similar advantages and disadvantages to processing in inert gases. However, chemical reactions between the process gas and the specimen become possible. Hydride or carbide formation may be favored in some circumstances.

A further factor to consider when using reducing gases is that they may form explosive mixtures with air or oxygen. However, H_2 can be diluted with an inert gas to a concentration which will always be too low to be such a hazard.

4.4 Particulate Contaminants

Particulate contaminants can result in chemical contamination of a sample by adhering to and possibly by dissolving in it. For example if 10^6 particles, average diameter 0.1 μm , of similar molecular weight to the specimen material, adhered to a 0.5 cm diameter specimen, this would comprise about 1×10^{-8} impurity fraction. Many materials are mutually soluble to concentrations of more than 1 part in 10^8 and the particles would dissolve into liquid specimen.

Particulate contaminants can act as heterogeneous nucleation sites. In this capacity they will decrease the level of undercooling or supersaturation which can be achieved before nucleation occurs. The problem of particulate nucleation has only been addressed qualitatively in the context of containerless processing. The following comments can be made:

- o Laboratory experience shows that a number of molten materials can be undercooled by as much as 20% of their absolute melting point in containerless experiments. In many of these experiments, no system of particle control was used in the processing chamber⁽⁶⁾ so it is reasonable to assume that particles were present in the region around the undercooled liquid.
- o Critical nuclei are those of sufficient size to be thermodynamically stable. For metals they may be 100-1000 atoms in size. Once critical nuclei form, nucleation proceeds.

The critical size of an impurity nucleus depends on the way in which it interacts with the liquid. If the liquid wets the particle, it may be a potent nucleating agent. Non-wetting systems do not favor nucleation.

- o Particles can dissolve in a liquid at high temperature. This situation will not result in nucleation but in a small composition change in the material.
- o The laboratory observations that metals may be undercooled in experiments in gas-filled chambers where particles have formed by evaporation of the sample may be explained by thermophoresis transport effects.⁽⁷⁾ The thermophoretic force acting on particles makes them deviate from the flow streamlines in the non-isothermal conditions which would exist in a cold-wall chamber. Thermophoresis will transport particles away from hot regions into cooler ones, keeping the specimen relatively free of heterogeneous nuclei in a cold-wall chamber. This effect may be supplemented by a gas flow to entrain particles and remove them from the chamber. The gas

could then be filtered to remove particles before returning it to the chamber.

4.5 Summary

An environmental contamination control system can only be selected by considering the specific processing application requirements. No system is capable of providing gas of sufficient purity to prevent contamination of some metallic specimens. Evaporation can be used to remove contaminants and gas can be used to entrain the condensate which forms.

Reaction of gaseous impurities with a specimen removes them from the gas and places them on the surface of the specimen. Surface impurities can subsequently be removed from the specimen by evaporation and decomposition. Alternately the specimen could be replaced with another one and the "getter specimen" discarded.

Outgassing and evaporation from specimens provide sources of contamination which are independent of the purity of the processing environment. The use of a recirculating system with serial gas purification and particle removal offers the advantage that the gas can be purified to a level where reaction with the specimen does not occur.

The importance of particles in the region around a specimen needs to be addressed in the context of a specific system. Several systems, such as the equiatomic TiAl alloys⁽⁸⁾, can be undercooled without the need for particle removal from the processing chamber. Other systems, such as nickel, cannot be undercooled and this is attributed to nucleation by impurity (oxide) particles⁽⁹⁾.

The effects of small (submicron) particles in the region surrounding a liquid specimen depends on the system involved. This requires that an analysis is carried out for each system and the need for further research is suggested.

Finally, thermophoresis effects and gas flows may be used to remove particles from the vicinity of the specimen in gas-filled processing chambers.

5. Recommendations

Recommendations must be prefaced by stating the situations in which they apply. The best system for processing a given material will depend on the materials properties and the experimental constraints which apply. There are cases where a "perfect" system can be defined but probably not constructed. In many cases, mutually excluding effects make compromises necessary in order to engineer a practical system. A number of generalized systems have been specified and these are used as the basis for defining the requirements for processing systems.

The following generalized systems will be used as examples.

1. Processing a reactive material without the presence of particles. eg. Ni.
2. Processing a reactive material. eg. TiAl.
3. Processing an unreactive material without the presence of particles. eg. Pt-Rh alloys.
4. Processing an unreactive material. eg. gold.

The first situation is the most complex case considered. The gas must be purified and stripped of particle contaminants. All of the systems have the requirement that the processing chamber windows are kept free of condensed material. Recommendations are made on the basis of these considerations.

5.1 Case 1

It is recommended that processing is carried out in a gas. This will reduce or prevent deposition of condensate on the processing chamber windows. The gas can be used to remove particles formed, for example, by condensation of vapor and remove them from the region around the specimen. In microgravity, a further advantage of processing in a gas atmosphere is that the gas may be used to damp specimen motion.

In the case of reactive materials, gaseous impurity concentrations may be sufficient to produce some reaction with the specimen. This situation exists in all processing systems, vacuum and cleaned gas. The "self gettering" by reaction of trace impurities can provide an atmosphere which is free from any reactive impurities. This can be achieved in two ways: First, condensed phases formed by reaction between gas and the specimen surface can be evaporated or decomposed at high specimen temperatures and the products removed by entraining them in a gas stream. Second, metal vapor emanating from a hot specimen will react rapidly with gaseous impurities and the reaction products can be removed from the gas stream.

Gas recirculation has been suggested⁽¹⁰⁾ for systems requiring high purity. Recirculation is recommended for this application because the gas is then in a closed system and once it is purified it will no longer react with the specimen. Particles entrained by flowing gas past a specimen can be removed from the gas by filtering it before it is passed back into the chamber.

A schematic layout of the recommended system is shown in Figure 2. The processing chamber would be constructed from high quality materials such as polished stainless steel or aluminum. The latter is preferred because it is light and of comparable quality in other respects.^(11,12)

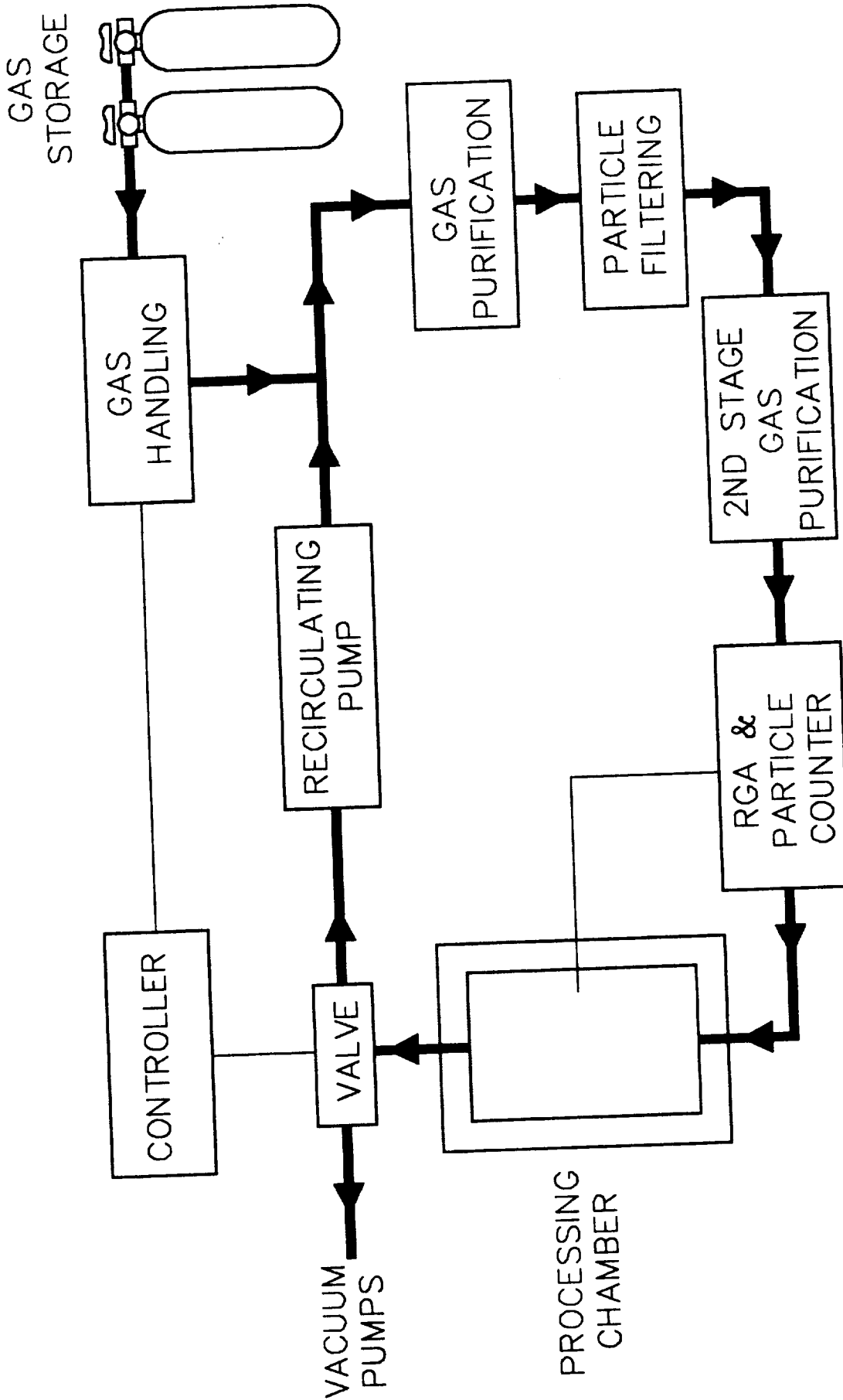


FIGURE 2 -- FLOW DIAGRAM OF CONTAMINATION CONTROL

To achieve the highest purity, the system would be evacuated and baked out, then backfilled with ultra high purity inert gas at moderate pressure (0.1 atm.). The gas is further purified and cleaned by a getter system and a particle filter placed in series with the processing chamber. Gas entering the chamber will have a concentration of chemical contaminants of about 1 part in 10^9 , still sufficient to react with some materials. When a specimen is heated in the processing chamber, the impurity concentration in the gas will decrease until it reaches a level below which reactions cannot occur.

5.2 Case 2

A purity requirement similar to that in case 1 exists. For this reason, it is desirable to use a closed system. If particle removal is not required, a recirculating system is not essential. A system similar to the one shown in Figure 1 could be used to good effect. The system could be simplified by eliminating the recirculation and filtering components.

5.3 Case 3

The less stringent requirements on gas purity would enable operation in a gas at moderate pressure. There would be no need to further purify the gas. Situations may exist in which the impurity content of the gas is less than that of the specimen, the specimen may then provide a source of contamination of the gas. A recirculating system would be necessary to entrain and remove particles from the vicinity of the specimen, these would then be removed by filtering the gas.

5.4 Case 4

This is the simplest case considered. Processing could be carried out in a closed chamber in high purity inert gas or under reduced pressure. Operation in a gas is preferable for the reasons stated earlier in this report.

6. Recommendations for Further Work

Several areas related to the problem of contamination control which require further work have been identified. The work can be divided into two categories. Those relating to fundamental scientific questions, which may be specific to a particular system and those relating to hardware development and advances in technology.

6.1 Scientific Issues

Cleaning of metals at high temperature: As described in section 4.2, some metals can be cleaned of oxide and nitride by high temperature processing. There is a possibility of removing other impurities by gasification in oxygen. These aspects of

purification would depend on the thermodynamic and kinetic limitations which apply to a given system. A study of the systems of interest would be required in order to determine how effective these techniques would be.

Size of critical nuclei: The size of a critical nucleus required to induce nucleation of a liquid material is influenced by a number of factors, some of which are discussed in section 4.5. The way in which these factors interact are not well understood and will be specific to a given system. Further work will be required to define the requirements for a specific system.

Gas Cleanliness: The required cleanliness for processing a particular material will depend on the level of contamination which can be tolerated and on the kinetics of the formation of the contaminating species. Research would be required to determine the practical limits which would apply to working with a particular system.

6.2 Instrumentation Issues

Particle Entrainment: Laminar gas flow can be used to entrain particles and transport them from the area around the specimen. A detailed design requirements analysis of a laminar flow system would be needed to define the scope and capabilities of the system.

Gas analysis: The development of miniaturized gas analysis systems with low energy requirements is an area which requires further research. Spectroscopic techniques lend themselves well to gas and particle chemical analyses. The technology exists for constructing a miniaturized spectrometer system for monitoring of gas purity and composition. A requirements analysis and engineering definition would be required to enable a system to be designed. Research is also required to evaluate and define the scope of the measurement problem.

Prevention of window coating: Deposition of material onto windows and viewing ports reduces their transmission. This represents a major problem in situations where accurate noncontact temperature measurement is necessary. Several approaches might be used to prevent deposition. One way is to reduce the rate of deposition to very low levels is to use a gas atmosphere in the processing chamber. In situations where this is not possible, mechanical techniques could be used to prevent or remove deposition. This problem warrants further analysis and evaluation.

Pumps: Recirculating systems require pumps to move the gas through the purification system and chamber. The pumps must be clean and non-contaminating. The technology for pumping gas has been developed for application to controlled atmosphere glove boxes. This technology could be used as the basis for design of recirculating systems for use in processing chambers. The

adaptation of these pumps will require a design analysis to determine the engineering requirements of the pumps.

7. References

1. L. Brewer and G.M. Rosenblatt, "Thermodynamics of Suboxide Vaporization" *Trans. Met. Soc.*, 224, 1268 (1961).
2. J.K.R. Weber, R.A. Schiffman, S. Krishnan and P.C. Nordine, "Containerless Processing and Property Measurements of High Temperature Liquids and Solids" *Proc. VII European Symposium on Materials and Fluid Sciences in Microgravity*, Oxford, UK, 10-15 Sep., 1989.
3. F.D. Richardson and J.H.E. Jeffes, "The Thermodynamics of Substances of Interest in Iron and Steel Making from 0°C-2400°C" *J. Iron Steel Inst.* 160, 261 (1948).
4. D.A. Toy, "Purifying at the Point of Use Keeps Your Gasses at Their Cleanest" *Semiconductor International*, pp 64-72, June (1990).
5. S. Krishnan, J.K.R. Weber, P.C. Nordine, R.A. Schiffman, R.H. Hauge and J.L. Margrave, "Optical Properties of Liquid Silicon, Aluminum, Titanium, and Niobium" Submitted, *High Temp. Sci.*, Nov., 1990.
6. R. Bayuzick, N.D. Evans, W.H. Hofmeister and M.B. Robinson, "Microgravity Containerless Processing in Long Drop Tubes" *Proc. 2nd Symposium on Space Industrialization*, Marshall Space Flight Center, Huntsville, AL, Feb., 1984, pp. 243-259.
7. D.I. Fotiadis and K.F. Jensen, "Thermophoresis of Solid Particles in Horizontal Chemical Vapor Deposition Reaches" *J. Crystal Growth* 102, 743 (1990)
8. J.K.R. Weber and S. Krishnan, Progress Report NASA Contract # NAS8-37472, Nov. 26, 1990.
9. W. H. Hofmeister, Vanderbilt University, private communication.
10. R.H. Hauge, Rice University, private communication.
11. H. Ishimaru, "Developments and Applications for All-Aluminum Alloy Vacuum Systems" *MRS Bulletin*, pp23-34, July, 1990.
12. H. Ishimaru, "All-Aluminum-Alloy Ultra High Vacuum System for a Large-scale Electron-Position Collider" *J. Vac. Sci. Technol.* A2, 1170 (1984).

Appendix I Gas Quality Analysis

1. Introduction: There are two aspects to gas quality analysis. The first is chemical analysis and the second is particle analysis. Chemical analysis requires that the composition of the gas is measured with respect to gaseous impurities, these can be assumed to be homogeneously distributed throughout the gas. Particle analysis is a measure of the concentration and size distribution of solid particles suspended and entrained in a gas.

2. Chemical Analysis: Gaseous impurities in a gas can conveniently be monitored with a mass spectrometer. A relatively simple and robust system is the quadrupole mass spectrometer. Ions are generated and accelerated into a quadrupole tube. The impurities are then separated by their ion mass.

Infrared emission spectroscopy is a well established technique to determine the chemical composition of gases and vapors. This method may be applied to measurements of the composition of impurity species present in a processing chamber. The design of a system for use in this application would require development of sensor technologies.

3. Particle Analysis: Light is scattered by particles suspended in a gaseous medium which allows the measurement of their concentration and size distribution.

Several systems are available which measure the concentration of particles by this technique. The measured concentration and size distribution depends on the detector placement. In situations where particles precipitate from the gas, measurements will not represent the bulk concentration.

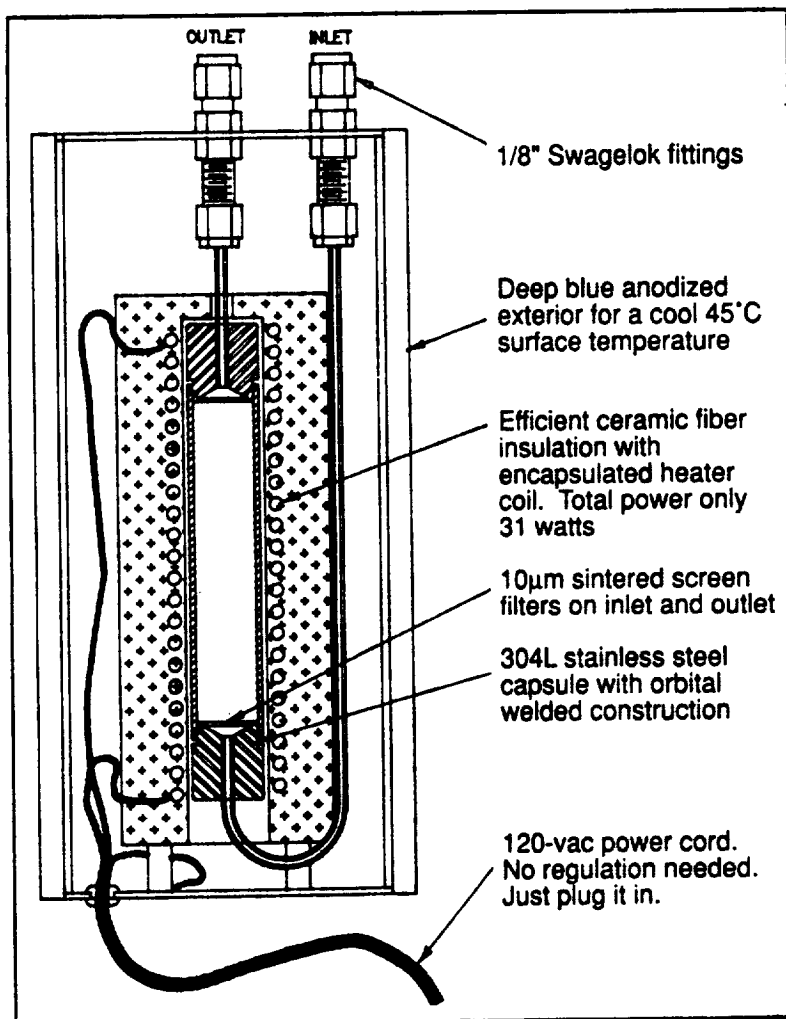
The basis of this instrumentation exists. Development work to miniaturize aerosol particle measuring equipment has been carried out at NASA Lewis Research Center. The use of solid-state lasers and detectors in combination with fiber optic light guides have resulted in miniaturization of the instrumentation for light scattering measurements. Design studies to integrate this technology into a processing facility are recommended

* J.M. Bassler and J.L. Margrave, "High Temperature Applications of Infrared Spectroscopy", Chapter 10 in Characterization of High Temperature Vapors, Ed. J.L. Margrave, Wiley, 1967.

The SAES Pure Gas GC50 purifier designed specifically for gas chromatography.

The GC50 is an economical and convenient way to boost the instrument sensitivity. The following table shows the purity of typical 5N cylinders before and after purification with the GC50.

Impurities in Gas Stream	Nitrogen		Helium or Argon	
	Inlet (ppb)	Outlet (ppb)	Inlet (ppb)	Outlet (ppb)
H ₂ O	2000	< 20	2000	< 20
O ₂	3000	< 2	2000	< 2
CO, CO ₂	1000	< 10	500	< 10
CH ₄	500	< 500	300	< 10
other hydrocarbons	100	< 10	100	< 10
H ₂	1000	< 10	100	< 10
N ₂	-	-	5000	< 10



Cutaway of the SAES Pure Gas GC50 ppb purifier.

Gas analysis in gas chromatography is dependent upon the purity of the carrier gas, regardless of the type of sensor mounted on the GC. In the case of trace analysis, ultrahigh-pure carrier gas is necessary for the GC spectrum to show only minor fluctuations in purity.

The SAES Pure Gas GC50 is so effective in removing gaseous impurities that the outlet concentration is below the sensitivity of commercially available instrumentation.

Features

- purifier life – 12 months at maximum flow rate with impurity level shown above
- maximum flow rate is 200 scc/min
- standard voltage heater (no control unit)
- easy to use
- negligible maintenance
- easily adaptable to any type of GC
- 1/8" compression fittings
- replaceable cartridge

If you are a user, ask SAES Pure Gas how to install a GC50 in your gas chromatograph.

If you are a manufacturer, ask SAES Pure Gas how to improve the performance of your instrument by including a GC50 as OEM standard equipment.

SAES Getters S.p.A.
Head Office
Via Gallarate, 215/217
20151 Milano, Italy
Tel +39-2-3020.1 (20 lines)
Fax +39-2-3340.3636

SAES Pure Gas, Inc.
Headquarters
4175 Santa Fe Road
San Luis Obispo, CA 93401
Phone (805) 541-9299
Fax (805) 541-9399

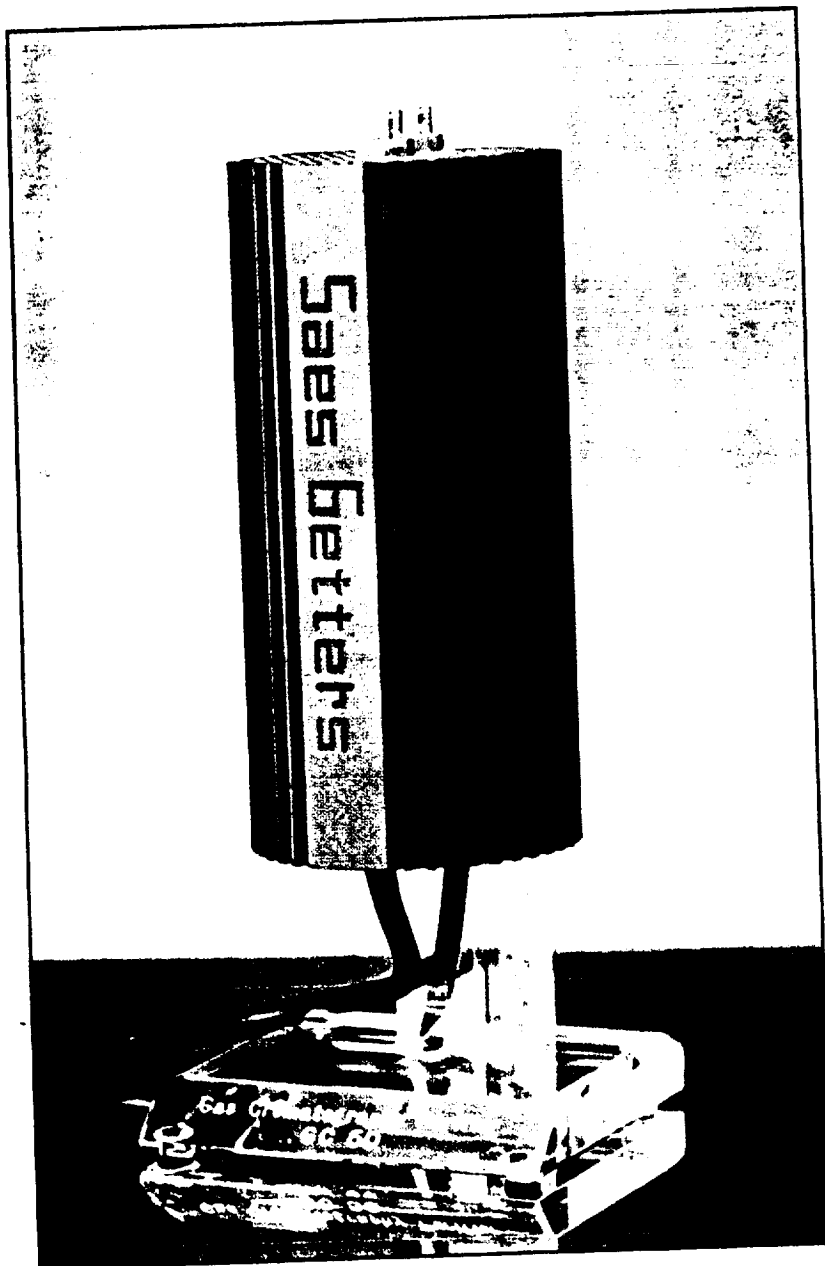
SAES Getters Japan Co., Ltd.
8-1-8 Nishi-Golanda
Shinagawa-Ku, Tokyo 141
Tel +81-3-494-1908
Fax +81-3-494-1938

Hankuk Getters Corp.
Shin Bong 2nd Bldg., 3rd Floor
835-6 Yeok Sam Dong
Kang Nam Ku Seoul, Korea
Tel +82-2-556-3815/6
Fax +82-2-556-3817



The GC50 ppb purifier for gas chromatography.

Specifically designed for the purification of GC carrier gases, the GC50 removes impurities to the low ppb level and below.



*The SAES Pure Gas GC50 ppb purifier for gas chromatography.
Height: 9" (22.86 cm), OD: 4" (10.16 cm).*

Improves

**99.999% carrier gas
to 99.99999% quality
for any type of gas
chromatography**

- lowers carrier-gas background noise
- increases detection limits
- ensures greater reproducibility
- protects columns from moisture and oxygen contamination
- provides ppb-level purity at a low cost

**saes
getters**

ORIGINAL PAGE IS
OF POOR QUALITY

Comprehensive

You can have point-of-use or proximate purification and filtration with **Nanochem Systems**.

Systems that can purify many process gases and remove a host of impurities.

Nanochem purifies a wide range of process gases such as Silane, Dichlorosilane, Chlorine, Ammonia, Hydrogen Chloride, Hydrogen, Argon, Nitrogen, Helium, Xenon, Krypton and more.

Reliable

With **Nanochem**, purification is reliable — regardless of extremely high impurity surges. The purifiers remove O₂ and H₂O to less than 10 ppb consistently. At the point-of-use, impurities from upstream leaks, improper cylinder changes, gas system components and process cross-contamination are virtually eliminated.

The built-in particle filter is baked-out and purged with "Nanochem Pure" inert gas to remove all traces of trapped moisture and oxygen. The purifier is ready to go to work, no filter preconditioning is required.

Cost Effective

Nanochem removes process gas impurities like O₂, H₂O, CO₂, CO and trace dopants in a single operation. The chlorinated gas purifiers remove moisture and particulates.

Compare that to other gas purifiers . . . they demand *several* devices to remove a combination of impurities and still don't accomplish the purity of **Nanochem**.

Simple

Nanochem Systems require no utilities for operation and come with standard VCR® type connections for easy in-line installation and replacement.

You'll know when a replacement is needed because **Nanochem** lets you know — thanks to the unique fiber optic end-point detection system.

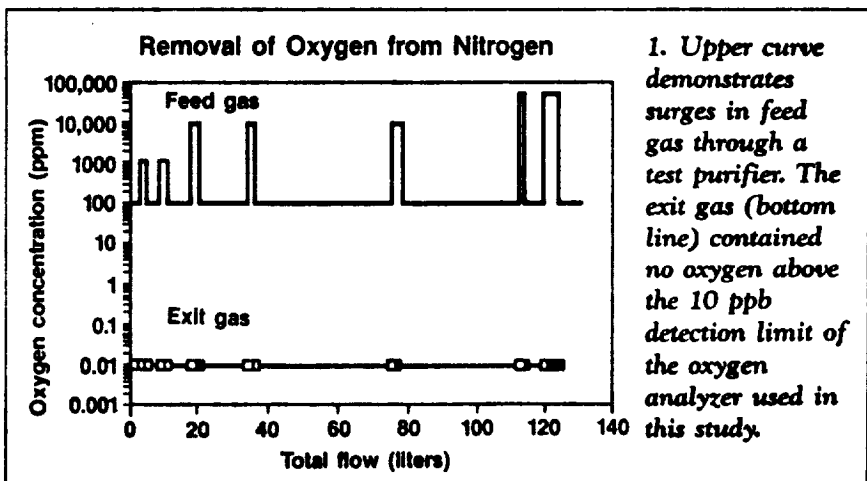
Compact

Semi-Gas D-Series and L-Series Purifiers (for point-of-use applications from 0 to 20 slpm) give you truly astounding gas purification in a compact unit.

Meanwhile, the **N-Series** is designed for proximate or area application (20 to 100 slpm) and the **P-Series** for high flow area application (100 to 900 slpm). Both **N-** and **P-Series** systems come complete within an exhaustable enclosure. **P-Series Surface Mount Purifiers** are available for inert house gas purification.

Nanochem's Unique Features

1. **Nanochem Systems** deliver 99.999999% purity without the need to heat or cool.
2. End-point detection is built in.
3. **Nanochem Systems** work consistently without need for regeneration.
4. They're compact and lightweight.
5. They have zero to nominal power requirements.
6. Flexible installation options:
 - inside process tool.
 - proximate to process tool.
 - inside source gas cabinet.
7. **Nanochem Systems** are precision fabricated with electropolished, orbital-fusion-welded 316L stainless steel.
8. You also get in-line, pre-equilibrated particle filtration (<0.01μ particle retention).
9. Every **Nanochem System** is assembled and tested in our class 100 clean work area.



Nanochem® Purifiers

GASES PURIFIED AND COMMON IMPURITIES REMOVED BY THE NANOCEM FAMILY OF PRODUCTS

GAS PURIFIED	NANOCEM PRODUCT NUMBER	COMMON IMPURITIES REMOVED
Argon (Ar) Helium (He) Krypton (Kr) Neon (Ne) Nitrogen (N ₂) Xenon (Xe)	1400 1400 1400 1400 1400 1400	Oxygen, Water, Oxides of Carbon Sulphur and Nitrogen
Ammonia (NH ₃) Butane (C ₄ H ₁₀) Carbon Tetrafluoride (CF ₄) Ethane (C ₂ H ₆) Hexafluoroethane (C ₂ F ₆) Methane (CH ₄) Propane (C ₃ H ₈)	1600 1600 1600 1600 1600 1600 1600	Oxygen, Water, Oxides of Carbon Sulphur and Nitrogen, Contaminant Halogen Compounds
Hydrogen (H ₂)	3000	Oxygen, Water, Oxides of Carbon Sulphur and Nitrogen, Complex Hydrocarbons
Silane (SiH ₄)	IV	Oxygen, Water, Oxides, Chlorine, Chlorosilanes, Trace Dopants
Hydrogen Chloride (HCl)	DP-85	Water
Dichlorosilane (DCS)	DP47	Water, Trace Dopants

Consult Semi-Gas Systems for information on the purification of other gases.

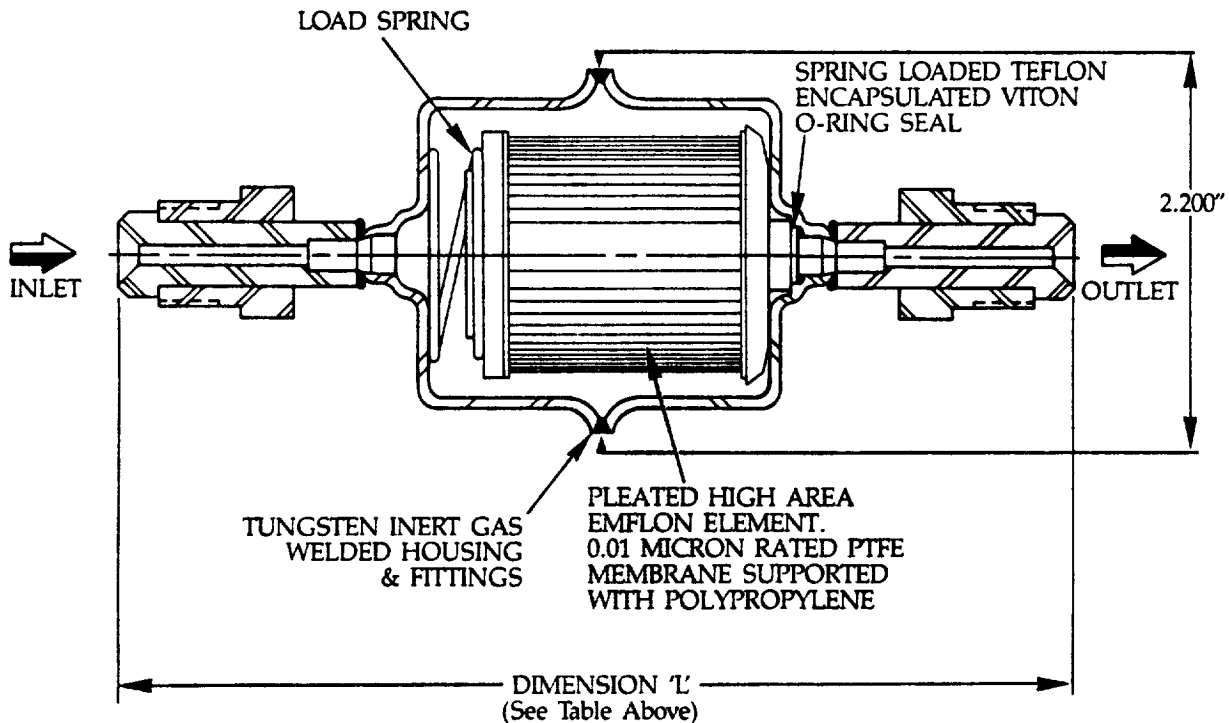
Part Numbers/Ordering Information

GLF6101  SGLF6101 

Code	Standard Fitting Options*	Nominal Length (L) — Inches	
		GLF	SGLF
SM4S	1/4" Compression Seal (Swagelok Compatible)	5 9/16"	4 3/16"
SM6S	3/8" Compression Seal (Swagelok Compatible)	5 13/16"	4 7/8"
VM4	1/4" Gasket Seal, Male (VCR Compatible)	5 9/16"	4 15/16"
VM6/B	3/8" Gasket Seal, Male (VCR Compatible)	5 13/16"	5"

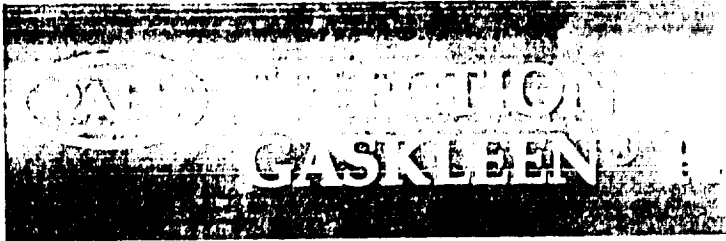
* Other fittings available on request.

**Engineering Drawing:
Gaskleen® Gasline Filter Assembly**



Pall Ultrafine Filtration Company
 East Hills, New York 11548
 (516) 484-5400, 1-800-645-6532
 Telex: 968855 TWX: 510-223-0606
 FAX: 516-484-5228

Serves Electronics, Pharmaceutical,
 Biological, Veterinary, Fermentation, Bioprocessing,
 Food and Beverage Industries.



ORIGINAL PAGE IS
OF POOR QUALITY

Description

The Pall Gaskleen® in-line gas filter is specifically designed to effectively remove submicron-size, yield-reducing particles from front end processing gases. This convenient device assures 0.01 micron absolute filtration efficiency and long service life. Unlike other gas line filters, the Gaskleen filter assembly will not shed particles.

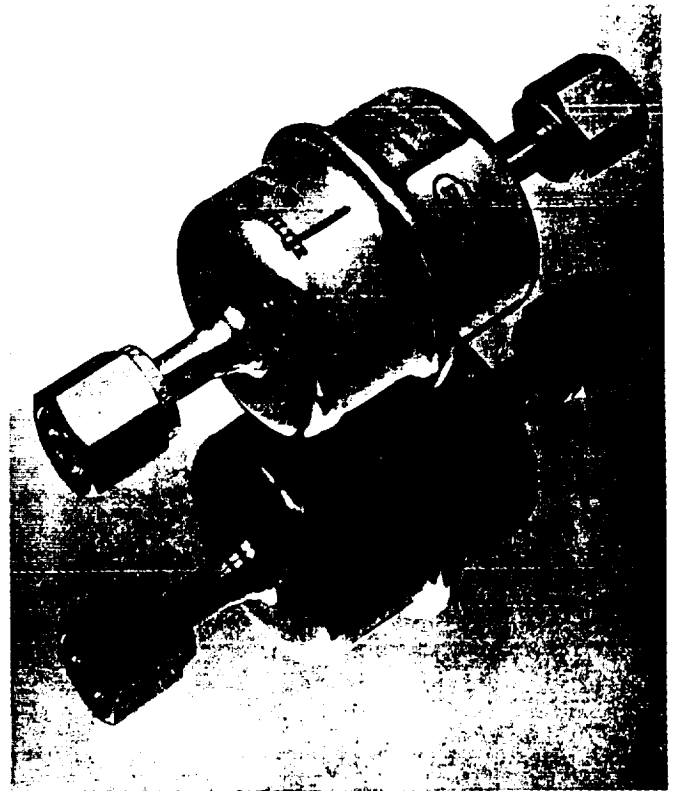
All filter components are compatible with specialty gases. The welded, 316L stainless steel housing withstands high operating pressure and ensures maximum safety and compatibility. The standard Swagelok† and VCR†† compatible fittings allow quick installation into any system.

The Pall Gaskleen is available in a standard length (GLF 6101) and shortened version (SGLF 6101). For complete specifications see below.

All Gaskleen filters are packaged in special double bags with nitrogen to prevent moisture and oxygen contamination. An outside, aluminized Mylar®, vapor barrier bag is used with an inner safety bag to ensure cleanliness.

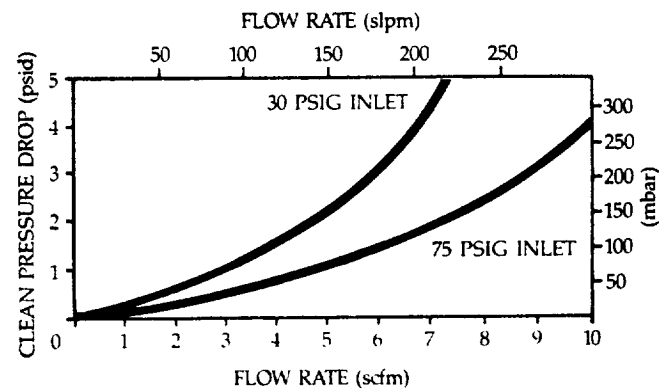
Assembly Characteristics

- 0.01 micron Emflon® (PTFE) medium with polypropylene end caps and support layers
- 316L electropolished stainless steel housing
- 20-25 RMS internal surface finish
- 750 psig operating pressure at 100°F
- Teflon††† encapsulated Viton††† O-ring
- 100% helium leak tested to 10⁻⁷ atm cc/sec; design tested to 10⁻⁹ atm cc/sec
- Choice of various 316L stainless steel fittings including VCR and Swagelok compatible fittings
- 0.5 ft² effective filtration area for both the standard and shortened versions
- Manufactured, nitrogen purged and packaged in a clean room
- Filter element 100% integrity tested



Gaskleen® Filter Assembly

Pressure Drop vs. Gas Flow Rate



† Trademark of Crawford Fitting Company
 †† Trademark of Cajon Company
 ††† Trademark of E.I. du Pont de Nemours & Company

Represented By
ENPRO INCORPORATED
 121 S. LOMBARD ROAD
 ADDISON, ILLINOIS 60101
(708) 629-3504

Appendix V Pumps.

Further development and design analysis are required to design instrumentation for application of this technique to particle counting in containerless processing systems.

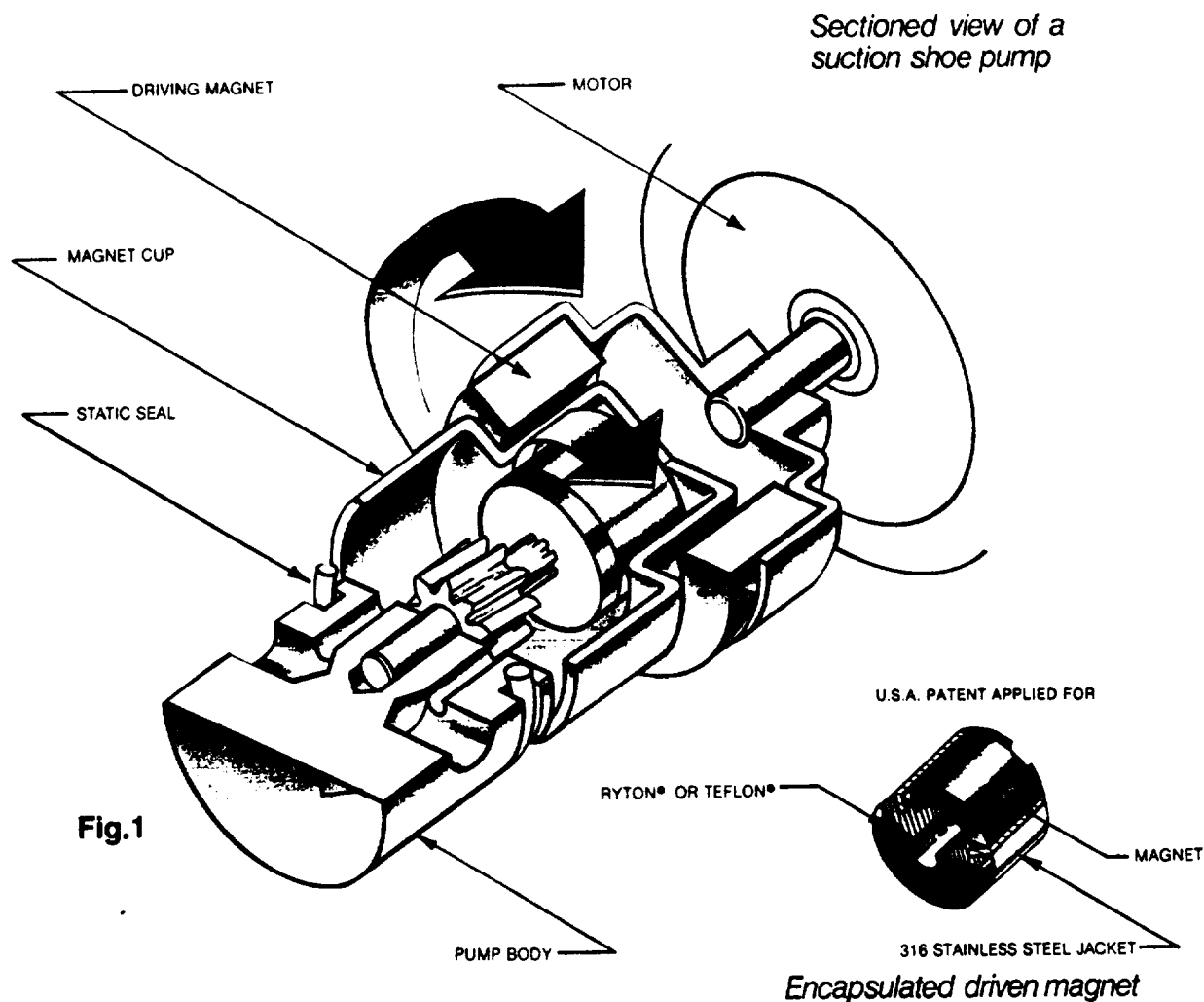
There are two areas which require further evaluation. The first is to determine the optimum location for the pump in a gas recirculating system. If the gas is used to entrain particles, the pump must produce sufficient gas flow velocity and volume to provide the required level of particle removal.

The second consideration is the type of pump which is best suited to the application. The following types of pump may be used for this application:

- o Gear pumps provide a continuous pressure head and flow rate. Magnetic coupling eliminates the need for rotating shaft seals and minimizes pump-related sources of contamination. Gear pumps may be used in low pressure and can be evacuated and baked out to provide a high degree of cleanliness.
- o Diaphragm pumps separate the driving components from the gas handling components by a diaphragm. Double diaphragm pumps may be used to provide continuous flow.

Product literature is enclosed on a number of pumps. There is a need for further research and evaluation to provide a pump system suitable for the application proposed here.

* NASA Conference Publication 10033, NASA Laser Light Scattering Advanced Technology Development Workshop-1988, Edited, W.V. Meyer, Cleveland, Sep. 7 and 8, 1988.



Freedom from leaks/contamination

The conventional means of sealing pumps is by using some type of shaft seal. These shaft seals are dynamic seals (moving seals between the shaft and the pump housing) and allow areas where leakage and contamination can occur. Dynamic seals also create additional friction that the motor must overcome. Magnetically coupled pumps eliminate shaft seals.

Magnetically coupled pumps utilize a static seal (see Fig. 1) that is not subjected to wear from moving parts. Using a static seal greatly reduces maintenance and virtually eliminates the possibility of contamination or leakage.

How the magnetic coupling works

The driven magnet is connected to the pumping parts and is sealed within a magnet cup (see Fig. 1). The driving magnet encircles this cup. The two magnets align themselves pole-to-pole and rotate together with no slippage until the decoupling limit is exceeded.

Decoupling

Decoupling occurs when the pump load exceeds the coupling torque between the magnets. This feature can act as a safety device to protect pump and motor from inadvertent damage. To recouple the magnets bring the motor to a complete stop, eliminate the cause of decoupling and restart.

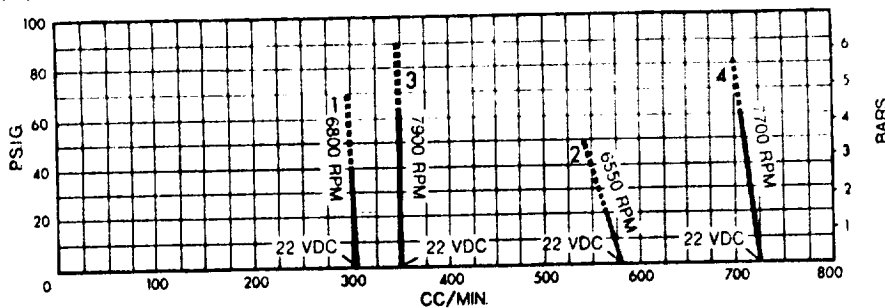
Encapsulated magnet

In magnet drive pumps the driven magnet is exposed to the fluid being pumped. To insure that the fluid remains contaminant-free, Micropump™ encapsulates driven magnets in 316 stainless steel and Rytan® or Teflon® (see Fig. 1)

SECTION K

FOR APPLICATIONS REQUIRING TEFLON®/316 STAINLESS STEEL

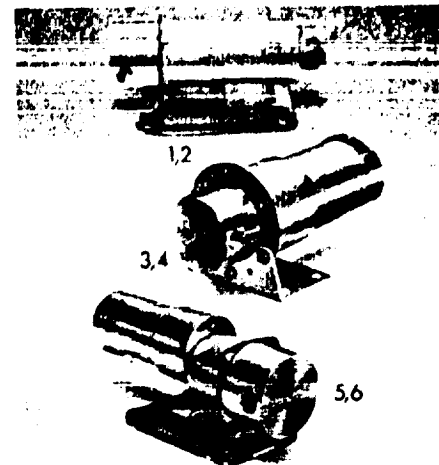
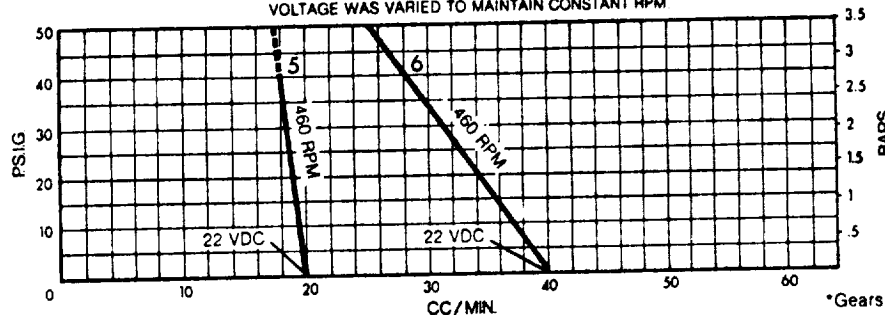
MAGNETIC DRIVEN GEAR PUMPS



INTERMEDIATE PERFORMANCES CAN EASILY BE ACHIEVED BY VARYING VOLTAGE INPUT TO THE MOTOR

— CONTINUOUS DUTY - - - - - INTERMITTENT DUTY

PERFORMANCES SHOWN ARE CONSTANT RPM CURVES. VOLTAGE WAS VARIED TO MAINTAIN CONSTANT RPM



MATERIALS IN CONTACT WITH FLUID:
GRAPHITE, TEFLON® &
316 STAINLESS STEEL

MAX. SUCTION VACUUM: 28.5" (724mm) Hg*

MAX. SYSTEM PRESSURE: 600 PSIG (41 BARS)

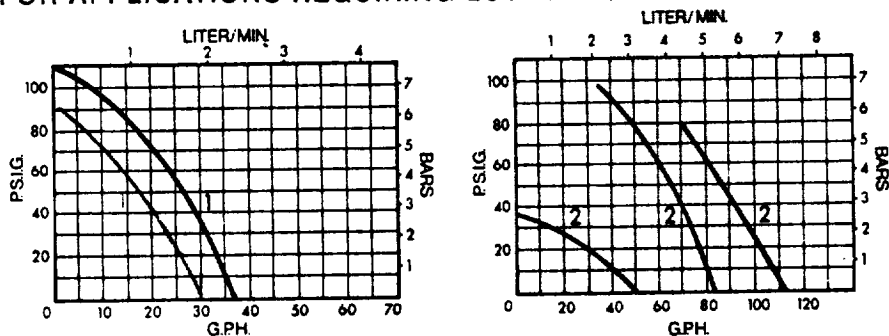
TEMPERATURE RANGE: -100°F. to 275°F.

*Gears wetted with H₂O dependent upon atmospheric pressure. (-73°C. to 135°C.)

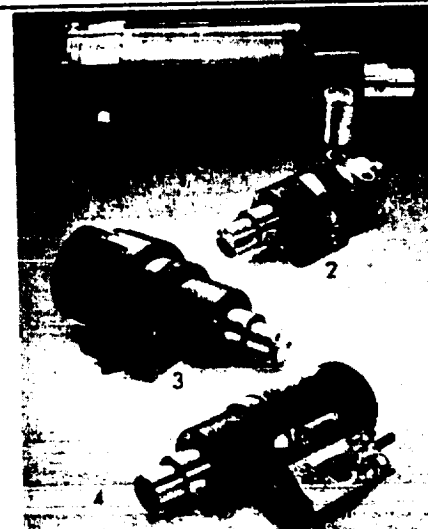
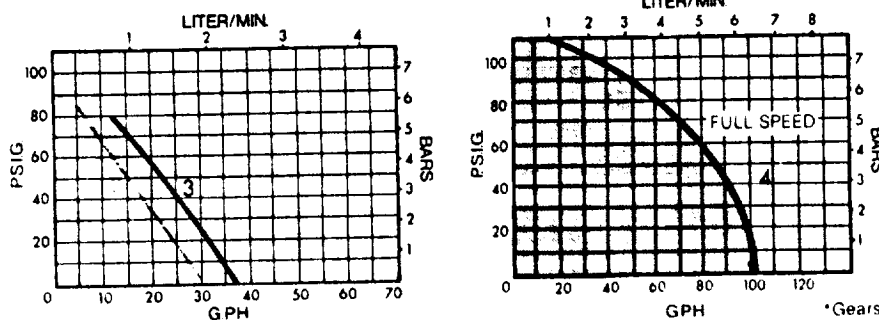
REF. NO.	MODEL NO.	MOTOR			DIMENSIONS				WEIGHT		PRICE	SERVICE KIT NO.		
		PUMP-MOTOR	VOLTS	@ HERTZ	AMPS*	H" x W" x L"	cm x cm x cm	LBS.	Kg					
1	180-336	0-24VDC	—	1.9	2.0	1.5	4.2	5.1	3.8	10.7	1.3	6	\$319.00	82135
2	182-336	—	—	—	—	—	—	—	—	—	—	—	313.00	82136
3	181-346	—	—	6.8	2.4	2.5	5.1	6.1	6.4	13.0	1.5	7	313.00	82135
4	183-346	—	—	—	—	—	—	—	—	—	—	—	313.00	82136
5	180-361	—	—	1.8	2.3	1.9	5.0	5.8	4.8	13.0	1.0	5	320.00	82135
6	182-361	—	—	—	—	—	—	—	—	—	—	—	314.00	82136

* AT STALL

FOR APPLICATIONS REQUIRING LOW PULSELESS FLOWS



— 50Hz



MATERIALS IN CONTACT WITH FLUID:
TEFLON® & 316 STAINLESS STEEL

MAX. SUCTION VACUUM: 28.5" (724mm) Hg*

MAX. SYSTEM PRESSURE: 300 PSIG (20 BARS)

BY-PASS ADJUSTS: 10 PSIG (.7 BARS) to MAX. PRESSURE

TEMPERATURE RANGE: -50°F. to 210°F.

*Gears wetted with H₂O dependent upon atmospheric pressure. (-45°C. to 98°C.)

REF. NO.	MODEL NO.	MOTOR			DIMENSIONS				WEIGHT		PRICE	SERVICE KIT NO.		
		PUMP-MOTOR	VOLTS	@ HERTZ	AMPS	H" x W" x L"	cm x cm x cm	LBS.	Kg					
1	120-519	115/230	60/50	2.0/1.0	5.2	6.1	14.1	13.2	15.5	35.8	20.6	9.4	\$555.00	81051
2	120-955	AIR PRESSURE			5.1	2.9	7.3	13.0	7.4	18.5	3.2	1.5	388.00	81051
3	120-605	115	60/50	1.5	4.3	4.2	8.8	10.9	10.7	22.4	6.6	3.0	340.00	81051
4	120-415	115	60/50*	2.1	3.5	4.8	9.1	9.4	8.6	20.6	5.25	2.4	408.00	81051





INTERSONICS
I N C O R P O R A T E D

SURVEY AND EVALUATION OF BEAM HEATING SYSTEMS
FOR APPLICATIONS IN CONTAINERLESS EXPERIMENTATION

Report on NASA Contract #NAS8-37592

By

J.K. Richard Weber
Shankar Krishnan
D. Scott Hampton
Dennis R. Merkley
Charles A. Rey

January 21, 1991

Preface

This work was carried out under NASA contract NAS8-37359 through NASA Marshall Space Flight Center, Huntsville, AL. The work was conducted by a team of scientists and engineers who have experience in the design and construction of flight hardware and in the application of containerless techniques to high temperature research.

The report contains recommendations for beam heating systems which could be used to achieve the high temperatures required for containerless microgravity materials experimentation and property measurements.

Table of Contents

1. EXECUTIVE SUMMARY 1

2. INTRODUCTION 1

3. SCOPE OF THE PROBLEM 2

3.1 Heat Balance 2

3.2 Energy Absorption and Delivery Efficiency 4

3.3 Conversion Efficiency 6

4. BEAM-HEATING SYSTEMS 7

4.1 Lamps 7

4.2 Electron Beam Heating 7

4.3 Laser Beam Heating 8

4.3.1 Solid State 8

4.3.1.1 Diode Lasers 8

4.3.1.2 YAG, YLF and Crystal Hot Lasers 9

4.3.2 CO₂ Laser Beam Heating 9

4.4 Solar Heating 10

4.5 Electromagnetic Heating 10

4.6 Microwave Heating 10

5. DISCUSSION 10

5.1 Lamp Heating 11

5.2 Electron Beam Heating 12

5.3 Laser Beam Heating 12

5.4 Solar Heating 13

5.5 Electromagnetic Heating 13

5.6 Microwave Heating 13

5.7 Power Supplies and Cooling Requirements 13

5.8	Safety Considerations	15
6.	RECOMMENDATIONS	16
7.	REFERENCES	16
8.	APPENDICES	17
	Figure 1	3
	Figure 2	5
	Figure 3	14

1. EXECUTIVE SUMMARY

The factors which can be used to select a non-contact heating system are described and discussed. For materials at high temperatures in a cold-wall chamber, radiation is the principal method of heat transfer. By selecting the heating beam wavelength and shape, energy transfer to the specimen can be optimized for many materials of potential interest.

The range of beam heating devices which may be used are discussed and recommendations are made for systems which would be well suited for heating of groups of materials such as glasses, ceramics, metals, and alloys.

Laser beam heating has been identified as the most versatile system of beam heating. The range of wavelengths available makes it possible to optimize a system for a particular group of materials. Because stray and reflected light are monochromatic, their interference with pyrometric and other optical measurements can be minimized.

A number of areas which warrant further investigation have been identified and work is recommended in the areas of electromagnetic heating and in design and testing of laser beam heating systems.

2. INTRODUCTION

High temperature containerless materials research and processing creates the need for non-contact heating methods. Energy efficient heating systems need to be developed for use in space-based applications. The purpose of this report is to evaluate approaches for heating materials to the high temperatures required for containerless experimentation.

High temperatures may be achieved by positioning an object inside a hot-wall furnace and allowing it to come to thermal equilibrium. This approach can be used to achieve modest temperatures but do not have useful capabilities above about 2000 K. Much of the interest in containerless research and property measurement requires materials to be heated to temperatures above 2000 K [1]. At these higher temperatures, the heat balance between the specimen and its surroundings favors non-isothermal or "beam heating" techniques.

The application of beam heating a specimen inside a cold-walled chamber offers several potential benefits:

- o Efficient use of heating power
- o High rates of temperature change
- o Clean, chemically pure environment
- o Non-intrusive
- o Minimizes waste heat burden on cooling system

3. SCOPE OF THE PROBLEM

Containerless experiments on materials at temperatures of up to 4000 K have been proposed. In a hot-wall furnace, the specimen temperature does not exceed the furnace wall temperature and the furnace cavity must be raised to the temperature required for the experiment. This uses energy to heat the furnace cavity wall as well as the specimen. Energy which is not used to heat the specimen provides an additional burden on cooling systems.

Beam-heating is inherently efficient because energy is used directly to heat the specimen in a cold environment. The power required for heating then depends on three factors:

- o Heat flow balance between the specimen and its surroundings.
- o Energy absorption and delivery efficiency.
- o Conversion efficiency of electrical energy into the heat beam.

3.1 Heat Balance

A hot specimen can lose heat to its surroundings by three mechanisms, conduction, convection and radiation. At temperatures above about 1500K, in a vacuum or gas at normal pressure, the predominant mechanism of heat transfer is radiation. For the purpose of the present discussion, conductive and convective losses will be ignored.

The equation which describes energy transfer from freely radiating body is Planck's equation:

$$W(\lambda, T) = \int_{\lambda_1}^{\lambda_2} \frac{C_1}{\lambda^5 [\exp(C_2/\lambda T) - 1]} d\lambda \quad (1)$$

where $W(\lambda, T)$ is the spectral radiance in $Wm^{-2} sr^{-1}$, c_1 is the first radiation constant = $1.1911 \times 10^8 W \mu m^4 sr^{-1}$, c_2 is the second radiation constant = $1.4388 \times 10^4 \mu m K$, λ is the wavelength in μm , and T is the absolute temperature of the radiating surface.

Planck's law applies to a perfectly emitting surface, i.e. a blackbody. Radiation from real surfaces requires a multiplicative factor, the spectral emissivity, ϵ_λ , where the λ subscript denotes the wavelength dependence. Values of spectral emissivity lie in the range from 0.0 to 1.0 and may vary widely with wavelength and temperature. Figure 1 shows examples of how the spectral emissivity of several groups of materials varies with wavelength.

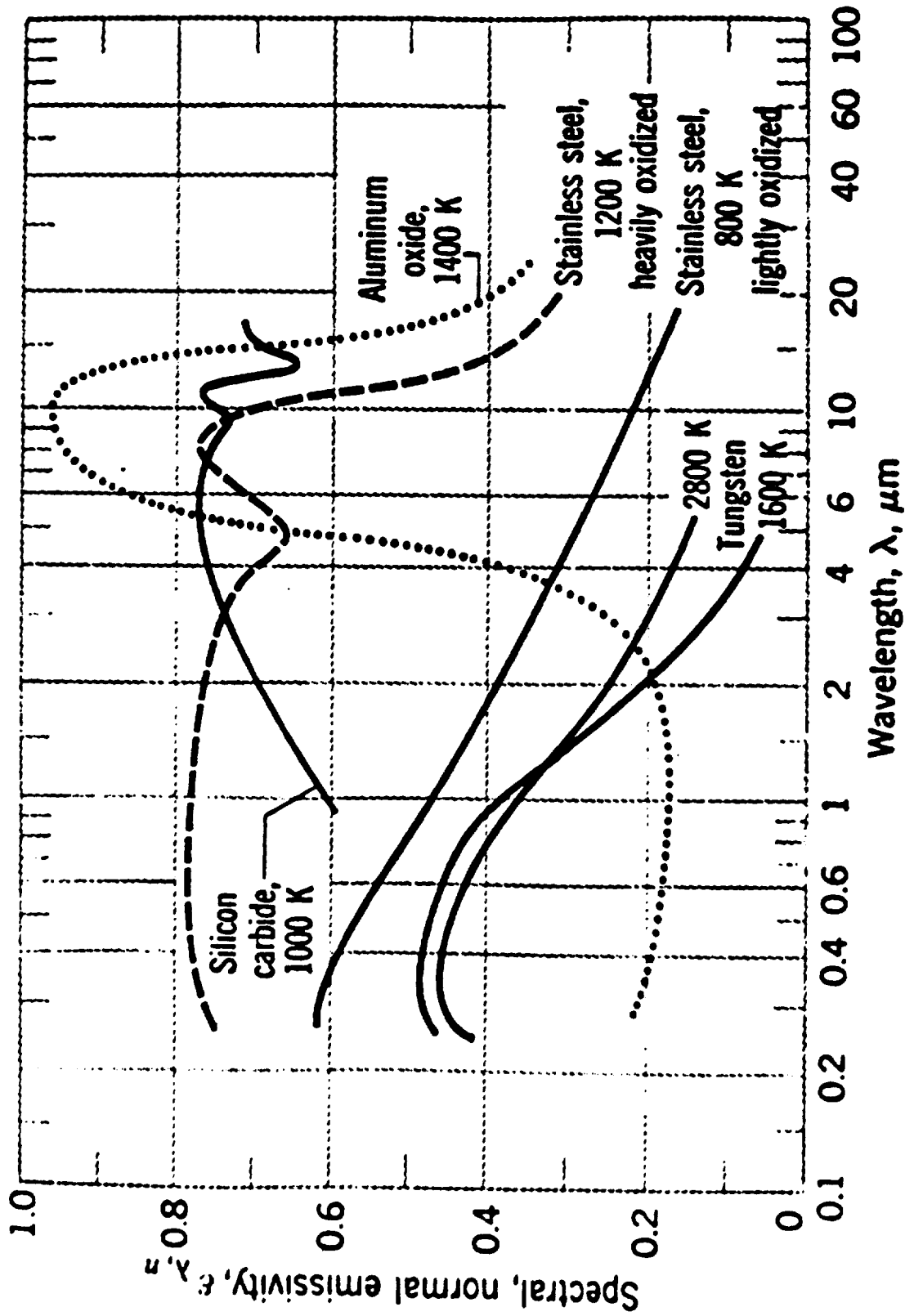


Figure 1. Wavelength dependence of emissivity for groups of materials of interest for beam heating. This figure is substantially as given in "Introduction to Heat Transfer" by F.P. Incropera and D.P. DeWitt, Wiley, 1990.

The total radiation heat loss from a surface at temperature T (K) is given by integration of eqn. 1 for all wavelengths. This gives the Stefan-Boltzmann equation:

$$W(T) = A \epsilon \sigma T^4$$

where W (T) is the radiant intensity in watts, A is the effective area of the radiating surface and σ is the Stefan-Boltzmann constant = $5.67 \times 10^{-8} \text{ Wm}^{-2} \text{ K}^{-4}$. The value of ϵ , the total emissivity, is a function of the material. Figure 2 shows the energy radiated per unit area by a blackbody as a function of its surface temperature.

The amount of energy radiated by a real material will depend on its total emissivity. Table 1 lists typical values of total emissivity for several materials.

TABLE 1

MATERIAL	Temp Range (K)	ϵ at 0.65 μm	ϵ (total)
Graphite	1000-3000	0.8-0.93	0.7-0.8
Copper	300 -1000	0.10	0.05
Platinum	1500	0.30	0.20
Tungsten	2000	0.43	0.28
Al ₂ O ₃ (Sapphire)	2000	0.005	0.005
Al ₂ O ₃ (Po. Cryst)	2000	0.30	0.45

The total emittance of many materials can be a strong function of temperature and can change sharply during a phase transition. For example, the value for solid sapphire at the melting point is about 0.005, but when the solid melts, this increases to about 0.90; so the rate of heat loss increases by a factor of about 200. In practice, this means that for sapphire, the radiative loss per cm² would increase from 0.8 W to about 150 W on melting.

A simple way to decrease the radiative heat loss from a material is to decrease the surface area of the specimen. A 0.2 cm sphere requires only 4% of the power that a 1.0 cm sphere would to maintain it at the same temperature.

3.2 Energy Absorption and Delivery Efficiency

When a specimen is beam heated in a cold-wall chamber, its equilibrium temperature will be reached when the rates of absorption and radiation of energy are equal. Radiation reaching a surface can be absorbed, reflected or transmitted. Only the component which is absorbed will heat the material. For any given wavelength, the absorption is equal to the emission when the material is in thermal equilibrium with its surroundings.

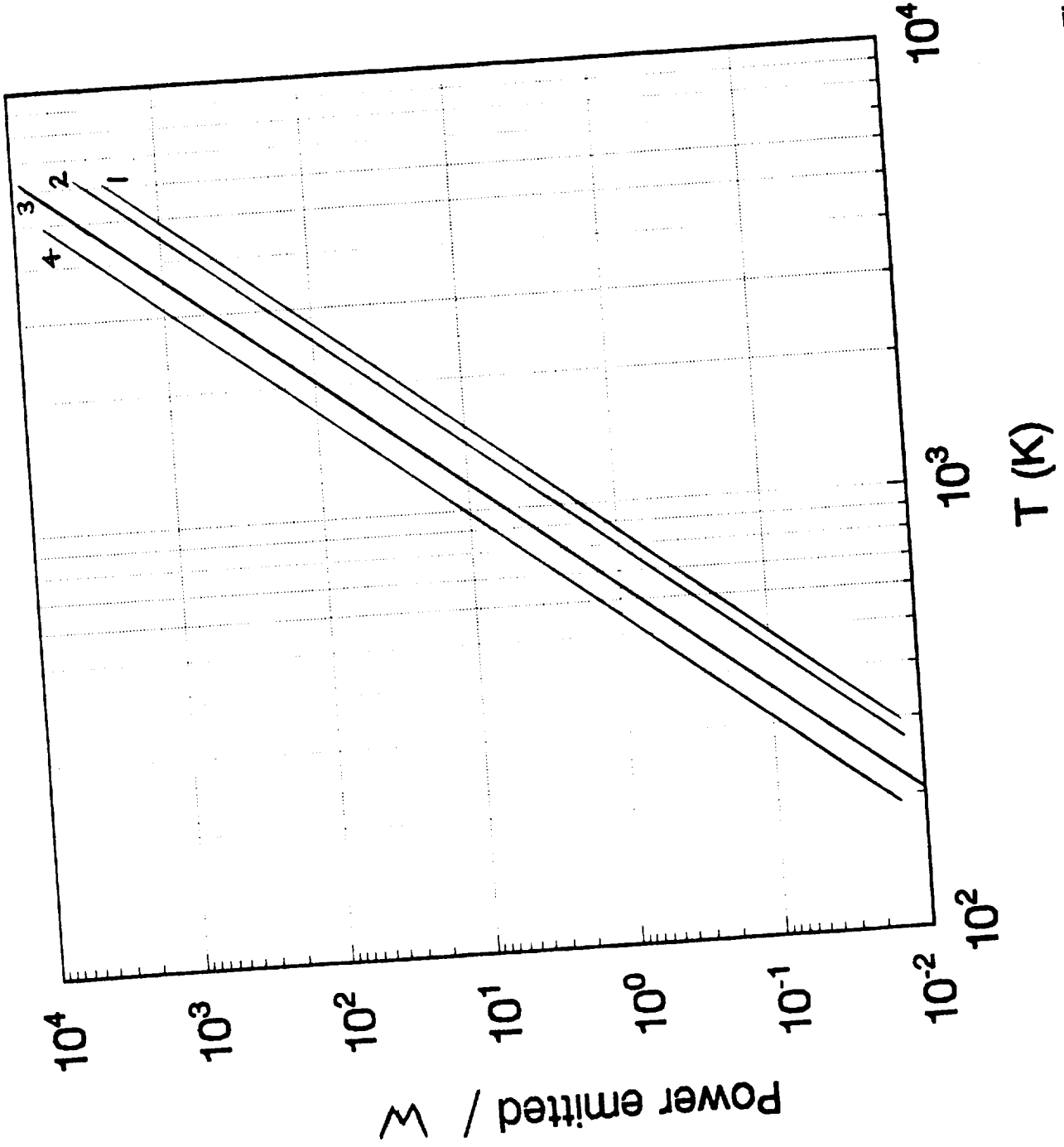


Figure 2. Energy radiated by a blackbody as a function of its surface temperature. The lines on the plot correspond to the surface areas of 0.25, 0.5, 1.0, and 2.0 cm² respectively.

Figure 1 suggests that for heating beams which cover the uv-ir (0.2 - 10 μm) spectrum, the wavelength of the heating beam can be selected to include areas of the spectrum where the material absorbs strongly. For example, many ceramics, such as aluminum oxide, mullite, zirconia, magnesia, and yttria absorb well in the 5-12 micron wavelength range, consequently they may be heated efficiently with beams which have energy concentrated in this range. Metals absorb well in the shorter wavelength 0.2-0.5 micron range and can therefore be heated most efficiently with radiation in this range.

Table 2 lists typically generic properties of various materials in terms of their absorbance, transmittances and reflectance. This table is relevant to beam-heating in the visible and IR regions of the spectrum.

TABLE 2

MATERIAL	ABSORBS	TRANSMITS	REFLECTS
TRANSITION METALS	UV, VIS	-	IR
METALLIC ALLOYS	UV, VIS	-	IR
SEMICONDUCTORS	ABOVE BANDGAP	BELOW BANDGAP	ABOVE BANDGAP
OXIDE GLASS	MWIR	VIS, IR	-
OXIDE, NITRIDE CERAMICS	MWIR	VIS, IR	-
POLYMERS	SWIR	IR, VIS	-

For efficient heating the energy from the heating beam needs to be directed to the surface of the specimen. The size of the beam and the ratio of the area of the heating beam to the area of the specimen will affect the thermal homogeneity of the specimen. A minimum requirement for efficient heating is that the specimen intercepts the whole cross section of the heating beam.

3.3 Conversion Efficiency

Conversion efficiency is the ratio of the output beam power from a device to the power supplied to it. Typical conversion efficiencies for particular devices are presented in section 4.

The most efficient method of beam heating a particular material may not be to use the device with the highest conversion efficiency. The optimum efficiency occurs when the product of conversion efficiency and absorption by the specimen is maximized.

4. BEAM-HEATING SYSTEMS

A number of approaches to beam heating can be devised. The choice of beam heating wavelength is determined by the absorption characteristics of the material to be heated and this is discussed further in Section 5.

4.1 Lamps

Lamps provide a spectral distribution which is centered in the near IR and visible region of the spectrum. Light can be produced either by a resistively heated incandescent filament or by a gas discharge in a sealed envelope. The spectral distribution which results is determined by the properties and temperature of the filament (up to about 3000K) or the temperature of the gas discharge (>5000K) and the absorption of the envelope. Heating can be achieved in a vacuum or gas environment.

Arc lamps have been used in a number of heating applications [2-4] including semiconductor processing and in KC 135 experiments [4]. For heating applications, light is focussed with reflecting lenses so that it provides even illumination of the specimen.

Arc lamps provide near point-source illumination and can be imaged to provide a concentrated beam. Filament type lamps, such as tungsten halogen, cannot be focused as well as arc lamps and this can limit their efficiency in some applications. The overall efficiency of lamp heating systems is generally rather low when the losses are due to optical collection and delivery to the sample are considered.

A number of other factors must be considered. In the case of arc lamps, the large change in impedance during starting requires a complex control system and creates a large amount of electromagnetic interference when the lamps are operated. For example, a 1kW xenon arc lamp typically requires 20 kV for ignition, then goes through a transition period requiring 250 volts before settling to 25V at 40 Amps to sustain the arc. Systems must therefore, be heavily protected against a number of interference problems generated by the lamp.

Lamps have the advantage that they are simple and readily available. Their spectral distribution makes them well suited to heating of some ceramics, silicon and other materials which absorb in the near IR region. However, the spectrum generated by lamps also covers the range over which hot bodies emit most of their radiation. This means that pyrometry has to be carried out at a wavelength where a significant amount of scattered and reflected light from the specimen can interfere with the measurement. This can be a major disadvantage of lamp heating in cases where noncontact temperature and property measurements are needed.

Information on commercially available lamps is given in Appendix I.

4.2 Electron Beam Heating

This technique uses a potential difference (typically 5-100 kV) between an electron gun and the specimen to accelerate electrons from the gun to the

specimen. Electron beam heating can be used to heat conducting materials including metals, alloys and carbon.

Electron guns are available in a range of output power from several hundred to several kilowatts. Electron beam heating can be efficient and the temperature of the target can be controlled by altering the emission current from the electron gun.

The principal limitations of electron beam heating are that it requires a vacuum to operate, heating may be localized and specimen charging can lead to loss of positioning stability and may result in a significant decrease in heating efficiency. These effects place restrictions on the types of experiments which could be carried out and the materials which could be processed.

4.3 Laser Beam Heating

Laser light is monochromatic and may be focussed with refracting optics or conducted with light guides. Laser beams may be propagated through a vacuum or a gaseous medium and laser beam heating has been widely used in ground-based experimentation [5-7] and in manufacturing operations. [8]

Two types of lasers are available; solid state (diode and pumped crystal host) and gas lasers. Depending on the lasing medium, a wide range of wavelengths from UV to IR are available.

4.3.1 Solid State

During the last decade there have been significant developments in the area of solid state laser technology. The development of high power, stacked arrays of laser diodes can provide a stable, high power system for heating applications. These may be operated in continuous wave (cw) or pulsed mode (also referred to as quasi -cw) depending on their construction. Quasi-continuous wave operation can be achieved by operating a set of pulsed laser diodes serially to provide overlap between the pulses.

4.3.1.1 Diode Lasers

Diode lasers are high intensity light sources made from a semiconductor such as gallium, aluminum, and arsenide (GaAlAs), in which the aluminum concentration controls the bandgap, and hence the emission wavelength. The wavelength can be about 670-1000 μm depending on the composition of the lasing medium. Diodes can be operated in continuous wave (cw) or quasi-cw (Q-cw long pulses, low repetition rate) modes. The design may consist of Single Quantum Wells (SQW) or Separate Confinement Hetero structures (SCH). Table 3 [9-11] summarizes the characteristics of selected laser diode systems. The efficiency figures presented in Table 3, represent typical values which may be achieved in ideal circumstances. For heating applications, the efficiency would depend on the duty cycle.

TABLE 3

Examples of Laser Diode Specifications

Device type	Mode*	Average Power	Nominal Conversion Efficiency
SQW-SCH	CW	3.8 W	40%
Linear Array	CW	12 W	40%
Stacked Two-dimensional Arrays	Q-CW	120 W	39%

* Quasi-CW devices require power supplies which can deliver large peak power pulses.

Product specifications for a representative selection of moderately high power laser diodes is given in Appendix II. One of the pioneering manufacturers of laser diodes is Spectra Diode Laboratories (San Jose, CA), they have increased the cw power and developed pulsed arrays for multi-beam devices.

Laser diode technology is rapidly evolving and higher power diodes which can operate at high efficiency with long duty cycles are becoming available. Engineering technologies include the development of fiber coupled diode lasers to provide 10 W from a 64 element bundle (Laser Diode Inc., New Brunswick, NJ). This offers a useful combination of high power and a convenient system for energy delivery to a specimen.

4.3.1.2 YAG, YLF and Crystal Hot Lasers

Flash lamp, discharge lamp or diode pumped solid state YAG or YLF lasers which lase in the wavelength range from 1-1.3 μm . These devices have potential applications in heating of some metals and ceramics.

The lasing medium is a stable crystal and has a long life expectancy. However, flash lamp pumped systems have a short life expectancy due to failure of the tube. Diode pumping is a more reliable system, but conversion efficiencies are very low. Typically, the YAG laser does not exceed 3% conversion of electricity into laser energy.

4.3.2 CO₂ Laser Beam Heating

Continuous wave CO₂ lasers provide radiation at 10.6 μm (MWIR) and beam heating has been applied in a number of materials processing and property measurement applications [5-8]. Research at Intersonics has demonstrated that the use of laser beam heating in combination with electromagnetic, aerodynamic or aero-acoustic levitation provides a convenient technique for attaining high temperatures [12].

Sealed tube gas lasers do not require a supply of gas. The lasing gases are sealed into the tube. Advances in sealed tube CO₂ lasers have resulted in compact units such as the Synrad r-f excited laser which operates from avionics power and generates 60 W cw laser power. Further information on sealed tube lasers is provided in Appendix III.

4.4 Solar Heating

The surface temperature of the sun is approximately 6000 K. However, the power density at the surface of the Earth is only about 0.13 W/cm². This means that in order to collect 100 W, a collecting area of about 700 cm² would be required. The spectral distribution is centered around 0.5 um and the majority of the energy is in the visible and near IR regions of the spectrum.

Experiments have demonstrated heating of materials to temperatures in excess of 2000K by use of focused solar radiation. The main limitation of using solar radiation directly is that it is difficult to control the heating rate in a useful way. The use of solar cells in combination with accumulators offers a possible means of supplementing the limited power which is available in flight hardware.

4.5 Electromagnetic Heating

Induction heating occurs when electrically conductive materials are exposed to high power rf fields, such as those developed by an electromagnetic levitator. In conventional electromagnetic levitators, control of the positioning forces and the heating power are linked and increasing the temperature of the specimen also increases the forces on it.

Recent developments have resulted in an ability to decouple heating and levitation [13] functions and enable heating of materials which can be positioned independently. Electromagnetic heating is limited to materials which conduct electricity; however, operation at higher frequencies extends the range of materials which can be EM heated.

4.6 Microwave Heating

Microwaves can be generated efficiently with magnetron tubes. The waves may be propagated into a tuned cavity to heat materials within it. The effectiveness of heating is a function of the absorption efficiency of material. This may be strong function of temperature resulting in "thermal runaway" when certain materials are heated.

Microwave heating has been developed for processing certain ceramic materials. [14] The use of microwave heating in materials experiments has been suggested by Barmatz [15] and heating of ceramics to high temperatures has been demonstrated.

5. DISCUSSION

Beam heating offers a useful means of heating specimens. Because beam heating is non-intrusive, it can enable maximum quiescence to be achieved in microgravity

processing experimentation. Many beam heating techniques provide a large degree of control, enabling precise temperature control to be achieved.

As indicated by Figure 1 and Table 2, the optimum heating technique for a particular material depends on the optical characteristics of the surface. In general metals absorb well at short wavelengths in the UV whereas ceramics and glasses absorb well at somewhat longer wavelengths in the IR. Metals can be heated by electromagnetic induction or electron beam heating. Any of these can be used in combination with a positioning system.

Table 4 summarizes the techniques of beam heating which may be applied in containerless processes. The conversion efficiencies are representative of the range which may be achieved.

TABLE 4

Summary of Beam Heating Methods

METHOD	SPECTRUM	TYPICAL CONVERSION EFF.*
LAMPS		
Tungsten-Halogen	0.25-2.4 μm	15-25%
Arc/Gas-Discharge	0.25-3.5 μm	10-25%
Electron Beam		5-25%
LASERS		
CO ₂	10.6 μm	5-10%
YAG	1.06 μm	1-4%
Laser Diodes	0.78-0.83 μm	15-50%
Solar	0.3-1.5 μm	-
Electro-magnetic Induction		5-10%
Microwave		30-50%

* Ratio of output beam power to total electrical power to operate device.

5.1 Lamp Heating

Lamp heating can be inexpensive and rugged. It provides a convenient system for heating most materials up to temperatures of 2-3000 K. Lamp heating is limited by its low efficiency which is largely due to light collection and focussing difficulties and the wide spectrum over which the energy is distributed. Large amounts of reflected light interfere with pyrometry and imaging of the specimen. In addition, arc lamp systems create a harsh environment for electrical equipment which complicates the overall system engineering task.

5.2 Electron Beam Heating

This technique can potentially provide high efficiency for heating metals. However, it requires a vacuum of $\leq 10^{-7}$ Torr for operation and this restricts its use. Experiments requiring a gas atmosphere can not utilize electron-beam heating and any of the advantages of using a gas atmosphere processing [16] can therefore not be realized.

The way in which the electron beam is focussed determines how efficiently the specimen is heated. In order to minimize beam disturbance by an rf field in an electromagnetic levitator, a small diameter beam would be required and this may produce localized heating, resulting in hot spots or ablation of the specimen. This effect would be most pronounced in larger specimens because of the very large power densities required to balance the radiative losses at high temperatures. These effects could be diminished if the levitation technique did not displace the electron beam.

The efficiency of electron beam heating will depend on two factors. The first factor is the amount of power used to energize the electromagnets necessary to steer the electron beam. The second is the amount of power absorbed by the specimen. Because the specimen is not grounded, it will become charged, resulting in heating of the chamber walls rather than the specimen.

5.3 Laser Beam Heating

Figure 1 shows that for a given group of materials, there is an optimum wavelength at which an energy beam will be absorbed. The wide range of lasers which are available provides a means of delivering power at the optimum wavelength for heating.

The following potential advantages of laser beam heating techniques are identified:

- o Stable, controllable power output
- o Choice of wavelengths
- o Can operate in a vacuum or most gaseous atmospheres
- o Readily focussed to provide optimum illumination of a specimen surface
- o Monochromatic light- reflected portion of beam does not interfere with pyrometry
- o High conversion efficiencies are possible

Laser beam heating systems have been demonstrated on Earth to be well suited to heating of a variety of materials. Sealed tube gas lasers, with laser diode technology, offers feasibility approaches to space qualified laser systems, but there are several areas of laser beam heating which require further development.

For example, if laser diodes are used, techniques would need to be developed to prevent light reflected from a specimen from entering the laser cavity. This has been addressed by Buoncristiani [17] of NASA Langley Research Center and a design suggested by him for using light from several lasers on a single specimen is presented in Figure 3.

Further work would be required to design optical systems capable of delivering power to the specimen. A variety of optics are available for this purpose and it is likely that an efficient system could be developed from these components. Systems based on cylindrical lenses and reflecting optics would enable maximum utilization of the energy emitted by the laser.

5.4 Solar Heating

This technique has the desirable quality that the source of energy is free. However, the requirements for experimentation in microgravity are that the source be controllable and available when required. Solar heating is limited in this regard. It may also be a difficult engineering task and could require considerable dislocation of the spacecraft facilities.

5.5 Electromagnetic Heating

This technique is well established for processing of metals. Electromagnetic heating efficiencies vary widely. Optimum heating occurs only when the output impedance of the generator and the impedance of the load are matched. This situation can be realized in practice only in a few cases. The SEL development [13, 18] aims to improve the impedance matching between the amplifier and load to increase the power utilization efficiency.

The reader is referred to the literature for a detailed discussion of the factors which may be optimized to provide efficient electromagnetic heating [19].

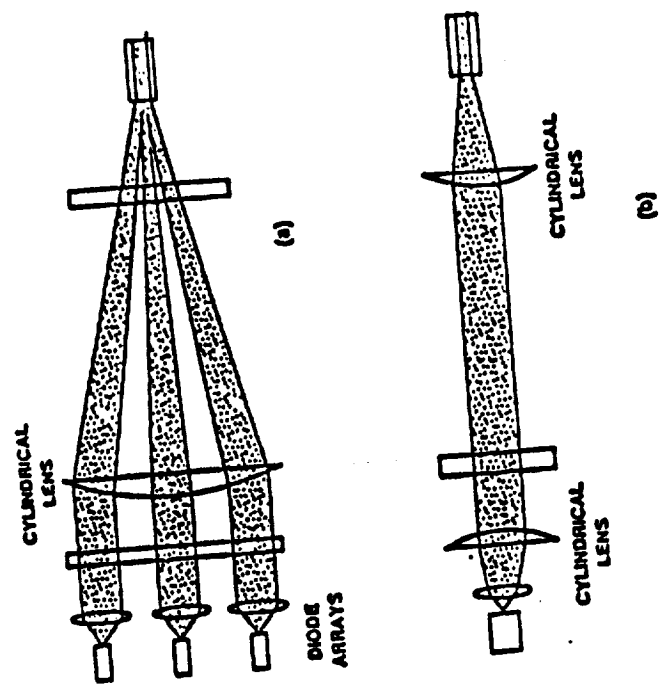
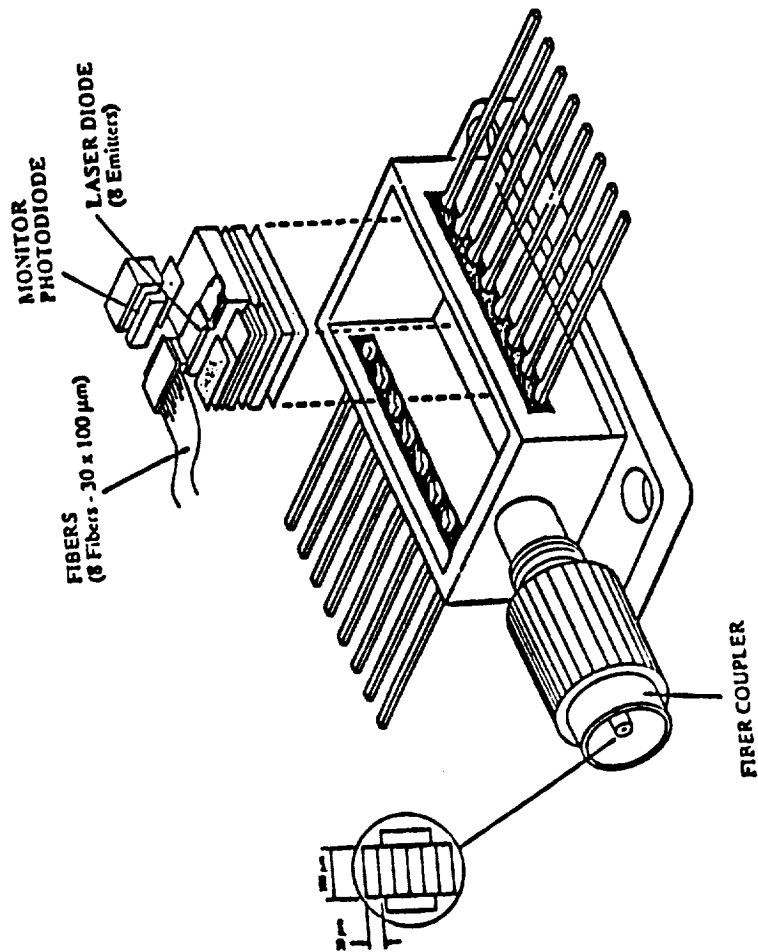
5.6 Microwave Heating

Microwave heating has the potential to provide a useful technique for processing of some ceramic materials. In many situations, heating is from the "inside out" leading to inverse temperature gradients. This may offer the potential for novel processing techniques. This issue of thermal runaway would need to be addressed in certain applications.

5.7 Power Supplies and Cooling Requirements

Systems designed to supply high power to specimens for heating purposes must be capable of delivering the energy efficiently to the heating device. Factors to be evaluated (and common to all systems in varying degrees) are the amount of electromagnetic interference produced by the high power devices and the amount of cooling required. Specific power supply requirements vary for each of the approaches discussed and some of them are summarized below.

Concepts for Optical Power Delivery



Scalable Lens Focus

Optical Fiber Ribbons

Figure 3. Optical systems for coupling laser diodes together to provide increased power and focusing of beams for heating specimens. Fiber coupling can provide 80 - 85% energy transmission

- o The impedance of an arc lamp changes significantly during its warm up period when the arc is struck and initiated. This requires a power supply capable of operating with a varying load.
- o Electron beam heating will require a large potential in order to provide for remote placement of the electron gun relative to the specimen. An accelerating potential of 50-100 kV would be required for operation of a typical electron beam welder, and similar potentials might be required for beam heating.
- o Sealed tube gas lasers require a high voltage supply.
- o Laser diodes operate at low voltage and high current which can be supplied by solid-state systems.

5.8 Safety Considerations

Safety aspects of the various techniques must also be considered since this is a primary concern in micro-gravity experiments. Some of these are common to all techniques. For example, hot specimens must be contained both from the standpoint of burn potential as well as outgassing of potentially dangerous materials. Other aspects are technique specific. The following is a summary of some of the safety issues that would need to be addressed:

- o Lamps - Lamps produce very hot surfaces which must be protected from and/or cooled. Arc lamps have a unique hazard of requiring high voltage (~20kv typical) for ignition. They also emit large amounts of UV and generally operate at a high internal pressure (20 atmospheres and higher) of xenon gas or mercury vapor. This is both an explosion and a harmful gas hazard.
- o Electron Beam - Electron beam heating requires very high supply voltages (up to 100 kv). Highly accelerated electrons may result in x-ray emission from some specimens.
- o Lasers- High power lasers pose a potential threat to the human eye and also require a high voltage power supply. Lasers with dangerous gases can probably be avoided leaving only the potential for relatively small amounts of carbon dioxide, helium, nitrogen, and/or argon. Solid state lasers leave only the potential eye threat as a hazard since they do not require gas or high voltage.
- o Microwaves - Leakage of microwaves would need to be prevented by shielding power. Any high energy heating system has the potential for creating a safety hazard. Therefore, all systems of this type require interlocks and failsafe designs to reduce the risks associated with a malfunction or operator error.

6. RECOMMENDATIONS

The approaches which provide the most potential for enhanced heating capabilities are laser beam heating and electromagnetic heating.

The most versatile method identified is laser beam heating because this can be tailored to meet the requirements of most material heating applications. Lasers may be propagated through a vacuum or gaseous medium. Laser beams may be focussed to provide the optimum heating configuration for a particular specimen, dual-sided or multiple-point heating systems can be designed with reflecting optics or light guides.

The following areas requiring further development and/or study have been identified:

- o Development of improved impedance matching systems for use in electromagnetically heated systems
- o Specification of laser beam systems for heating of ceramics and metals
- o Design and testing of a laser diode beam heating system
- o Consideration of a high power CO₂ laser system for space application

7. REFERENCES

1. Proc First Workshop on Containerless Experimentation in Microgravity, Ed. E.H. Trinh, JPL, Pasadena, CA, 17-19 Jan. 1990.
2. Y. Ikegami, E. Mori and M. Saito, "Development of and Acoustic Levitation Device with a Mirror Furnace", Proc. #rd European Symposium on Materials Science in Space, (1979) pp. 121-125.
3. C.A. Rey, D.R. Merkley, G.R. Hammarlund and T.J. Danley, Quarterly Report, Contract NAS8-33742, 15-Oct-1987.
4. C.A. Rey and D.R. Merkley, Quarterly Report, Contract NAS8-33742, 15-Jul-1988.
5. P.C. Nordine, J.K.R. Weber, S. Krishan and R.A. Schiffman, "Vapor Pressure and Enthalpy of Vaporization of Pure Boron", High Temp. Sci., submitted, March, 1991
6. J.K.R. Weber, R.A. Schiffman, S. Krishnan and P.C. Nordine, "Containerless Processing and Property Measurements of High Temperature Liquids and Solids", Proc. VIIth European Symposium on Materials and Fluid Sciences in Microgravity, Oxford, UK, 10-15 Sep., 1989.
7. J.P. Coutures, J.C. Rifflet, D. Billard and P. Coutures, Proc. 6th European Symposium on Materials Under Microgravity, Bordeaux, 2-5 Dec., 1986.

8. S. Copley, "Shaping Ceramic With A Carbon Dioxide Laser", Proc. 120th TMS Meeting, 17-21 Feb. 1991, New Orleans, LA.
9. A.M. Buonchristiani, "Solid-State Lasers for Use in Non-Contact Temperature Measurements", Proc. Non-contact Temperature Measurement Workshop, JPL, Pasadena, CA, 17-19 Jan., 1989.
10. W. Streifer, D.R. Scrifes, G.L. Harnagel, D.F. Welch, J. Beger and M. Sakamoto, IEEE J. Quantum Electronics, 24, 883-894 (1988).
11. D. Botez "Recent Development in High-Power Single Element Fundamental Method Diode Lasers" Laser Focus, March 1987 pp.68-79
12. J.K.R. Weber, D.S. Hampton, S. Krishnan, D. Merkley, P.C. Nordine, J.K. DeVos and M. Zartarski "Containerless Liquid Phase Processing of Ceramic Materials; The Structure of Aluminum Oxide, Formed From The Undercooled Melt" in preparation
13. T.J. Danley, R.A. Schiffman, J.K.R. Weber, S. Krishna, P.C. Nordine, C.A. Rey and P.A. Bruno, "Stabilized Electromagnetic Levitation", Proc. XXVIII COSPAR, The Hague, The Netherlands, 25 Jun-6 Jul., 1990.
14. "Microwave Processing of Materials" ed. W.H.Sutton, M.H.Brooks and, I.J. Chatrisky,
15. M. Barmatz "Ground-based and Microgravity Containerless Positioning Technologies and Facilities" in Ref. 1
16. J.K.R. Weber, D.R. Merkley and C.A. Rey, "Study and Evaluation of the Feasibility of Providing Improved Contamination Control for Electromagnetic Levitation Systems, Rpt. Contract NAS8-37593, March 1, 1991.
17. A.M. Buoucrisiani and A.L. Fripp Private Communication
18. J.K.R. Weber, T.J. Danley, R.A. Schiffman, C.A. Rey, S.Krishnan and P.C. Nordine, "Stabilized Electromagnetic Levitator", Phase I final report, NASA contract NAS8-38468.
19. R.T. Frost and C.W. Chang, "Theory and Applications of Electromagnetic Levitation", Materials Processing in the Reduced Gravity Environment of Space, Proc., MRS Symposium, 9, 71 (1982).

8. APPENDICES

APPENDIX I

The enclosed specifications relate to the Canrad Hanovia xenon arc lamps. These were used in the KC-135 flights of the High Temperature Acoustic Levitator [4].

APPENDIX II

Diode lasers

Laser diode technology is rapidly evolving. In 1990, Spectra Diode Labs introduced the SDL-2480 series, a 3-Watt CW diode laser array with a 500 um aperture and the SDL-3200 series, quasi-CW laser array with 60-Watt peak powers at 12 mJ/pulse. As a five bar stack, the specifications for the SDL-3200 series range from 300-1200 W peak power with energies of 60-240 mJ/pulse. In 1991, Spectra Diode Labs. plans to bring out 60 W/300 W quasi CW arrays that operate at 10% duty factors to provide 6-30 W of average power.

APPENDIX III

Synrad CO₂ laser.

CANRAD-HANOVIA XENON COMPACT ARC LAMPS

Xenon lamps are available from Canrad-Hanovia in standard ratings from 150 watts to 30 kw, and in custom configurations to meet the most exacting application's requirements. Xenon lamps provide high intensity light with a color temperature of 6000°K. Generally, Xenon lamps up to 10 kw require forced air cooling; and lamps over 10 kw must be liquid cooled.

In addition to high output in the visible portion of the spectrum (440 nm to 700 nm), Xenon Compact Arc Lamps are also an excellent source of IR radiation.

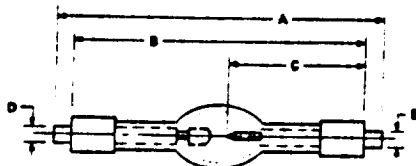
Diffused arc lamps are also available in Xenon format. The plasma of the arc is remarkably stable during operating, with "hot spots" virtually eliminated. The result is a more uniform pupil illumination.

Standard Xenon Compact Arc Lamps rated up to 10 kw are available with ozone-free quartz envelopes to absorb extreme UV. Diffused lamps range from 150 watts to 3500 watts in quartz or ozone-free envelopes.

Typical Lamp Configurations

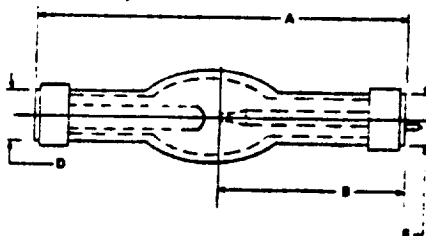
All Xenon Compact Arc Lamps, other than AC Lamps, require a minimum open circuit of 70 volts during ignition. AC Lamps require 115V up to 2500 watts and 200V above 2500 watts.

Outline 1



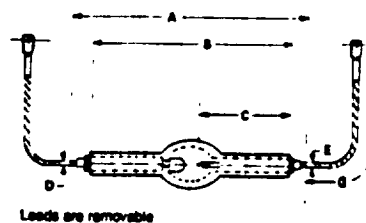
Unless otherwise indicated, all bulbs are clear fused quartz. Special electrical and/or mechanical configurations are available.

Outline 2



able in all types of Canrad-Hanovia Compact Arc Lamps.

Outline 3



Xenon compact arc lamps/150 to 10,000 watts

Lamps operated anode up $\pm 30^\circ$.

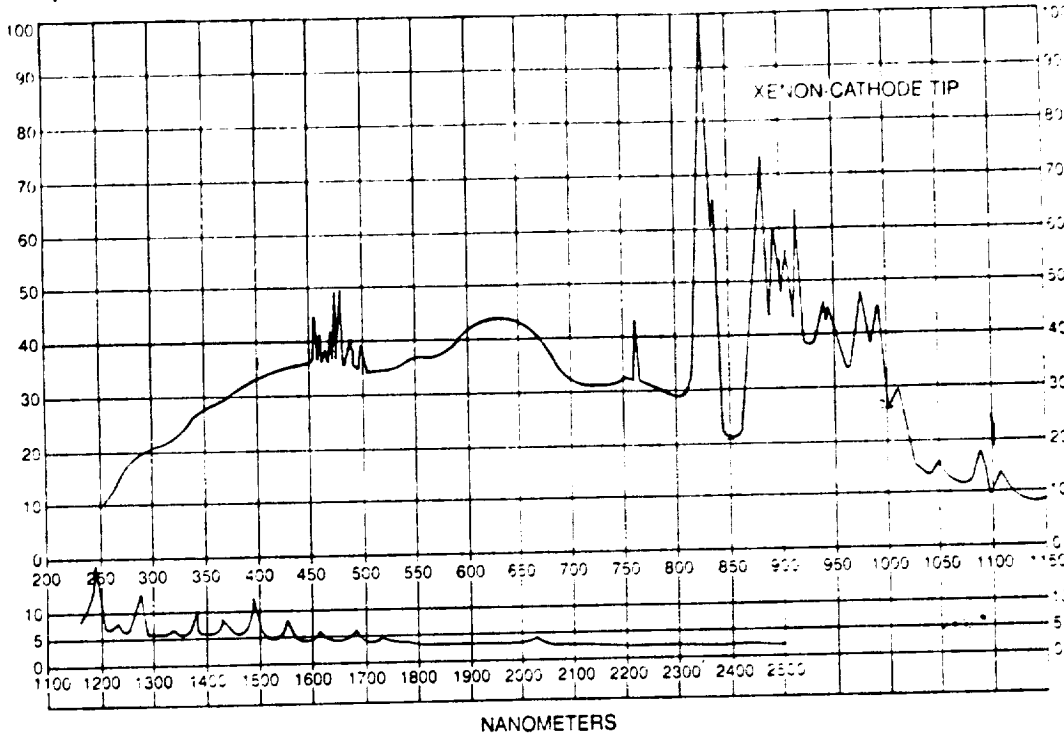
Watts	Lamp Type	Notes	Power Rated (Watts)	Operating		Luminous Flux (Lumens)	Horizontal Intensity (CDs)	Luminance Avg. (CDs/mm ²)	Over Area (mm ²)	Cold Arc Gap (mm)	Bulb Diam. (mm)	Avg. Life (Hrs.)	Mechanical Dimensions: See Outline #1				
				Voltage (Volts)	Current (Amps)								Length			Anode Dia. D	Cathode Dia. E
150	L5122-000	1	150	20	7.5	2200	300	470	5x1.5	19	18	1000	4 1/2	3 1/2	1.84	44	44
	901C0011		150	20	7.5	2200	300	470	5x1.5	19	18	1000	4 1/2	3 1/2	1.84	44	44
	L5236-100		150	20	7.5	2200	300	470	5x2.0	25	20	1000	5 7/8	4 1/2	2 1/2	4/7mm	4/7mm
	L5324-000	1	150	20	7.5	2200	300	470	5x2.0	25	20	1000	5 7/8	4 1/2	2 1/2	4/7mm	4/7mm
300	914C0010		300	15-20	15-20	6000	700	390	75x1.5	20	20	1000	5 1/2	4 1/2	2.08	44	44
500	L5269-000	1	500	14-20	30	9000	1500	3500	3x3	89	25	200	4 1/2	3 1/2	1.70	.87	80
	959C1980		500	14-20	30	9000	1500	3500	3x3	89	25	200	4 1/2	4 1/2	2.56	.87	80
700	991C0010	1	700	23	30	21,000	2300	400	1x2.5	31	29	1000	7	6 1/2	3.25	.44	44
1,000	L5179-000	1	1000	23	43.5	30,000	3000	400	1x3	40	38	1000	8 1/2	8 1/2	4.13	44	44
	976C0010		1000	23	43.5	30,000	3000	400	1x3	40	38	1000	8 1/2	8 1/2	4.13	44	44
	982C0980	1	1000	23	43.5	30,000	3000	400	1x3	40	38	1000	8 1/2	8 1/2	4.13	32	39
2,200	491C1390		2200	20-24	100	81,000	8000	680	1x4	5	57	1000	13 1/2	11 1/2	5.47	38	31
	L5289-000	1	2200	20-24	100	81,000	8000	680	1x4	5	57	1000	13 1/2	11 1/2	5.47	38	31
5,000	966C0390		5000	32-36	147	210,000	21,000	600	1x8	10-11	71	1000	16 1/2	14 1/2	6.72	38	31
7,000	L5341-000	1	7000	46	150	300,000	30,000	700	1x8	14	80	500	17.03	15.45	6.71	38	31
10,000	L5463-000		10,000	52-58	200	500,000	50,000	4000	*	14	100		16.97	15.39	6.71	38	55

NOTES 1 Ozone-free quartz bulb

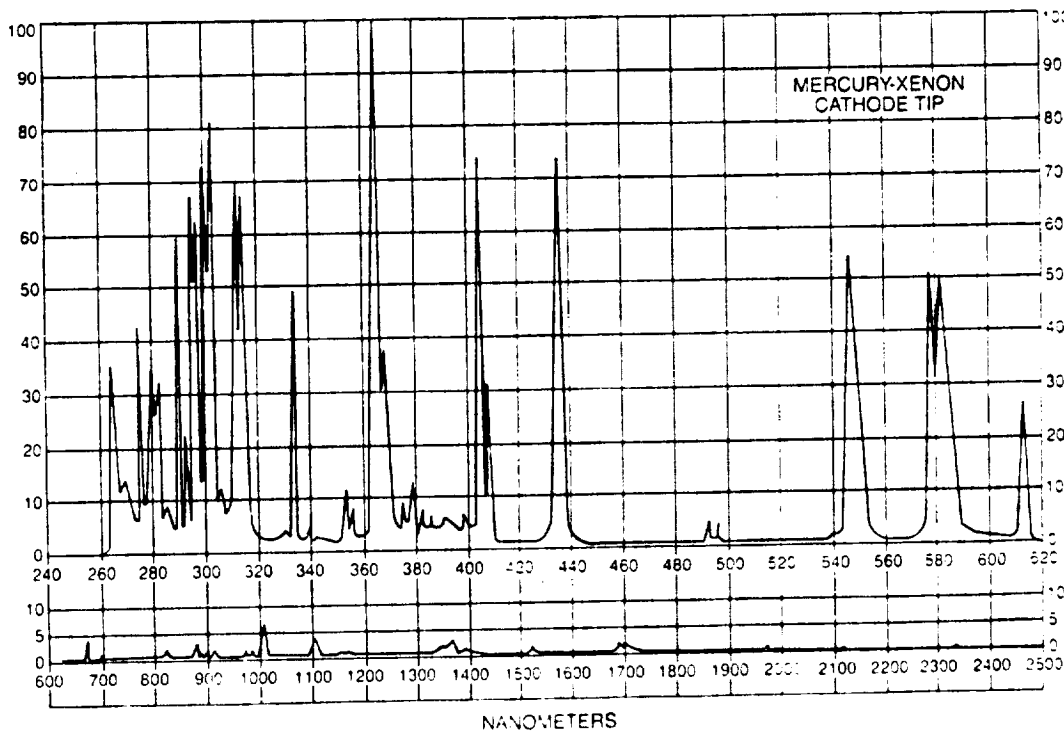
* 2mm diameter circle with center 0.5mm from cathode lip

Spectral emission curves

Spectral emission for Xenon Compact Arc Lamps



WAVELENGTH NANOMETERS	OUTPUT
300	0.1894
310	0.104
330	4.472
340	4.245
45	5.626
500	5.214
550	5.224
600	6.472
650	5.649
750	4.687
800	8.914
850	6.284
900	6.788
950	5.848
1000	2.871
1050	1.953
1100	1.402
1150	1.593
1200	0.846
1250	0.896
1300	0.795
1350	0.931
1400	0.919
1450	1.118
1500	0.751
1550	0.513
1600	0.515
1650	0.352
1700	0.28
1750	0.345
1800	0.306
1850	0.306
1900	0.306
1950	0.268
2000	0.345
2050	0.230
2100	0.230
2150	0.230
2200	0.230
	100.000



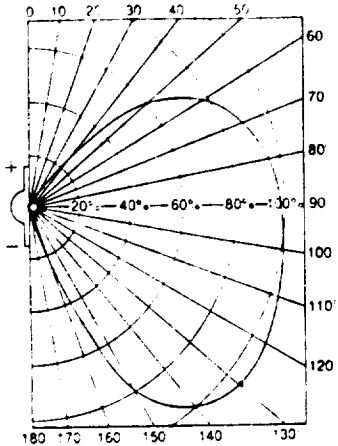
WAVELENGTH NANOMETERS	OUTPUT
260	2.205
270	0.778
280	0.883
290	4.201
300	3.883
310	7.308
320	1.372
330	0.448
340	0.886
350	4.131
360	0.538
370	0.488
380	0.504
390	0.319
400	0.207
410	0.498
420	0.196
430	0.207
440	0.196
450	0.196
460	0.196
470	0.196
480	0.196
490	0.196
500	0.196
510	0.196
520	0.196
530	0.196
540	0.196
550	0.196
560	0.196
570	0.196
580	0.196
590	0.196
600	0.196
610	0.196
620	0.196
630	0.196
640	0.196
650	0.196
660	0.196
670	0.196
680	0.196
690	0.196
700	0.196
710	0.196
720	0.196
730	0.196
740	0.196
750	0.196
760	0.196
770	0.196
780	0.196
790	0.196
800	0.196
810	0.196
820	0.196
830	0.196
840	0.196
850	0.196
860	0.196
870	0.196
880	0.196
890	0.196
900	0.196
910	0.196
920	0.196
930	0.196
940	0.196
950	0.196
960	0.196
970	0.196
980	0.196
990	0.196
1000	0.196
1010	0.196
1020	0.196
1030	0.196
1040	0.196
1050	0.196
1060	0.196
1070	0.196
1080	0.196
1090	0.196
1100	0.196
1110	0.196
1120	0.196
1130	0.196
1140	0.196
1150	0.196
1160	0.196
1170	0.196
1180	0.196
1190	0.196
1200	0.196
1210	0.196
1220	0.196
1230	0.196
1240	0.196
1250	0.196
1260	0.196
1270	0.196
1280	0.196
1290	0.196
1300	0.196
1310	0.196
1320	0.196
1330	0.196
1340	0.196
1350	0.196
1360	0.196
1370	0.196
1380	0.196
1390	0.196
1400	0.196
1410	0.196
1420	0.196
1430	0.196
1440	0.196
1450	0.196
1460	0.196
1470	0.196
1480	0.196
1490	0.196
1500	0.196
1510	0.196
1520	0.196
1530	0.196
1540	0.196
1550	0.196
1560	0.196
1570	0.196
1580	0.196
1590	0.196
1600	0.196
1610	0.196
1620	0.196
1630	0.196
1640	0.196
1650	0.196
1660	0.196
1670	0.196
1680	0.196
1690	0.196
1700	0.196
1710	0.196
1720	0.196
1730	0.196
1740	0.196
1750	0.196
1760	0.196
1770	0.196
1780	0.196
1790	0.196
1800	0.196
1810	0.196
1820	0.196
1830	0.196
1840	0.196
1850	0.196
1860	0.196
1870	0.196
1880	0.196
1890	0.196
1900	0.196
1910	0.196
1920	0.196
1930	0.196
1940	0.196
1950	0.196
1960	0.196
1970	0.196
1980	0.196
1990	0.196
2000	0.196
2010	0.196
2020	0.196
2030	0.196
2040	0.196
2050	0.196
2060	0.196
2070	0.196
2080	0.196
2090	0.196
2100	0.196
2110	0.196
2120	0.196
2130	0.196
2140	0.196
2150	0.196
2160	0.196
2170	0.196
2180	0.196
2190	0.196
2200	0.196
2210	0.196
2220	0.196
2230	0.196
2240	0.196
2250	0.196
2260	0.196
2270	0.196
2280	0.196
2290	0.196
2300	0.196
2310	0.196
2320	0.196
2330	0.196
2340	0.196
2350	0.196
2360	0.196
2370	0.196
2380	0.196
2390	0.196
2400	0.196
2410	0.196
2420	0.196
2430	0.196
2440	0.196
2450	0.196
2460	0.196
2470	0.196
2480	0.196
2490	0.196
2500	0.196
	100.000



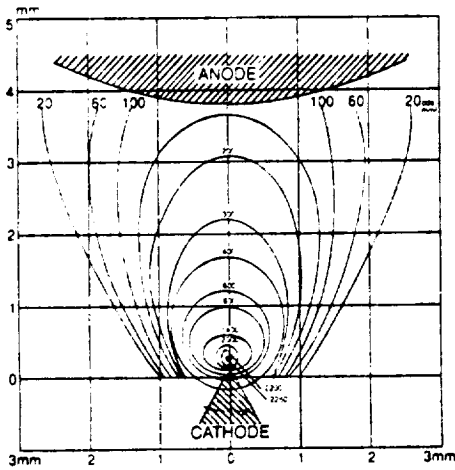
CANRAD-HANOVIA, INC.
 100 Chestnut Street, Newark, NJ 07105
 (201) 589-4300, Telex 13-8531

ORIGINAL PAGE IS
 OF POOR QUALITY

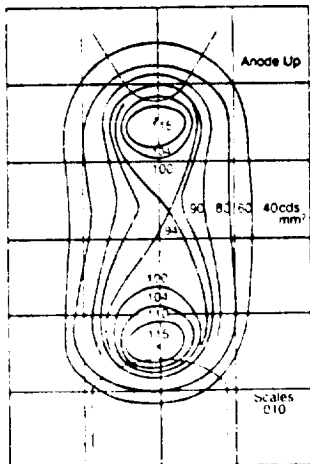
Typical intensity-luminance data



Relative Light Intensity Distribution of Typical Compact Arc Lamp



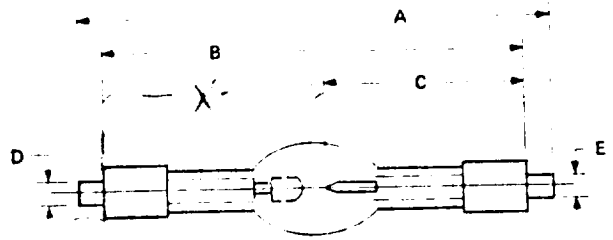
Luminance Distribution in Arc of Typical Compact Arc Lamp at 100 Amps



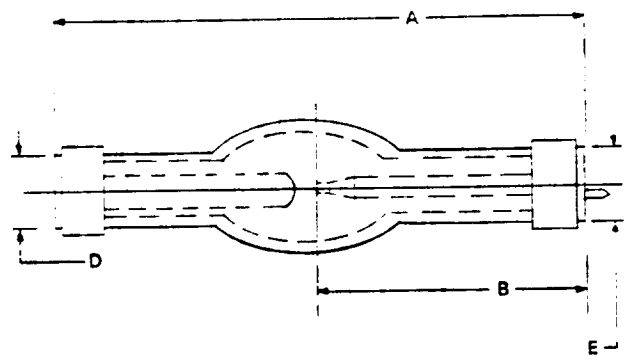
Luminance Distribution of Typical Diffuse Mode Compact Arc Lamp at 8.5 Amps

Typical lamp configurations

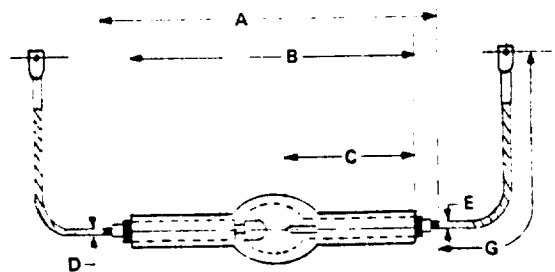
Outline 1



Outline 2



Outline 3



Leads are removable

All Xenon and Mercury-Xenon Compact Arc Lamps, other than AC Lamps, require a minimum open circuit of 70 volts during ignition. AC Lamps require 115V up to 2500 watts and 200V above 2500 watts

Unless otherwise indicated all bulbs are clear fused quartz.

Special electrical and/or mechanical configurations are available in all types of Canrad-Hanovia Compact Arc Lamps.

**ORIGINAL PAGE IS
OF POOR QUALITY**

SCALABLE, END-PUMPED, DIODE LASER PUMPED Nd:YAG LASER*

T. Y. Fan and A. Sanchez
Lincoln Laboratory, Massachusetts Institute of Technology
Lexington, Massachusetts 02173-0073
(617) 276-6737

The highest efficiency diode laser pumped lasers with good beam quality have been demonstrated using an end-pumped geometry. However, end-pumped lasers have been limited to low power because of difficulties in scaling. Some techniques used to scale end-pumped lasers include polarization coupling, higher power pump sources,¹ multiple pump sources using fiber coupling,² and providing multiple "ends" by using many gain elements.³ Here we present an alternate method for scaling an end-pumped laser which is compatible with all the above techniques. Our technique takes advantage of the difference in beam quality from the diode laser in the planes perpendicular and parallel to the junction.

Figure 1 shows a schematic of our experiment in the planes parallel and perpendicular to the junction of the diode arrays. Each of the three linear diode arrays (SDL-2430-C) were collimated and the collimated beams focused into a Nd:YAG rod using cylindrical optics. The Nd:YAG rod was coated with a high reflector at 1.06 μm on one face and an antireflection coating on the other. The output mirror has 97.5% reflectivity at 1.06 μm . Preliminary results are shown in Fig. 2. Laser operation was obtained with each diode array operating separately. In each case the output was in a TEM₀₀ mode and the laser cavity was not realigned for operation for each diode array separately. With all three arrays operating the output was still TEM₀₀ and we were able to obtain nearly four times the output power compared with pumping with a single array.

Simple scaling arguments indicate that over an order of magnitude pump power increase in the same mode volume can be obtained compared with using a single array. This technique thus allows higher pump intensity at the gain medium which is desirable for low gain, tunable lasers, and quasi-three-level lasers.⁴

REFERENCES:

1. D. L. Sipes, *Appl. Phys. Lett.* **47**, 74 (1985).
2. K. Kubodera and J. Noda, *Appl. Opt.* **21**, 3466 (1982).
3. J. Frauchiger, P. Albers, and H. P. Weber, to be presented, Topical Meeting on Tunable Solid State Lasers, paper TuC2.
4. T. Y. Fan and R. L. Byer, *IEEE J. Quantum Electron.* **QE-23**, 605 (1987).

* This work was performed for the Strategic Defense Initiative Organization under U. S. Navy sponsorship.

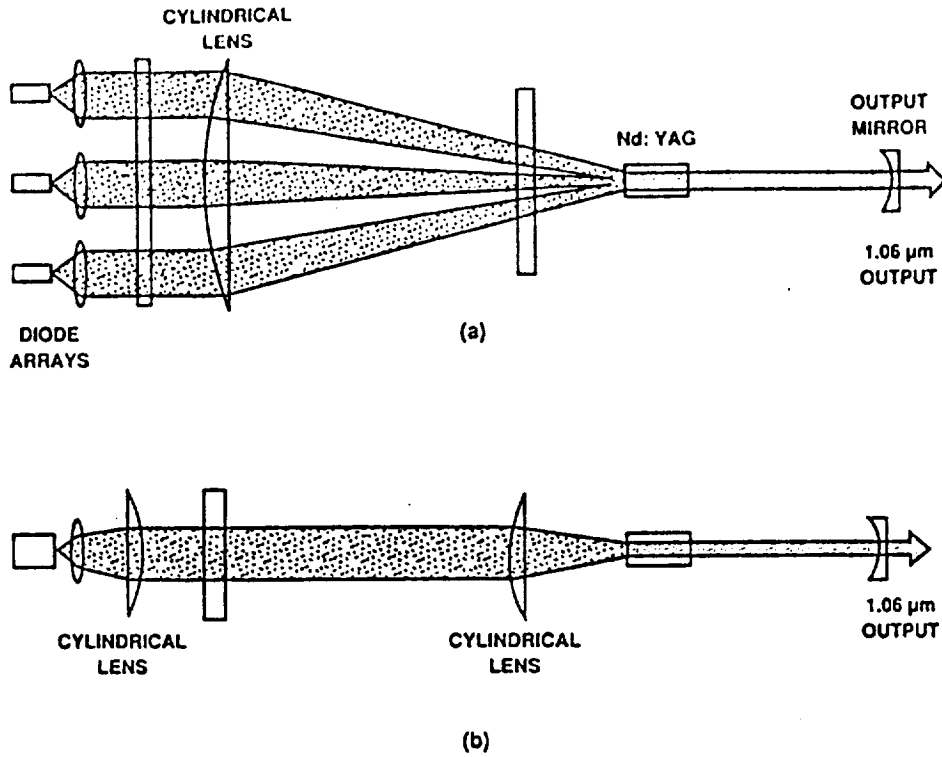


Fig. 1. Schematic of the scalable end-pumped laser experiment. (a) Plane perpendicular to the junction. (b) Plane parallel to the junction.

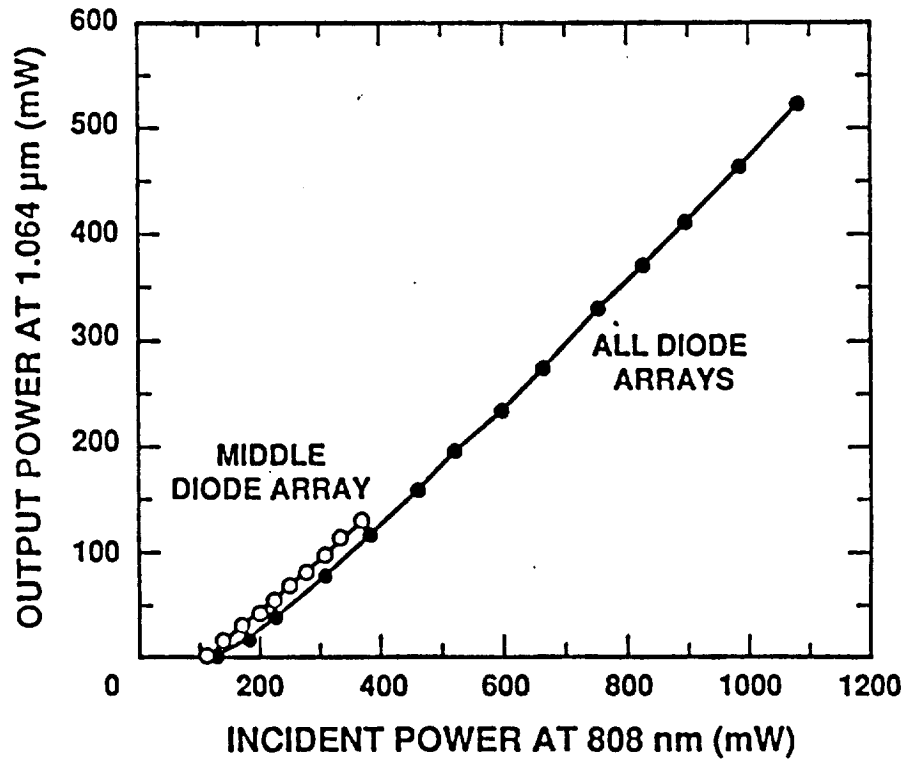


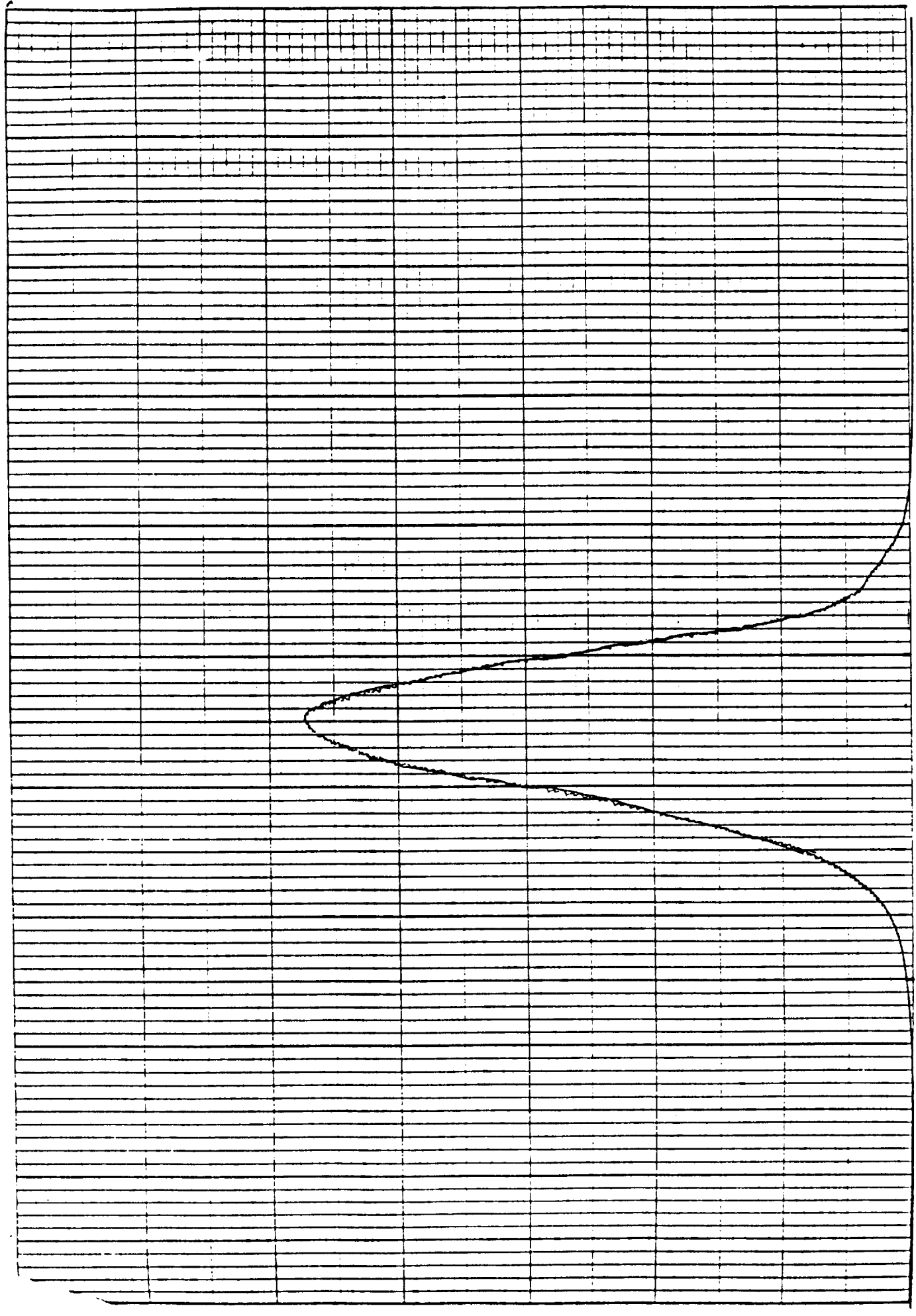
Fig. 2. Continuous wave output power as a function of input power for the middle array and all three arrays. The output for the other arrays operating individually was slightly less than the one shown.

3072 | WAVELENGTH | MICHE J RDE | SOCKET N/A

0014 | SERIAL NUMBERS MATCH | OPERATOR'S MANUAL


S/N# 061

SDL3490S



790 Wavelength (nm) 795 800 805 810

THE 48-5 "DUO-LASE" 50W CO₂ LASER



Synrad's "DUO-LASE" family of lasers combines two standard Synrad laser tubes for twice the output power of a standard laser. In model 48-5 the output beams from two 25 watt sealed CO₂ laser tubes are combined optically to provide a single, diffraction limited beam at 50 watts. This optical technique is unique in the laser industry and features a multitude of advantages for most applications over the conventional approach of intra-cavity folding to achieve high power output in a relatively short and compact laser body.

The DUO-LASE technique capitalizes on the long production history of Synrad's 48-1 and 48-2 "all-metal" lasers, over 1,000 of which have been manufactured. This assures the user a mature product with proven reliability. These lasers are also economical since they are built from high production volume modules that comprise our proven 10 and 25 watt sealed, RF-excited CO₂ lasers. The only new elements are the optical beam combiner and the water cooled chassis assembly.

Care has been taken to totally separate all power and control functions between the two laser sections achieving essentially failsafe operation for applications that can be served with the power of one laser. Any one electronic or laser tube failure will only affect that section leaving the second channel unaffected and available for use.

Even though about 500 watts of RF power is generated internally to the laser, the unit is transistorized with our modular approach using our standard 120 watt RF drivers. There is no warm up time as seen in the commonly used vacuum tube RF power supplies.

The DUO-LASE technique is also applicable for combining two of our CO lasers as well as for combining two 10 watt CO₂ lasers in a shorter package.

Applications for the 48-5 as well as other DUO-LASE products are limited to thermal applications (cutting, drilling, melting, vaporizing, engraving, etc.) These lasers can not be used for applications requiring a single frequency as two wavelengths are emitted at the same time. Ideal applications are medical as well as industrial use in the computer aided cutting of cloth, plastic, wood or thin metal products.

The optical combining technique is based on the fact that each laser is linearly polarized, allowing the use of a polarization sensitive beam combiner to achieve 98% efficiency in combining the two beams. The two components of the resulting beam are spatially parallel and colinear. The normal temporal and spatial variations of a single laser are reduced by combining the output of two lasers. Output polarization is random and therefore superior for many cutting applications.

The unit is self-contained (one unit) requiring only the application of AC or DC prime power (depending on model), cooling water, and a control signal. It is therefore ideally suited for overhead installation as a cutting tool in sail lofts. No RF cable runs are required.

ORIGINAL PAGE IS
OF POOR QUALITY

SPECIFICATIONS 48-5 CO₂ LASER

Wavelength	10.57 to 10.63 microns	
Power output (W)	Typical	60
	Min. on delivery	50
	End of life*	40
Power stability	(30 sec. warm up)	± 5%
Mode Quality	TEM ₀₀ equivalent	95% purity
Beam size (mm)		3
Beam divergence (mR)		5
Polarization		Random
Modulation	To 5 khz	
Electrical control	TTL input (+3.5V) to 10 khz	
Cooling water	1.5 gallons/minute at less than 20°C	
Electrical input	115 VAC version (48-5-115): 90-130 VAC, 50 to 400 Hz, 12A 28 VDC version (48-5-28): 28-32 VDC, 44 A max.	
Weight	44 lbs. (20 kg) max.	
Size	5.6×4.32×35" (142×110×890 mm)	

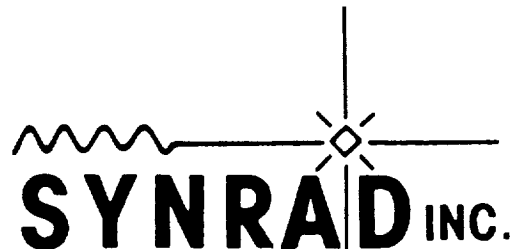
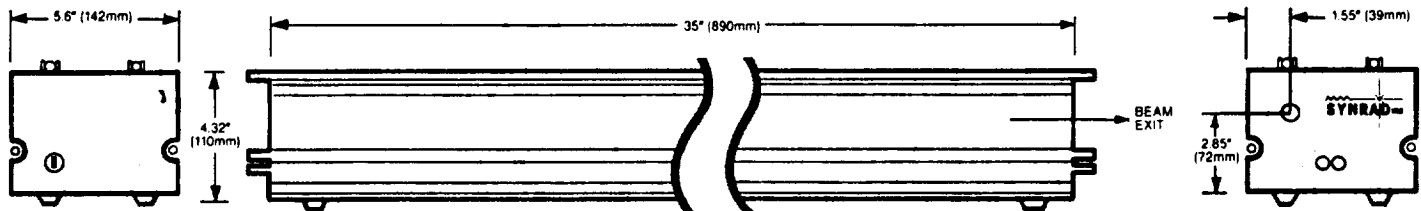
*This power level is guaranteed for 12 months regardless of operating hours, assuming normal intermittent commercial use.



INVISIBLE LASER RADIATION -
AVOID EYE OR SKIN EXPOSURE
TO DIRECT OR SCATTERED
RADIATION

100W CO₂ MAX

CLASS IV LASER PRODUCT



11816 North Creek Parkway North,
Suite 103
Bothell, WA 98011-8205

(206) 483-6100
FAX: (206) 485-4882

5 Watt GaAlAs Linear Array Laser Diode

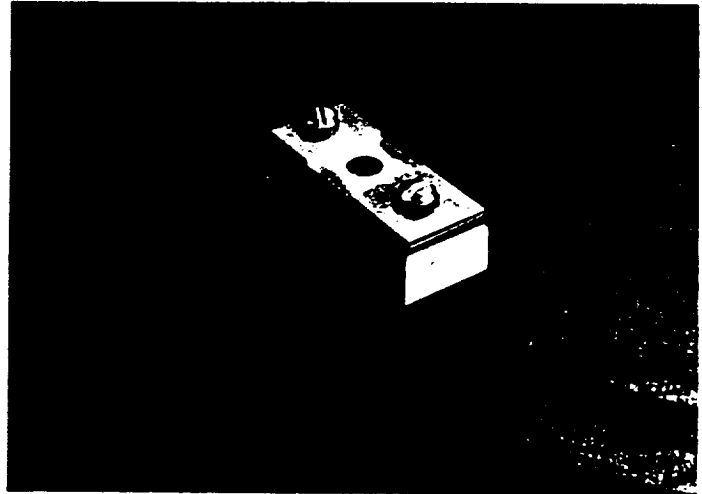
SDL-3480-L

5 Watt CW Optical Power

Monolithic Linear Array

High Efficiency Quantum
Well Structure

Reliable, 25 mW Per Emitter



ORIGINAL PAGE IS
OF POOR QUALITY

General Description

The high optical power and linear array format provided by the SDL-3480-L serves applications such as optical pumping of solid state lasers, beacons, and high power illuminators. With an emitting aperture of 1 cm x 1 μ m, the array can be easily coupled to side pumped Nd:YAG, or Nd:YLF rods or slabs. This highly efficient source is ideal for systems with limited energy or heat transfer budgets.

The SDL-3480 consists of twenty 10-stripe phase coupled emitters spaced on a monolithic 1 cm laser diode "bar". Individual stripes are spaced on 10 μ m centers. 10-stripe phased arrays each have an aperture of 100 μ m. Spacing of phased arrays is 0.5 mm. A total of 200 individual stripes, each operating at a power level of approximately 25 mW, sum incoherently to provide 5 W of optical power. The bar is bonded to a metal submount with the "P" surface (active junction) toward the submount for minimum thermal resistance. All emitters are driven in electrical parallel.

Reliability is enhanced by the relatively low energy emitted per stripe and the heat spreading spaces between groups of phased arrays. High optical power and high efficiency is achieved by a quantum well active layer structure that provides low threshold and excellent electrical to optical conversion efficiency.

The linear array output facet is directly available, facilitating placement of optical elements or intimate coupling to laser media. The copper heatsink is designed to be readily mounted to an external thermoelectric element and heat removal system. Options include wavelength selection for Nd:YAG and Nd:YLF. The diode array must be temperature tuned to the rare earth absorption band.

Spectra Diode Labs

SDL-3480-L Specifications (Typical Values @ 25°C)

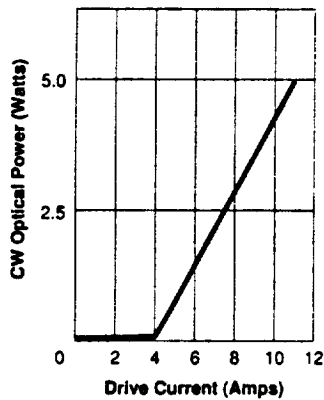
Parameter	Optical			Emitting Dimensions (W X H)	Beam Divergence $\theta_{\perp}, \theta_{\parallel}$	Spectral Width	Electrical			Thermal
	CW Output Power	Differential Quantum Efficiency	Total Conversion Efficiency				Threshold Current	Operating Current	Series Resistance	Recommended Case Temperature
Model	W	W/A	%	μm	deg FWHM	nm	A	A	Ω	$^{\circ}\text{C}$
SDL-3480-L	5	0.7	25	1 cm x 1 μm	50 x 10	3	4	11	0.03	0 to 25

Absolute Maximum Ratings

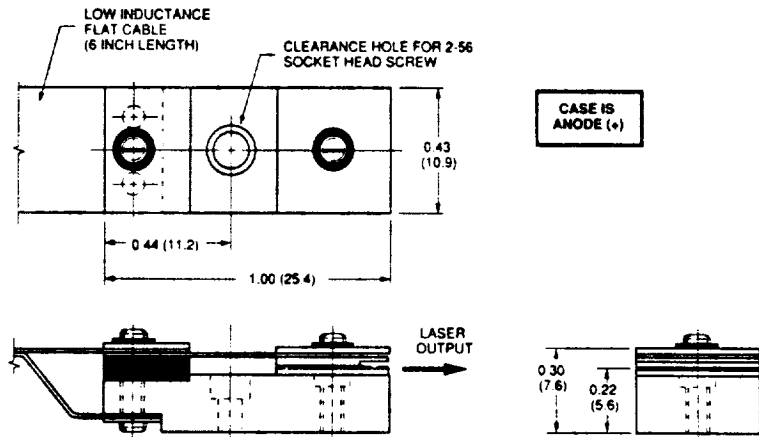
CW Output Power	5.2 Watts
Reverse Voltage	3 Volts
Case Operating Temperature	-20 to 30 $^{\circ}\text{C}$
Storage Temperature Range	-55 to 80 $^{\circ}\text{C}$

- Other Specifications:
 - Temperature coefficient of wavelength is approximately 0.27 to 0.3 nm/ $^{\circ}\text{C}$.
 - Temperature coefficient of threshold current can be modeled as: $I_{TH2} = I_{TH1} \exp[(T_2 - T_1)/T_0]$ where T_0 is a device constant of about 140.
 - Temperature coefficient of operating current is approximately 0.5 to 0.7%/ $^{\circ}\text{C}$.
- Forward Voltage is typically: $V_f = 1.5 \text{ V} + I_{op} \times R_s$
- Wavelength range of cw laser diodes is approximately 790 to 830 nm. Wavelength selection is available as an option. Refer to Price List for wavelength selection range, variance and price.

Typical Light-Current Response



"L" Bar Plate Package [Dimensions in inches (mm)]



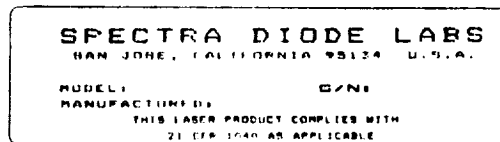
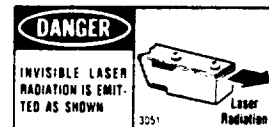
The laser light emitted from this laser diode is invisible and may be harmful to the human eye. Avoid looking directly into the laser diode or into the beam along its optical axis when the device is in operation.

Operating the laser diode outside of its maximum ratings may cause device failure or a safety hazard. Power supplies used with the component must be employed such that the maximum peak optical power cannot be exceeded.

CW laser diodes may be damaged by excessive drive current or switching transients. When using power supplies, the laser diode should be connected with the main power on and the output voltage at zero. The current should be increased slowly while monitoring the laser diode output power and the drive current.

Shipping

Because of the small size of these devices, each of the labels shown is attached to the individual shipping container. They are illustrated here to comply with 21 CFR 1040 as applicable under the radiations control for health and safety act of 1968.





CONTAINERLESS PROCESSING AT HIGH TEMPERATURES USING ACOUSTIC LEVITATION

C. A. Rey, D. R. Merkley, S. Hampton, J. DeVos,
D. Mapes-Riordan, and M. Zatarski

Intersonics, Incorporated
3453 Commercial Avenue
Northbrook, IL 60062

ABSTRACT

Containerless processing of a specimen while it is heated to high temperatures can be accomplished using acoustic levitation. This involves the creation of sufficiently strong and suitably shaped acoustic fields and it is more easily achieved in the microgravity of space. This technique permits the heating, melting, reacting, cooling, and solidification of a substance without contamination or heterogenous nucleation caused by contact with the container. It further enables the processing of materials for which there is no acceptable crucible material. These acoustic containment techniques have been demonstrated in space at temperatures to 1800K in early sounding rocket and space shuttle experiments.

Newly developed approaches can improve the processing capabilities at higher temperatures and provide more contamination-free environments. Advanced techniques are described which facilitate the development of inert or reducing atmospheres in excess of 2000K. Recent testing, in the laboratory and aboard the NASA KC-135 aircraft, of a high temperature acoustic positioner has demonstrated the effectiveness of a specimen motion damping system and the control of specimen spin. These new techniques can produce the extremely quiescent states which help enable the study of deep undercooling processes. The high degree of specimen stability also permits more accurate measurement of high temperature material properties.

INTRODUCTION

Materials processing is conducted at elevated temperatures in many research and manufacturing areas. Materials science and high temperature chemistry are examples of areas which traditionally involve the use of a crucible to contain molten materials. This crucible produces unwanted interactions between the container and the material being processed, resulting in a number of undesirable effects. The container may provide unwanted heterogenous nucleation sites, contaminate the materials or be partially or completely dissolved by the material being processed. In addition, the container may react unfavorably or be incompatible with the surrounding gas, which frequently is required in order to control the chemistry during processing. For some materials there may be no container available which has a sufficiently high melting point.

Containerless processing can eliminate all of the unwanted effects of the crucible. The technique which will be described here uses a method of acoustic levitation which is capable of positioning conductive or nonconductive materials. A suitably shaped acoustic field pattern is created which

constrains the motions of the material being processed. The difficulty of acoustically generating sufficiently large levitating or positioning forces limits the application of this technique in the earth's gravitational field. While some acoustic containerless processing can be achieved on earth, as the processing temperatures increase, the acoustic forces become weaker. As a result it becomes difficult to support specimens with the densities of common materials. By going into an orbital space environment, i.e., microgravity, positioning of specimens for containerless processing is more easily achievable. Such acoustic containment techniques were first demonstrated in space in early sounding rocket and space shuttle experiments. These early approaches used small resistively-heated furnaces combined with appropriate acoustic transducers and positioning components. Materials have been processed at temperatures up to 1800K in an air atmosphere.

Experiments performed in microgravity may also benefit from some additional advantages of the microgravity environment. For example, isostatic pressures will exist throughout the liquids being processed. Buoyant and convective effects are avoided and separation due to density differentials in the liquid melt are eliminated. Additionally, there exists the potential for maintaining an extremely quiescent state during the sequence of melting, processing, reacting, cooling, and solidification.

This paper describes a newly developed approach which can improve processing capabilities, achieve higher temperatures and provide a more contamination-free processing environment.

EXPERIMENTAL APPROACH

Acoustic levitation involves producing an acoustic field which has nodes in the acoustic pressure distribution which are continuous in time. One method of producing this condition is to generate standing waves in an acoustically resonant tube. In general, the stationary acoustic field pattern, which can be produced by exciting various resonances within an acoustic chamber, exerts restoring forces on an object which has a density different than that of the acoustic medium. This continuous acoustic force is given by the negative gradient of the potential energy function.

Similar gradients can be easily produced in a nonresonant fashion by using the interference of multiple acoustic beams.² The acoustic field generated by this interference pattern can produce large potential energy gradients by suitably focusing the acoustic waves. Acoustic nodes can be shaped to form closed "energy wells" capable of exerting restoring forces sufficiently large to position materials without a container. This was first demonstrated at temperatures up to 1800K in an electric furnace with a single axis acoustic positioning system flown on sounding rockets in 1979 and 1980. This was also successfully demonstrated³ with the Single Axis Acoustic Levitator (SAAL) flown in 1983 and 1985 as part of the Materials Experiment Assembly carried in the space shuttle. During these experiments, reluctant glass forming materials were shown to be less susceptible to heterogenous nucleation due to the absence of a container.⁴

Intersonics, Incorporated's new acoustic positioning system uses multiple transducers in order to produce stronger restoring forces and more symmetrically-shaped energy wells. The use of multiple transducers provides enhanced capabilities and more flexible operating parameters.' These additional capabilities include the ability to control specimen position, spin, and the shape of liquid drops. The specimen position control capability allows the use of a closed-loop control system, which greatly enhances the positioning stability of the system. The spin control feature can be used to prevent rotation of the specimen or to produce spin in order to increase specimen isothermality. By modulating the acoustic amplitude, the shape of a liquid specimen can be altered and the drop may be excited into various modes of oscillation.

An application of these techniques has been developed in a High Temperature Acoustic Levitator (HAL). This system utilizes three independent orthogonal positioning axes. The transducer arrangement is shown schematically in Fig. 1. Unlike the heated furnace levitation system referred to earlier, this system uses radiant beam heating. This is produced using ellipsoidal reflectors to focus light from three high power Xenon arc lamps. Fig. 2 is a General Assembly Drawing of this test setup. This equipment has been tested in the laboratory and in short (20 second) periods in the low-gravity environment aboard a NASA KC-135 low gravity test facility.

RESULTS

The abilities to spin, control position and produce damping of residual motions of the specimen have been demonstrated with this device. Fig. 3 is a picture of a specimen being positioned during the heating stage of an experiment. Fig. 4 indicates the typical residual gravitational levels which are encountered during the low gravity period while the KC-135 aircraft is engaged in a parabolic maneuver. These residual g-levels produce fluctuating forces which tend to disturb the stability of the specimen within the acoustic positioning system.

The intensity of the acoustic field necessary to limit the specimen displacement to less than one mm for specimens of varying densities is indicated in Fig. 5. These values were calculated based on acoustic positioning force calibration data and were confirmed during recent KC-135 HAL testing. The confirmation of this analysis resulted in a modification to the equipment to provide dynamic control of the acoustic energy well position and also provide damping of specimen motions. This technique uses three optical sensors which detect the specimen position. The sensor signals are used to determine the magnitude of the velocity vector of the specimen along each of the three orthogonal acoustic axes. This information is then used to shift the energy well position in an amount proportional to the velocity of the specimen and in a direction opposite to that velocity. The result is the equivalent of a viscous drag force which damps oscillations of the specimen. Fig. 6 is a diagram of the motion damping system.

The motion damping system was tested on the KC-135 in March of 1990. Fig. 7 shows the residual motion frequently observed on a specimen without the benefits of the damping circuit. Fig. 8 is an example of acoustic positioning utilizing the damping technique. Additional perturbations and instabilities have been observed during the heating of the specimen. With velocity damping, these perturbations can be reduced to very small levels. In some cases the residual

RMS amplitude of the specimen motion is less than 0.1 mm. Specimen temperatures in excess of 1400K have been obtained in KC-135 test flights of the HAL system.

Testing of this system has indicated that stable positioning can be achieved under ambient and heated conditions, including the transient states of heat-up and cool-down. Successful demonstration of the HAL and the motion damping system has been carried out on earth at temperatures in excess of 2000K.

CAPABILITIES ANALYSIS

The capabilities for continuous processing of dense materials at high temperatures using HAL are given in Table I. The breadboard equipment which has been used in this investigation is limited in maximum temperature by the efficiency of the Xenon arc lamp heating system. An improved arc lamp or laser heating system will replace the arc lamps in order to increase the processing temperature capabilities. The system described here was not completely enclosed and the processing gas was that of the environment, i.e., air. In order to process materials in different gas mixtures or avoid oxidation or contamination of metal or alloys, the processing region can be enclosed in a sealed chamber. The processing gas may then be suitably selected in order to meet the needs of the experiment. Rapid cooling, which takes place mainly due to radiation losses, is on the order of 200K per second for a specimen at 1800K. This could be increased by using an appropriate quenching gas and by increasing the acoustic field intensity. The specimen is held in the region of an acoustic pressure node which is also the position of the velocity anti-node. Because of this and the high acoustic intensity, the velocity of the surrounding gas molecules is very large. This greatly increases the conductive heat flow to the gas from the surface of the specimen. This can more than double the cooling rates.

CONCLUSION

Intersonics, Incorporated High Temperature Levitator is capable of processing specimens of up to 6 mm diameter in a high-purity environment without the contaminating effects of a container at high temperatures and with relative quiescence. Some applications would include the study of deep undercooling of metals, alloys and glass forming materials. Property measurements can be made on reactive materials. Ceramic superconductors as well as semiconductor materials could be investigated in a highly contamination-free environment.

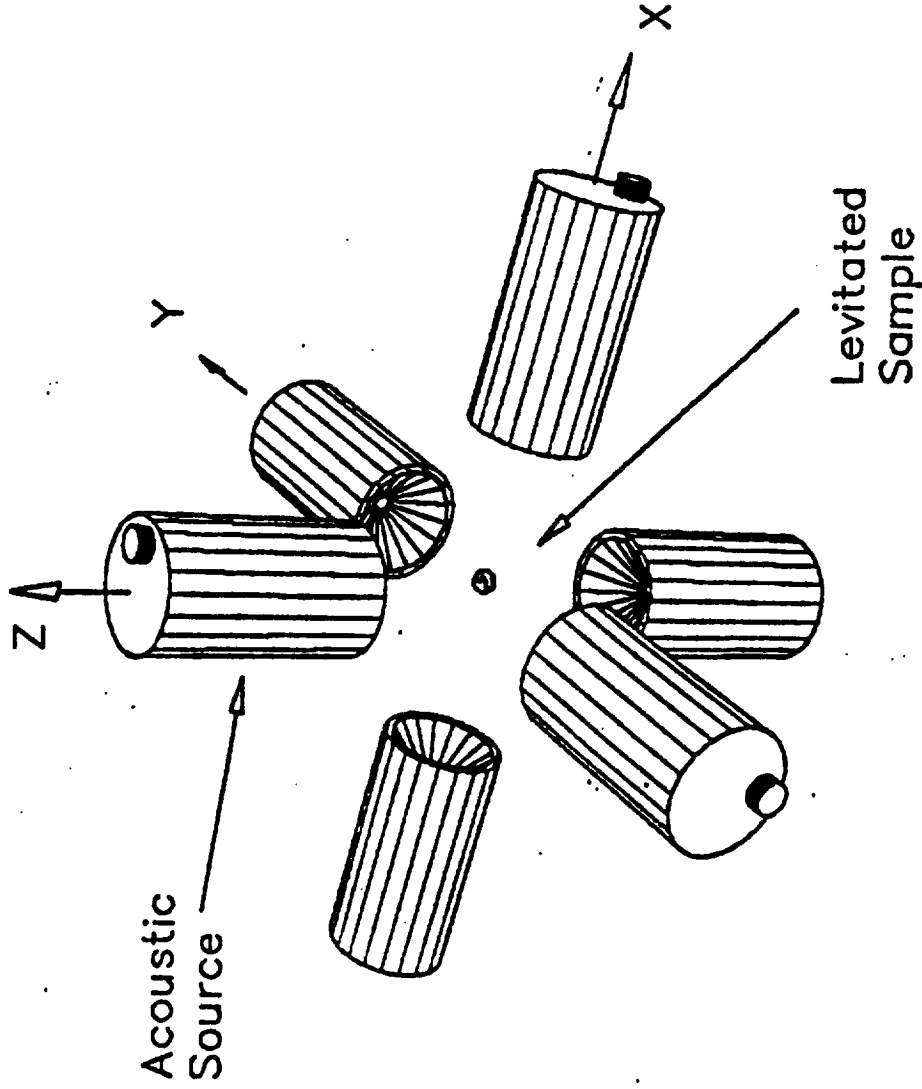
Continuing improvements of the acoustic processing system are under investigation at Intersonics, Incorporated and further enhancements of the processing capabilities are being developed. Similar versions of the HAL could be carried aboard sounding rockets and, if longer duration experiments were required, on space shuttle or free flying orbital carriers.

The authors wish to acknowledge the support for this work from the National Aeronautics and Space Agency.

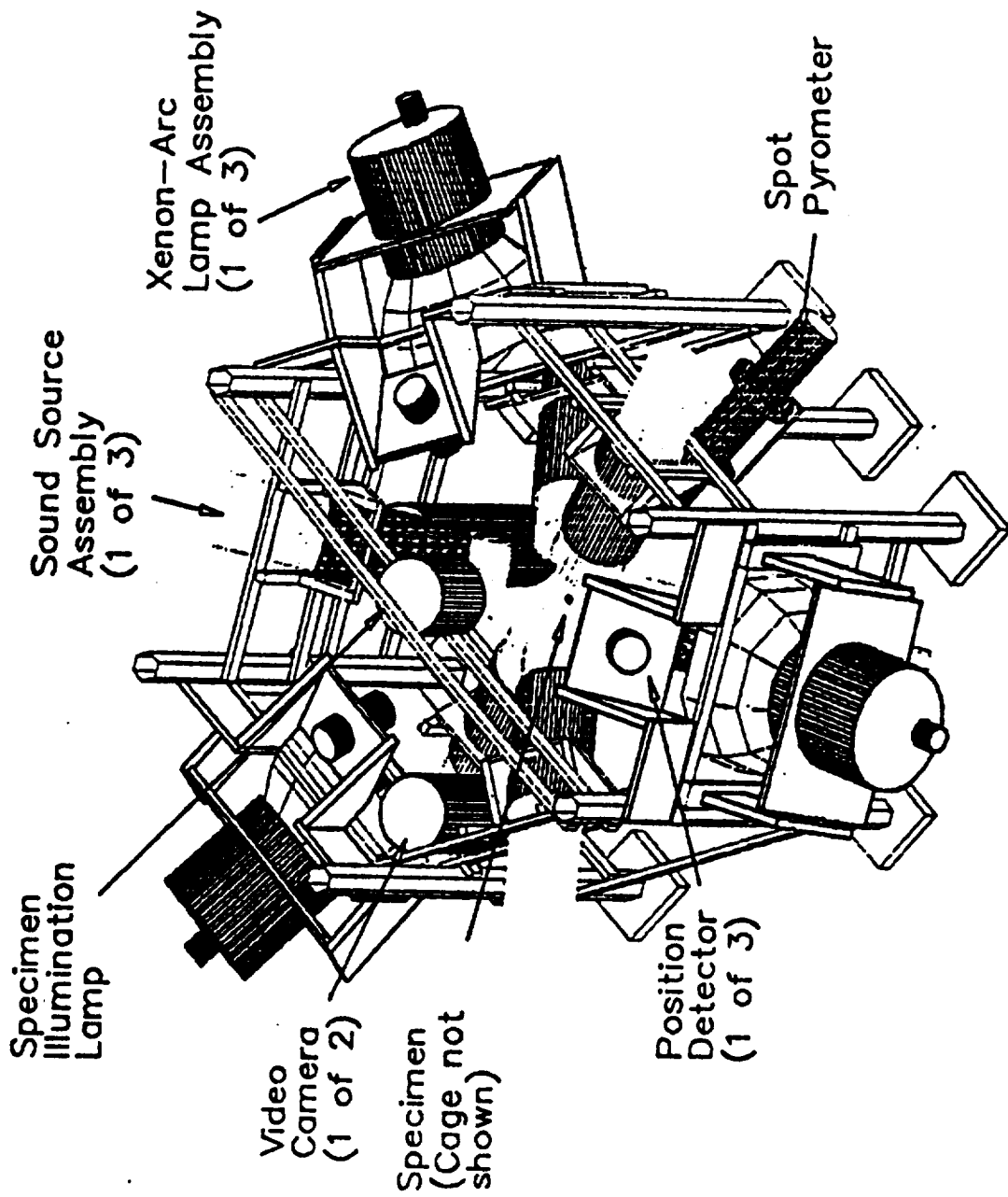
References:

1. "Acoustic Levitation Materials Processing Systems," Charles A. Rey, et al, 17th Aerospace Sciences Meeting, AIAA, New Orleans, January, 1979.
2. "A New Acoustic Levitation Device Using the Interference Sound Field From Two Opposed Radiators," Charles A. Rey, Thomas J. Danley, Dennis R. Merkley, and Gregory R. Hammarlund, 114th Ann. Mtg. of Acoustical Society of America, 1987.
3. "Acoustic Levitation Technique for Containerless Processing at High Temperature in Space," Charles A. Rey, Dennis R. Merkley, Gregory R. Hammarlund, and Thomas J. Danley, METALLURGICAL TRANSACTIONS, Vol. 19A, November, 1988.
4. "Glass Formation in Microgravity," C. S. Ray and D. E. Day, Mat. Res. Soc. Symp. Proc. Vol. 87 (1987).
5. "Specimen Translational Control Capabilities Using an Opposed Radiator Acoustic Levitation System," Charles A. Rey, Dennis R. Merkley, Gregory R. Hammarlund, and Thomas J. Danley, 114th Ann. Mtg. of Acoustical Society of America, 1987.

HAL ACOUSTIC POSITIONING ARRANGEMENT



RESEARCH IN THIS AREA LED TO DEVELOPMENT OF A NEW TECHNIQUE FOR ACOUSTICALLY POSITIONING A SAMPLE BY USING MULTIPLE OPPOSED FOCUSED ACOUSTIC TRANSDUCERS. BY USING THREE PAIR OF OPPOSED SOUND SOURCES, THE SUPERPOSITION OF THE THREE INTERFERENCE FIELDS PRODUCES VERY SYMMETRIC ENERGY WELLS, AND THUS AN EXTREMELY STABLE LEVITATION ENVIRONMENT. IN ADDITION, THE CAPABILITY FOR MANIPULATION OF THE SAMPLE IS GREATLY ENHANCED.



HIGH TEMPERATURE ACOUSTIC LEVITATOR (HAL)

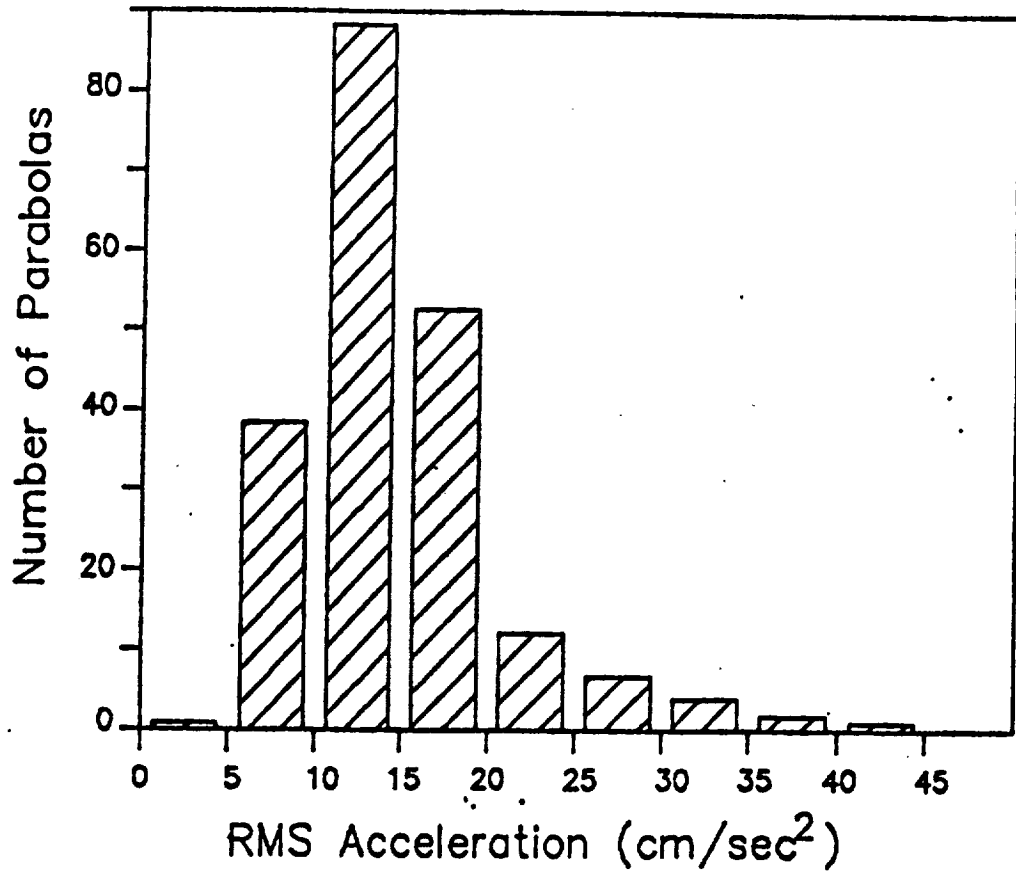
ORIGINAL PAGE IS
OF POOR QUALITY



Operational prototype of high temperature 3-axis acoustic levitator-positioner. The levitated sample is heated with a xenon-arc lamp. Processing of solid or liquid materials up to 2500K (4040°F) is possible.

Figure 3

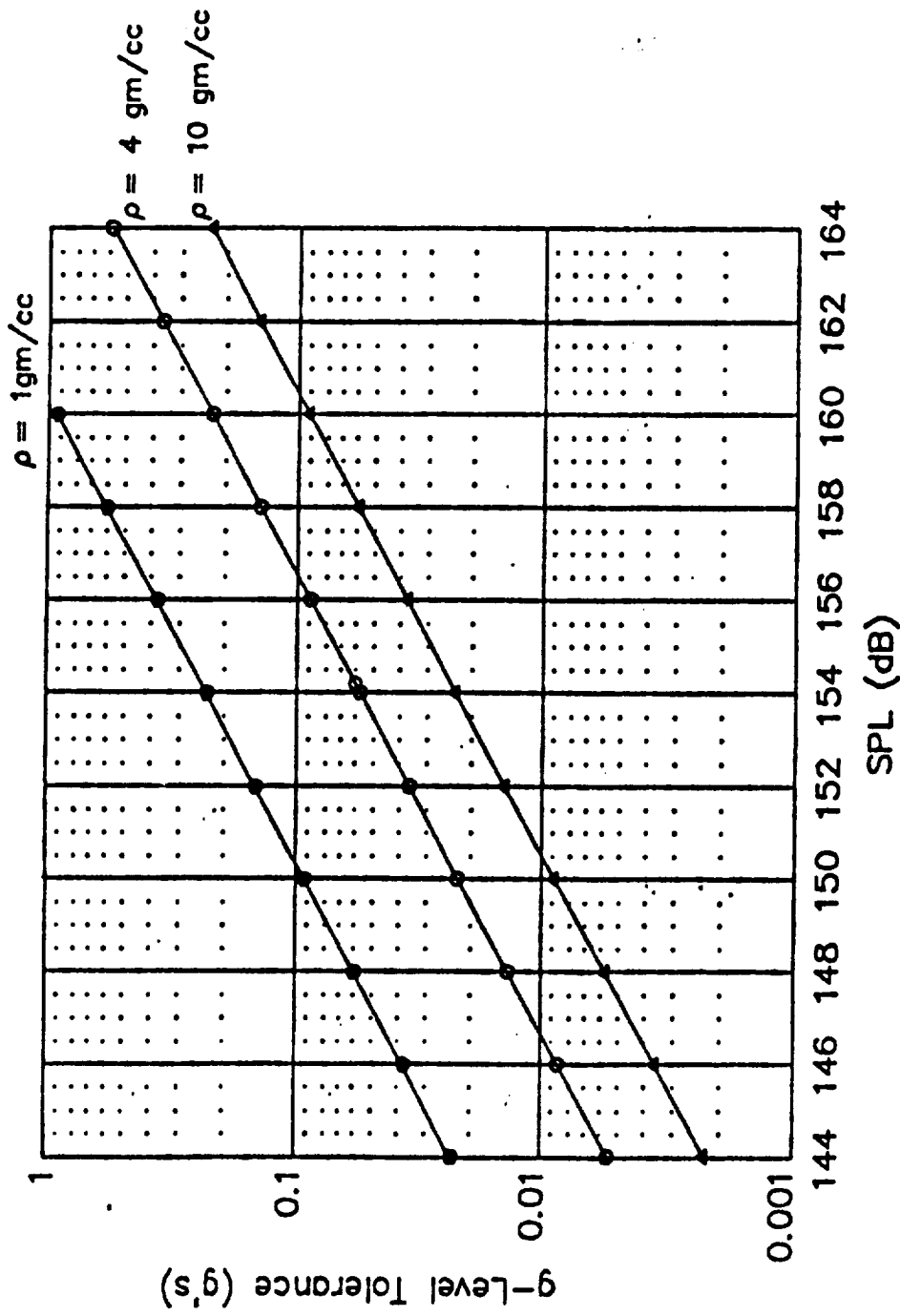
RESIDUAL ACCELERATION
(FOR KC-135 AIRCRAFT DURING PARABOLIC MANEUVER)



DURING THE RECENT TESTING OF HAL ON NASA'S KC-135 AIRCRAFT APPROXIMATELY 300 PARABOLAS WERE PERFORMED. THIS FIGURE SHOWS THE TYPICAL GRAVITATIONAL LEVELS ENCOUNTERED. THE RMS RESIDUAL ACCELERATION LEVELS WERE CALCULATED FROM DATA OBTAINED FROM ACCELEROMETERS POSITIONED NEAR THE ACOUSTIC LEVITATION ASSEMBLY.

Figure 4

g-Level Tolerance (g's) vs. SPL (dB)



Specimen displacement = 1 mm

Frequency = 20 kHz

Spherical Specimen Diameter = 3 mm

USING THE EQUATIONS FOR ACOUSTIC POSITIONING FORCE, THIS FIGURE SHOWS THE ACOUSTIC PRESSURE LEVELS REQUIRED TO SUCCESSFULLY POSITION A SPECIMEN FOR VARIOUS RESIDUAL GRAVITATIONAL FORCES THAT ARE NOT FLUCTUATING. THREE CURVES ARE SHOWN FOR SPECIMEN DENSITIES OF 1, 4 AND 10 GM/CM³. THE CALCULATIONS ASSUME A 20 KHZ SOURCE AND A MAXIMUM SPECIMEN DISPLACEMENT OF 1 MM.

ACOUSTIC POSITIONING SYSTEM

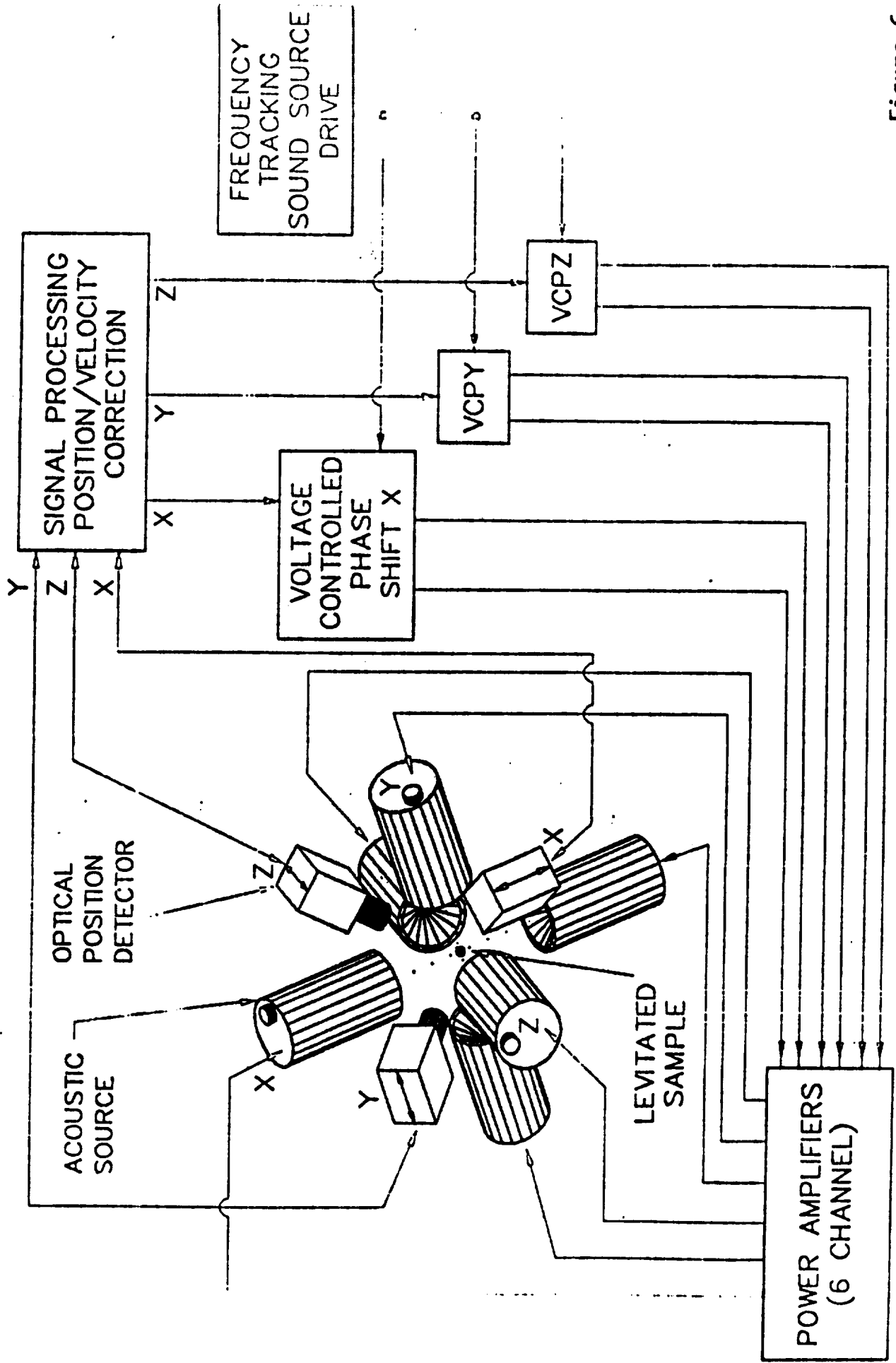
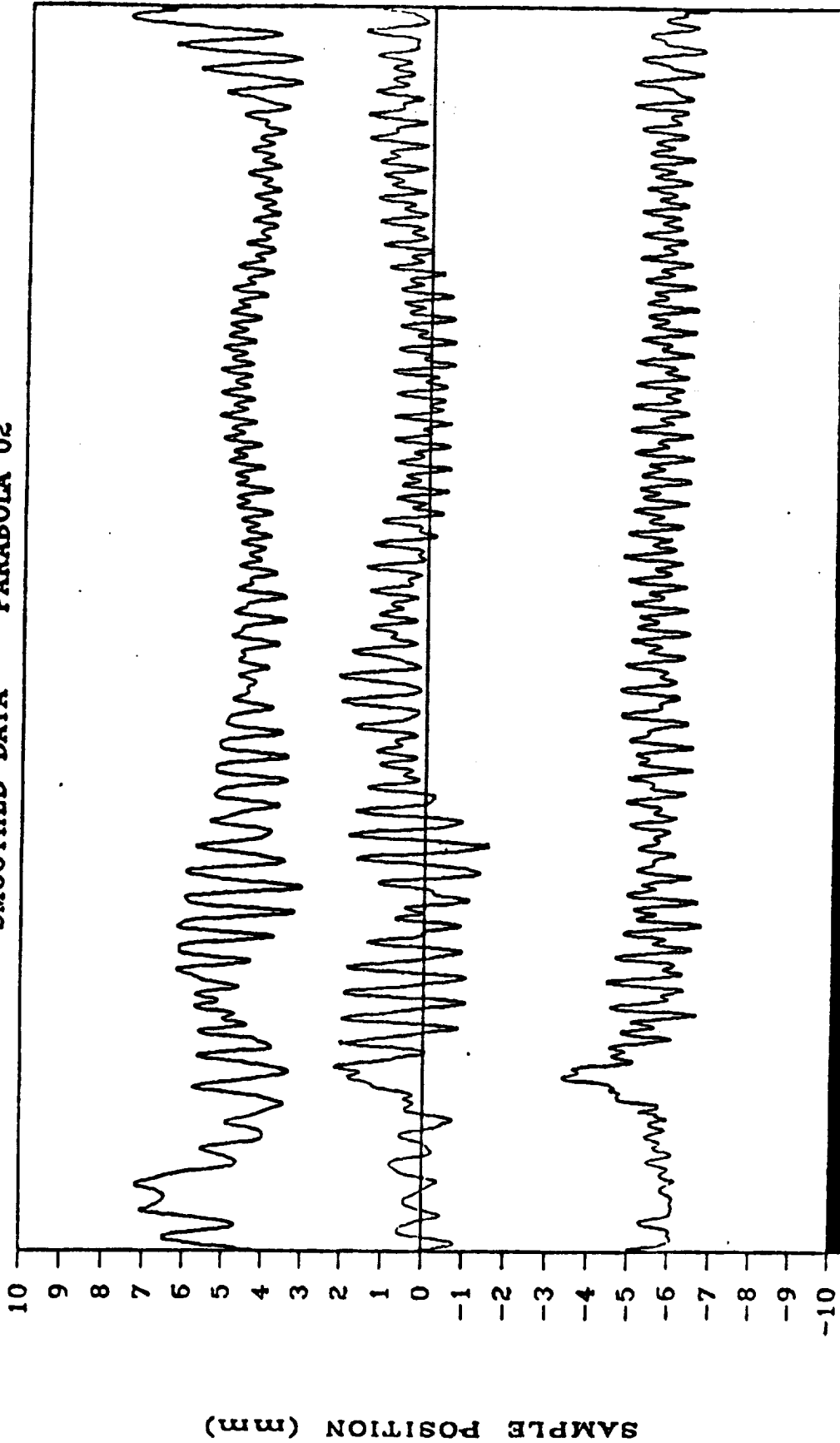


Figure 6

HAL KCI35 TESTS JAN 11, 1990

SMOOTHED DATA PARABOLA 02

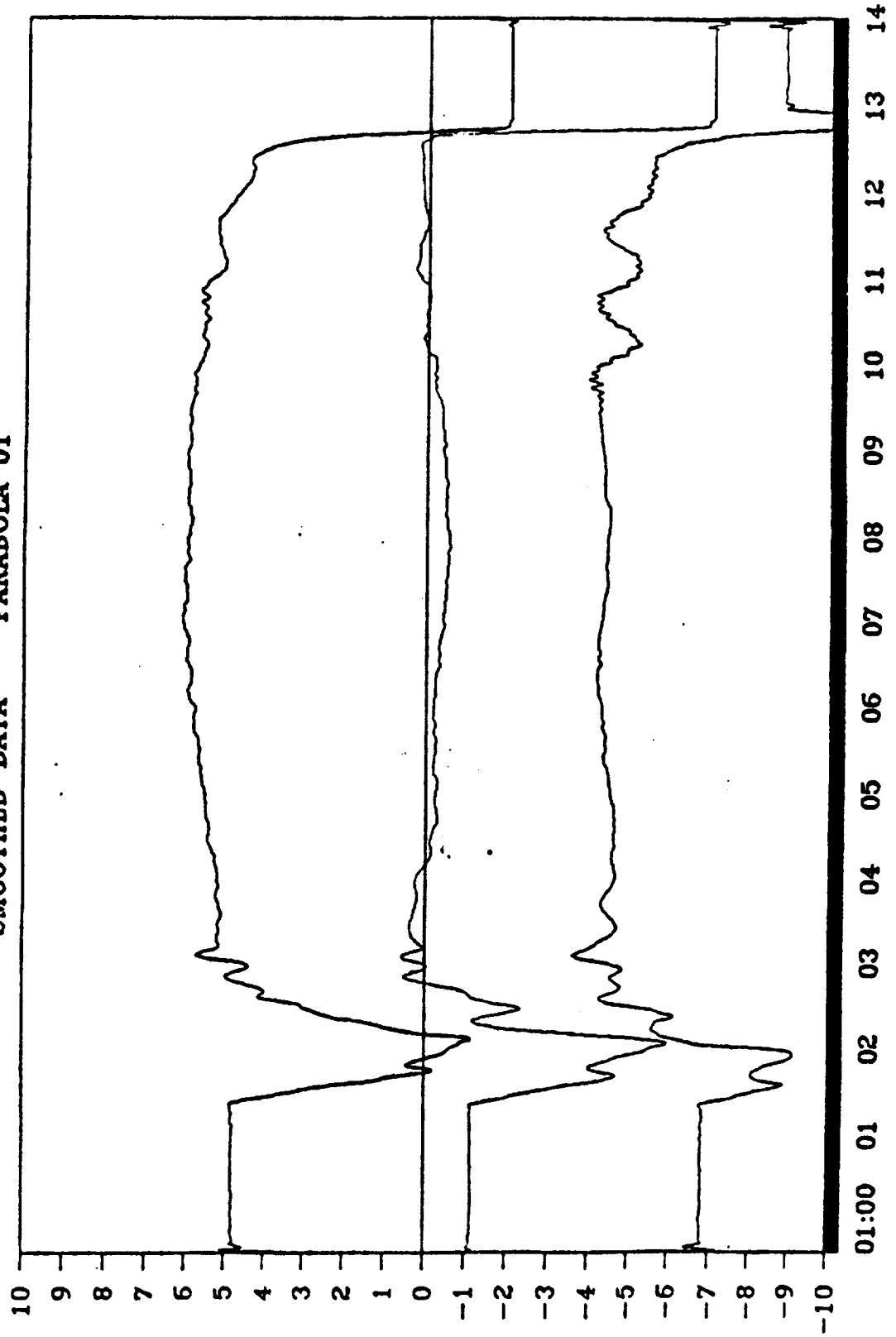


52:53 54 55 56 57 58 59 00 01 02 03 04 05 06 07 08 09 10 11 12 13

— POS1 + 5 — POS2 — POS3 - 5 - - - - - FR

HAL KCI35 TESTS MARCH 22, 1990

SMOOTHED DATA PARABOLA 01



EXPERIMENT CLOCK TIME
—— POS1 + 5 - - - - POS3 - 5

SAMPLE POSITION (mm)

HAL SCIENCE CAPABILITIES

TEMPERATURES DESIGN GOAL	300 TO 2200K > 3000K
ISOTHERMALITY *	FAIR TO GOOD WITH SPIN
TEMPERATURE CONTROL PRECISION	PRECISION (~ 1°C)
GAS PURITY PARTICULATE CONTAMINATION	EXCELLENT (AS GOOD AS PROCESS GAS)
PROCESS GAS	~ ANY
SPECIMEN MOTION	< 0.5 mm RMS
SPECIMEN DENSITY	ANY
SPECIMEN DIAMETER	UP TO 6 mm
HEAT RATES *	VERY FAST, 0 TO OVER 200°C/SEC
COOLING RATES *	VERY FAST, 0 UP TO 200°C/SEC FASTER WITH GAS QUENCH
SPIN CONTROL	GOOD, NO OR VERY LOW SPIN
OPTICAL ACCESS	VERY CONVENIENT
HEATERS	XENON ARC OR LASER BEAM
CARRIER	KC-135, SOUNDING ROCKET SPACELAB, SPACE STATION

* SAMPLE PROPERTIES AND SIZE DEPENDENT

